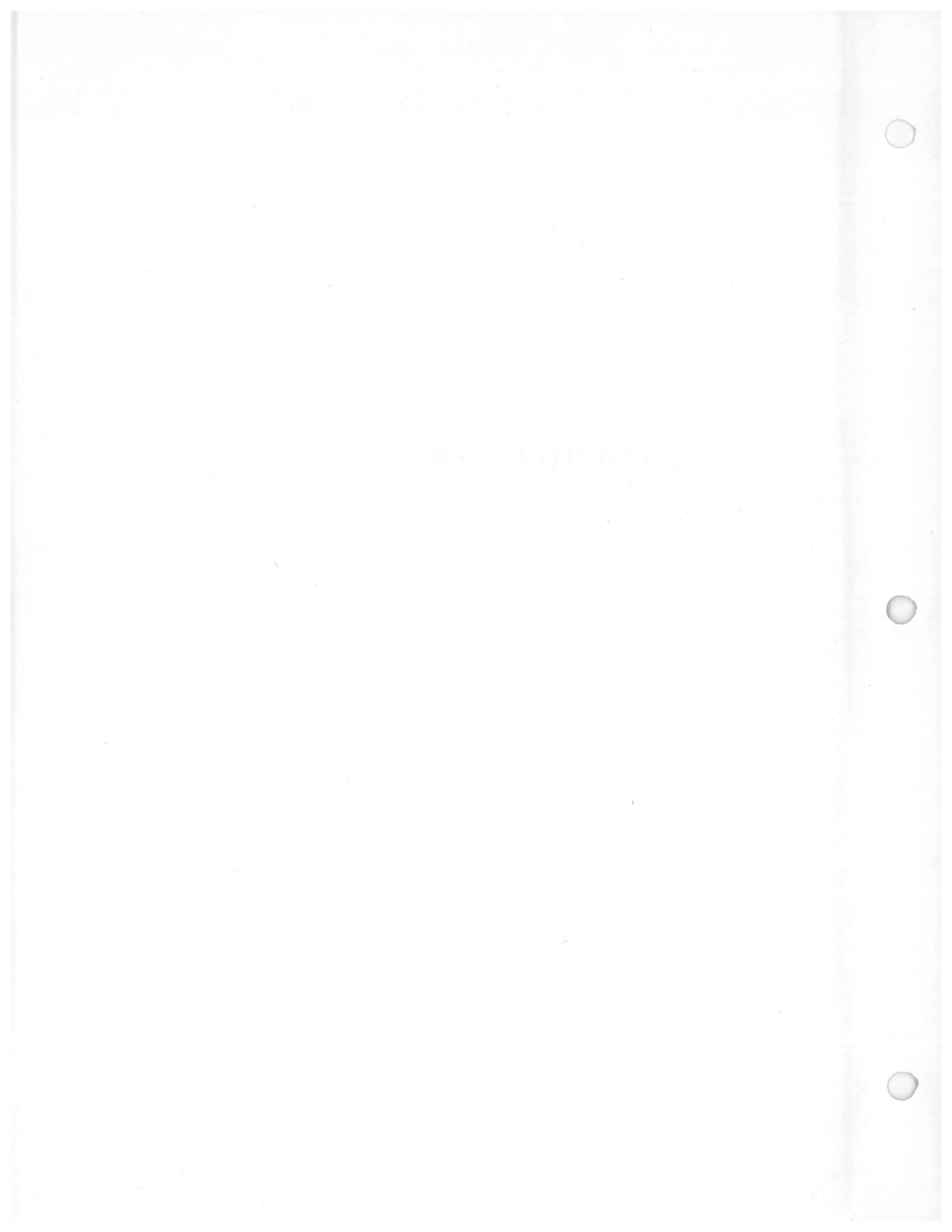


REPORT NO. AE62-0774

# LIQUID HYDROGEN TECHNOLOGY

SEPTEMBER 1962

Prepared by  
GENERAL DYNAMICS ASTRONAUTICS  
A DIVISION OF GENERAL DYNAMICS CORPORATION  
San Diego, California





# GENERAL DYNAMICS | ASTRONAUTICS

## CONTENTS

List of Illustrations	vii
List of Tables	xv
Foreword	xvii
Summary	xix
1. MANUFACTURE	1
1.1 Major Liquid Hydrogen Producers	1
1.2 Price of Liquid Hydrogen	2
1.3 Production Processes	3
2. TRANSPORTATION	9
3. HYDROGEN SAFETY	13
3.1 General Properties of Hydrogen	13
3.2 Flammability and Detonation Hazards	13
3.3 System Design Considerations	17
3.4 Operational Considerations	20
3.5 Personnel Considerations	22
4. MATERIALS	25
4.1 Material Problems Associated with Liquid Hydrogen	25
4.2 Compatibility of Specific Materials	32
References	43
5. CRYOGENIC INSULATION	47
5.1 Types of Insulation	47

# GENERAL DYNAMICS | ASTRONAUTICS

5.2	Flight Insulations	55
	References	61
6.	TRANSFER	63
6.1	Cooldown Characteristics	63
6.2	Transfer Methods	72
6.3	Nomenclature	84
6.4	Subscripts	85
6.5	Greek Symbols	86
	References	87
7.	LIQUID HYDROGEN MEASUREMENTS	89
7.1	Introduction	89
7.2	Temperature Measurements	89
7.3	Pressure Measurements	97
7.4	Flowmeters	101
7.5	Level Sensors	102
7.6	Liquid/Gas Detectors	104
7.7	Hydrogen Leak Detectors	104
8.	PROPULSION SYSTEMS	105
8.1	Chemical Propulsion	105
8.2	Nuclear Propulsion	108
8.3	Electric Propulsion Systems	111
8.4	Solar Propulsion	114
9.	SLOSHING	119
9.1	Mechanical Pendulum Analogy	119
9.2	Damping the Fluid Motion	123
	References	127

## GENERAL DYNAMICS | ASTRONAUTICS

10. VORTEXING	129
10.1 Scaling Model Test Results	129
10.2 Antivortex Designs	133
11. PROPELLANT HEATING	137
11.1 Introduction	137
11.2 Environmental Heating	137
11.3 Onboard Heat Sources	148
11.4 Nomenclature	163
11.5 Greek Symbols	166
Appendix	167
References	169
12. ZERO-GRAVITY BEHAVIOR	171
12.1 Zero-Gravity and Simulated Zero-Gravity Testing Methods	171
12.2 The Behavior of Liquid Hydrogen at Zero Gravity	172
12.3 Zero-Gravity Liquid/Gas Separators	185
References	190
13. SPACE STORAGE	191
13.1 Thermal Protection	191
13.2 Meteoroid Hazard	195
13.3 Nomenclature	210
13.4 Greek Symbols	212
13.5 Subscripts	212
References	215
14. PROPERTIES	217
14.1 Definition of Terms	217
14.2 Definition of Symbols and Abbreviations	221
14.3 Physical Constants and Miscellaneous Information	223

## GENERAL DYNAMICS | ASTRONAUTICS

14.4 Thermal Properties	247
14.5 Nuclear Properties	269
14.6 Conversion Factors	278
References	279
Bibliography	283

# GENERAL DYNAMICS | ASTRONAUTICS

## ILLUSTRATIONS

1. Air Products' liquid hydrogen facility at West Palm Beach, Fla.	2
2. Condensed flow chart of Air Products' liquid hydrogen production cycle.	4
3. Characterization of nuclear spins of orthohydrogen and parahydrogen.	6
4. Converter cold box for liquefying hydrogen.	7
5. Vacuum-insulated transfer lines for liquid hydrogen.	9
6. Liquid hydrogen trailer.	10
7. Minimum ignition energies for hydrogen-air mixtures at one atmosphere.	14
8. Suggested spacing for liquid hydrogen storage tanks.	18
9. Liquid hydrogen storage tank, Sycamore Canyon Test Site.	19
10. Water deluge system, Sycamore static test stand.	24
11. Astronautics' cryogenic tensile testing setup.	29
12. Low-strain-rate plastic deformation as a function of time for A110AT titanium alloy.	34
13. Low-strain-rate notched stress rupture curves for A110AT titanium alloy at various hydrogen levels.	35
14. Applied stress for delayed failure and reduction in area at failure for A110AT titanium alloy, un-notched specimens.	36
15. Foaming polyurethane insulation on Centaur forward bulkhead.	49
16. Typical failure in fiberglass sealer on outside insulation test with liquid hydrogen.	56
17. External foam-filled honeycomb insulation with a repair plug.	58
18. Wrinkled skin of vacuum insulation.	60
19. Internal foam-filled honeycomb insulation after 20 pressure cycles in liquid hydrogen.	60

## GENERAL DYNAMICS | ASTRONAUTICS

20. Percent cooldown of concentrated masses.	67
21. Dimensionless parameters for calculating mass flow rate ( $\bar{w}_2$ ) of discharge gas for unrestricted flow.	67
22. Friction factor as a function of reynolds number.	69
23. Proportionality constant for curved lines.	69
24. Dimensionless parameters for calculating mass flow rates ( $\bar{w}_2$ ) of discharge gas for restricted flow.	70
25. Dimensionless parameters for calculating discharge pressure ( $P_2$ ) for restricted gas flow.	70
26. Typical gas-pressurization transfer systems.	74
27. Tank pressurization analytical model.	75
28. Maximum and minimum limits for pressurant gas requirements.	76
29. Effect of sloshing on propellant heating.	79
30. Solubility of helium in liquid hydrogen as a function of pressure.	80
31. Simplified cross-section of Centaur liquid hydrogen pump.	81
32. Platinum resistance thermometer.	90
33. Typical flight vehicle telemetry temperature bridge.	91
34. General-purpose bridge circuit for temperature measurements.	93
35. Thermopile.	95
36. Typical thermistor probe.	96
37. Gas-pressure temperature probe.	98
38. Helical Bourdon tube transducer.	99
39. Strain-gage pressure transducer.	99
40. Typical differential pressure transducer.	100
41. Typical turbine flowmeter.	101
42. Vibrating paddle liquid-level sensor or liquid/gas detector.	103
43. Centaur upper stage with Atlas booster just prior to liftoff.	106
44. Proposed reactor-in-flight-test vehicle.	109

## GENERAL DYNAMICS | ASTRONAUTICS

45. Typical liquid hydrogen flow for nuclear vehicle.	110
46. Electric arc-heated thrust device.	112
47. Electric resistance-heated thrust device.	113
48. Solar-powered space ship prototype.	115
49. Artist's concept of solar-powered space ship.	116
50. Tank model and coordinates for pendulum analogy.	121
51. Nondimensional sloshing parameters for pendulum analogy; flat-bottom cylindrical tank (first mode).	124
52. Sloshing test setup at Astronautics.	125
53. Typical baffle configuration.	126
54. Annular ring baffles in a test tank.	128
55. Slosh height definition.	128
56. Atlas antivortex membranes.	133
57. Proposed Saturn antivortex device.	135
58. Ground heat load to hydrogen tank.	138
59. Variation of solar heat flux with distance to the sun.	142
60. Unit heating rates in interplanetary space.	143
61. Distance from sun on typical interplanetary trajectories.	144
62. Geometry of planetary thermal radiation to a flat plate.	147
63. Geometry of planetary albedo to a flat plate.	149
64. Through-connection heat-leak parameter.	150
65. Typical hydrogen tank support.	151
66. Intertank heat transfer as a function of conductivity (including convection and radiation in tank).	152
67. Hydrogen tank stratification model.	154
68. Liquid oxygen temperature stratification in Atlas missile 4-B.	157
69. Astronautics' drop-test facilities for hydrogen zero-g test program.	173
70. Aircraft zero-g trajectory.	174

## GENERAL DYNAMICS | ASTRONAUTICS

71. Free-floating test capsule and personnel during Astronautics zero-g aircraft tests.	174
72. Test capsule and personnel viewed through a porthole of the nitrogen-filled bag, Astronautics aircraft zero-g tests.	175
73. Centaur liquid/liquid model.	176
74. Configuration of liquid hydrogen at zero g for typical nuclear vehicle.	179
75. Liquid/gas interface around a center vent tube at zero g.	180
76. Schematic drawing of Centaur zero-g liquid/gas separator.	188
77. Test prototype of Centaur zero-g liquid/gas separator.	189
78. Method for attaching laminar insulation to allow rapid outgassing in space.	194
79. Component parts of a thermal-meteoroid protection system.	195
80. Typical thermal/meteoroid protection systems.	196
81. Closeup of typical crater on outside surface of Atlas 109-D fragment.	197
82. Aluminum bumper with 3-in. spacing.	198
83. Mass-velocity distribution of meteoroids.	200
84. Meteoroid flux.	201
85. Skin thickness vs. threshold meteoroid mass.	205
86. Hole area vs. meteoroid mass.	206
87. Effectiveness of different bumper materials.	207
88. Effectiveness of bumper spacing and bumper thickness.	207
89. Reverse side of bumper space 0.25 in. from hull plate.	208
90. Dependence of total penetration on bumper spacing.	209
91. Effectiveness of 10 different core materials.	211
92. Experiment showing the advantage of energy-absorbing core material.	212
93. Sectioned honeycomb core after hypervelocity impact to bumper-honeycomb core-hull system.	213
94. Variation of target ballistic limit as a function of number of sheets and core material.	214



## GENERAL DYNAMICS | ASTRONAUTICS

95. Compressibility factor for liquid hydrogen as a function of temperature.	225
96. Compressibility factor for saturated hydrogen vapor as a function of temperature.	226
97. Compressibility factor for gaseous hydrogen as a function of temperature.	227
98. Sound velocity in hydrogen as a function of temperature and pressure.	229
99. Refractive index of liquid normal hydrogen as a function of temperature.	230
100. Dielectric constant of saturated liquid parahydrogen as a function of temperature (NASA-recommended values).	231
101. Density of solid and liquid hydrogen as a function of temperature.	232
102. Saturated vapor density of $e\text{-H}_2$ as a function of temperature.	233
103. Density of hydrogen at low temperatures.	234
104. Density of gaseous hydrogen at high temperatures.	235
105. Hydrogen phase changes as a function of temperature and pressure.	236
106. Vapor pressure of solid hydrogen as a function of temperature.	237
107. Vapor pressure of liquid equilibrium hydrogen as a function of temperature.	238
108. Vapor pressure of liquid normal hydrogen as a function of temperature.	239
109. Viscosity of liquid hydrogen as a function of temperature.	240
110. Viscosity of hydrogen.	241
111. Surface tension of liquid hydrogen as a function of temperature.	242
112. Hydrogen dissociation as a function of temperature and pressure.	245
113. Orthohydrogen/parahydrogen composition at equilibrium as a function of temperature.	246
114. Latent heat of vaporization of liquid hydrogen as a function of temperature.	249
115. Heat of conversion from normal hydrogen to parahydrogen.	250
116. Heat capacity of solid hydrogen as a function of temperature.	251
117. Heat capacity of liquid hydrogen and saturated vapor as a function of temperature.	252

## GENERAL DYNAMICS | ASTRONAUTICS

118. Heat capacity of hydrogen at low pressure, $C_p$ .	253
119. Heat capacity of hydrogen at high pressure, $C_p$ .	254
120. Heat capacity ratio ( $C_p/C_v$ ) of hydrogen as a function of temperature and pressure, $C_p/C_v = 1.4$ .	255
121. Heat capacity ratio ( $C_p/C_v$ ) of hydrogen as a function of temperature and pressure, $C_p/C_v = 1.4$ .	256
122. Heat capacity correction from normal hydrogen to parahydrogen.	257
123. Thermal conductivity of liquid hydrogen as a function of temperature.	258
124. Thermal conductivity of gaseous hydrogen at 14.7 psia as a function of temperature.	259
125. Thermal conductivity of hydrogen.	260
126. Temperature-entropy diagram for normal hydrogen ( $0^\circ$ to $270^\circ\text{R}$ ).	261
127. Temperature-entropy diagram for normal hydrogen ( $234^\circ$ to $540^\circ\text{R}$ ).	262
128. Temperature-entropy diagram for normal hydrogen ( $504^\circ$ to $1,080^\circ\text{R}$ ).	263
129. Temperature-entropy diagram for parahydrogen ( $36^\circ$ to $180^\circ\text{R}$ ).	264
130. Temperature-entropy diagram for parahydrogen ( $140^\circ$ to $540^\circ\text{R}$ ).	265
131. Enthalpy-entropy diagram for parahydrogen ( $500^\circ$ to $5,000^\circ\text{R}$ ).	266
132. Prandtl number of hydrogen as a function of temperature and pressure.	267
133. Prandtl number of hydrogen as a function of temperature and pressure.	268
134. Absorption cross-sections for hydrogen as a function of neutron energy.	269
135. Total neutron cross-section of liquid normal and parahydrogen as a function of neutron energy.	270
136. Total neutron cross-sections for hydrogen as a function of neutron energy.	271
137. Total neutron cross-sections for hydrogen as a function of neutron energy.	272
138. Total neutron cross-section for hydrogen as a function of neutron energy.	273
139. Range of protons in hydrogen as a function of proton energy.	274
140. Energy loss of protons in hydrogen as a function of proton energy.	275
141. Range of electrons and positrons in hydrogen as a function of energy.	276

## GENERAL DYNAMICS | ASTRONAUTICS

- |      |  |     |
|------|--|-----|
| 142. | Energy loss of electrons and positrons in hydrogen, including density correction, as a function of energy. | 277 |
| 143. | Total absorption coefficients of x-rays and gamma rays for hydrogen.                                       | 277 |

SECRET

# GENERAL DYNAMICS | ASTRONAUTICS

## TABLES

I. Low-temperature characteristics of metals.	26
II. Relative index for comparing thermal shock resistance of materials.	33
III. Structure-insensitive properties of uranium.	37
IV. Properties of modified and unmodified Teflon.	41
V. Properties of load-bearing insulations.	44
VI. Representative thermal conductivities of insulations.	48
VII. Total hemispherical emissivity of metals.	54
VIII. Equivalent lengths of screwed fittings and valves.	71
IX. Propulsion methods using hydrogen.	107
X. First-mode sloshing parameters for pendulum analogy (cylindrical, flat-bottom tank).	122
XI. Liquefaction unit weight.	192
XII. Hydrogen triple points.	224
XIII. Critical constants.	224
XIV. Boiling point at 14.696 psia.	224
XV. Compressibility of solid hydrogen as a function of pressure at 7.6°R.	226
XVI. Expansivity of solid hydrogen as a function of temperature.	226
XVII. The virial equations of state.	228
XVIII. Sound velocity in ideal gaseous normal hydrogen as a function of temperature.	243
XIX. Dielectric constant of liquid parahydrogen as a function of temperature and pressure.	244
XX. Dissociation of hydrogen molecules as a function of temperature at a pressure of one atmosphere.	245

## GENERAL DYNAMICS | ASTRONAUTICS

XXI. Heat of dissociation of hydrogen for the reaction $H_2 \rightleftharpoons 2H$ .	247
XXII. Latent heat of fusion of solid hydrogen.	247
XXIII. Equations for computing thermal conductivity of normal parahydrogen.	248
XXIV. Isotopic mass.	269

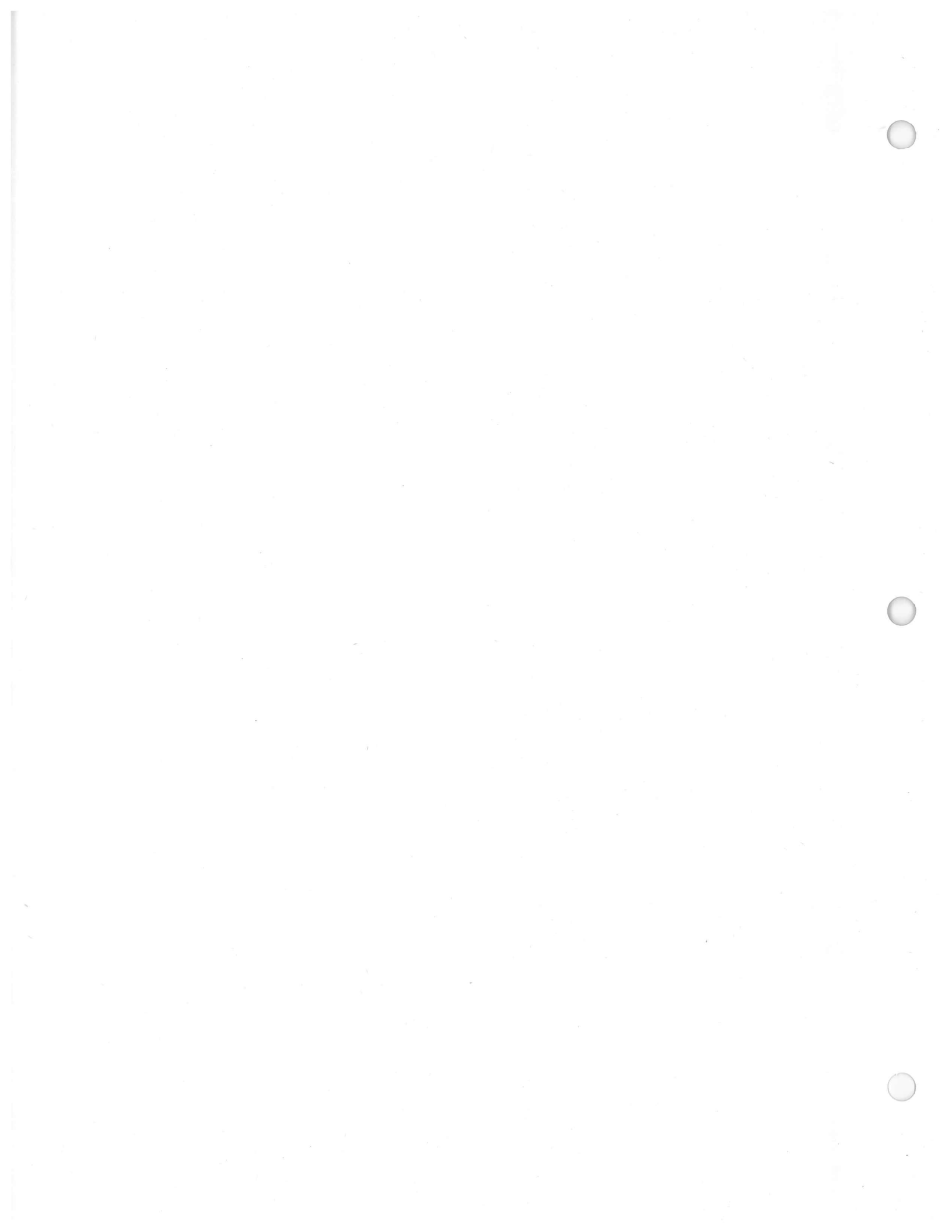
# GENERAL DYNAMICS | ASTRONAUTICS

## FOREWORD

This report summarizes a continuing study of liquid hydrogen technology being conducted by General Dynamics Astronautics, A Division of General Dynamics Corporation. Work is performed on a company-funded basis (under REA No. 114-9640). The report is intended to serve as a standard reference on liquid hydrogen properties, handling, and storage, with primary emphasis on space vehicle applications. Preliminary findings in this study were published as Appendix F of the Nuclear Test Stage Preliminary Design Study final report (Astronautics Report No. AE61-1151).

This report was compiled and edited by Richard T. Parmley, Astronautics research engineer. The following individuals contributed to the indicated portions of this study:

R. S. Dummer	Space Heating
R. N. Franklin	Measurements
J. Hertz	Materials (Insulation)
C. V. Hopkins	Technical Editing
A. H. Jazwinski	Meteoroid Protection
C. C. Love	Propellant Heating
O. H. McDermed	Nuclear Heating
C. Melfi	Aerodynamic Heating
H. N. Norton	Measurements
G. W. Oliver	Materials (Lubricants)
J. Shirley	Zero G
J. F. Watson	Materials (Metals)
W. E. Willcutt	Manufacturing
S. A. Yalof	Materials (Plastics)





# GENERAL DYNAMICS | ASTRONAUTICS

## SUMMARY

This report contains information on liquid hydrogen as related to its use as a propellant for space vehicles. The following 14 areas are included:

1. **Manufacture.** This section includes plant locations, plant capacities, cost, production processes, and future expansion plans of the four major liquid hydrogen producers in the United States.
2. **Transportation.** Current methods for transporting liquid hydrogen are discussed.
3. **Hydrogen Safety.** The four main hazards associated with the use of liquid hydrogen were investigated with respect to the design and operation of a liquid hydrogen system. These four hazards are: (1) the ease of ignition of hydrogen in air over a wide composition range; (2) the low-temperature embrittlement some materials experience in liquid hydrogen; (3) the extremely high pressures that are attained if liquid hydrogen is vaporized in a closed system; and (4) the danger of frostbite to personnel exposed to the extreme subzero temperatures of liquid hydrogen. Overpressure equations for hydrogen-oxygen explosions are included.
4. **Materials Compatibility.** Four general types of material problems are encountered with liquid and gaseous hydrogen contact. These are: low-temperature embrittlement, thermal shock, chemical reactions of materials with hydrogen, and hydrogen embrittlement of metals. The specific materials discussed in detail are aluminum alloys, stainless steel alloys, titanium alloy, high temperature alloys, uranium, graphite, lithium hydride, seal materials, lubricants, and insulations.
5. **Cryogenic Insulation.** Evacuated and nonevacuated insulations are covered. Thermal conductivity values and equations for computing the thermal effectiveness of different insulating systems are included. Flight-weight insulations are discussed.
6. **Transfer.** Equations are given for calculating the following cooldown characteristics: pressure oscillations, conditions necessary to maintain single-phase

## GENERAL DYNAMICS | ASTRONAUTICS

flow, cooldown time, and mass of  $\text{LH}_2$  needed to cool the transfer system. Transfer methods (gas pressurization and pump) are discussed; equations are given for calculating gas-pressurization requirements; critical pump design areas are covered; methods for transferring  $\text{LH}_2$  at zero gravity are summarized.

7. Cryogenic Measurements. Ground and flight-type sensors, including some circuitry, are covered in the following six areas: temperature, pressure, flow, level sensing, liquid/gas detection, and leak detection.
8. Propulsion Methods. Propulsion methods currently using  $\text{LH}_2$ , or contemplating the use of  $\text{LH}_2$ , are summarized. These include chemical, nuclear, electric, and solar propulsion systems.
9. Sloshing. A mechanical pendulum analogy, identical to the perfect fluid hydrodynamic equations for sloshing fluids, is given for computing the forces and moments on a cylindrical tank. Equations are given for computing the damping effect mechanical baffles and wall-wiping action have on fluid motion.
10. Vortexing. The similitude of liquid motion is discussed in order to correlate scale-model test results with full-scale prototypes. Designs for eliminating vortex motion of emptying fluids from a tank are shown.
11. Propellant Heating. Equations for calculating the heat contribution from environmental and onboard sources are given for: ground hold conditions prior to liftoff, aerodynamic heating, space heating (planetary radiation, albedo, and solar radiation), heat-transfer rates at an  $\text{LH}_2/\text{LO}_2$  bulkhead and in through connections, and volumetric nuclear heat deposition from a reactor for a baffled and nonbaffled tank, including the subsequent temperature and vapor pressure rise.
12. Zero-Gravity Behavior. Methods used for studying liquid hydrogen at zero gravity are discussed. The configuration of liquid hydrogen at zero gravity is dominated by surface tension effects and can be predicted. The perturbing effects on the equilibrium configuration of complex shapes, mechanical disturbances, and heat transfer into the tank are included. The use of static and dynamic devices for separating hydrogen vapor from liquid is discussed, along with limitations on these devices.
13. Space Storage. Storage of  $\text{LH}_2$  in space requires adequate thermal and meteoroid protection. The storage state (solid, slush, or liquid) is discussed along with some advanced insulation concepts. The meteoroid hazard is defined as well as present data will allow; equations are given for calculating hole areas, depth of penetration, and  $\text{LH}_2$  flow from a meteoroid punctured tank. Discussion of

## GENERAL DYNAMICS | ASTRONAUTICS

bumper systems, used to protect the  $\text{LH}_2$  tank from puncture, is given in three parts: bumper materials, bumper spacing, and energy-absorbing core materials.

14. Properties. The physical, thermodynamic, and nuclear properties of solid, liquid, and gaseous hydrogen are given.

1951-1952



# 1

## MANUFACTURE

### 1.1 MAJOR LIQUID HYDROGEN PRODUCERS

The National Bureau of Standards was asked in 1950 to assist the Los Alamos Scientific Laboratory on a major research project involving the application of low-temperature techniques. For this purpose the NBS Cryogenic Laboratory was established in Boulder, Colo., starting actual operations in the spring of 1952. As a result, the NBS Cryogenic Laboratory became the first large-scale producer of liquid hydrogen with a capacity of 1,000 lb. per day.

Recognizing the substantial potential inherent in liquid hydrogen for high specific impulse chemical rockets and nuclear vehicles, the Air Force Air Research and Development Command and the Air Materiel Command subsequently initiated the engineering design and construction of large-scale liquid hydrogen production facilities.

The first two plants were completed in 1957 and 1958, the first by Air Products, Inc., at Painesville, Ohio (capacity 6,000 lb. per day) and the second by the Stearns-Roger Manufacturing Co. at Bakersfield, Calif. (capacity 4,000 lb. per day). These plants have been operated for the Air Force by the companies for initial testing and development purposes in support of Air Force programs.

Later, the Air Force awarded a contract to Air Products for the construction of production facilities of even larger tonnage in West Palm Beach County, Fla. Two production facilities were constructed. The initial one was completed in 1958 with a capacity of 12,000 lb. per day. The second facility, completed in January 1959, has a capacity of 60,000 lb. per day. It is the largest liquid hydrogen production facility operating in the United States (see Figure 1).

Also in 1959, the Linde Co. opened a 14,000-lb.-per-day facility at Torrance, Calif. Linde has just completed a facility which will match the 60,000 lb. capacity of the large Air Products plant. This facility, located in Fontana, Calif. is in operation.

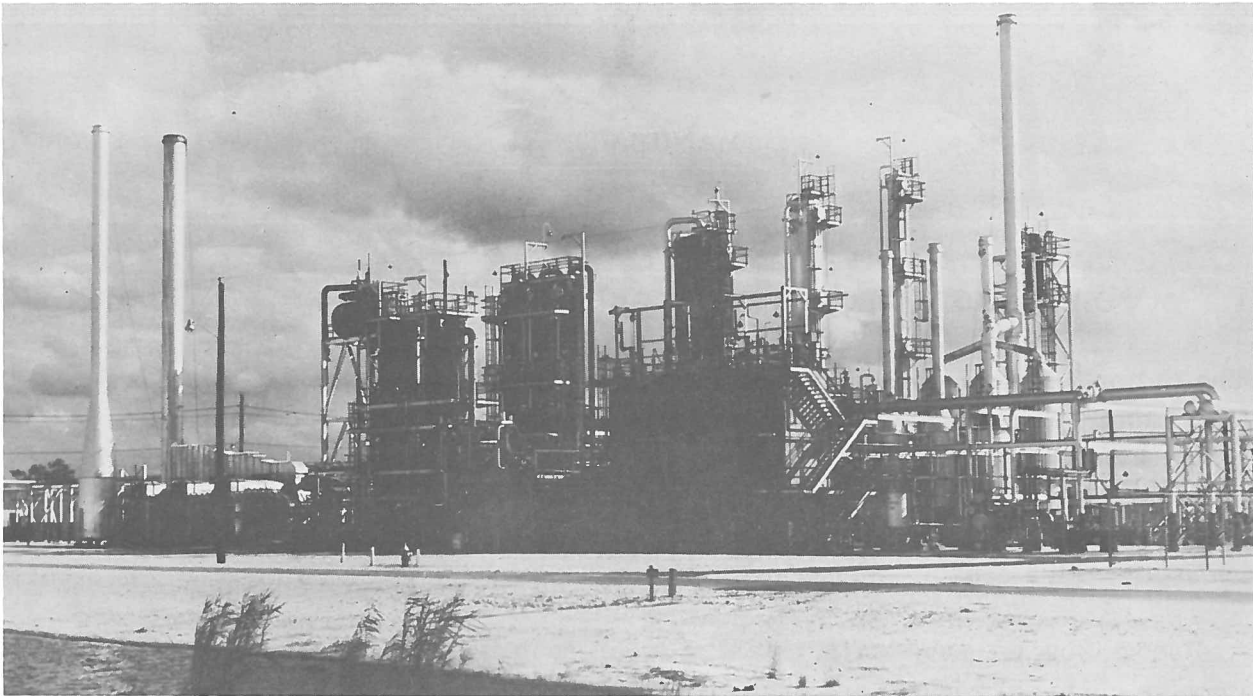


Figure 1. Air Products' liquid hydrogen facility at West Palm Beach, Fla.

Air Products is currently constructing a large plant in Long Beach, Calif. that will also have a capacity of 60,000 lb. per day. The plant will be completed by January 1963.

At present, there are no other major liquid hydrogen plants under construction. Many small facilities in the United States manufacture liquid hydrogen on a laboratory scale.

In summary, the United States now has a capability of producing 157,000 lb. of liquid hydrogen per day. When the new Air Products plant goes into operation, this capability will jump to 217,000 lb. per day.

## 1.2 PRICE OF LIQUID HYDROGEN

The price of liquid hydrogen was quoted by manufacturers at between 49 to 57 cents per pound, excluding the cost of transportation. However, all manufacturers agreed that improved production methods and large quantity production would drop the price.

### 1.3 PRODUCTION PROCESSES

The basic processes by which liquid hydrogen is manufactured can be broken down to four steps (in practice, some of these steps are combined in one operation):

1. Impure hydrogen gas is produced from basic raw materials.
2. Contaminants are removed from the hydrogen feed gas.
3. The hydrogen is converted from a composition of 75% orthohydrogen/25% parahydrogen to greater than 95% parahydrogen by the use of a catalyst.
4. The pure hydrogen gas is liquefied.

Air Products' production process, which is typical for large-scale hydrogen facilities, is described in the following paragraph.

**1.3.1 PRODUCTION OF HYDROGEN FEED GAS.** Air Products uses the Texaco partial oxidization process. Natural gas is reacted with oxygen under a pressure of 400 psig and a temperature in excess of 2,000°F to form hydrogen. The impure hydrogen is first scrubbed with water to remove free carbon and catalytically reacted with steam in shift converters to increase the hydrogen concentration (see Figure 2 for the entire production cycle). Linde's new Fontana plant will also obtain hydrogen from natural gas by the Texaco partial oxidation process.

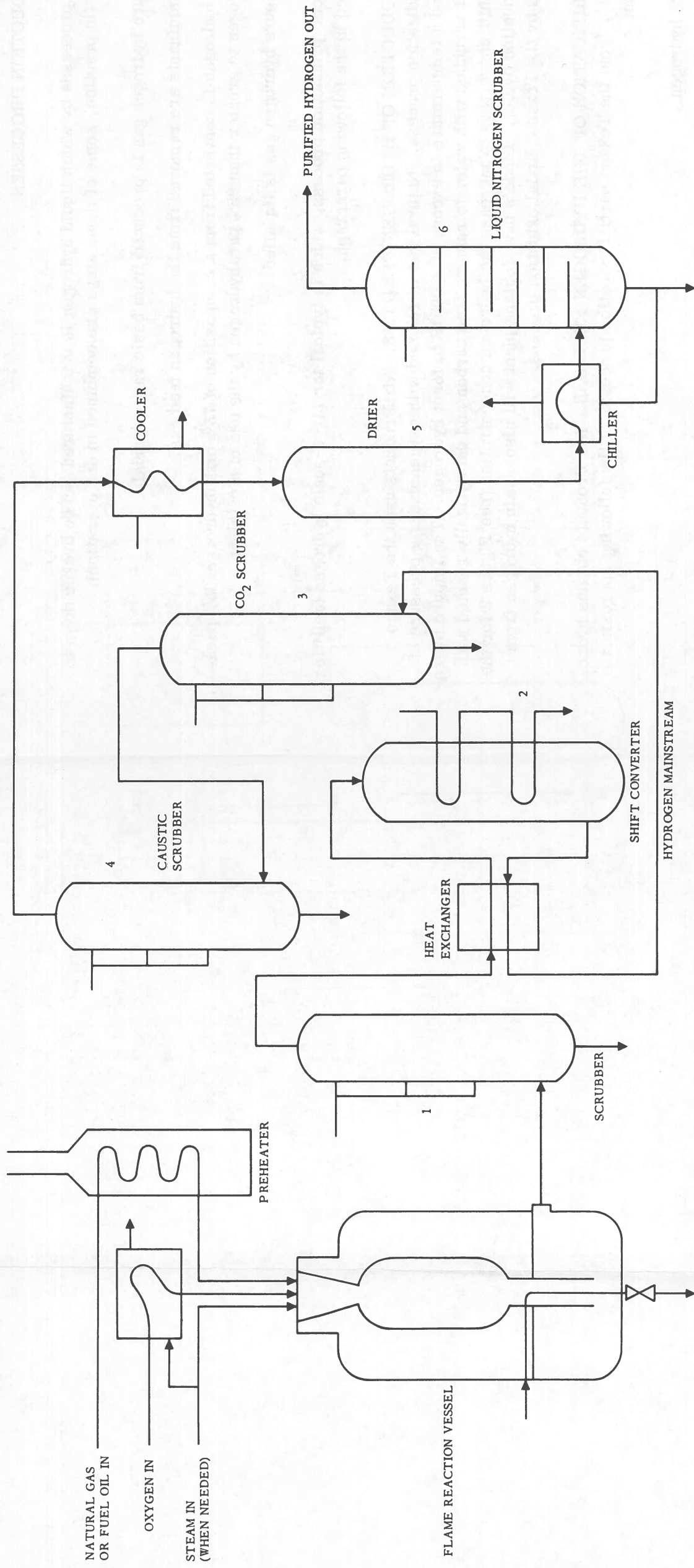
**1.3.2 PURIFICATION OF THE HYDROGEN FEED GAS.** Air Products obtains hydrogen feed gas, from the Texaco partial oxidation process, of the following approximate composition:

1. 98.8% hydrogen.
2. Saturated water vapor.
3. 0.01% carbon dioxide and acid gases.
4. 0.6% methane.
5. 0.3% argon and nitrogen.
6. 0.3% carbon monoxide.

The water vapor is removed by absorption over silica gel at 40°F and 600 psig.

The carbon dioxide and acid gases are removed by scrubbing with monoethanolamine solution and a caustic solution. Methane is absorbed over activated charcoal at -270°F



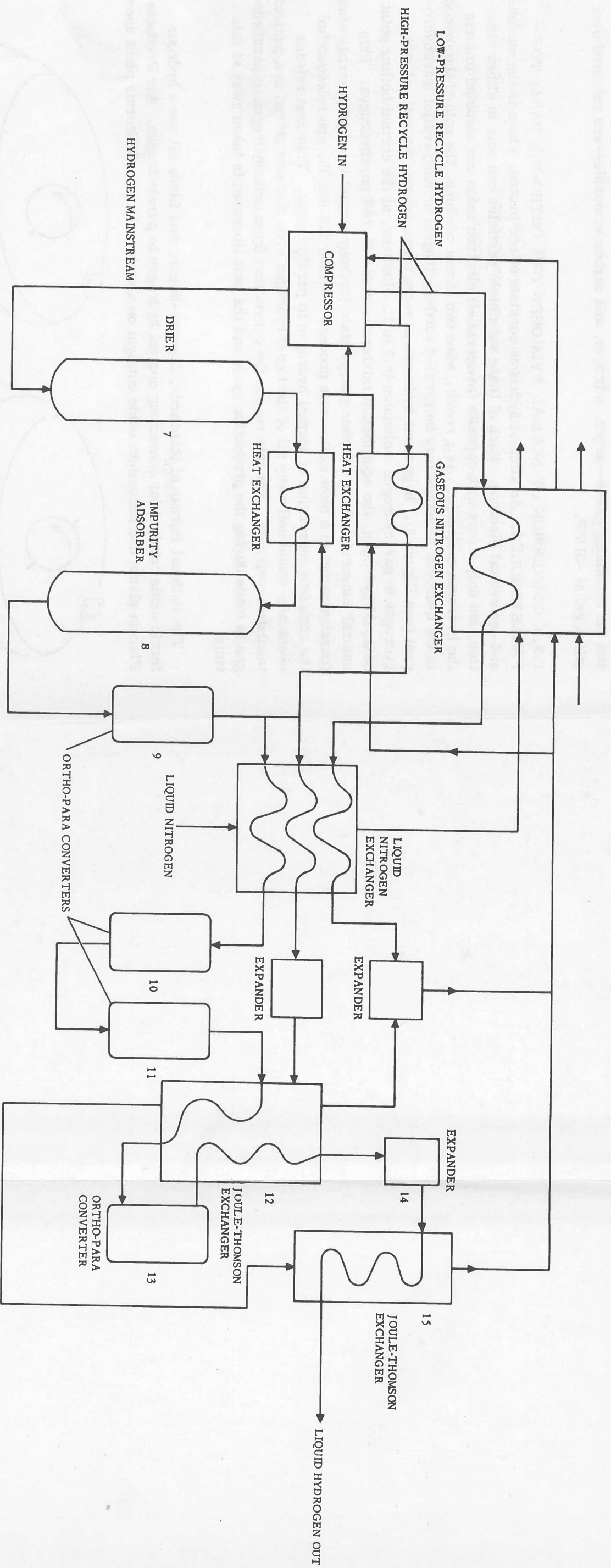


In the top of the flame reaction vessel, natural gas or fuel oil, oxygen & steam are separately injected, mixed & ignited through a big nozzle burner at 400 psig & 2,000°F. Steam is added only with heavy oils or slurried coal. The flame is quenched by a jet of water near the bottom of the vessel, in the proper zone, to give up its partial oxidation products, hydrogen & carbon monoxide. This gas is run through a water scrubber (1) to remove free carbon & through a shift converter (2) to catalytically convert the carbon

monoxide & steam to hydrogen & carbon dioxide. Principal impurities left in the gas are carbon dioxide, water vapor, methane, argon, nitrogen & carbon monoxide. The carbon dioxide is removed by a monoethanolamine scrubber (3) & a caustic scrubber (4). Water vapor is removed in the silica gel drier (5) at 40°F & 600 psig & methane is absorbed on activated charcoal in liquid nitrogen scrubber (6) at -270°F. The hydrogen then passes into the compressor.

Figure 2. Condensed flow chart of Air Products' liquid hydrogen production cycle (sheet 1 of 2).





From the compressor the hydrogen passes through another drier (7), a heat exchanger to cool the gas to  $-315^{\circ}\text{F}$  & over silica gel (8) to remove carbon monoxide, argon, & nitrogen. Residual contaminants such as oil from the compressors are removed in this step also. From here the gas passes through the first of a series of ortho-para converters using chromium oxide catalyst on alumina to convert the gas to greater than 95% parahydrogen. From the first converter (9) the hydrogen is cooled by a liquid nitrogen exchanger, passed through two more ortho-para converters (10, 11) & into the Joule-Thomson exchanger (12). From here the hydrogen passes through the final ortho-para

converter (13), back through the Joule-Thomson Exchanger (12), through a high-speed turboexpander (14), & into the final Joule-Thomson exchanger (15). In this final liquefying stage, the cold, highly compressed gas is swiftly expanded through centrifugal expanders (14) which drop its temperature to the liquefaction level in the Joule-Thomson exchanger (15). About 15% of the hydrogen drops out as liquid; the rest is recycled as shown. The liquid nitrogen used in the heat exchangers & the oxygen gas used in the flame reaction vessel are obtained in a separate air-fractionating system.

Figure 2. Sheet 2 of 2.

and the remaining gases--argon, nitrogen, and carbon monoxide--are removed over silica gel at  $-315^{\circ}\text{F}$ .

**1.3.3 CONVERSION OF NORMAL HYDROGEN (75% ORTHO-25% PARA) TO PARAHYDROGEN.** An atom of hydrogen consists of one proton, which is the nucleus, and one orbital electron. Each of these subatomic particles can spin in either direction, but only atoms with opposite (antiparallel) electron spins can combine to form the hydrogen molecule. As a result, when two atoms combine, the spin of the protons in the hydrogen molecule may be parallel (ortho-hydrogen) or antiparallel (parahydrogen) (see Figure 3). In gaseous hydrogen at room temperature, the ratio of ortho-hydrogen to parahydrogen molecules is 3 to 1. However, at the normal boiling point of liquid hydrogen, the equilibrium mixture contains 99.79% parahydrogen. This natural conversion from a higher energy state (ortho-hydrogen) to a lower energy state (parahydrogen) is a slow exothermic process in which 226 Btu/lb. are released for the complete conversion of normal hydrogen to parahydrogen. This heat release eventually would boil away all of the liquid hydrogen even if it was stored in a perfectly insulated container. For this reason the conversion from ortho-hydrogen to parahydrogen is made during the production cycle and the heat liberated is taken away at this time.

The National Bureau of Standards, Stearns-Roger, and Linde all use a hydrous ferric oxide catalyst for converting normal hydrogen to parahydrogen. Air Products' Florida plants use chromium oxide catalyst on alumina; the new California plant uses

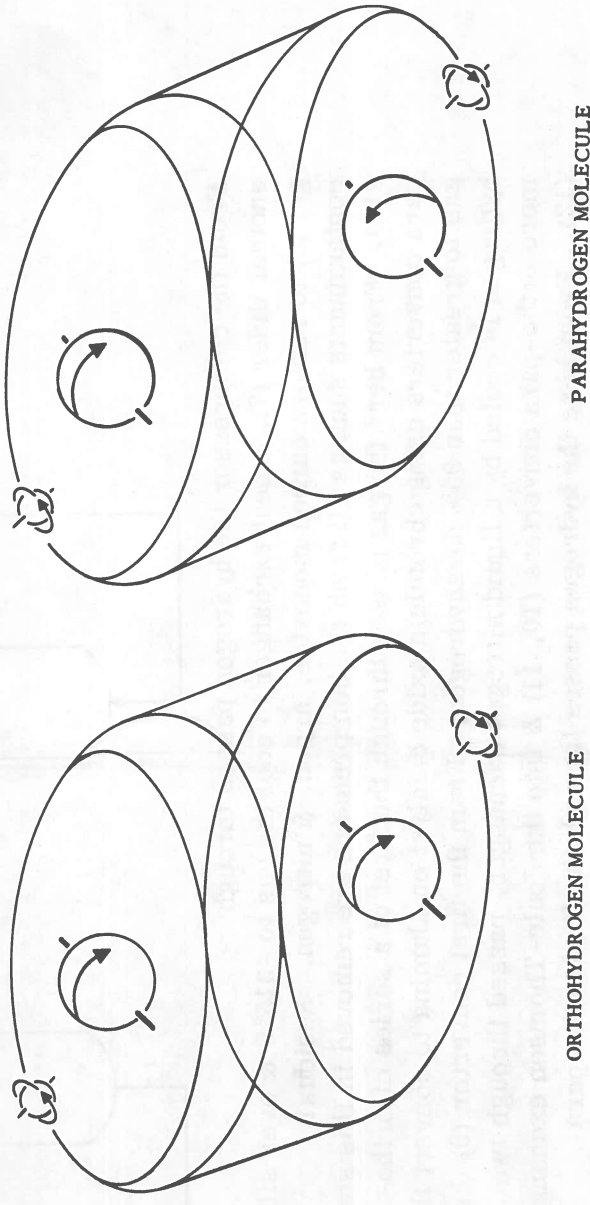


Figure 3. Characterization of nuclear spins of ortho-hydrogen and parahydrogen.

## GENERAL DYNAMICS | ASTRONAUTICS

hydrous ferric oxide. In all cases, the liquid hydrogen produced is greater than 95% parahydrogen.

**1.3.4 LIQUEFACTION PROCESSES.** Air Products uses a liquid nitrogen process and high-speed turboexpanders to provide low-temperature refrigeration for liquefaction of the hydrogen. Figure 4 shows the converter cold box where the hydrogen gas is liquefied.



Figure 4. Converter cold box for liquefying hydrogen.

GENERAL INSTRUCTIONS

1. The first part of the report should be a brief summary of the work done.

2. The second part should contain a detailed description of the methods used.

3. The third part should contain the results of the work done.

4. The fourth part should contain a discussion of the results.

5. The fifth part should contain the conclusions of the work done.

6. The sixth part should contain a list of references.

7. The seventh part should contain a list of symbols and abbreviations.

8. The eighth part should contain a list of figures and tables.

9. The ninth part should contain a list of appendices.

10. The tenth part should contain a list of errata.

11. The eleventh part should contain a list of acknowledgments.

12. The twelfth part should contain a list of references.

13. The thirteenth part should contain a list of symbols and abbreviations.

14. The fourteenth part should contain a list of figures and tables.

15. The fifteenth part should contain a list of appendices.

16. The sixteenth part should contain a list of errata.

17. The seventeenth part should contain a list of acknowledgments.

18. The eighteenth part should contain a list of references.

19. The nineteenth part should contain a list of symbols and abbreviations.

20. The twentieth part should contain a list of figures and tables.

21. The twenty-first part should contain a list of appendices.

22. The twenty-second part should contain a list of errata.

23. The twenty-third part should contain a list of acknowledgments.

24. The twenty-fourth part should contain a list of references.



## 2

## TRANSPORTATION

At present, liquid hydrogen is transported from the producer to the user by one of three methods. If the user is located near a production plant, the liquid hydrogen can be transferred through insulated lines. Pratt & Whitney's rocket engine test facility receives liquid hydrogen from the large Air Products plant in West Palm Beach County, Fla. in this manner (see Figure 5).

For transfer of smaller quantities over extended distances, an insulated trailer with truck, which holds 6,000 to 7,000 gal., has been used by all four major producers (see Figure 6). Losses have averaged around 0.8% per day using vacuum-perlite insulation. A 10-day trip is considered to be the maximum time that is practical for shipping liquid hydrogen by trailer.



Figure 5. Vacuum-insulated transfer lines for liquid hydrogen.

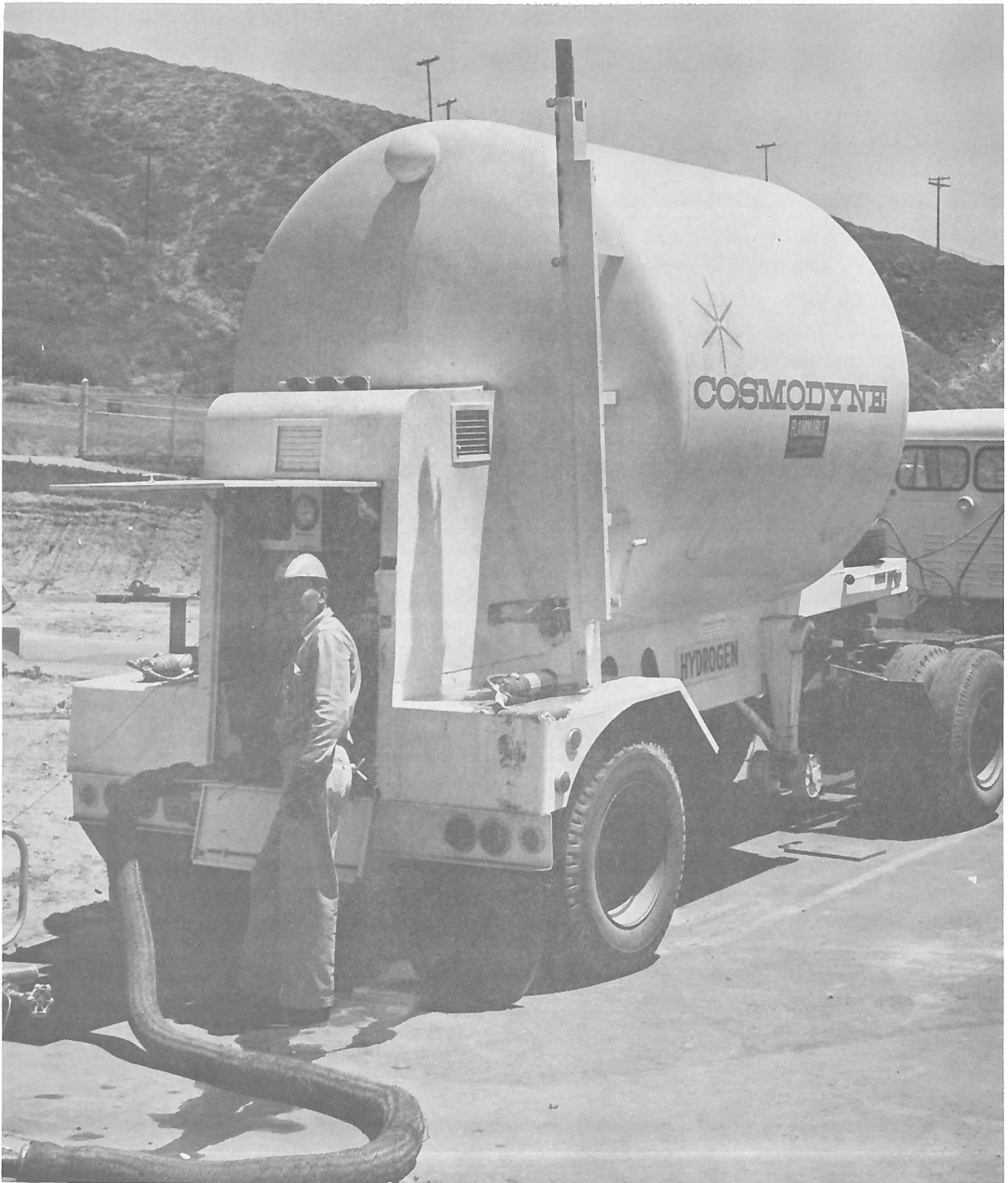


Figure 6. Liquid hydrogen trailer.

## GENERAL DYNAMICS | ASTRONAUTICS

Linde has also shipped 28,000 gal. of liquid hydrogen by rail in a specially designed insulated tank car. This is about the largest practical size that can be shipped by rail.

Shipping large quantities of liquid hydrogen by ship transport appears feasible although it has not been attempted. Liquid natural gas is being shipped commercially overseas by this method.

Bulk shipment of liquid hydrogen by air has not yet been attempted because of higher shipping costs.





# 3

## HYDROGEN SAFETY

### 3.1 GENERAL PROPERTIES OF HYDROGEN

Hydrogen is a colorless, odorless gas. It is nontoxic and essentially noncorrosive at room temperature. It ignites readily in the presence of air or oxygen (if an ignition source is present), burning with a colorless flame if no impurities are present. Hydrogen is a good reducing agent at elevated temperatures.

Due to its low density and low molecular weight, gaseous hydrogen will rise and disperse rapidly in the atmosphere. Its density is approximately 1/14 that of air; however, gaseous hydrogen at a temperature just above its boiling point (36.5° to 41°R) is denser than dry ambient air (68°F) and will settle initially until it warms slightly.

Hydrogen liquefies at a temperature of -423°F and one atmosphere pressure, with a resulting density 1/14 that of water.

### 3.2 FLAMMABILITY AND DETONATION HAZARDS

The principal hazard associated with gaseous or liquid hydrogen is its ease of ignition over a wide flammability range in air and oxygen. Detonations can occur although they are more difficult to initiate. Sparks, flames, detonations, and temperatures in excess of 1,000°R will all ignite hydrogen-air mixtures. The combustion limits of hydrogen in air range from 4% to 74% hydrogen by volume. Substitution of oxygen for air raises the upper limit to 94%. The limiting compositions for detonation lie between the upper and lower combustion limits. For confined or unconfined mixtures of hydrogen and air the range is approximately 18% to 59% hydrogen by volume.

Hydrogen-oxygen mixtures can be ignited by minute ignition sources (see Figure 7). For example, the electrostatic spark experienced by a person touching a door knob is 50 to 1,000 times greater than the threshold energy necessary for ignition of hydrogen-air mixtures.

Consequently, tests were run (by A. D. Little, Inc.) to determine if dangerous electrostatic charges can be generated in well-grounded systems during storage and

## GENERAL DYNAMICS | ASTRONAUTICS

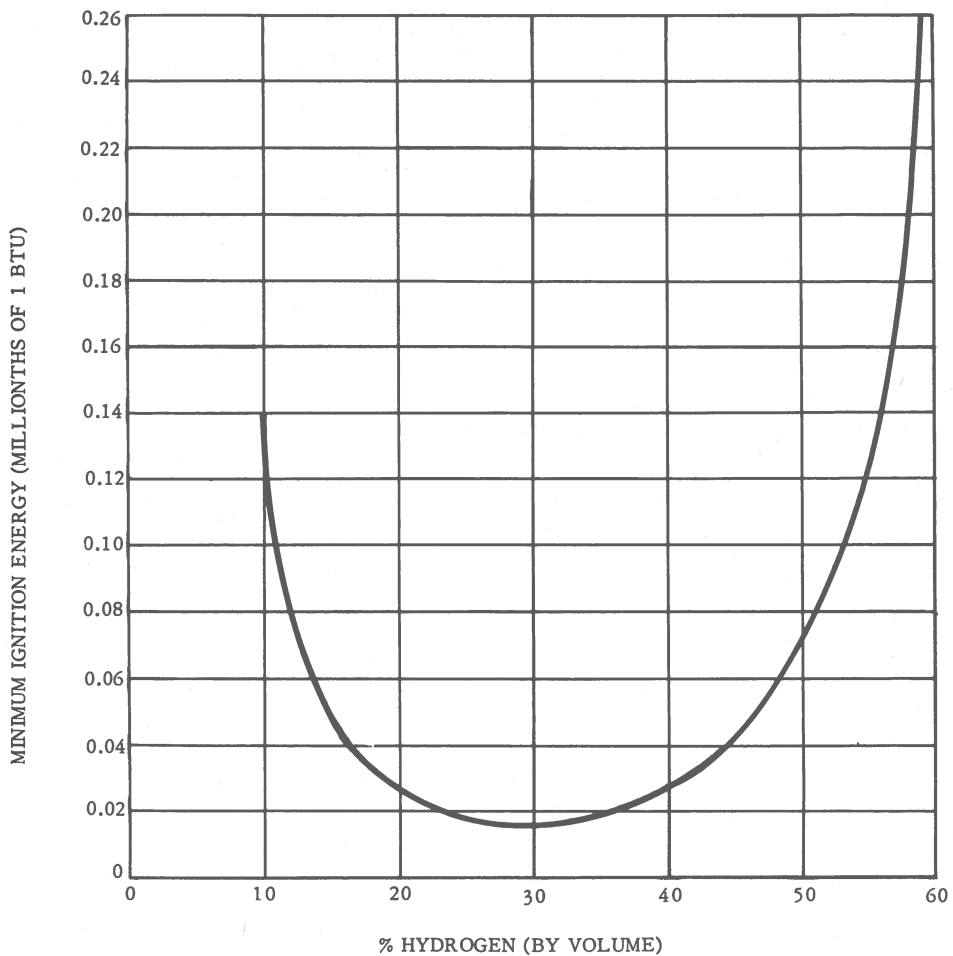


Figure 7. Minimum ignition energies for hydrogen-air mixtures at one atmosphere.

transfer of liquid hydrogen. It was found the maximum field strength for two-phase flow was on the order of 10 volts per centimeter. Since the breakdown potential of hydrogen is normally 17,500 volts/cm, the charge was insufficient to cause spark ignition (by three orders of magnitude). Field strengths during single-phase flow were less than 1 volt/cm.

Field strengths built up in a 5,000-gal. tank during liquid hydrogen transfer were even smaller, 0.01 volts/cm. However, because of the extremely low electrical conductivity of hydrogen, these small charges will persist over long periods of time in storage. (The relaxation time is approximately 1,000 times that of jet fuels.)

## GENERAL DYNAMICS | ASTRONAUTICS

Other tests were made by A. D. Little to determine the consequences of gross spillage of liquid hydrogen, as would be the case if a storage tank or transfer line ruptured. It was found that when liquid is spilled in this manner, initially all heat supplied to the liquid comes from the ground. After approximately 3 min., some heat contribution is made by condensation of air into the hydrogen pool. The evaporation rate of the diked liquid hydrogen pool is on the order of 5 to 7 in./min. It was found that ignition of the vapor does not significantly affect the rate of evaporation of the liquid although a crushed rock bed greatly increases the evaporation rate.

During these spill tests, the voluminous vapor cloud was ignited by a spark or flame prior to, and up to 8 sec. after, the spill. Upon ignition, the fireball would consume almost all of the material within the confines of the vapor cloud and the remaining material in the liquid pool would burn within a few minutes. The vapor cloud would remain close to the ground for a few seconds and then rise slowly and drift downwind.

No detonations were recorded in any of the tests. A number of spill tests were also made in which the vapor clouds were ignited by means of explosive igniters such as 2- and 4-gram pentolite charges. In none of these tests did the vapor cloud detonate. It was concluded that nonideal mixing in the spill tests inhibited the detonation.

Hydrogen-oxygen mixtures have a high explosive potential. On a weight basis, a 5-to-1 ratio of liquid oxygen to liquid hydrogen has 3.3 times as much explosive power as an equivalent weight of TNT. Substituting air for liquid oxygen and using a 1-to-5 weight ratio increases the explosive power (f), surprisingly enough, to 6.6 times that of TNT. The maximum overpressures that would be generated by an  $\text{LO}_2/\text{LH}_2$  explosion at a 5-to-1 weight ratio can be represented by the following equations:

$$\Delta P_{\text{air burst}} = \frac{4,120}{Z^3} - \frac{150}{Z^2} + \frac{39.5}{Z}$$

$$\Delta P_{\text{surface burst}} = \frac{4,204}{Z^3} + \frac{276.4}{Z^2} + \frac{42.58}{Z}$$

## GENERAL DYNAMICS | ASTRONAUTICS

where:

$\Delta P$  = overpressure (psi)

$$Z = \frac{R}{(3.3W)^{1/3}}$$

R = slant range (ft.)

W = weight of  $LO_2/LH_2$  (lb.)

For a 1-to-5 weight ratio of air to  $LH_2$ ,

$$Z = \frac{R}{(6.6W)^{1/3}}$$

Spillage tests have shown that instantaneous ignition prevents a detonation from reaching its full potential, the explosive values being bracketed between 0.05 f and 0.2 f. For delayed ignition, f values will increase to a maximum and then decrease with time. Factors that are involved in determining the explosion potential of a spillage as a function of time include amount of spillage, geometry of spillage (confined or unconfined spaces), rate of vaporization, mixing rate, and types of ignition sources.

Experimental work indicates that it takes a strong initiator to detonate an unconfined mixture of hydrogen and air. In tests with a mixture of 32% hydrogen and 68% air, the stoichiometric ratio of hydrogen to oxygen, no detonation occurred when the mixture was ignited with a hot wire, a spark source, or a squib. When ignited with a 2-gram charge of pentolite, the mixture detonated.

Tests were also run on mixtures of liquid hydrogen and solid oxygen and liquid hydrogen/solid air. A hot wire would not ignite the solid air/liquid hydrogen mixture unless the oxygen content was enriched. When pure solid oxygen crystals were subjected to impact in liquid hydrogen, they detonated in a manner similar to RDX, a solid explosive. Impact tests on crystals of air in liquid hydrogen produced no explosions. A drop height of 275 cm and a drop weight of 3.3 kg were used.

## GENERAL DYNAMICS | ASTRONAUTICS

### 3.3 SYSTEM DESIGN CONSIDERATIONS

At Astronautics' Point Loma Test Site, Sycamore Canyon Test Site, and Cryogenic Tensile Testing Laboratory the following safety rules were followed in designing the liquid hydrogen test facilities:

1. **Elimination of Ignition Sources.** All liquid and gaseous hydrogen equipment, fixed or movable, is grounded. All electrical equipment within a hazardous area is explosionproof. Most electrical and mechanical equipment is located outside the hazardous area. When it was not practical to do this, the equipment located in a hazardous area was mounted at a level below any potential hydrogen leak sources when possible. Since hydrogen is lighter than air, the danger of ignition is lessened by this arrangement. Also, the equipment will sustain little if any damage in case of fire.
2. **Choice of Construction Materials.** Materials used in the gaseous and liquid hydrogen systems were chosen for their toughness at liquid hydrogen temperatures, corrosion resistance, and thermal shock resistance. These properties are discussed in detail in Chapter 4.
3. **Storage Areas.** Multiple liquid hydrogen storage tanks should be spaced the approximate distances shown in Figure 8. Liquid hydrogen storage tanks at the two test sites are located near the edge of a cliff to allow runoff from a gross spillage accident to be dumped into a remote area (see Figure 9). A shallow dike surrounding the tank, capable of holding a volume 10% greater than the capacity of the tank, can also be used. The area beneath the storage tanks is covered with crushed rock to increase the liquid hydrogen evaporation rate if spillage occurs.

All hydrogen equipment is located out of doors at the test sites. In the tensile testing laboratory, the air is changed three times per minute to rapidly dilute any escaping hydrogen gas.

Insulation materials used in liquid hydrogen storage tanks (expanded perlite-vacuum) and transfer lines (high vacuum or carbon-dioxide filled spaces) are compatible with liquid oxygen. Condensation of liquid air in insulation not compatible with liquid oxygen forms a potentially explosive mixture. Organic materials are not suitable for use as liquid hydrogen insulation.

4. **Transfer Systems.** Dead-end tubing, voids, and pockets are avoided in designing transfer lines for gaseous and liquid hydrogen. "Positive" seal designs are used on all hydrogen transfer equipment. This includes a "cold" seal on the

## GENERAL DYNAMICS | ASTRONAUTICS

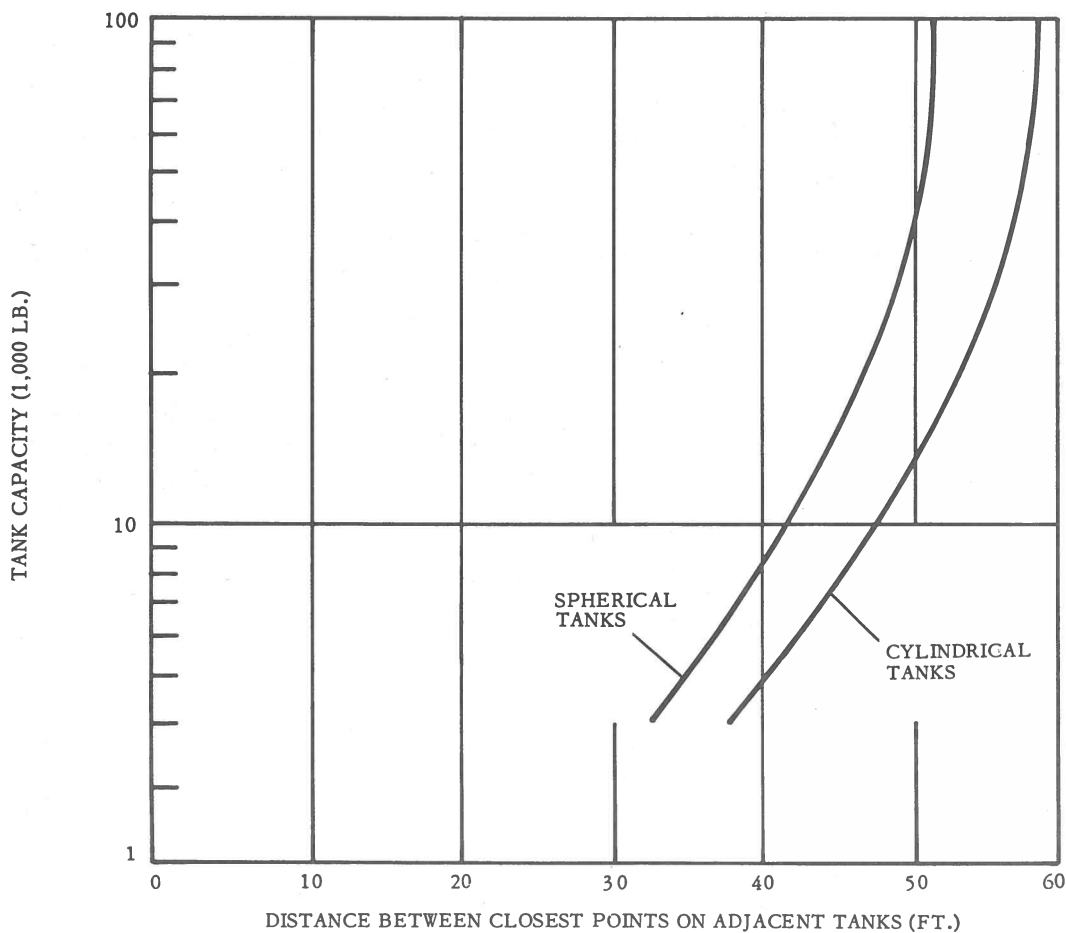


Figure 8. Suggested spacing for liquid hydrogen storage tanks.

liquid hydrogen line and a "warm" backup seal. Suitable expansion joints are used on all liquid hydrogen systems. The transfer lines are mounted on V-notched rollers that allow the line to move in any direction in a horizontal plane.

The over-all system for transferring hydrogen has been designed so that, in case of fire or explosion, the affected area can be isolated from the rest of the system. Remotely operated pneumatic valves are placed in strategic locations to allow the flow of additional hydrogen to the emergency area to be stopped. A filter located at the storage tank outlet removes foreign solids such as solidified gases during the transfer of liquid hydrogen.

5. Venting Systems. Pressure relief devices are used on all equipment where an excessive pressure may build up. This is especially important in systems where trapped residual liquid hydrogen may vaporize with explosive force if the

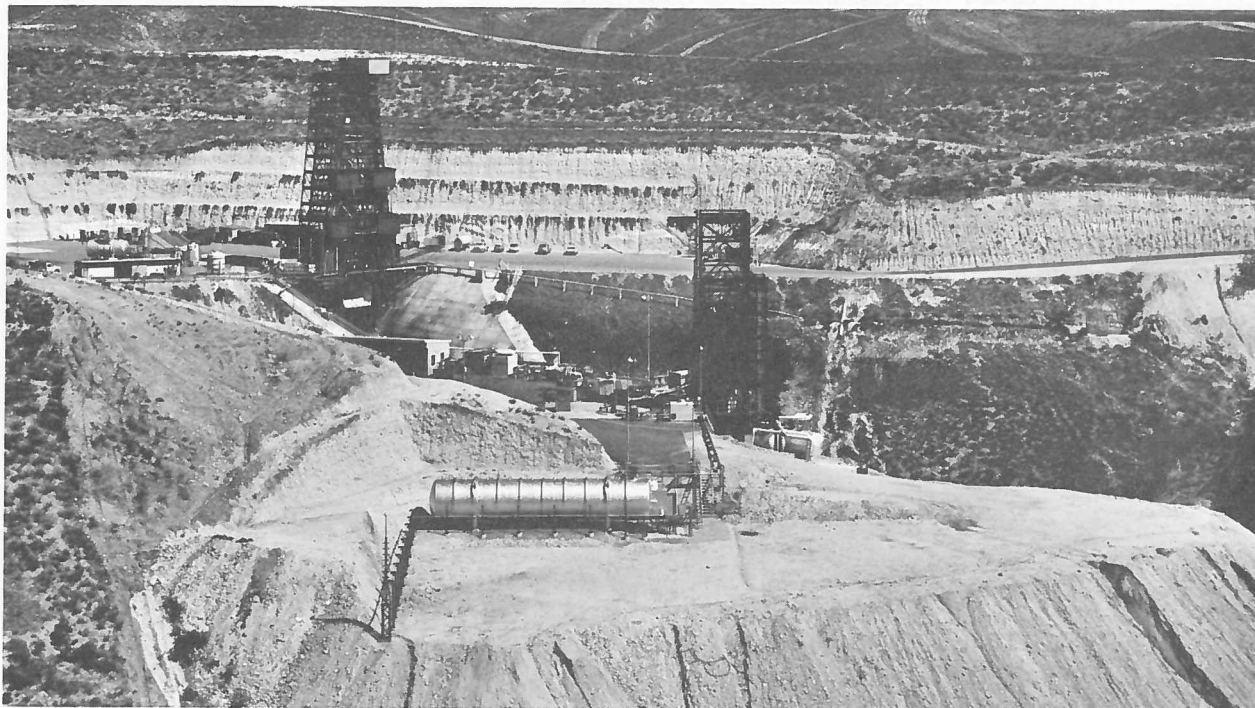


Figure 9. Liquid hydrogen storage tank, Sycamore Canyon Test Site.

insulation is faulty, i. e., in a transfer line between two valves. As an example, the pressure rise due to 1 cu. ft. of liquid hydrogen vaporizing and warming to 68° F in a volume of 10 cu. ft. is 1,154 psi.

Rupture discs are used as backup devices on the storage tanks. The rupture discs are designed to handle the worst possible case, i. e., complete insulation failure, causing a rapid pressure rise in the system.

All vented hydrogen gas is released through stacks of suitable height in a remote location. A stack height of approximately 20 ft. is used at the test sites. Some plants use a propane flame to continuously burn vented hydrogen if the rate released exceeds 30 lb./min. To prevent air backup in the hydrogen vent stack, a mechanical cover is provided that vents gas smoothly. Vent covers used previously at the test sites had a tendency to "chatter," causing pressure surges in the system. As an additional safety measure, the stack is purged with nitrogen when hydrogen is not being vented. Pressure relief devices on transfer lines are connected to the vent stack.

6. Emergency Warning Systems. Portable hydrogen leak detectors made by Mines Safety Appliance Co. are used to detect dangerous accumulations of

## GENERAL DYNAMICS | ASTRONAUTICS

hydrogen gas. Detectors, permanently mounted in various locations on the static test stand, are connected to an automatic buzzer/flashing red light warning system. These detectors are used during a tanking/static firing sequence.

Pressure gages are located in hydrogen systems to detect excessive pressure rises or pressure drops. A pressure drop below one atmosphere in a hydrogen system is dangerous because air will diffuse into the system if any leaks are present.

7. Personnel Safety Devices. Safety showers with eye wash basins are located at the test sites in areas where hydrogen fires may start.

### 3.4 OPERATIONAL CONSIDERATIONS

The following safety procedures are in use at Astronautics:

1. Elimination of Ignition Sources. All tools used in a hydrogen area are of the spark-resistant, beryllium-copper type. Cigaretts, lighters, combs, open flames, matches, and other ignition sources are not allowed in a hydrogen area. Appropriate warning signs are prominently displayed. Laboratory coats worn in the tensile testing area are made of cotton, a relatively static-free material. Before liquid hydrogen is transferred from one system to another, both systems are grounded (to a common ground) at a safe distance.
2. Elimination of Hazardous Mixtures. Before any container or system is filled with gaseous or liquid hydrogen, it is leak-tested. In the case of storage tanks, transfer lines, or other double-walled vessels, the leak-testing is done as the assembly progresses. Otherwise, the cost of repairing a leak would be prohibitive after the final assembly is complete. Leak-testing is accomplished by x-raying 100% of the welds and leak-checking each individual part as it is completed. The testing is done at a pressure 50% above the maximum use pressure. One recommended approach for detecting leaks in the system consists of the following steps:
  - A. Locate any gross leakage with bubble fluid using clean filtered air as the pressurizing gas.
  - B. After the gross leaks have been repaired, give the system a final check with a mass spectrometer-type detector using helium gas.

Before any system or container is filled with liquid hydrogen the following steps are performed:



## GENERAL DYNAMICS | ASTRONAUTICS

- A. Reduce the oxygen content in the system below the flammable limits.
- B. Remove any residual gas that might condense and freeze out.
- C. Cool the system down to liquid hydrogen temperatures.

Methods for accomplishing the above steps are:

### A. Method 1.

- (1) Evacuate the system to 3 psia. Admit liquid nitrogen, in a spray if possible. This starts the cooldown process and brings the system back to atmospheric pressure, at which point the oxygen content is below the flammable limits.
- (2) Continue the cooldown at atmospheric pressure with liquid nitrogen to near-equilibrium conditions.
- (3) Evacuate the system to a 50-micron pressure.
- (4) Introduce liquid hydrogen and continue the cooldown to equilibrium temperature, allowing sufficient time for residual nitrogen gas to be purged from the system.

### B. Method 2.

- (1) Pump the system down to 50 microns at room temperature.
- (2) Admit nitrogen gas until the pressure reaches 300 microns. This brings the oxygen content below the flammable limits.
- (3) Admit liquid nitrogen and cool down to the equilibrium temperature, allowing sufficient time for residual nitrogen gas to be purged from the system.

### C. Method 3.

- (1) Purge the system with nitrogen gas until the oxygen content drops below 1%.
- (2) Admit hydrogen gas and purge the system of nitrogen.
- (3) Introduce liquid hydrogen toward the end of the hydrogen-gas purge to start the cooldown process.

## GENERAL DYNAMICS | ASTRONAUTICS

D. Method 4. (This method has been used successfully on the Centaur hydrogen tank.)

(1) Purge air from the tank by introducing helium in the top of the tank. Since helium is considerably lighter than air, the helium-air mixture remains stratified, and air is pushed out the tank bottom outlet. This purge is continued until chemical analysis shows the vented gas to be essentially pure helium. Chemical analysis is run only at the beginning of the program to determine the length of time necessary for a complete purge under specified conditions.

(2) Admit liquid hydrogen.

After the static test run is completed, the stratified purging cycle is reversed: Purge hydrogen from the tanks by admitting nitrogen gas at the tank bottom outlet. The lighter hydrogen gas is vented out the top of the tank through a vent stack located on top of the static test stand. The purge is stopped after a specified time when the vented gas composition drops below 1% hydrogen by volume, as determined by previous experimentation.

A slight positive pressure is maintained in all hydrogen systems to prevent air from diffusing in through leaks. Liquid hydrogen is transferred by vaporizing a portion of the liquid in a heat exchanger and using the resultant gas for pressurizing the system. All systems are cleaned thoroughly before filling with gaseous or liquid hydrogen. Suitable cleaning processes are used to remove any metal scale, dirt, or soluble contaminants in the system. Storage areas for combustible materials are kept outside of hydrogen areas. Good housekeeping is maintained at all times.

### 3.5 PERSONNEL CONSIDERATIONS

All Astronautics personnel who are going to work with liquid hydrogen are given a basic six-hour safety course. The following subjects receive particular emphasis:

1. Hazards. Hydrogen is extremely flammable in both air and oxygen. Burning can be initiated by a small amount of energy as shown in Section 3.2. It is emphasized that part or all of the flame may be invisible. When hydrogen and air or oxygen are mixed in a confined or partially confined space, an explosion hazard exists. Due to its extremely low temperature, skin contact with liquid hydrogen or components at liquid hydrogen temperature causes severe frostbite

## GENERAL DYNAMICS | ASTRONAUTICS

or low-temperature "burns." If liquid hydrogen is trapped in a closed system and allowed to vaporize, dangerously high pressures will build up.

2. Operating Instructions. All personnel working with hydrogen are thoroughly versed on the proper operation and safety features of the system. Two men are always present when work is done in a hydrogen area.
3. Protective Clothing. Proper clothing and protective devices are provided for personnel when transferring liquid hydrogen. This list of safety clothing includes asbestos gloves, rubber boots, rubberized suit and cap. Protective clothing is loose fitting to permit easy removal.
4. First Aid. If a person receives a low temperature "burn," he is instructed to keep the affected skin areas sterile and summon medical attention as soon as possible.
5. Hydrogen Fires. For small hydrogen fires, carbon-dioxide fire extinguishers are available. If a fire occurs at the Sycamore Canyon Test Site, an extensive water deluge system allows the entire stand and vehicle, or any individual portion of the stand or vehicle, to be sprayed with enormous quantities of water (see Figure 10). In addition, a nitrogen gas purge is used in the diffuser flame bucket to dilute unburned hydrogen to a safe level. When the hydrogen fire is extensive, the most important single thing personnel can do is to shut off additional hydrogen flow into the emergency area. It is more effective to let a large hydrogen fire burn itself out than to try to fight it directly. It is emphasized that if the hydrogen flow is not shut off after the fire has been put out, the hydrogen may reignite. If a hazardous amount of hydrogen collects in the area, as indicated by combustible mixture detectors, personnel are instructed to ventilate the area immediately to dilute the hydrogen-air mixture below flammable limits.

Personnel working in a hydrogen area receive thorough instructions on what to do in case of a hydrogen fire or explosion. This includes the following major items:

- A. Location of remotely operated shutoff valves in the hydrogen system.
- B. Methods for fighting hydrogen fires.
- C. Location of fire-fighting equipment, fire alarm boxes, and telephones.
- D. First-aid treatment for burns.



Figure 10. Water deluge system, Sycamore static test stand.

## 4

## MATERIALS

## 4.1 MATERIAL PROBLEMS ASSOCIATED WITH LIQUID HYDROGEN

4.1.1 LOW-TEMPERATURE EMBRITTLEMENT OF METALS. A material property of increasing importance to rocket vehicle designers is toughness, which is often referred to in terms of resistance to brittle fracture, or notch sensitivity (References 1, 2, and 3)\*. Toughness, which measures resistance to fracture under shock-type loads or conditions of biaxial and triaxial stress, is of vital importance to the vehicle designer because his structures are subjected to shock-type loads which occur during engine firing, action of quick-closing valves, etc. Structures will contain built-in stress concentrations of varying degrees of notch acuity due to random inclusions in the metal, welding defects, tool marks, assembly eccentricities, and so on. These conditions all favor brittle failure, and they become even more severe at cryogenic temperatures.

The tendency of the various alloys toward brittle or catastrophic failure is measured by means of a notched/un-notched tensile ratio. To obtain this ratio, the tensile strength of a notched tensile specimen is divided by the tensile strength of a smooth tensile specimen. The trend of the resulting ratio as a function of temperature yields an index of a given material's tendency toward catastrophic failure. The notched/un-notched tensile ratios given in Table I were determined by the Materials Research Group at Astronautics. One of their tensile testing setups for determining this ratio at cryogenic temperatures is shown in Figure 11.

4.1.2 THERMAL SHOCK RESISTANCE. Resistance to thermal shock is a measure of the ability of a material to resist weakening or fracture when subjected to sudden heating or cooling. No standard tests exist which will accurately evaluate this property since shape is an important factor, as in the case of brittle fracture of metals at low temperature. However, the properties which appear to be necessary for good thermal shock resistance are high tensile strength ( $F_{tu}$ ), high thermal conductivity ( $k$ ), low modulus of elasticity ( $E$ ), and a low coefficient of thermal expansion ( $\alpha$ ). The ratio  $\frac{F_{tu} (k)}{(E) (\alpha)}$  gives a relative measure of the thermal shock resistance of a material

---

\* References are listed at the end of each chapter.

# GENERAL DYNAMICS | ASTRONAUTICS

Table I. Low-temperature characteristics of metals (sheet 1 of 3).

ALLOY	TEST TEMPERATURE (°F)	DIRECTION	TENSILE STRENGTH $F_{tu}$ (1,000 PSI)	NOTCHED TENSILE STRENGTH $F_{tu}$ ( $K_t = 6.3$ ) (1,000 PSI)	NOTCHED/ UN-NOTCHED TENSILE RATIO
ALUMINUM ALLOYS					
2014-T6	78	LONG.	73.1	74.5	1.02 (REF. 10)
	-100	LONG.	76.4	79.2	1.04
	-320	LONG.	87.1	85.5	0.98
	-423	LONG.	104	97.8	0.94
2014-T6	78	TRANS.	71.5	70.0	0.98
	-100	TRANS.	74.1	71.0	0.96
	-320	TRANS.	78.7	78.7	1.00
	-423	TRANS.	102	84.5	0.83
2219-T81	78	LONG.	67.5	64.4	0.95 (REF. 10)
	-100	LONG.	73.3	68.6	0.94
	-320	LONG.	85.2	77.4	0.91
	-423	LONG.	102	93.4	0.92
2219-T81	78	TRANS.	67.2	66.0	0.98
	-100	TRANS.	72.3	67.0	0.93
	-320	TRANS.	84.6	76.1	0.90
	-423	TRANS.	102	91.3	0.90
5052-H38	78	LONG.	45.1	48.3	1.07 (REF. 10)
	-100	LONG.	47.0	50.5	1.07
	-320	LONG.	62.6	63.2	1.01
	-423	LONG.	89.7	80.6	0.90
5052-H38	78	TRANS.	45.9	51.1	1.11
	-100	TRANS.	47.0	54.2	1.13
	-320	TRANS.	59.0	64.1	1.09
	-423	TRANS.	81.2	78.2	0.96
5086-H34	78	LONG.	47.8	48.7	1.02 (REF. 10)
	-100	LONG.	48.9	50.3	1.03
	-320	LONG.	65.4	61.9	0.95
	-423	LONG.	95.3	71.4	0.75

# GENERAL DYNAMICS | ASTRONAUTICS

Table I. Sheet 2 of 3.

ALLOY	TEST TEMPERATURE (°F)	DIRECTION	TENSILE STRENGTH $F_{tu}$ (1,000 PSI)	NOTCHED TENSILE STRENGTH $F_{tu}$ ( $K_t = 6.3$ ) (1,000 PSI)	NOTCHED/ UN-NOTCHED TENSILE RATIO
5086-H34	78	TRANS.	46.9	46.8	1.00
	-100	TRANS.	47.6	47.6	1.00
	-320	TRANS.	61.9	55.0	0.89
	-423	TRANS.	85.7	58.4	0.68
5456-H343	78	LONG.	58.6	54.2	0.92 (REF. 10)
	-100	LONG.	59.8	50.5	0.84
	-320	LONG.	72.7	49.5	0.68
	-423	LONG.	83.5	55.1	0.66
5456-H343	78	TRANS.	60.4	52.8	0.87
	-100	TRANS.	61.2	48.7	0.80
	-320	TRANS.	70.9	48.2	0.68
	-423	TRANS.	80.3	49.7	0.62
STAINLESS STEELS					
301 SS, 60% COLD-ROLLED	78	LONG.	205	235	1.15 (REF. 11)
	-100	LONG.	244	231	0.99
	-320	LONG.	321	268	0.83
	-423	LONG.	317	249	0.79
301 SS, 60% COLD-ROLLED	78	TRANS.	215	232	1.08
	-100	TRANS.	248	236	0.95
	-320	TRANS.	313	244	0.78
	-423	TRANS.	300	162	0.54
304 SS, 40% COLD-ROLLED	78	LONG.	176	191	1.09 (REF. 11)
	-100	LONG.	198	216	1.09
	-320	LONG.	251	262	1.04
	-423	LONG.	279	303	1.09
310 SS, 60% COLD-ROLLED	78	LONG.	174	180	1.03 (REF. 11)
	-100	LONG.	233	248	1.06
	-320	LONG.	278	296	1.06
	-423	LONG.	285	308	1.08

GENERAL DYNAMICS | ASTRONAUTICS

Table I. Sheet 3 of 3.

ALLOY	TEST TEMPERATURE (°F)	DIRECTION	TENSILE STRENGTH $F_{tu}$ (1,000 PSI)	NOTCHED TENSILE STRENGTH $F_{tu}$ ( $K_t = 6.3$ ) (1,000 PSI)	NOTCHED/ UN-NOTCHED TENSILE RATIO
TITANIUM ALLOY					
A110AT	78	LONG.	118	158	1.34 (REF. 12)
	-100	LONG.	142	175	1.23
	-320	LONG.	196	226	1.15
	-423	LONG.	247	239	0.97
A110AT	78	TRANS.	120	159	1.33
	-100	TRANS.	157	190	1.21
	-320	TRANS.	199	220	1.11
	-423	TRANS.	244	208	0.85
HIGH-TEMPERATURE ALLOYS					
K-MONEL (AGE-HARDENED)	78	LONG.	154	144	0.93 (REF. 13)
	-100	LONG.	166	155	0.93
	-320	LONG.	183	174	0.95
	-423	LONG.	200	198	0.99
INCONEL-X (AGED)	78	LONG.	174	168	0.97 (REF. 13)
	-100	LONG.	189	174	0.92
	-320	LONG.	214	184	0.86
	-423	LONG.	233	199	0.85
HASTELLOY B, 40% COLD-ROLLED	78	LONG.	191	220	1.15 (REF. 13)
	-100	LONG.	222	245	1.10
	-320	LONG.	228	265	1.16
	-423	LONG.	283	308	1.09

when compared to other materials. The higher the ratio is, the more resistant the material is to fracture from thermal shock. Due to a lack of low-temperature data, the preceding ratio has been calculated for ambient conditions only.

4.1.3 CHEMICAL REACTIONS. Liquid hydrogen and low-temperature gaseous hydrogen are considered to be essentially noncorrosive (Ref. 4). However, at elevated temperatures, gaseous hydrogen forms hydrides with some metals, e. g., uranium and titanium, and reduces metal oxides less active than iron to their elemental state.





Figure 11. Astronautics' cryogenic tensile testing setup.

## GENERAL DYNAMICS | ASTRONAUTICS

These include copper, silver, and gold. Oxides of beryllium, titanium, uranium, iron, tantalum, niobium, nickel, aluminum, magnesium, chromium, and zinc are unaffected.

The ease of ignition of hydrogen in air is well known and is covered in Section 3.2.

Above 1,000°F, graphite begins reacting with hydrogen to form methane gas.

**4.1.4 HYDROGEN EMBRITTLEMENT OF METALS.** The ability of small quantities of hydrogen to drastically embrittle metals has long been recognized. Only recently, however, a new facet of hydrogen embrittlement, which involves the ability of hydrogen to produce delayed failure, has been observed and studied. Delayed failure, or, as it is also termed, static fatigue, is defined as the property of a material to fail under the action of a sustained load, even though it is capable of supporting a higher load for a finite period of time. One of the phenomena encountered in steels heat-treated to relatively high-strength levels and exposed to a hydrogen atmosphere under certain conditions is the occurrence of brittle delayed failures in service.

Since the recognition of hydrogen embrittlement of steels, considerable evidence has been obtained to show that this phenomenon occurs in many other metals. It is now well established that under certain conditions hydrogen can have an adverse effect on the mechanical properties of some titanium alloys, and to a lesser extent on some other ferrous and nonferrous alloys.

**4.1.4.1 Characteristics of Delayed Hydrogen Embrittlement in Steels.** The chief effects of hydrogen embrittlement are a marked decrease in ductility on slow straining and a propensity toward delayed failures under static loads, even at stresses far below the yield strength. Static fatigue is characterized by a discontinuous crack growth that continues to ultimate failure of the metal.

A critical hydrogen concentration in the metal must be obtained to initiate a crack. The rate of the crack growth depends on the hydrogen concentration and distribution within the metal, and the applied stress. For metals with a uniform hydrogen distribution, a definite incubation period is necessary before initiation of the first crack is noted. For a given material and notch geometry, the applied stress multiplied by the incubation time is a constant.

Temperature, strain rate, and the previous state of the metal have characteristic effects on the hydrogen embrittlement phenomena, as follows:

1. Hydrogen embrittlement disappears at low and high temperatures and, consequently, is most severe in an intermediate temperature range.
2. Hydrogen embrittlement is inversely proportional to the strain rate; that is, it decreases with increasing strain rate.
3. In general, steels are more susceptible to hydrogen embrittlement when heat-treated to a high strength level than in the annealed condition.

If the conditions under which the metal is charged with hydrogen are not too severe, complete recovery of ductility is obtainable. On the other hand, when the strength level of the metal and the hydrogen content are high, baking treatments are not able to produce complete recovery of the initial ductility.

#### 4.1.4.2 Characteristics of Delayed Hydrogen Embrittlement in Titanium Alloys.

Hydrogen embrittlement in titanium and its alloys manifests itself in either high- or low-strain-rate embrittlement and thus differs in this respect from steels. In general, the low-strain-rate embrittlement of titanium is similar to steels and depends on hydrogen content, ultimate tensile strength, temperature, rate of application, and magnitude of stress. Low-strain embrittlement has been shown to occur in all-alpha and all-beta alloys as well as alpha-beta alloys (Ref. 5 and 6).

High-strain-rate embrittlement (such as occurs at impact speeds) is attributed to hydride formation in the titanium. Alpha stabilizing additions such as aluminum seem to increase the solubility of hydrogen in titanium and, consequently, lower the sensitivity of the alloy to hydride-induced impact embrittlement (Ref. 7).

Although the effects of hydrogen in titanium are in many ways similar to those in steels, there are several major differences. The amount of hydrogen required to embrittle titanium alloys is an order of magnitude greater than for steel. Steels will outgas at room temperature; titanium alloys will not. Titanium forms a hydride; steel does not. Also, some titanium alloys creep a significant amount at room temperature, while little or no creep is found in steels at this temperature.

#### 4.1.4.3 Hydrogen Embrittlement of Other Metals.

Hydrogen has been shown to have an embrittling effect on other materials such as nickel, vanadium, zirconium, niobium, and several austenitic nickel-chromium-iron alloys (Ref. 6, 8, and 9).

## 4.2 COMPATIBILITY OF SPECIFIC MATERIALS

4.2.1 ALUMINUM ALLOYS 2014, 2219, 5052, 5086, AND 5456. Notched/un-notched tensile ratios indicate that aluminum alloys 2014, 2219, and 5052 retain their toughness down to liquid hydrogen temperatures. Although the notched/un-notched tensile ratio of aluminum alloy 5086 drops considerably at liquid hydrogen temperatures, the notched tensile strength increases with decreasing temperature. This trend indicates adequate toughness at  $-423^{\circ}\text{F}$  (see Table I). All of the aluminum alloys listed exhibit good thermal shock resistance (see Table II). None reacts with hydrogen to form hydrides or shows any hydrogen embrittlement tendencies.

### 4.2.2 STAINLESS STEELS

4.2.2.1 Type 301. Notched/un-notched tensile ratios indicate that 301 stainless steel exhibits excessive brittleness at liquid hydrogen temperatures (see Table I). Type 301 stainless steel has good thermal shock resistance, although it is the poorest of the structural alloys considered (Table II). It does not form hydrides with hydrogen to any significant extent.

Tests run at Astronautics show that 301 stainless steel, cold-rolled to a high strength level, was severely embrittled by hydrogen in a chemical milling operation (Ref. 14). Baking treatments at  $500^{\circ}\text{F}$  for 4.5 hours reduced the hydrogen embrittlement considerably but did not eliminate it. At first this hydrogen embrittlement may seem contrary to expectations since 301 stainless steel is known as an austenitic stainless steel. However, although 301 is austenitic in the annealed condition, severe cold-working transforms the alloy to a low-carbon martensite. In addition, cold-working is known to make steels more susceptible to hydrogen embrittlement.

4.2.2.2 Types 304 and 310. Notched/un-notched tensile ratios indicate that 304 and 310 stainless steels retain their toughness down to liquid hydrogen temperatures (Table I). They have good thermal shock resistance, on the same order of magnitude as 301 stainless steel (Table II). Neither 304 nor 310 stainless steel will react chemically with hydrogen.

In the annealed condition, both 304 and 310 are known to be austenitic stainless steels. Therefore, under normal conditions, molecular hydrogen will not embrittle 304 or 310 stainless steel.

4.2.3 A110AT TITANIUM ALLOY. Notched/un-notched tensile ratios indicate that A110AT titanium alloy retains its toughness down to  $-423^{\circ}\text{F}$  (see Table I).

# GENERAL DYNAMICS | ASTRONAUTICS

Table II. Relative index for comparing thermal shock resistance of materials\*.

ALLOY	DENSITY (PCF)	TENSILE STRENGTH, F <sub>tu</sub> (1,000 PSI)	THERMAL CONDUCTIV- ITY, k (BTU/FT. HR. -° F)	MODULUS OF ELASTICITY, E (MILLIONS OF PSI)	LINEAR THERMAL EXPANSION COEFFICIENT, α (μ IN. /IN. /° F)	RELATIVE INDEX OF THERMAL SHOCK RESISTANCE $\frac{(F_{tu}) (k)}{(E) (\alpha)}$
ALLUMINUM ALLOYS						
2014	0.101	72	89.5	10.6	12.8	48
2219	0.100	67	80	10.3	13	40
	(ESTIMATED)		(ESTIMATED)	(ESTIMATED)	(ESTIMATED)	
5052	0.097	45	80	10.2	13.2	27
5086	0.096	47	80	10.3	13.3	27
5456	0.096	59	68	10.3	13.3	29
STAINLESS STEELS						
301	0.29	210	9.4	25	9.4	8.4
304	0.29	176	10.3	28	9.6	6.7
310	0.29	174	7.5	30	8.0	5.4
TITANIUM ALLOY						
A110AT	0.161	119	46	16	5.2	66
HIGH-TEMPERATURE ALLOYS						
K-MONEL	0.306	154	10.9	26	7.8	8.3
INCONEL-X	0.300	174	8.7	31	6.4	7.6
HASTELLOY						
B	0.334	191	6.5	31	5.6	7.2
URANIUM						
DEPLETED	0.686	(CAST) 60 TO 85	17.2	29.8	a <sub>o</sub> AXIS 12.1 b <sub>o</sub> AXIS-0.8 c <sub>o</sub> AXIS 12.9	4.9
LITHIUM HYDRIDE						
LITHIUM HYDRIDE	0.025	(ESTIMATED) <1	5.37	10	39	<.015
GRAPHITE						
GRAPHITE	0.054	WITH GRAIN	66-84	1.21	1.3 TO 1.5	44
	0.069	1.1 TO 1.3				
		AGAINST GRAIN	63-70	1.15	1.4 TO 2.1	
		1.0 TO 1.2				

\* VALUES LISTED ARE FOR ROOM TEMPERATURE, APPROXIMATELY 70° TO 80°F.

## GENERAL DYNAMICS | ASTRONAUTICS

A110AT titanium alloy has the best thermal shock resistance of the structural metals considered. It is an order of magnitude better than 301 stainless steel (Table II). A110AT will start absorbing hydrogen rapidly at about 570°F to form titanium hydride. This hydride formation was shown to consist of a thin surface layer on the metal. Below 450°F, no hydride formation occurs (Ref. 15).

Hydrogen embrittlement of A110AT titanium is characterized by low strain embrittlement when the hydrogen content exceeds approximately 300 ppm. Below 300 ppm, delayed failure of sharp notched specimens at low strain rates is characterized by continuous flow or creep with no measurable crack formation until the latter stages. Above 300 ppm, an incubation period is required before a crack forms. During this period little or no plastic flow occurs (see Figure 12). It is interesting to note that a small quantity of hydrogen, 175 ppm, greatly improves the creep resistance of this alloy without causing any embrittlement or hydrogen-induced failures. At 285 ppm there is some evidence of hydrogen embrittlement, although a considerable amount of creep occurs. Above 300 ppm, hydrogen embrittlement causes delayed failures (see Figure 13).

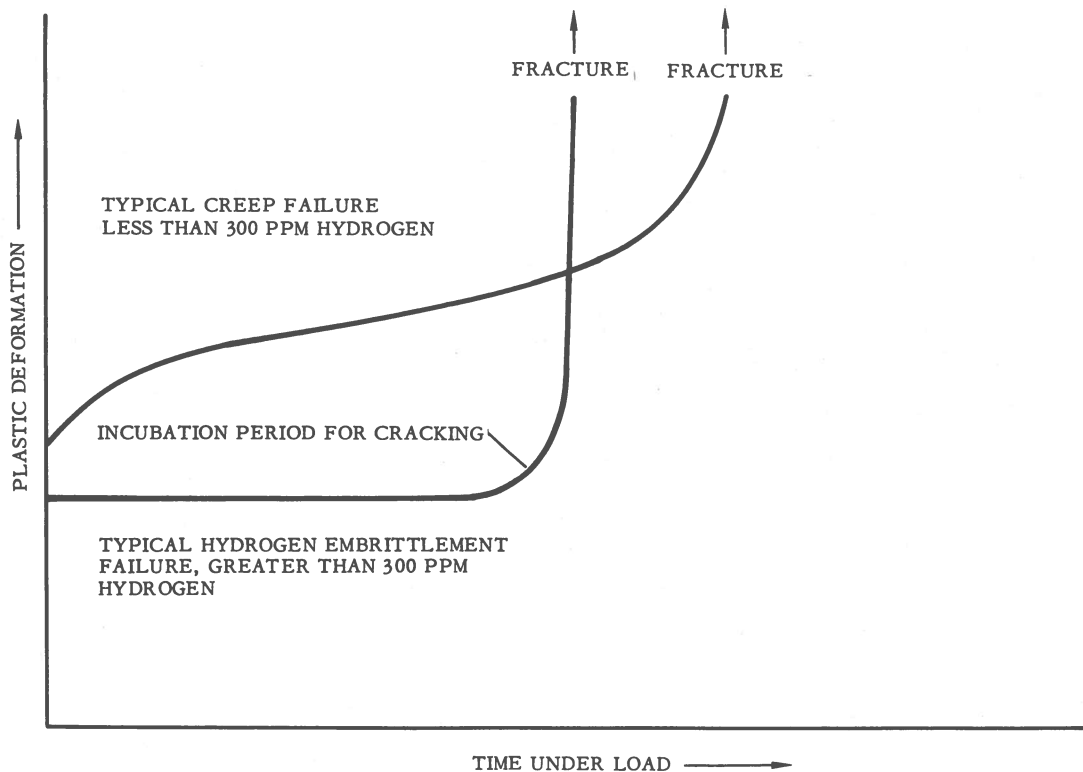


Figure 12. Low-strain-rate plastic deformation as a function of time for A110AT titanium alloy.

## GENERAL DYNAMICS | ASTRONAUTICS

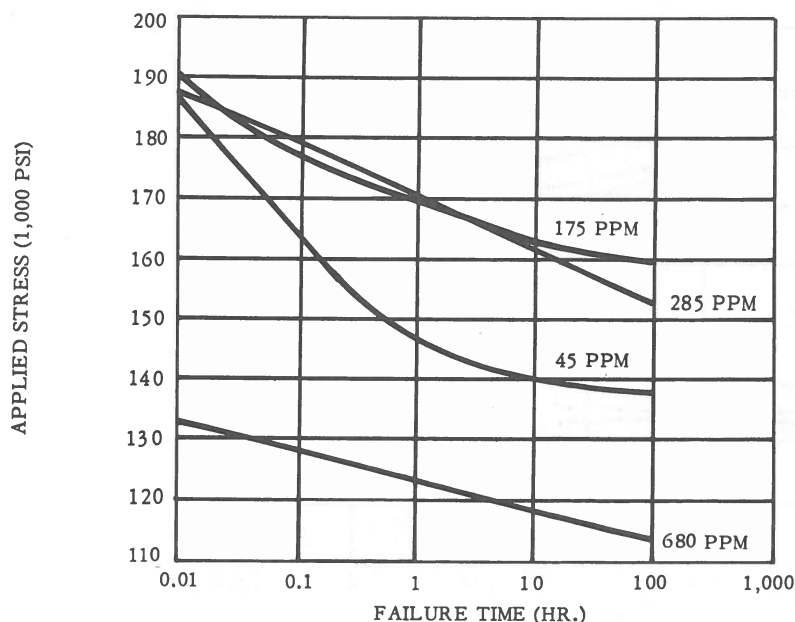


Figure 13. Low-strain-rate notched stress-rupture curves for A110AT titanium alloy at various hydrogen levels.

Un-notched stress rupture data also illustrate the incidence of low-strain-rate hydrogen embrittlement. At 160 ppm hydrogen, no embrittlement was noted, while data obtained at the 285-ppm level exhibited some embrittlement. At 690 ppm, the alloy was brittle in all low-strain-rate rupture tests (see Figure 14).

In a normal un-notched tensile test, A110AT titanium alloy was ductile at the 690-ppm hydrogen level.

### 4.2.4 HIGH-TEMPERATURE ALLOYS

4.2.4.1 K-Monel (Age-Hardened), Inconel X (Aged), and Hastelloy B. Notched/un-notched tensile ratios indicate that K-Monel, Inconel X, and Hastelloy B alloys retain their toughness down to liquid hydrogen temperatures (see Table I). K-Monel, Inconel X, and Hastelloy B exhibit good thermal shock resistance, on the same order of magnitude as 301 stainless steel (see Table II). None of the alloys listed--K-Monel, Inconel X, or Hastelloy B--reacts with hydrogen to any extent.

Studies on nickel and nickel-chromium-iron alloys indicate they are embrittled by hydrogen in a manner similar to steels (Ref. 6), as follows:

1. The embrittlement decreases with increasing strain rate.

## GENERAL DYNAMICS | ASTRONAUTICS

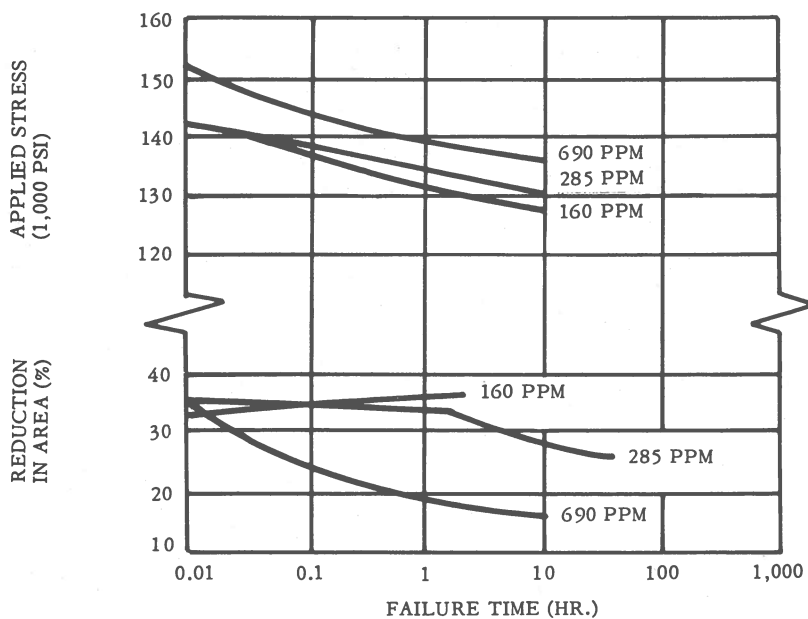


Figure 14. Applied stress for delayed failure and reduction in area at failure for A110AT titanium alloy, un-notched specimens.

2. The brittleness disappears at low and high temperatures (below  $-300^{\circ}$  and above  $500^{\circ}\text{F}$  for pure nickel).
3. Embrittlement decreases with increasing chromium and iron content.
4. Hydrogen of 4 to 5 ppm embrittles the nickel-chromium-iron alloys.

Additional studies on copper indicated that it is not embrittled by hydrogen.

An extrapolation of these results to K-Monel (66% nickel, 29% copper, 3% aluminum); Inconel X (73% nickel, 15% chromium, 7% iron, 2.5% titanium, 0.9% aluminum, 1% columbium); and Hastelloy B (62% nickel, 28% molybdenum, 5% iron) indicates that:

1. None of the three alloys will show embrittlement at high strain rates.
2. Below  $-300^{\circ}$  and above  $500^{\circ}\text{F}$ , hydrogen embrittlement is not a problem even if the alloys were highly charged with hydrogen previously.
3. Judging by their chemical composition, K-Monel would show the least hydrogen embrittlement, followed by Hastelloy B and then Inconel X.



## GENERAL DYNAMICS | ASTRONAUTICS

4. A hydrogen concentration in the order of 4 to 5 ppm is necessary to produce hydrogen embrittlement.

4.2.5 URANIUM. Some of the physical properties of uranium are highly dependent upon the prior metallurgical history. These include the linear coefficients of thermal expansion, modulus of elasticity, tensile properties, thermal conductivity, and impact strength. For this reason the values listed in Table II can only be considered representative and will vary widely depending on the metal's prior history. Other properties, including density and heat capacity, are structure-insensitive. These properties are shown in Table III.

Table III. Structure-insensitive properties of uranium.

TEMPERATURE (°F)	DENSITY (PCF)
77	1,189
392	1,179
752	1,041
1,202	1,144
1,224	1,134
1,292	1,132

TEMPERATURE (°F)	HEAT CAPACITY, C <sub>p</sub> (BTU/LB. °R)
32	0.0275
212	0.0292
392	0.03135

PURE URANIUM TRANSFORMS FROM THE ALPHA TO THE BETA PHASE AT  
1,224°F & FROM THE BETA TO THE GAMMA PHASE AT 1,416°F.

Uranium is a dense, silvery metal that oxidizes in air to a straw color within a few minutes. On standing for several days, the oxide film darkens to a blue-black color. Due to the difference in density between uranium and its oxides, the oxide film spalls off when the thickness becomes sufficiently great. Therefore, the oxide film does not offer protection to the uranium.

Uranium reacts with hydrogen to form uranium hydride, UH<sub>3</sub>. Due to the difference in density between uranium and uranium hydride, the hydride continuously spalls off to expose a fresh uranium surface. The uranium hydride formed is a brownish-black to brownish-gray pyrophoric powder, 4 to 5 microns in diameter.

## GENERAL DYNAMICS | ASTRONAUTICS

Studies have shown that uranium powder reacts with hydrogen at the low temperature of  $-112^{\circ}\text{F}$ , reaching a maximum rate at  $437^{\circ}\text{F}$  of  $1.5 \times 10^{-3}$  grams/sq. cm/min. The rate decreases from  $437^{\circ}\text{F}$  on up, due to the decomposition of uranium hydride. This decomposition pressure is 1 psia at  $600^{\circ}\text{F}$ , rising to 12 psia at  $800^{\circ}\text{F}$ .

Although no information is available on the low-temperature embrittlement of uranium, it has a fair resistance to thermal shock, about half again as good as 304 and 310 stainless steels.

**4.2.6 GRAPHITE.** Graphite has one of the most anisotropic structures known. The physical properties of the final product are highly dependent upon the choice of raw materials and the method of forming. Manufactured graphite is not one specific material but a family of materials. Each member of the family is essentially pure carbon but varies in such things as the orientation of the crystallites, the size and number of pore spaces, the degree of graphitization, and so on.

Graphite can be manufactured from almost any organic material that leaves a high carbon residue when heated. Petroleum coke, a refinery by-product, is by far the major source of graphite. In manufacturing graphite, the volatile fractions are first removed and the coke is crushed and sized. The crushed raw material is combined with coal tar pitch and formed. The formed material is then baked at  $1,380^{\circ}$  to  $1,650^{\circ}\text{F}$  for 30 to 72 days. This baking process develops an infusible carbon bond. The final step in graphite manufacture is the conversion of carbon to graphite. This is known as graphitizing and requires a temperature in the  $4,700^{\circ}$  to  $5,400^{\circ}\text{F}$  range.

Graphite has excellent thermal shock resistance (Table II). Fracture due to thermal shock is almost unknown. For example, graphite at a temperature of  $3,000^{\circ}\text{F}$  has been quenched in water without damage. The thermal shock resistance is due to its low thermal coefficient of expansion and unusually high thermal conductivity (comparable to aluminum with the grain and comparable to brass against the grain).

Graphite's resistance to gas flow erosion has been tested by directing a helium jet with a velocity of 900 fps and a temperature of  $3,600^{\circ}\text{F}$  at the graphite. After 24 hours the only erosion noted was the removal of particles previously loosened by machining (Ref. 16). Graphite does not begin reacting with hydrogen until the temperature is in excess of  $1,000^{\circ}\text{F}$ .

**4.2.7 LITHIUM HYDRIDE.** Lithium hydride is a white, crystalline solid which may be fabricated into blocks. It can be made by reacting lithium metal with hydrogen at

## GENERAL DYNAMICS | ASTRONAUTICS

1,100°F. It is essentially stable in an inert atmosphere or in hydrogen to its melting point at 1,256°F. Lithium hydride must be canned, as it reacts rapidly with moisture.

Lithium hydride blocks are fabricated by either hot or cold pressing. The major difference is the amount of force required to compress the lithium hydride powder. A 900°F hot-pressed block will reach 98% of theoretical density with 2,500 psia pressure, while cold pressing requires 20,000 psia to approach 92% of the theoretical density. An inert atmosphere must be maintained over the heated die, since the material is extremely sensitive to atmospheric oxygen and moisture at elevated temperatures.

At General Dynamics|Fort Worth, lithium hydride has been heated to 1,000°F while confined in stainless steel containers, with a 12% to 15% volume expansion noted. Lithium hydride does not start decomposing until it is heated above its melting point. At this temperature the decomposition pressure is only 0.4 psia.

Lithium hydride has poor thermal shock resistance (see Table II).

4.2.8 SEALS FOR LIQUID HYDROGEN APPLICATIONS. Sealing at LH<sub>2</sub> temperatures involves the general problems of: (1) dynamic systems, and (2) static systems.

These systems must be adapted to the amounts of leakage that can be tolerated and the deflection required under load. The considerations which must be kept in mind when designing cryogenic seals include such factors as differential thermal expansion, minimization of seal area, directing pressure to work towards effecting a seal, using thin seal materials (films, composites, etc.) to maintain plasticity at low temperatures, and the selection of effective tolerances and surface finishes.

Dynamic systems include such designs as composite envelope seals where a film of containing material (e.g., Mylar, FEP Teflon, Kynar) is provided with support by a homogeneous special filler; various lip seal configurations, including the extremely thin reed or washer seal; delicate diaphragm seals which provide accurate closure at low pressures; and various hybrid lip seals which employ pneumatic pressures for more positive actuation.

Static (and semistatic) seal design encompasses situations where seals must bridge large spans (high deflection), sealing against mismatch defects, to designs where extreme vacuum or pressure tightness and usually very slight deflections are required. Static seals employ almost all techniques described in the previous paragraph regarding dynamic sealing and additionally some unique techniques.

## GENERAL DYNAMICS | ASTRONAUTICS

Helium-pressurized pneumatic seals are employed in sealing large panels, fairings, and insulation cones where slight leakage is permissible. They usually are fabricated from Mylar and pressurized with helium gas. Lightweight, simplicity, and ease of actuation are principal advantages of this system. Where high deflection and low leakage are required, the composite seal system described in the paragraph on dynamic seals is usually employed.

The most common LH<sub>2</sub> static seals employed are those using thin plastic films, sheets, and fluorocarbon composites clad in fluorocarbon film envelopes. These are the conventional gaskets.

Where frequent disassembly is not required, dichromate cured polysulfide sealants have been used successfully in LH<sub>2</sub> systems. This system is frequently employed for repairs, effective sealing being practicable by casting a catalyzed film on the exterior of a joint which is to be sealed for LH<sub>2</sub> service.

High compression load seals such as the knife-edge designs, Teflon-coated toroidal rings, crushed rubber, and "X" or "K" cross-section seals are employed in maintaining ultra-low leakage and high vacua in cryogenic systems.

4.2.9 LUBRICANTS. Knowledge of lubrication for moving parts in contact with LH<sub>2</sub> is still in its infancy. Consequently, few lubricating systems have been investigated extensively. Some of the more successful lubricating systems being used are described in this section.

Liquid hydrogen's low temperature has both beneficial and detrimental effects on lubrication properties. Heat produced by friction is removed rapidly; however, conventional lubricants such as oils and greases freeze solid at this temperature. In fact, the best oils and greases are not usable below -100°F and few can be employed even to -65°F. Consequently, self-lubricating materials are needed for LH<sub>2</sub> lubrication. (Self-lubricating materials may be defined as those which will lower the shear forces significantly when sliding or rolling against an opposing surface.)

4.2.9.1 Ball Bearing Lubrication. Material selection for the ball bearings and races does not pose too significant a problem; however, material choice of the bearing separators or cages is limited by the fact the cage must be constructed of sacrificial material. Metallic cages or separators have never been successful. To date, both micarta and modified Teflon have been used. Micarta has a tendency to wear faster than the modified Teflon. Modified Teflon can be recommended as a lubricant

## GENERAL DYNAMICS | ASTRONAUTICS

because of its self-lubricating properties and resulting freedom from "cold welding," noncorrosiveness, excellent machinability, and vibration damping properties. Some disadvantages of modified Teflon include low structural strength (the filler material improves this property somewhat), low thermal conductivity, high thermal coefficient of expansion, low nuclear radiation stability, and operational limitation to low speeds.

Modified Teflon is much better than unmodified Teflon because the incorporation of fillers improves mechanical strength and wear properties while retaining self-lubricating properties and chemical inertness (see Table IV). Wear rates are reduced by a factor of several thousand. Other benefits include lower mold shrinkage, lower thermal expansion, and higher thermal conductivity. Filler materials used in modified Teflon include aluminum silicate ceramic fibers, graphite, molybdenum disulfide, and glass fibers. A 60% Teflon, 40% glass fiber with molybdenum disulfide composition has been found satisfactory for bearing separators.

Table IV. Properties of modified and unmodified Teflon.

	TEFLON	MODIFIED TEFLON		
		DURIOD 5600	DURIOD 5650	DURIOD 5870
MECHANICAL PROPERTIES				
TENSILE STRENGTH, LONG. (PSI)	1,500 to 3,000	2,600	4,500	7,000 to 8,000
TENSILE STRENGTH, TRANSVERSE (PSI)	1,500 to 3,000	1,800	3,000	4,000 to 6,000
HARDNESS (SHARE)	D 50 to 65	D 66	D 72	D 73
PHYSICAL PROPERTIES				
COEFFICIENT OF THERMAL EXPANSION 73° TO 140°F, (μIN./IN./°F)	55	16,20*	19,22*	16,50*
THERMAL CONDUCTIVITY (BTU-IN./HR.-FT. <sup>2</sup> -°F)	1.7	2.22	1.89	2.1

\*LONGITUDINAL & TRANSVERSE, RESPECTIVELY.

4.2.9.2 Lubrication of Plane Bearing, Sliding, or Rotating Surfaces. Dispersions of Teflon or fluorinated ethylene-propylene (FEP) bonded to sandblasted surfaces at elevated temperatures are the preferred coatings. It is not advisable to use conventional (resin - bonded) solid film lubricants at this time because not enough is known of their performance in an LH<sub>2</sub> environment. Teflon requires a cure temperature of 700°F; FEP may be fully cured at 500°F followed by a flash heating to 550°F. These cure

temperatures allow steels to be coated but make use of aluminum alloys marginal. However, dielectric heating units that heat the coating but leave the metal cool could be used for aluminum coating. Coating thicknesses normally range between 1 mil and 5 mils. It is important that the coating thickness be kept small and a good bond be made to the metal; otherwise, the coating will break away when thermally shocked with  $\text{LH}_2$ .

4.2.10 INSULATION. A number of approaches to cryogenic insulation are being employed in space vehicle application and a discussion of these follows.

4.2.10.1 Internal Insulation. The use of internal insulation (normally organic foam or reinforced foam) reduces the bonding problems normally associated with liquid hydrogen applications, since the bond line approaches ambient temperature. A room temperature curing adhesive can then be used rather than the heat-cured systems normally associated with external-type insulations in which the bond line is at  $-423^\circ\text{F}$ . Internal insulation also minimizes the danger of possible damage during ground handling. Internal insulation has a lower average temperature and temperature gradient across it during flight than does external insulation.

Associated with these advantages are a series of disadvantages. The most difficult problem is obtaining a nonpermeable inner seal. Permeability of the inner seal by gaseous hydrogen under pressure will result in a large increase in the thermal conductivity of the internal insulation. Internal insulation also presents the possibility of engine fouling from thermal cracking of the inner skin. An added requirement that the insulation must withstand because of its location is water immersion. This results from required tank cleaning procedures and possibly water calibration of the tank. Internal insulation also prohibits the use of low-temperature design allowables on the tank materials, and is usually an expensive manufacturing process.

4.2.10.2 External Insulation. Foam and reinforced-foam insulations, as well as materials such as balsa, cork, etc., can be applied externally to a liquid hydrogen tank as well as internally. The external insulation systems are usually divided into two categories, bonded and jettisonable. The bonded systems have the disadvantage of requiring the adhesive to withstand shear, tension, peel, thermal and mechanical fatigue, vibration, etc., at temperatures down to  $-423^\circ\text{F}$ , while the jettisonable-type system requires a helium purge system to prevent ice and liquid air formation. Sealing between panel edges and tank, and jettisoning the panels are two major problems with nonbonded systems. However, they are compensated by a greater efficiency than the internally and externally bonded systems. Both of the external systems are subject to damage during ground handling, and both are subjected to high average

## GENERAL DYNAMICS | ASTRONAUTICS

temperatures and large temperature gradients across the insulation during flight through the atmosphere. The helium purge system must be sealed properly or it too will be subject to gas permeation of the core and subsequent increases in thermal conductivity (k factor). Heat leaks through attachments and bracketry may also be a problem with external insulations.

The advantages of external systems are discussed in detail in Section 5.2.3. Briefly, these advantages include: utilization of low-temperature design allowables on certain portions of the tank, relative ease of manufacture (particularly the non-bonded type), ease of repair, and ease in tank cleaning.

4.2.10.3 High-Efficiency Insulation. There are available a series of powder and multilayer insulations which are extremely efficient at low pressure (0.1 micron and lower). When the cold side temperature is at  $-423^{\circ}\text{F}$  and the hot side is at room temperature, the powder insulations such as perlite and silica aerogel at 0.1 micron result in k factors of the same order of magnitude as those obtained with a straight vacuum. The use of reflective shields such as aluminum foil, in combination with glass fiber paper or glass matting, will result in k factors as low as one-sixtieth that of a straight vacuum. The problems associated with the "super insulations" are numerous. They are usually nonload-bearing and require a vacuum-tight container; the powders are subject to settling; and the foil-type insulations are subject to lateral heat flow. However, many of these problems associated with laminar insulations can be eliminated by proper design as shown in the discussion of advanced insulation concepts in Chapter 13.

4.2.10.4 Miscellaneous Insulation Materials. Since most of the materials being used for cryogenic insulations are composites, it is almost impossible to list the mechanical and physical properties of the countless combinations that are available. Table V lists some general materials and their properties. It should be pointed out that these properties are dependent on density, temperature, formulation, etc., and are just typical values. The use of reinforced foams for cryogenic insulations is extensive, but the type of reinforcement controls the properties of the composites and once again the possible combinations are so great that they cannot be enumerated in this report.

### REFERENCES

1. The Relation of Microstructure to Brittle Fracture. J. R. Low, American Society for Metals, Cleveland, Ohio, p. 163, 1954.

# GENERAL DYNAMICS | ASTRONAUTICS

Table V. Properties of load-bearing insulations.

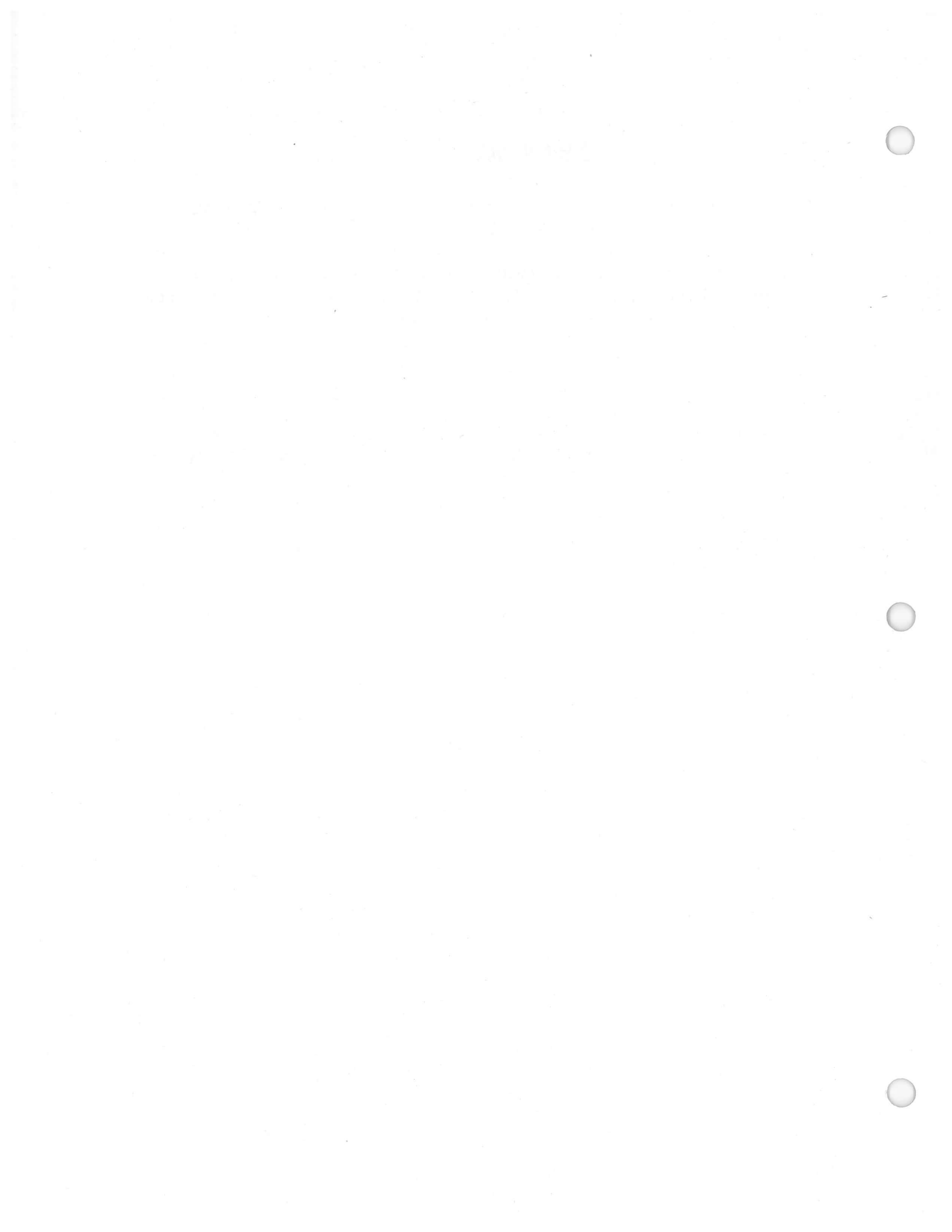
MATERIAL	DENSITY (PCF)	TENSILE STRENGTH (PSI)	MODULUS OF ELASTICITY (PSI)
POLYURETHANE FOAM (CO <sub>2</sub> BLOWN) PARALLEL TO RISE	2.0	40-65	1,500
POLYURETHANE FOAM (FREON 11 BLOWN) PARALLEL TO RISE	2.0	40-55	1,100
POLYSTYRENE FOAM	1.6-2.0	35-60	-
CORKBOARD	20.4	65	-
BALSA, END GRAIN	6.3	450-1,375	330,000
BALSA, FLAT GRAIN	6.0	70-110	14,000

2. Investigation of the Mechanism of Rapid Crack Propagation in Metals. M. E. Shank and J. E. Neimark, Watertown Arsenal Laboratory, File No. 893/179, August 1958.
3. Modern Concepts of Flow and Fractures. E. R. Parker, Transactions of ASM. 50, p. 52, 1958.
4. Compatibility of Rocket Propellants with Materials of Construction. Battelle Memorial Institute, DMIC Memo 65, p. 41, 15 September 1960.
5. Hydrogen Contamination in Titanium and Titanium Alloys. R. I. Jaffee et al., Part V, Hydrogen Embrittlement, WADC TR 54-616, February 1959.
6. Hydrogen Embrittlement in Steels, Titanium Alloys and Several Face-Centered Cubic Alloys. A. R. Troiano et al., WADC Report 59-172, April 1959.
7. Effects of Hydrogen on Alpha Titanium Alloys. G. A. Lenning, et al., Journal of Metals, Trans. Section 8, p. 1,235, October 1956.
8. Hydrogen Embrittlement of Tantalum at Ambient Temperatures. A. Claus and H. Forestien, Comp. Rend. Vol. 246, No. 23, p. 3,241, 1958.
9. Effect of Hydrogen on the Mechanical Properties of Columbium. T. W. Wood and R. D. Daniels, paper at AIME Meeting, February 1959.



## GENERAL DYNAMICS | ASTRONAUTICS

10. Mechanical Properties of Aluminum Alloys at Cryogenic Temperatures. J. L. Christian, Astronautics Report MRG-190, 2 December 1960.
11. The Effect of Cryogenic Temperatures on the Mechanical Properties of High Strength Sheet Alloys (Cold Worked Austenitic Stainless Steel). J. F. Watson and J. L. Christian, Astronautics Report ERR-AN-003, 16 May 1960.
12. Mechanical Properties of Titanium and Titanium Alloys at Cryogenic Temperatures. J. L. Christian, Astronautics Report MRG-189, 14 October 1960.
13. Low-Temperature Properties of K-Monel, Inconel-X, Rene 41, Haynes 25 and Hastelloy B Sheet Alloys. J. F. Watson and J. L. Christian, Astronautics Report.
14. The Susceptibility of Materials to Hydrogen Embrittlement from Chemical Milling Operations. R. L. Jones, Astronautics Report MRG-219, p. 12, 16 March 1961.
15. The Effects of Alloying Elements in Titanium. R. I. Jaffee et al., Defense Metals Information Center Report 136B, p. 43, 29 May 1961.
16. The Industrial Graphite Engineering Handbook. National Carbon Co., p. 5D.04.01, 1959.



# 5

## CRYOGENIC INSULATION

### 5.1 TYPES OF INSULATION

Use of liquid hydrogen propellant for flight vehicles requires highly efficient insulation to reduce boiloff losses to an acceptable value. The final choice of an insulation for a particular system represents a compromise of many factors. For ground handling systems, various practical considerations such as economy, convenience, weight, bulk, and ruggedness dictate the insulation choice. Flight-type insulations, on the other hand, must meet a different set of requirements. They must be able to withstand aerodynamic heating (external configuration only), acceleration, vibration, and shock, and still have the desirable properties of low density, ease of application to large tanks, thermal effectiveness, and high reliability.

The governing mechanisms of heat transfer through insulation are:

1. Radiation.
2. Conduction through the gas permeating the insulation.
3. Conduction through the solid material.

Radiation losses are directly proportional to the emissivity of the surface and the fourth power of the surface temperature. Conduction losses through residual gas are proportional to the pressure (within limits) while conduction losses through a solid are proportional to the thermal conductivity of the insulating material and the effective area of contact between the insulation and support structures.

**5.1.1 NONEVACUATED INSULATIONS.** The density and apparent mean thermal conductivity of the following insulations are shown in Table VI.

**5.1.1.1 Polyurethane Foam.** Polyurethane foams are made in densities from 1.5 to 20 pcf and range in cell structure from flexible (open cell), to semirigid (partly open cell), to rigid (closed cell). Polyurethane may be foamed in place using a selected monomer, foaming agent, and catalyst (see Figure 15).

# GENERAL DYNAMICS | ASTRONAUTICS

Table VI. Representative thermal conductivities of insulations.

INSULATION	DENSITY (PCF)	APPLIED VACUUM (MM OF Hg)	BOUNDARY TEMPERATURES, WARM & COLD SURFACE (°R)	APPARENT MEAN THERMAL CONDUCTIVITY ( $\frac{\text{Btu} \cdot \text{ft.}}{\text{FT.}^2 \cdot \text{HR.} \cdot \text{°R}}$ )
PLASTIC FOAMS				
POLYURETHANE (FREON-BLOWN)	2	NONE	540-37	$800 \times 10^{-5}$
POLYURETHANE	2	$2 \times 10^{-3}$	528-139	$850 \times 10^{-5}$
POLYSTYRENE	2	NONE	540-37	$1.560 \times 10^{-5}$
POLYSTYRENE	2	$6 \times 10^{-2}$	508-139	$1,150 \times 10^{-5}$
HONEYCOMB CORE				
PHENOLIC FIBERGLASS HONEYCOMB, 1/4-IN. CELLS	6.5	NONE	540-37	$6,600 \times 10^{-5}$
ABLATIVE INSULATIONS				
CORKBOARD	18-20	NONE	530-37	$2,300 \times 10^{-5}$
BALSA	8-10	NONE	530-37	$2,100 \times 10^{-5}$
POWDERS				
EXPANDED PERLITE	5 - 6	$< 10^{-3}$	540-37	$41 \times 10^{-5}$
SILICA AEROGEL	5	$< 10^{-3}$	540-137	$127 \times 10^{-5}$
OPACIFIED POWDERS				
LINDE CS-5	11.0	$< 10^{-3}$	540-163	$22 \times 10^{-5}$
SILICA AEROGEL WITH ALUMINUM POWDER (50% BY WEIGHT)	6	$< 10^{-3}$	540-137	$32 \times 10^{-5}$
LAMINAR INSULATIONS				
NRC-2	2.5	$10^{-6}$	530-139	$1.6 \times 10^{-5}$
LINDE SI-10	2.0	$10^{-6}$	530-36	$6.5 \times 10^{-5}$
LINDE SI-62	5.5	$10^{-6}$	530-36	$1.8 \times 10^{-5}$
LINDE SI-62 (COMPRESSED BY 15 PSI DIFFERENTIAL PRESSURE)		$10^{-6}$	530-139	$6.0 \times 10^{-5}$
LINDE SI-91	7.5	$10^{-6}$	530-36	$1.0 \times 10^{-5}$

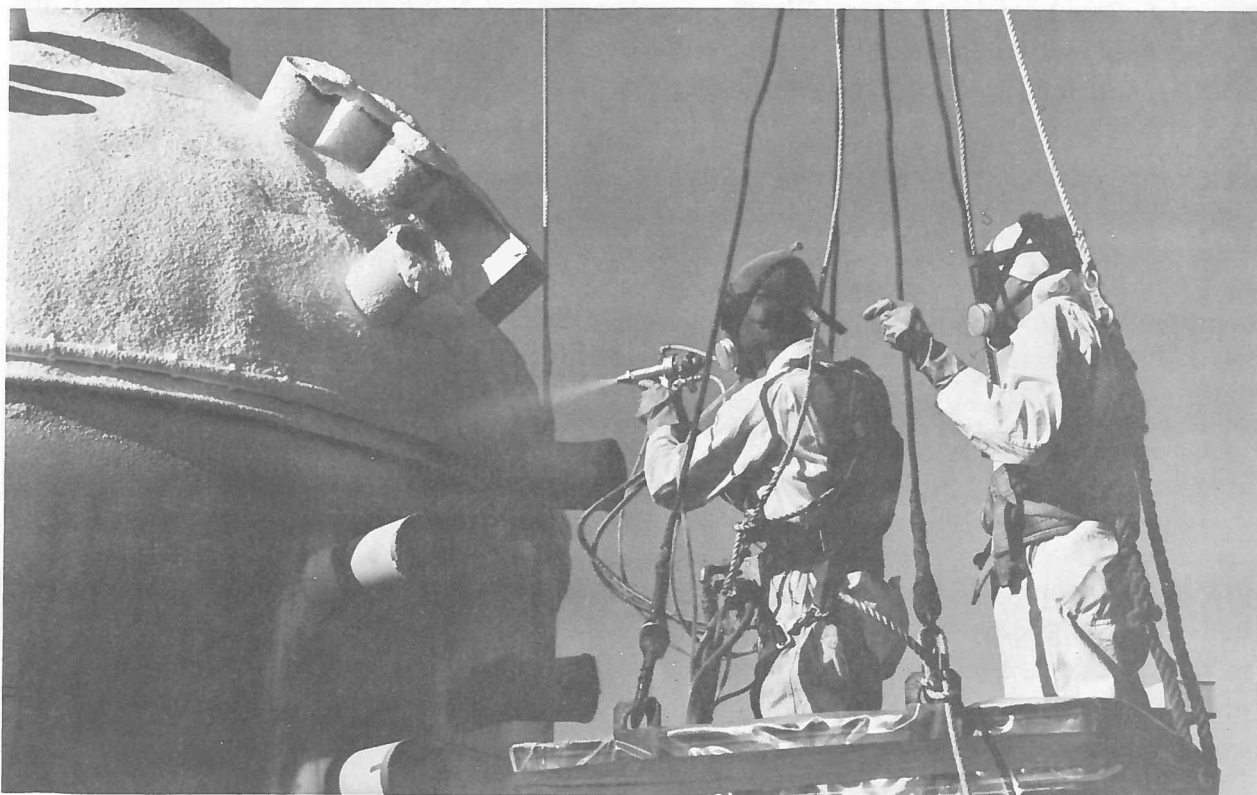


Figure 15. Foaming polyurethane insulation on Centaur forward bulkhead.

Repairs can be accomplished by the same technique. Although closed-cell foams are relatively impervious to gas diffusion, an airtight barrier should be placed on the surface of the foam to prevent air condensation at the cold surface. This barrier has the added advantage of providing a partial vacuum in the insulation due to the cryopumping action of liquid hydrogen.

5.1.1.2 Polystyrene Foam. Polystyrene foam is a low-density, closed-cell, rigid plastic foam. Normally polystyrene foam is received in bulk form from the manufacturer and machined to the desired shape. However, a process using granules of polystyrene containing a blowing agent and a temperature of 230° to 270°F does allow the plastic to be foamed in place.

5.1.1.3 Honeycomb Sandwich Panels. Fiberglass phenolic honeycomb panels with laminated fiberglass outer skins have been considered for space vehicle LH<sub>2</sub> tanks. Although the thermal effectiveness of honeycomb insulation is not as good as plastic foams (as shown in Table VI), its load-carrying capacity makes it attractive for space applications. This results in an over-all savings since thinner tank skins can be utilized.

5.1.1.4 Corkboard and Balsa Wood. Corkboard and balsa wood have been tested for use as externally bonded and sealed insulations for liquid hydrogen-fueled vehicles. This type of insulation is suitable for high-acceleration vehicles with large aerodynamic heating loads. Results of the study showed commercial composition corkboard was suitable but the use of balsa wood was marginal. The surface of the insulation had to be sealed to prevent air condensation; otherwise, the thermal conductivity value of the insulation rose approximately 50%. The maximum temperatures to which the insulation could be subjected to were found to be 1,100° to 1,350°F for composition corkboard, 700°F for balsa, and 450°F for foamed corkboard. The surface of these materials was charred and blackened after exposure to these temperatures.

5.1.2 VACUUM INSULATIONS. The density and apparent mean thermal conductivity of the following insulating systems are shown in Table VI.

5.1.2.1 Evacuated Plastic Foams. Isocyanate and urethane foams were evacuated to 1-50 microns pressure. The thermal conductivity of the foams dropped approximately 1/2 to 1/3 of the nonevacuated value. Evacuation of styrene foams improved them only moderately. Evacuated glass and silica foams showed no improvement over nonevacuated glass foams. The isocyanate, urethane, and styrene foams all supported the 1-atmosphere load without buckling. However, the time necessary to evacuate the foams was extremely long and high pumping rates had to be continued to maintain the vacuum. For example, at a pumping speed of 5 cfm per cubic foot of Styrofoam, it took 40 hours to obtain and maintain a 50-micron vacuum. Applied heat lowered these times somewhat.

5.1.2.2 Evacuated Powder Insulations. When an insulating space is filled with a low-density powder, the apparent thermal conductivity is approximately that of the gas. There is a marked reduction in thermal conductivity when the gas pressure is reduced to a value at which the mean free path of a molecule is comparable with interstitial distances. This pressure is on the order of 1 to 0.1 mm of Hg. Below  $10^{-3}$  mm of Hg, the rate of heat transfer is almost independent of pressure. The residual heat transfer is by conduction through the powder and by radiation. Heat-transfer losses can be reduced by a factor of approximately four over conventional powders if a metal opacifier such as aluminum or copper powder is added to the insulating powder in the approximate weight ratio of one to one. These reflective opacifiers make the insulation relatively opaque to thermal radiation. No significant difference was found between silver, nickel, copper, and aluminum powders. The metal powder must be well mixed with the insulating powder to prevent a conductive

## GENERAL DYNAMICS | ASTRONAUTICS

short circuit in the insulation. Evacuated powder insulations have maintained their thermal effectiveness for many years without re-evacuation.

The heat-transfer rate ( $q$ ) through a powder insulation of constant thickness is given by:

$$q = \frac{\bar{k}(T_2 - T_1) (\sqrt{A_1 A_2})}{t} \quad (\text{Ref. 1})$$

Where

$\bar{k}$  = means effective thermal conductivity between  $T_1$  and  $T_2$ ,

$T_1, T_2$  = temperatures of warmer and cooler surfaces, respectively,

$A_1, A_2$  = areas of warmer and cooler surfaces, respectively,

$t$  = thickness of insulation.

This equation is exact for concentric spheres. For cylinders, it is accurate to 5% if the thickness of the insulating space is not more than 50% of the radius of the inner cylinder.

**Expanded Perlite.** Expanded Perlite is a low-density, low-cost powder that has been used successfully in insulating the liquid hydrogen storage tank at the Sycamore Canyon Test Site.

**Santocel.** Santocel is a low-density insulating powder consisting of silica aerogel. It is a good desiccant, readily removing water vapor from air.

**5.1.2.3 High-Vacuum Insulation.** The use of high-vacuum insulations for cryogenic storage and transfer lines has been reduced to common practice. However, the production and maintenance of a high vacuum takes precise manufacturing techniques and high-vacuum pumping equipment. Outgassing from the containing surfaces and diffusion of gases through the metal walls tend to destroy the vacuum. Liquid hydrogen temperatures help maintain the vacuum through a cryopumping action. "Getters," i. e., materials that absorb residual gases, are often used in vacuum lines.

## GENERAL DYNAMICS | ASTRONAUTICS

When a vacuum on the order of  $10^{-6}$  mm of Hg is obtained, heat transfer between two surfaces is due almost entirely to heat radiation. The rate of radiant heat transfer is given by the equation:

$$q = \sigma E A (T_1^4 - T_2^4) \quad (\text{Ref. 2})$$

Where

$q$  = heat transfer rate,

$\sigma$  = Stefan-Boltzmann constant ( $1.73 \times 10^{-9}$  Btu/ft.<sup>2</sup> - hr. - °R),

$A$  = area (inner surface of concentric cylinders and spheres),

$T_1, T_2$  = temperatures of warmer and cooler surfaces, respectively,

$E$  = emissivity factor.

The appropriate values for  $A$  and  $E$  depend on the geometry of the radiating surface. Furthermore,  $E$  depends on the emissivities of the two surfaces, and in the case of concentric shapes, on whether the reflection is specular or diffuse. Diffuse reflections result in a higher radiant flux. In order to be on the conservative side, the following equations for  $E$  are for diffuse reflections.

### 1. Parallel Plates and Concentric Spheres

$$E = \frac{e_1 e_2}{e_2 + (1 - e_2) e_1} \quad (\text{Ref. 2})$$

### 2. Long Coaxial Cylinders

$$E = \frac{e_1 e_2}{e_2 + \frac{A_1}{A_2} (1 - e_2) e_1} \quad (\text{Ref. 2})$$



## GENERAL DYNAMICS | ASTRONAUTICS

where

$A_1, A_2$  = areas of cooler, warmer surfaces, respectively,

$e_1, e_2$  = emissivities of cooler, warmer surfaces, respectively.

Values of  $e_1$  and  $e_2$  depend markedly on the type of material, surface roughness, degree of oxidation, and temperature. Typical emissivity values for various metals are listed in Table VII (Ref. 3).

Experience at Astronautics Point Loma and Sycamore Canyon Test Sites has shown that high-vacuum transfer lines are expensive and difficult to maintain in the field. An alternative condensable gas insulating system has proven to be satisfactory. The space between the inner and outer line is filled with carbon dioxide. At liquid hydrogen temperatures, the carbon dioxide solidifies, forming a vacuum in the insulating void. This system has been maintenance-free since installation in mid-1961.

5.1.2.4 Laminar Insulations. Laminar insulations, also known as "superinsulations," derive their remarkable impedance to heat flux from the effect of multiple radiation barriers. High vacuum is essential for the proper functioning of this type of insulation to reduce gas conduction to a minimum. These radiation barriers consist of foils of highly reflective metals separated by a nonconductor.

The theoretical heat transfer across more than 10 reflective shields can be expressed within engineering accuracy by:

$$q = \frac{\sigma EA (T_1^4 - T_2^4)}{n + 1} \quad (\text{Ref. 4})$$

where

$q$  = heat-transfer rate,

$\sigma$  = Stefan-Boltzmann constant ( $1.73 \times 10^{-9}$  Btu/ft.<sup>2</sup>-hr.-°R),

$E$  = emissivity factor (see Section 5.1.2 on high vacuum insulation, and Table VII),

$A$  = area,

# GENERAL DYNAMICS | ASTRONAUTICS

Table VII. Total hemispherical emissivity of metals.

METAL	SURFACE PREPARATION	EMISSIVITY ( $\epsilon$ ) (AT 137° FOR 540° R BLACK BODY RADIATION)
ALUMINUM (0.001 IN.)	KAISER FOIL, UNANNEALED	0.018
ALUMINUM (0.001 IN.)	KAISER FOIL, UNANNEALED	0.03 (540° R)
ALUMINIZED MYLAR (0.0005 IN.)	ALUMINUM COATING, BOTH SIDES	0.04
COPPER (0.005 IN.)	ELECTROLYTICALLY CLEANED	0.017
GOLD (0.0015 IN.)	FOIL, SOLVENT-CLEANED	0.01
NICKEL (0.004 IN.)	FOIL, SOLVENT-CLEANED	0.022
SILVER	SOLVENT-CLEANED	0.008
STAINLESS STEEL, TYPE 301	SOLVENT-CLEANED	0.21 (535° R)
STAINLESS STEEL, TYPE 302 (0.005 IN.)	SOLVENT-CLEANED	0.048
TIN (0.001 IN.)	FOIL, CLEANED	0.013
ZINC (0.0065 IN.)	FOIL, SOLVENT-CLEANED	0.02

$T_1, T_2$  = temperatures of warmer, cooler surfaces, respectively,

$n$  = number of shields.

The actual observed heat leaks are usually several times higher than the calculated value due to the conductance through material separating the shields. It is interesting to note that the surface finish of the warm and cold surfaces has little effect on the over-all heat transfer rates of laminar insulation.

Aluminum foil is normally used for the radiation shields although aluminized Mylar has been tried due to its higher strength. Apparently the aluminum coating is transparent to some extent for the Mylar insulation was found to have about twice the thermal conductivity value of aluminum foil insulations (Ref. 4). Some of the spacer materials used include glass wool, fiberglass, paper, and nylon netting.

## 5.2 FLIGHT INSULATIONS

Liquid hydrogen tanks require insulation on the ground to minimize LH<sub>2</sub> boiloff and to prevent the condensation of air (which can create a potential safety hazard on the test stand or launch pad). Insulation of tanks is required during flight to prevent high boiloff rates and/or tank pressure rise due to aerodynamic and space heating. For airborne liquid hydrogen tanks the insulation must be lightweight and still have adequate strength to withstand the thermal, ground, and air loads which are imposed upon it. A second requirement for airborne liquid hydrogen tank insulation is reliability, which is even more important than weight. The insulation should be capable of performing its function whenever necessary with a minimum of upkeep and repair.

### 5.2.1 ENVIRONMENTAL CONDITIONS

5.2.1.1 Tanking and Ground Hold. Thermal shock occurs when the propellant tank is filled with liquid hydrogen. The thermal shock occurs because of the large difference in thermal contraction between the tank and the insulation.

With external insulation, the metal tank skin contracts almost instantaneously upon contact with the liquid hydrogen. Due to its lower thermal conductivity, the temperature of the insulation changes much more slowly than the tank skin; therefore, the insulation contracts much more slowly than the tank. Thermal stresses occur when the insulation resists the tank shrinkage (see Figure 16). The tank is loaded in biaxial tension, the insulation is loaded in biaxial compression, and the adhesive between the tank insulation is loaded in tension.

With internal insulation, the inner skin of the insulation contracts almost instantaneously and is loaded in tension, while the tank skin is loaded in compression. Local shear loads occur in the adhesive and insulation at the ends of the cylindrical tank, at the bulkhead tangency planes, and at small cutouts such as the access door and tank vent line for both external and internal insulations.

The severest thermal stress condition occurs upon initial contact with the liquid hydrogen. As the insulation attains thermal equilibrium, the thermal stresses decrease slightly due to the decrease in the temperature gradient. The initial tanking is more critical as far as structural integrity of the insulation is concerned than the ground hold which follows. To reduce the severity of the thermal shock, the internal temperature of the tank should be lowered to about -200°F by means of cold hydrogen gas prior to filling the tank with liquid hydrogen. The tank chilldown period is perfectly feasible and is currently being used on the Centaur.



Figure 16. Typical failure in fiberglass sealer on outside insulation test with liquid hydrogen.

5.2.1.2 Maximum Aerodynamic Pressure. Maximum aerodynamic pressure for a boost vehicle normally occurs between 30,000 and 40,000 ft. with the vehicle traveling at about Mach 2 and accelerating at about 2g. The maximum aerodynamic pressure is between 700 and 800 psf. The temperature of the outer skin of the vehicle is normally about room temperature at maximum  $q$ ; therefore, the thermal stresses are about the same as they are on the ground. The only insulation loading condition which occurs at maximum  $q$  that is different from the ground hold condition, is the increased pressure differential across the tank wall due to the decrease in atmospheric pressure with altitude. The effects of increased pressure differential across the tank wall are to decrease the compressive thermal stress in the outer skin, and to increase the tensile stress in the inner skin.

If the insulation is bonded directly to the pressurized tank it will not encounter problems due to aerodynamic flutter. For insulation that is not fastened rigidly to the tank, flutter is another design condition which must be considered. Flutter requirements will probably determine panel stiffness requirements for any insulation that is not fastened securely to the pressurized tank structure.

## GENERAL DYNAMICS | ASTRONAUTICS

5.2.1.3 **Maximum Acceleration.** The maximum vehicle acceleration normally occurs when the vehicle is outside of the earth's atmosphere; thus air loads are negligible at maximum g. The pressure differential across the tank wall is a maximum at this portion of the trajectory due to the absence of atmospheric pressure.

5.2.2 **DESIGN CONCEPTS.** The following insulation designs are typical of the concepts used on liquid-hydrogen-fueled Saturn stages. Both the Saturn S-IV and Rift stages are using the internally bonded insulation concept; the S-II uses externally bonded insulation; Centaur uses jettisonable panels on the cylindrical section of the tank and bonded external insulation elsewhere.

Some advanced insulation concepts are presented in Section 13.1.3.

5.2.2.1 **Bonded External Insulation.** The simplest, cheapest, and most easily fabricated method for insulating a liquid hydrogen tank is to bond the insulation directly to the tank. A typical externally bonded insulation would consist of honeycomb panels that would be bonded to the tank skins, filled with polyurethane foam, and covered with a fiberglass outer skin. Corkboard and balsa wood have also been considered as external insulation.

External bonded insulation has several advantages over internally bonded insulation. The external insulation must only be sealed against air and water vapor instead of the much smaller hydrogen molecule. The welded propellant tank serves as the seal against hydrogen. The propellant tank is protected from damage by the external insulation during ground handling, transportation, and flight. General Dynamics' experience with honeycomb sandwich on the Atlas and the B-58 indicates that this type of external insulation is rugged and not easily damaged. If the insulation is damaged, it is much easier to repair than the propellant tank; therefore, the tank protection feature is a definite advantage (see Figure 17). Insulation damage may be found and repaired quite readily from the outside of the tank, thus eliminating the need to enter the tank.

However, external insulation makes inspection of the propellant container structure more difficult, since visual inspection can only be performed from inside the tank. Moreover, no room temperature bonding material has yet been found for external insulation; therefore, application of heat is required both during fabrication and repair. This causes spot repair to become highly difficult and unreliable. All tests of external insulation conducted by Astronautics have shown laminations and cracking of the outer fiberglass layers. Sealed corkboard and balsa wood have not shown the same problem.

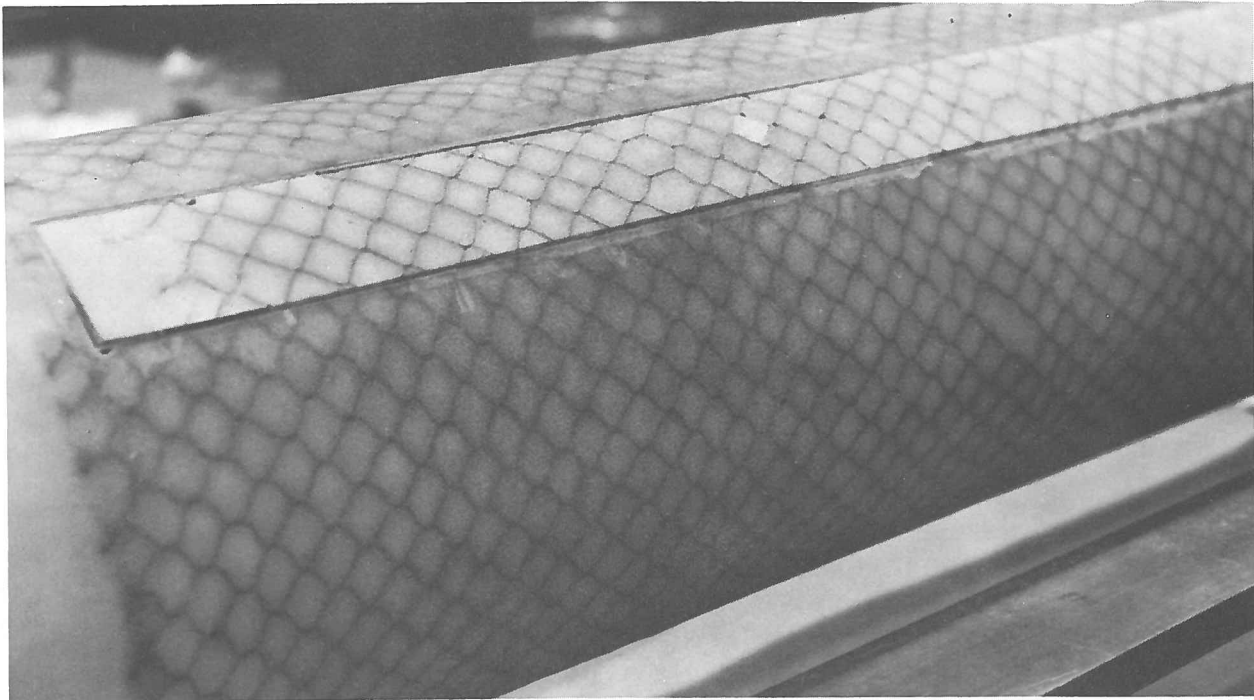


Figure 17. External foam-filled honeycomb insulation with a repair plug.

5.2.2.2 Helium-Purged External Insulation. Helium-purged external insulation is similar to the bonded insulation except that it is not bonded to the tank, and the resulting gap between the insulation and tank is purged with helium gas to prevent liquid air from forming. A typical insulation consists of a honeycomb core with a 1-in. cell size filled with 2 pcf of polyurethane foam. The insulation core has fiberglass faces on both sides, and these are sprayed with a sealer. The insulation panels are mechanically fastened together, and are also mechanically fastened to the tank.

This type of insulation is similar to that successfully in use on the cylindrical portion of the Centaur tank. If it is not necessary to jettison the insulation panels, they can be permanently fastened together with mechanical joints, thus eliminating the slip joints and spring straps which are used on Centaur. Mechanically fastening the insulation panels eliminates much of the helium leakage that occurs with the Centaur insulation panels. Permanently sealed expansion joints enable the tank to contract and expand due to temperature and pressure without loading the insulation. Thermal shock due to filling the tank with liquid hydrogen is not felt by this type of insulation since it is not bonded to the tank. The insulation does have a temperature gradient across it, but the rate of temperature change and thermal stress buildup is considerably less than for an insulation that contacts the tank or the liquid hydrogen.

## GENERAL DYNAMICS | ASTRONAUTICS

The helium-purged insulation can be easily repaired if the damage areas are small, but if large areas are damaged, the helium-purged insulation lends itself to replacing an entire panel more readily than does the bonded insulation. Repairs to the propellant tank are also easier to make for the helium-purged insulation than for a bonded insulation because no insulation or adhesive has to be removed from the tank.

**5.2.2.3 Canned External Insulation.** The canned external insulation gets its name from the manner in which it attaches to the outer skin. The outer skin is not bonded to the insulation, but is fastened at its edges and evacuated much in the same manner as foods are preserved, hence the name canned.

A typical insulation consists of foam-filled honeycomb similar to that used for the Centaur jettisonable insulation panels. The honeycomb is filled with polyurethane foam and is bonded to the tank. The outer skin can have several possible configurations; it can be 0.025-in. aluminum, 0.010-in. Mylar, or 0.010-in. fiberglass impregnated with silicone rubber.

This type of insulation is lightweight and relatively inexpensive, but several difficulties are anticipated with it. Some work has been done at Astronautics toward using evacuated metal skins as liquid hydrogen insulation. Vacuum insulation using 0.010-in. stainless steel skins has been fabricated and tested. The outer skin wrinkles as shown in Figure 18 are due to the vacuum. This type of insulation would not give a smooth outer tank skin during flight, and would therefore be subjected to local hot spots due to aerodynamic heating, as well as increasing the drag of the vehicle. If the evacuated space is vented to the atmosphere during flight, skin flutter would probably occur with catastrophic results. If it is attempted to permanently evacuate the insulation, an extremely low pressure would be required to prevent ballooning of the skin during the boost phase of flight. In the transition from vacuum bag to balloon, the skin is again subject to potentially catastrophic flutter problems. In addition to the skin flutter problems, difficulty is expected in obtaining and maintaining a hard vacuum over large surface areas with many joints.

**5.2.2.4 Bonded Internal Insulation.** The bonded internal insulation concept is similar to the bonded external insulation described previously. It consists normally of a honeycomb core filled with polyurethane foam and bonded to the inside of the tank (see Figure 19). The inner skin usually consists of a fiberglass wet layup with several coats of sealant.





Figure 18. Wrinkled skin of vacuum insulation.

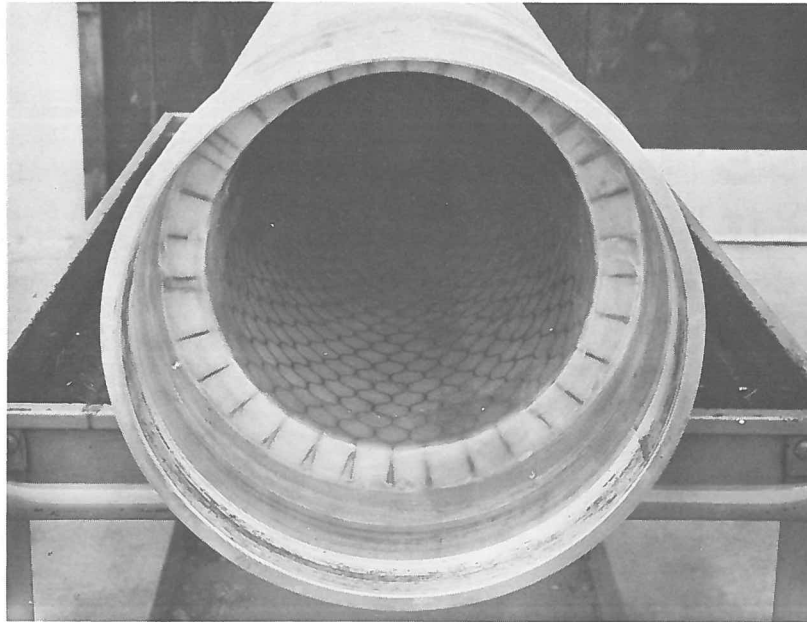


Figure 19. Internal foam-filled honeycomb insulation after 20 pressure cycles in liquid hydrogen.



## GENERAL DYNAMICS | ASTRONAUTICS

The bond to the tank wall is not subjected to thermal shock with this insulation technique, but the bond of the inner skin to the insulation is subject to thermal shock. The over-all vehicle weight with this type of insulation is higher than with the external insulation because low temperature design allowables cannot be used for the tank skins and because a large vapor pressure rise occurs due to aerodynamic heating, causing a tank weight increase even though the insulation by itself is about the same weight as the externally bonded insulation. Internal insulation need not be sealed against  $\text{GH}_2$ , though this would be advantageous. No adequate seal against  $\text{GH}_2$  is presently known. Internal insulation has just about as many local openings and attachment provisions as does the external insulation. Local flexing of the insulation occurs in the areas of baffle attachments inside the tank, which results in a low fatigue life for the insulation under temperature and pressure cycling. Internal insulation cannot be used if the tank is stiffened by means of stringers and frames which require either an excessive number of attachments through the insulation or insulation of the frames. Either of these requirements leads to a poor design because of the complications.

### REFERENCES

1. Cryogenic Engineering. R. B. Scott, D. Van Nostrand Co., Inc., August 1960, p. 205.
2. Storage, Transfer and Servicing Equipment for Liquid Hydrogen. B. M. Bailey et al., WADC Tech. Report 59-386, pp. 37-38, July, 1959.
3. Thermal Radiation Absorption by Metals. M. M. Fulk et al., Cryogenic Engineering, Vol. I, Plenum Press, pp. 227-228, 1954.
4. Engineering Aspects of Heat Transfer in Multilayer Reflective Insulation and Performance of NRC Insulation. M. P. Hnilicka, Cryogenic Engineering, Vol. 5, Plenum Press, 1960, p. 201.
5. Cryogenic Insulation Development. S. T. Stoy, Cryogenic Engineering, Vol. V, Plenum Press, 1960, p. 219.



## 6

## TRANSFER

Discussion of liquid hydrogen transfer can be broken into two topics: the cooldown characteristics associated with introducing cryogenic hydrogen into ambient temperature containers, and the transfer method used.

## 6.1 COOLDOWN CHARACTERISTICS

6.1.1 INTRODUCTION. When liquid hydrogen enters a warm transfer line, a liquid front forms. The incoming liquid advances a considerable distance down the line before being halted by the back pressure from the boiloff gas. Since the initial surge causes the liquid to contact a large area of line wall, the amount of gas formed normally exceeds the line-venting capacity, causing the liquid flow to reverse. The initial surge and reverse flow is followed by other surges of diminishing magnitude, decreasing gradually to a steady flow rate. The changing frequency (F) of these pressure oscillations can be predicted by the following equation:

$$F = \frac{1}{2\pi} \left( \frac{\gamma P}{l_g l_l \rho_l} \right)^{1/2} \quad (\text{Ref. 1})$$

where

$$\gamma = c_p/c_v \text{ of LH}_2,$$

$$P = \text{transfer pressure,}$$

$$l_g = \text{length of line filled with gas,}$$

$$l_l = \text{length of line filled with liquid,}$$

$$\rho_l = \text{liquid hydrogen density.}$$

## GENERAL DYNAMICS | ASTRONAUTICS

If a person stationed himself on the downstream side of the line, and looked through a glass window in the line, he would observe the following phenomena during the cool-down period:

Initially, gas would pass the window followed by droplets of liquid. Next, pulses of liquid flashing into gas would move down the line followed by an advancing front of stratified flow, both smooth and vigorously boiling. The stratified flow would be of short duration and would be almost immediately cleared out by slugs of liquid hydrogen. Progressing rapidly through the pipe, these slugs would occur more frequently until they eventually coalesced and filled the pipe. At this time the wall temperature approaches the liquid temperature and single-phase flow would be observed.

**6.1.2 CONDITIONS NECESSARY FOR SINGLE-PHASE FLOW.** Steady-state transfer of liquid hydrogen should be accomplished with single-phase flow rather than two-phase flow. Higher flow rates are possible and excessive pressure drops are avoided. The flow process is also considerably more predictable than two-phase flow. Consequently, it is desirable to be able to calculate under what conditions single-phase flow is maintained.

The following equation predicts what total pressure (P) is required at the inlet to maintain single-phase flow for a given heat input, flow rate, and size of transfer line:

$$P = P_f \text{ (pressure required by pipe friction)} \\ + P_{vp} \text{ (vapor pressure of liquid hydrogen)}$$

where:

$$P_f = \frac{0.1197 (\dot{m}^{1.821}) L}{D^{4.821}}$$

$$\log P_{vp} = 2.93029 - \frac{79.8210}{T + \frac{L}{\dot{m} c_{p,l}}} + 0.02093 \left( T + \frac{qL}{\dot{m} c_{p,l}} \right) \quad \text{(Ref. 2)}$$

$\dot{m}$  = LH<sub>2</sub> mass flow rate (lb./sec.),

L = line length (ft.),

## GENERAL DYNAMICS | ASTRONAUTICS

- $D$  = internal diameter of line (in.),  
 $T$  =  $\text{LH}_2$  temperature prior to transfer ( $^{\circ}\text{R}$ ),  
 $q$  = heat input to line (Btu/ft.-sec.),  
 $c_{p,l}$  = heat capacity of  $\text{LH}_2$  at constant pressure (Btu/lb.- $^{\circ}\text{R}$ ).

For uninsulated lines, the heat flux is 3,490 Btu/hr.-ft.<sup>2</sup> in still ambient air; in a 15-mph wind, the value is 6,020 Btu/hr.-ft.<sup>2</sup>. Heat inputs through insulated lines can be calculated using appropriate thermal conductivity values given in Chapter 5.

**6.1.3 COOLDOWN TIME FOR INSULATED LINES.** The time it takes for a transfer system to cool down to liquid hydrogen temperature can be estimated, approximately, with the following equation:

$$\tau \text{ (cooldown time)} = \frac{\Sigma(m_m)(\bar{c}_m)(\Delta T_m)}{(\bar{w}_2)(\Delta H)} \quad (\text{Ref. 3})$$

where:

- $\Sigma$  = summation,  
 $m_m$  = system cooldown mass,  
 $\bar{c}_m$  = temperature mean specific heat of cooldown mass,  
 $\Delta T_m$  = temperature change of cooldown mass,  
 $\bar{w}_2$  = time mean rate of mass flow of cooldown gas leaving system,  
 $\Delta H$  = latent heat of vaporization of  $\text{LH}_2$ .

Since  $\bar{c}_m$ ,  $\Delta T_m$ , and  $\Delta H$  are known, only  $m_m$  and  $\bar{w}_2$  have to be calculated.

**6.1.3.1 Calculation of Cooldown Mass.** If the transfer line consists of a thin-walled tube, the entire mass will cool to  $\text{LH}_2$  temperatures; therefore, the weight of the tube equals the cooldown mass ( $m_m$ ). However, if the line contains relatively thick sections such as valves and flanges, only partial cooldown occurs. A method for estimating the cooldown of the concentrated masses in the system is shown in Figure 20.

## GENERAL DYNAMICS | ASTRONAUTICS

This method involves the division of a given piece of concentrated mass into a series of slabs, and the calculation of the cooldown history from unidirectional transient conduction theory.

To make use of this plot, first calculate a cooldown time neglecting the concentrated masses. Next, represent each concentrated mass by an equivalent slab and obtain the percentage of cooldown from Figure 20. Add this percentage of the concentrated mass to the distributed mass. The total is used for calculation of a new cooldown time. Repeat the iterative process until the answer converges.

### 6.1.3.2 Calculation of Discharge Gas Flow Rate.

Unrestricted Gas Flow. The mass flow rate ( $w_2$ ) for unrestricted gas flow is a function of  $\frac{2f(L_e)}{D}$  and the ratio of the exit pressure ( $P_2$ ) to the supply pressure ( $P_1$ ) as shown in Figure 21, where:

$f$  = friction factor,

$L_e$  = equivalent length,

$D$  = internal diameter of transfer line.

To calculate  $w_2$  from Figure 21, the friction factor ( $f$ ) and equivalent length ( $L_e$ ) must be determined. The supply pressure, ( $P_1$ ), cross-sectional area of the pipe ( $A_1$ ), internal diameter of the line ( $D$ ), exit pressure ( $P_2$ ) (normally 15 psia), and constant ( $K$ ) are all known.

The friction factor ( $f$ ) can be determined if the flow turbulence is known. Values of  $f$  for smooth tubing are shown in Figure 22 as a function of the reynolds number ( $R_e$ ). If the reynolds number cannot be calculated, a good estimate for  $f$  is 0.002 to 0.003 since  $R_e$  is normally between  $10^6$  and  $10^7$  during cooldown.

The equivalent length of a transfer line takes into account pressure drops due to bends and obstructions. Therefore, by definition, the equivalent length equals the actual length for straight smooth tubing. Since this calculation is applicable only to unrestricted gas flow, the effect of bends is discussed here and the effect of obstructions is included in the following section on restricted flow.

GENERAL DYNAMICS | ASTRONAUTICS

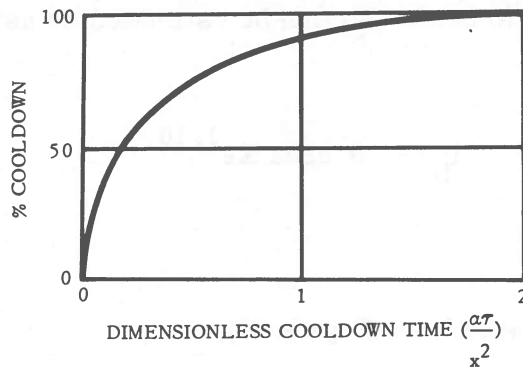


Figure 20. Percent cooldown of concentrated masses.

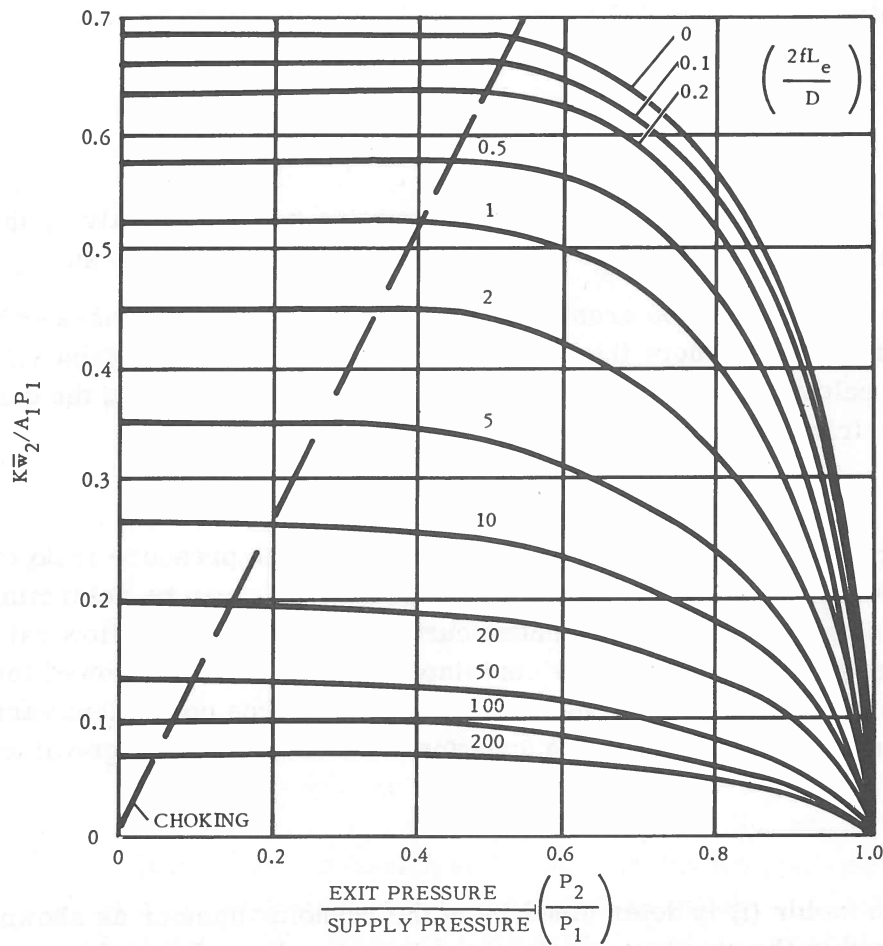


Figure 21. Dimensionless parameters for calculating mass flow rate ( $\bar{w}_2$ ) of discharge gas for unrestricted flow.

## GENERAL DYNAMICS | ASTRONAUTICS

The equivalent length due to bends ( $l_b$ ) can be estimated by using the following equation:

$$l_b = 0.0202 X \epsilon^{1.10}$$

where

$X$  = proportionality constant (see Figure 23),

$\epsilon$  = angle subtended by bend (deg.).

This value of  $l_b$  is added to the actual length of the line ( $L$ ) to get the total equivalent length ( $L_e$ ),

$$L_e = L + \Sigma l_b$$

**Restricted Gas Flow.** For the case of end restriction (i. e., vent valve), the gas flow rate becomes a function of the ratio of the discharge pressure to the supply pressure,  $\frac{2f(L_e)}{D}$ , and the area ratio (tube cross-section,  $A_1$ , over orifice cross-section,  $A_2$ ). For adiabatic flow cases where the discharge gas flow rate equals Mach 1, Figure 24 can be used to calculate  $w_2$ . The unknowns to be determined include the discharge pressure ( $P_2$ ), friction factor ( $f$ ), and equivalent length ( $L_e$ ).

The discharge pressure ( $P_2$ ) can be calculated from the pressure ratio curves in Figure 25 since  $P_1$ ,  $A_1$ ,  $A_2$ , and  $D$  are known and  $f$  and  $L_e$  can be determined as shown in the following paragraphs. These curves are plotted for a flow rate of Mach 1 at the discharge point. The flow rate contained in Figure 24 has allowed for contraction losses (vena contracta) at the orifice. Since the orifice coefficient varies between 0.7 and 0.9 for the pressure ratios in question at Mach 1, an average value of 0.8 was used.

The friction factor ( $f$ ) is determined from the Reynolds number as shown in Figure 22 and discussed in the previous section on unrestricted gas flow. For smooth tubing during cooldown, it normally varies between 0.002 and 0.003.



GENERAL DYNAMICS | ASTRONAUTICS

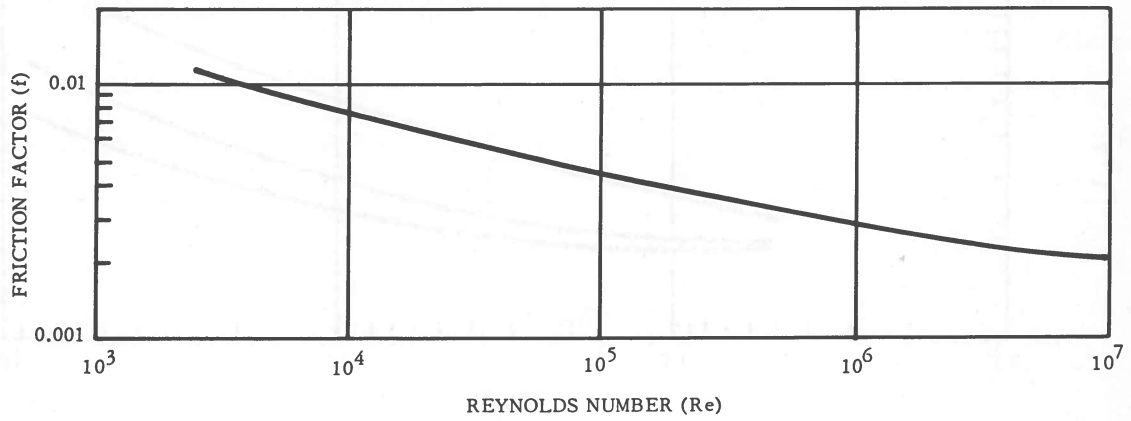


Figure 22. Friction factor as a function of reynolds number.

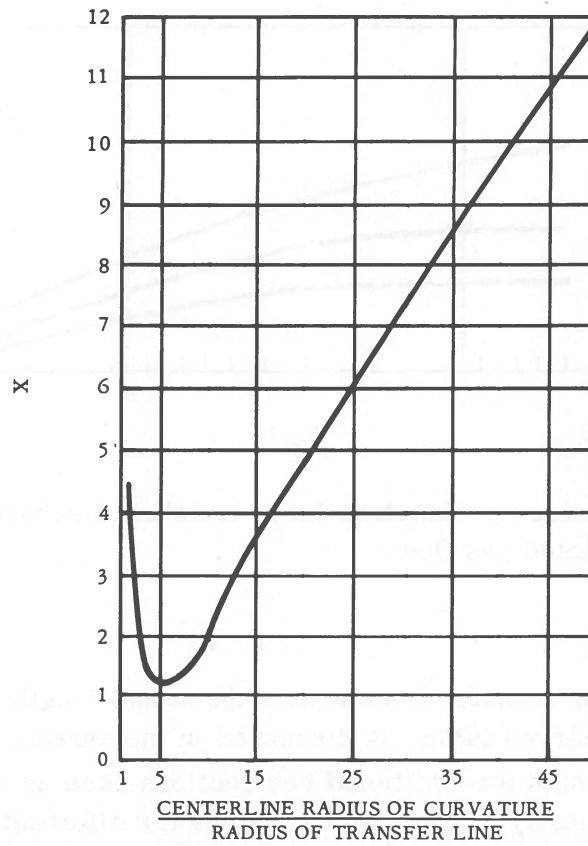


Figure 23. Proportionality constant for curved lines.

GENERAL DYNAMICS | ASTRONAUTICS

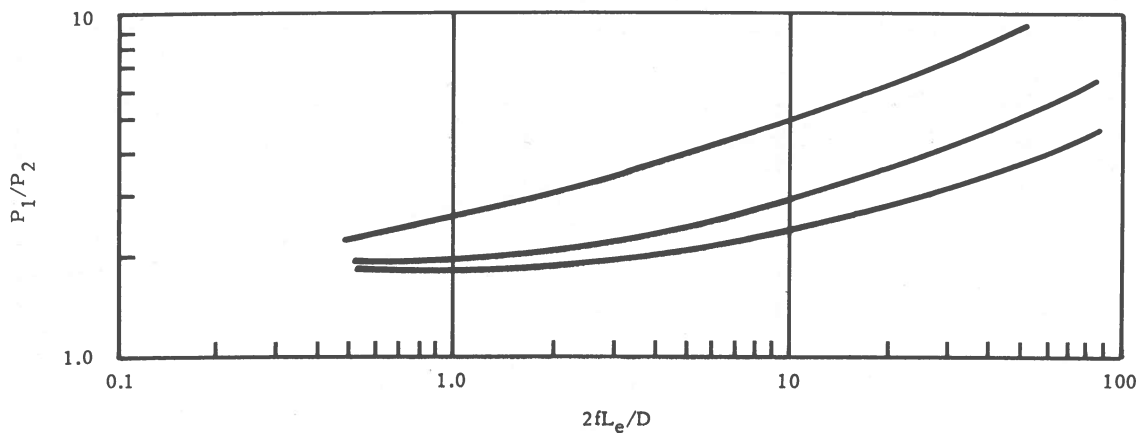


Figure 24. Dimensionless parameters for calculating mass flow rates ( $\bar{w}_2$ ) of discharge gas for restricted flow.

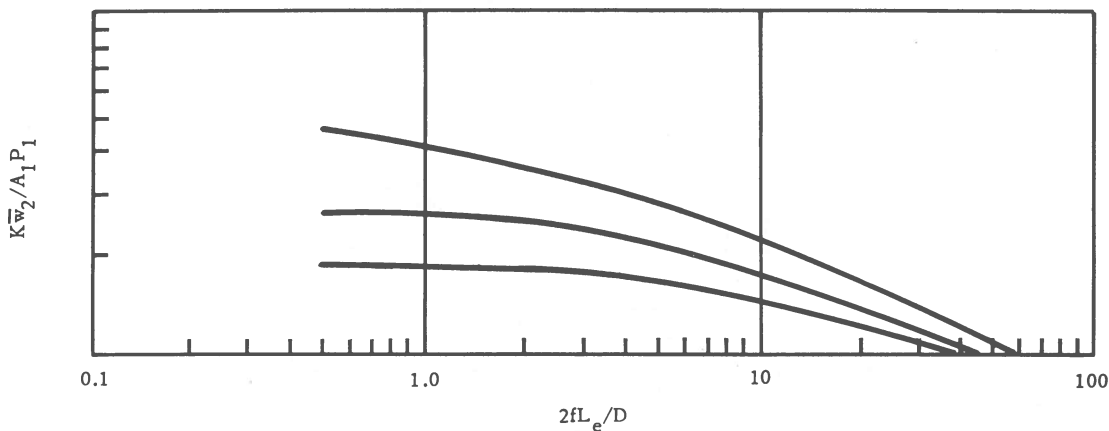


Figure 25. Dimensionless parameters for calculating discharge pressure ( $P_2$ ) for restricted gas flow.

The equivalent length for transfer lines equals the actual length for straight tubing and can be calculated for curved tubing as discussed in the unrestricted gas flow section. The equivalent length for additional obstructions such as valves and couplings must be determined empirically. Some typical values for different screwed fittings and valves are shown in Table VIII (Ref. 4). (Although screwed fittings are never used

## GENERAL DYNAMICS | ASTRONAUTICS

in LH<sub>2</sub> systems, these values do give some insight into the pressure drops that will be encountered. Most hydrogen couplings have a smooth interior, however, so the equivalent lengths would be somewhat less than those listed.) The total equivalent length of the line can be represented by the following equation:

$$L_e = L + \Sigma l_b + \Sigma l_o$$

where

$L$  = actual line length,

$l_b$  = equivalent lengths of bends,

$l_o$  = equivalent lengths of miscellaneous obstructions.

All of these calculations for restricted gas flow apply only to a discharge velocity of Mach 1. For cases where the exit velocity is less than Mach 1, a trial and error solution must be performed.

Table VIII. Equivalent lengths of screwed fittings and valves.

FITTING	EQUIVALENT LENGTH ( $l_o$ ) (IN LINE DIAMETERS)
45° ELBOWS	15
90° ELBOWS (STANDARD RADIUS)	32
90° SQUARE ELBOWS	60
180° CLOSE RETURN BENDS	75
T'S (USED AS ELBOW, ENTERING RUN)	60
T'S (USED AS ELBOW, ENTERING BRANCH)	90
GATE VALVES (OPEN)	7
GLOBE VALVES (OPEN)	300
ANGLE VALVES (OPEN)	170

6.1.4 LH<sub>2</sub> COOLDOWN MASS. The mass of LH<sub>2</sub> needed to cool down a transfer system depends on the flow rates used and length of the transfer line. For high flow

## GENERAL DYNAMICS | ASTRONAUTICS

rates and short transfer lines, the following equation approximates the LH<sub>2</sub> cooldown mass ( $m_l$ ) required:

$$m_l = \frac{m_m \bar{c}_m \Delta T}{\Delta H}$$

This equation assumes the gas is being vented at saturation temperatures (maximum case).

For low flow rates and long transfer lines, the following equation is applicable:

$$m_l = \frac{(m_m)(\bar{c}_m)(\Delta T)}{\Delta H + (\bar{c}_g)(\Delta T)}$$

where

$m_m$  = cooldown mass,

$\bar{c}_m$  = mean specific heat of cooldown mass,

$\Delta T$  = temperature change,

$\Delta H$  = latent heat of vaporization of LH<sub>2</sub>,

$\bar{c}_g$  = mean specific heat of hydrogen gas over  $\Delta T$  range.

This equation assumes the gas warms to ambient temperature before being vented (minimum case). For flow rates and line lengths between these two extreme cases, the cooldown mass of LH<sub>2</sub> will be bracketed between the maximum and minimum cases.

### 6.2 TRANSFER METHODS

As for cost, transfer of LH<sub>2</sub> in ground-based systems is more economically accomplished by dewar pressurization rather than by pumps for batch deliveries of 25,000 gal. or less and at flow and pressure combinations to 10,000 gpm and 200 psi. For delivered-liquid requirements of 25,000 to 500,000 gal., the flow and pressure combination required strongly influences the choice of the system having the lowest cost.

## GENERAL DYNAMICS | ASTRONAUTICS

It can be generally stated, however, that as the delivered-liquid requirements vary from 25,000 to 50,000 gal. and as the pressures increase to 200 psi, pumps become more favorable and pressurization systems less favorable in cost.

For airborne systems, combination pump-pressurization systems are used exclusively for the following reason: Gas pressurization systems require high pressures and consequently excessively heavy tanks to maintain the flow rates required. The combined pressurization system with the pump is needed to maintain an NPSH and prevent cavitation.

Advanced propulsion systems with low mass transfer and low chamber pressure requirements may use pressurized transfer due to its inherent reliability and simplicity.

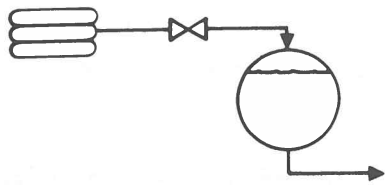
Several possibilities exist for transferring hydrogen at zero gravity. These methods are discussed in Section 6.2.3.

**6.2.1 GAS PRESSURIZATION.** Only two gases can be used to pressurize liquid hydrogen, hydrogen and helium. All other gases condense at this temperature. Helium is normally obtained from commercial high-pressure storage bottles. Hydrogen, on the other hand, may be obtained as high-pressure bottled gas or by vaporizing some of the stored liquid hydrogen. There are several possible variations to these transfer techniques as shown in Figure 26. For example, the vaporized gas can be stored in high-pressure bottles until required for transfer or admitted directly to the storage-vessel ullage. Both pumps and gravity flow have been used in actual designs to circulate  $LH_2$  to the heat exchangers.

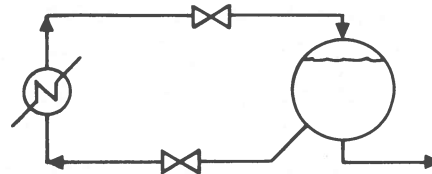
For ground-based  $LH_2$  transfer systems, it is necessary to know the pressurant gas requirements in order to specify sufficiently large transfer lines, heat exchangers, storage bottles, pumps, and compressors. For flight stages, it is even more critical to know the pressurization gas requirement for maintaining NPSH on the pump, in order to accurately calculate the weight of propellant required for pressurant. When pressurizing liquid hydrogen by warm gaseous hydrogen, there is a heat and mass exchange (condensation or evaporation) at the liquid-gas interface and at the cold inner walls of the ullage space in the tank (see Figure 27). These exchange processes at the boundaries of the ullage volume determine how much gas is required to pressurize a tank and displace a given amount of liquid.

The pressurization gas requirements can be bracketed between maximum and minimum limits by assuming: (1) the gas will be cooled to saturation, or (2) the gas will

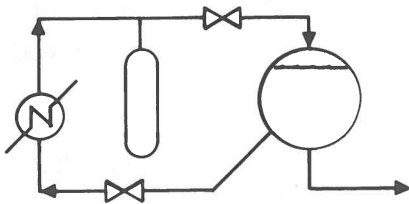
GENERAL DYNAMICS | ASTRONAUTICS



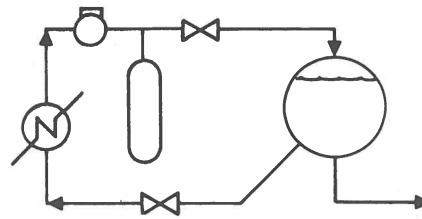
BOTTLED GAS SYSTEM



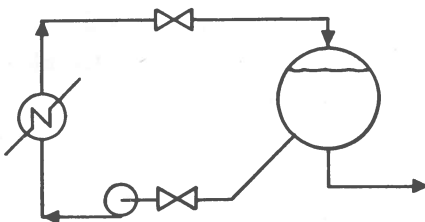
GRAVITY-FED, VAPORIZED GAS SYSTEM



STORED, VAPORIZED GAS SYSTEM (GRAVITY FED)



COMPRESSED & STORED, VAPORIZED GAS SYSTEM (GRAVITY FED)




PUMP-FED, VAPORIZED GAS SYSTEM

SYMBOLS:

 BOTTLED GAS (H<sub>2</sub> OR He)

 VALVE

 LH<sub>2</sub> STORAGE

 HEAT EXCHANGER

 GH<sub>2</sub> STORAGE

 COMPRESSOR


 PUMP

Figure 26. Typical gas-pressurization transfer systems.

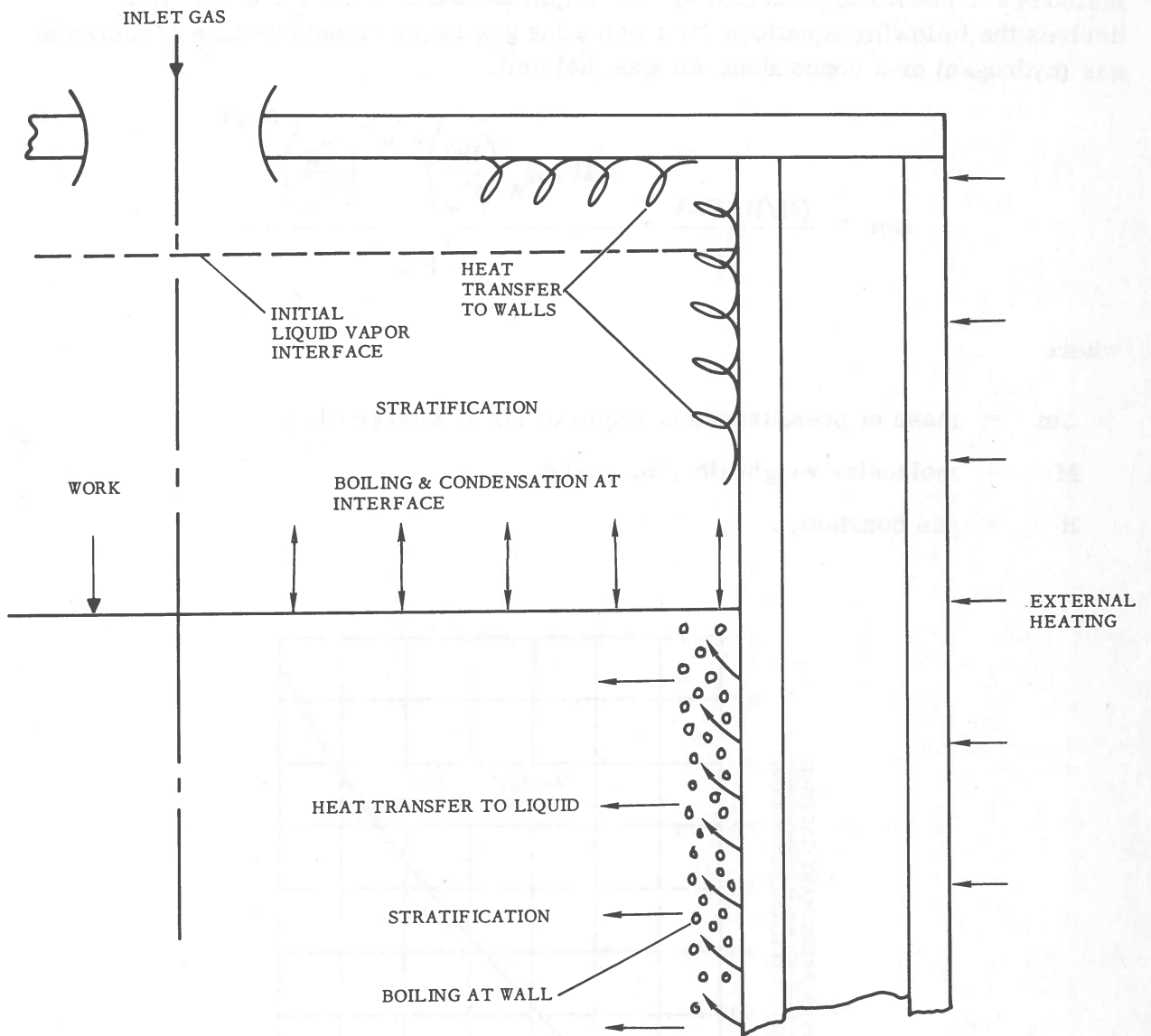


Figure 27. Tank pressurization analytical model.

## GENERAL DYNAMICS | ASTRONAUTICS

remain at the same temperature at which it entered the tank. As can be seen from Figure 28, the range between the maximum and minimum case is so wide that other methods are needed to calculate the gas requirements more accurately. Ref. 5 derives the following equations for calculating gas requirements using a condensable gas (hydrogen) or a noncondensable gas (helium):

$$\Delta m \approx \frac{(M/R) P \Delta V}{T_i} + \frac{0.150 Q_w \left( \frac{H\Theta}{C_w} \right)^{0.63} \left( \frac{C_g}{C_w} \right)^{0.40}}{c_{p,g} T_i}$$

where

- $\Delta m$  = mass of pressurant gas required for discharge (lb.),
- $M$  = molecular weight (lb./lb.-mole),
- $R$  = gas constant,

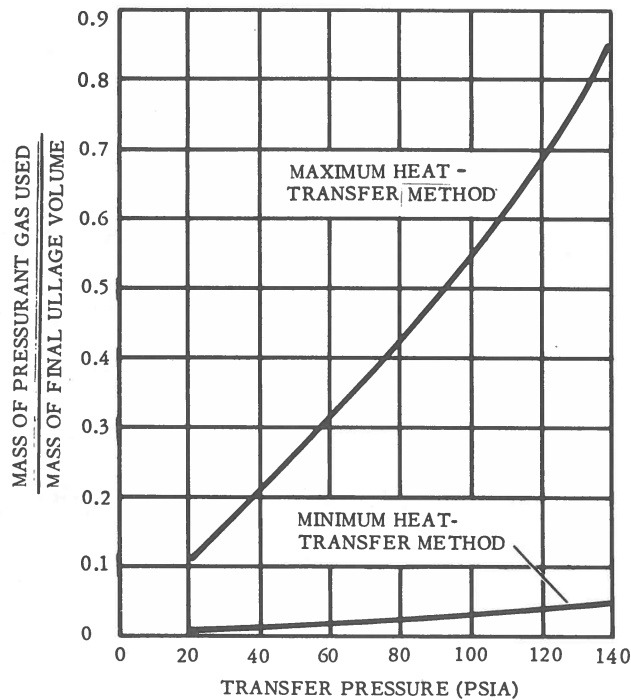


Figure 28. Maximum and minimum limits for pressurant gas requirements.



## GENERAL DYNAMICS | ASTRONAUTICS

- P** = tank pressure (psi),  
 **$\Delta V$**  = volume change of gas phase during discharge (cu. ft.),  
 **$T_i$**  = temperature of inlet gas ( $^{\circ}\text{R}$ ),  
 **$Q_w$**  = heat transferred to tank wall if wall heats to temperature of inlet gas (Btu),  
**H** = average heat-transfer coefficient between gas and wall (Btu/hr.-ft.<sup>2</sup>- $^{\circ}\text{R}$ ),  
 **$\Theta$**  = discharge time (hr.),  
 **$C_w$**  = mean heat capacity of wall per unit wall area ( $\overline{c_{p,w}}(\overline{\rho}_w)(\delta)$ ), (Btu/ $^{\circ}\text{R}$ -ft.<sup>2</sup>),  
 **$C_g$**  = mean heat capacity of gas phase per unit wall area ( $\overline{c_{p,g}}(\overline{\rho}_g)(D)$ ), (Btu/ $^{\circ}\text{R}$ -ft.<sup>2</sup>),  
 **$c_{p,g}$**  = specific heat of gas at constant pressure (Btu/lb.- $^{\circ}\text{R}$ ),  
 **$c_{p,w}$**  = specific heat of tank wall (Btu/lb.- $^{\circ}\text{R}$ ),  
 **$\rho_g$**  = density of gas (pcf),  
 **$\rho_w$**  = density of tank wall (pcf),  
 **$\delta$**  = wall thickness (ft.),  
**D** = inner tank wall diameter (ft.).

To solve the equation, the individual terms are calculated as follows:

1. All gas properties are evaluated at an average temperature between the inlet pressurant gas and saturation unless otherwise specified.
2. H is calculated from

$$H = 0.13 \frac{k_g}{y} \left[ \left( \frac{y^3 \rho_g^2 g \beta \Delta T}{\mu^2} \right) \left( \frac{c_{p,g} \mu}{k} \right) \right]$$

where

**$k_g$**  = thermal conductivity of gas (Btu/hr.-ft.<sup>2</sup>- $^{\circ}\text{R}$ ),

## GENERAL DYNAMICS | ASTRONAUTICS

- y = length of tank discharged (ft.),
- g = local gravitational acceleration (fps<sup>2</sup>),
- $\beta$  = thermal coefficient of expansion of tank wall per °R,
- $\Delta T$  = temperature driving force for heat transfer (°R),
- $\mu$  = viscosity of gas (lb./ft.-sec.).

$\Delta T$  has been found to average about 175°R during tests using ambient temperature gas. This value does not have to be known too accurately since H varies as the cube root of  $\Delta T$ .

The general applicability of these equations is not known. For the following test conditions, however, accuracy is within 10% for hydrogen and helium: an upright vacuum-insulated cylindrical tank with gas diffuser to prevent direct gas impingement on liquid surface, volume of 25 cu.ft., tank pressure range of 55 to 164 psi, discharge time range of 90 to 355 sec., ambient temperature pressurant, and no fluid sloshing. Sloshing will increase the heat transfer rate to the liquid as shown in Figure 29. Reference 6 gives another method for estimating gas pressurization requirements and work is being done at Astronautics to derive gas pressurization equations that will have general applicability.

When helium is used as the pressurant gas, a small fraction is soluble in liquid hydrogen. This solubility is shown as a function of pressure in Figure 30.

**6.2.2 PUMP TRANSFER.** Due to the many facets involved in pump design, it is beyond the scope of this section to go into design details. Instead, a brief description will be given of potential problem areas and of key features of LH<sub>2</sub> pump design. The flight-weight Centaur LH<sub>2</sub> pump will be used as an example.

Of all the mechanical pumping systems available, the centrifugal pump has repeatedly demonstrated its superiority over all other types, including the positive-displacement pump. The Centaur uses an axial flow inducer with a mixed-flow impeller-type pump made by the Pesco Division of Borg-Warner Corp. (see Figure 31). As with any mechanical pump, there are potential problem areas which, with careful design, can be solved. The four main problem areas include pump bearings, seals, tolerances between moving parts, and material selection.

**6.2.2.1 Pump Bearings.** The loads transmitted to the shaft of a centrifugal pump are carried principally by antifriction type bearings. The Centaur pumps use steel

# GENERAL DYNAMICS | ASTRONAUTICS

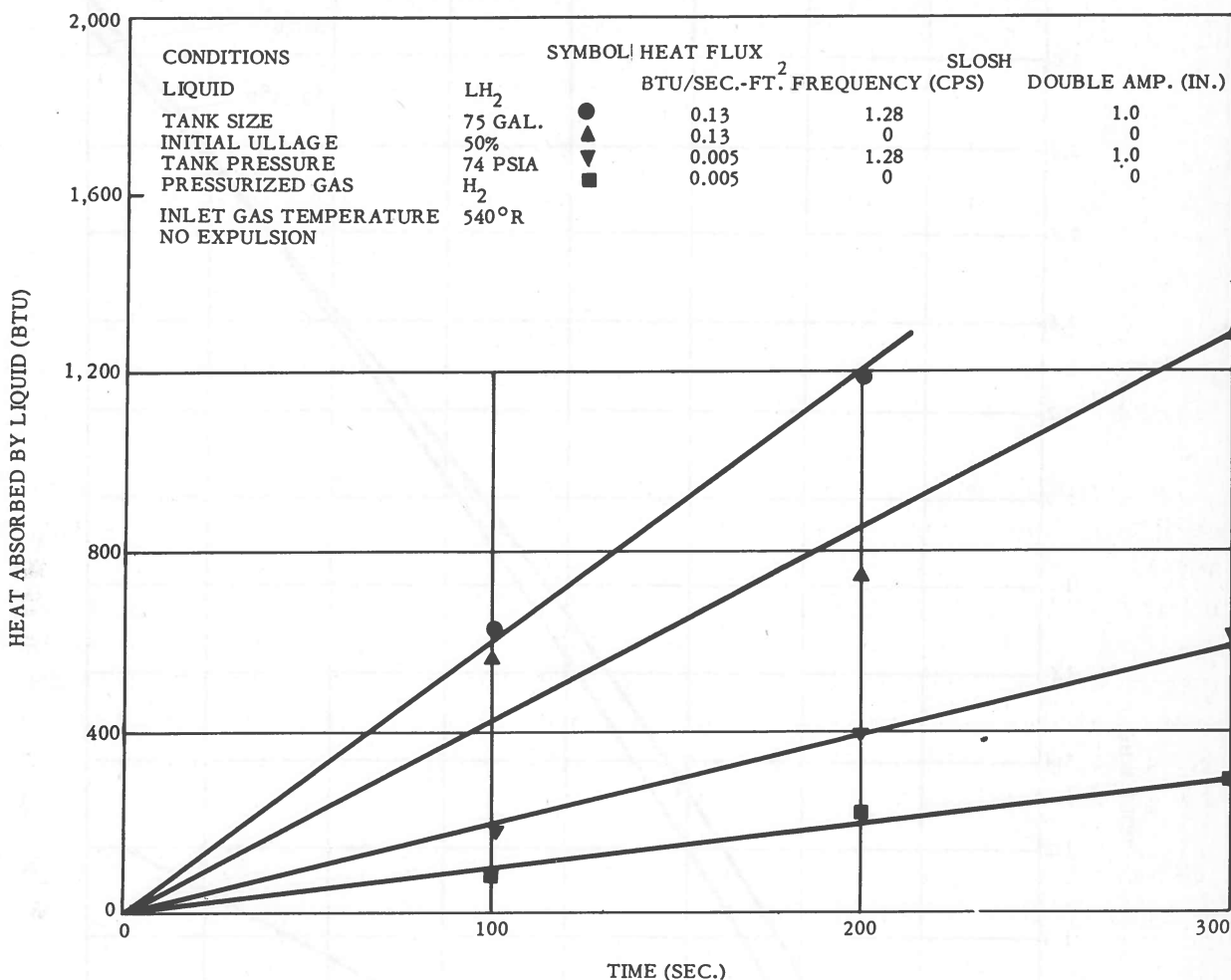


Figure 29. Effect of sloshing on propellant heating.

bearings in micarta cages lubricated by liquid hydrogen during use. When the bearings are operated in liquid hydrogen, contaminants comprised of any material or gas except hydrogen or helium will freeze out. The frozen particles have the same action on the bearings as dirt or grit has on conventionally lubricated bearings, i. e., they cause excessive wear. Consequently, it is important that the pump be purged with hydrogen or helium gas prior to introduction of liquid hydrogen.

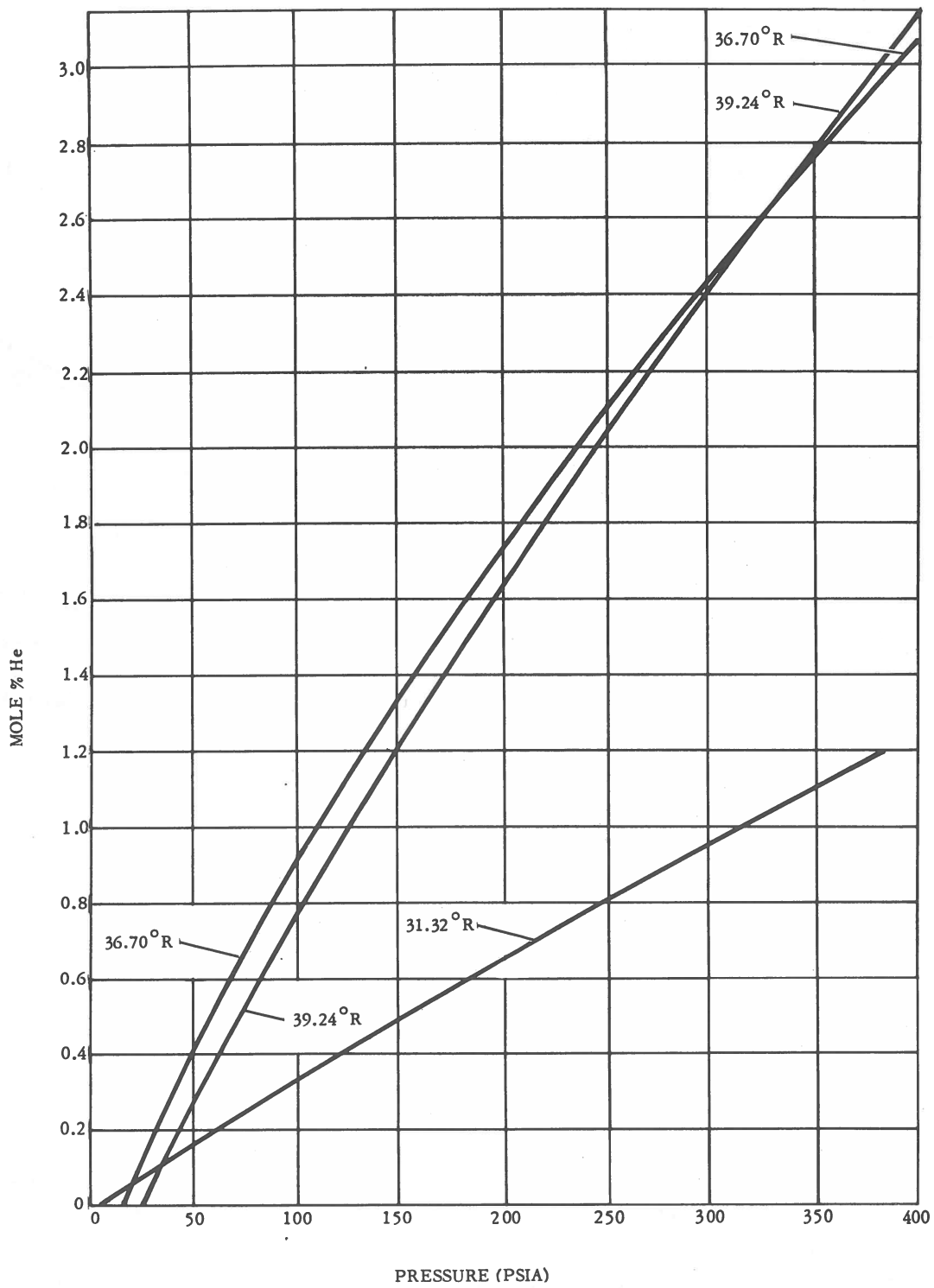


Figure 30. Solubility of helium in liquid hydrogen as a function of pressure.



6.2.2.2 Seals. If the pump is located outside the LH<sub>2</sub> tank, there is a problem of preventing hydrogen gas leakage past the shaft seal. Since it is not possible to prevent some leakage, the volume in the seal labyrinths must be purged with inert gas. Helium is good for this purpose but is expensive; nitrogen gas is acceptable if the seal area is kept above 150°R. When the pump is submerged directly in the fluid, as on Centaur, the shaft leakage is not a problem. Graphite compositions, carbon-impregnated Teflon, Kel-F, and polyurethane seals have all been used successfully.

6.2.2.3 Tolerances and Material Selection. Since the LH<sub>2</sub> pump is normally cooled rapidly to LH<sub>2</sub> temperatures, it is important that the thermal contraction coefficients of materials used are known accurately so the proper tolerances can be specified. For example, rapid cooling of improperly designed bearings could result in flattening, leading to rapid bearing failure. In addition, it is important that the materials do not become brittle at LH<sub>2</sub> temperatures. Material selection is discussed in Chapter 4.

Other design area considerations include head-capacity performance, cavitation performance, and pump insulation.

6.2.2.4 Head-Capacity Performance. The LH<sub>2</sub> head-capacity performance of a centrifugal pump is identical (with only minor differences) to its water performance and to the performance obtained with liquids which have viscosities equal to or less than water.

6.2.2.5 Cavitation Performance. The cavitation performance of pumps operated with liquid hydrogen is better than water or liquid nitrogen performance. NPSH requirements of the order of a few inches to a few feet are sufficient to prevent cavitation and subsequent deterioration of performance when handling LH<sub>2</sub>.

For multiple restarts in space under low-g, it is important that the liquid flow not vortex as it enters the pump. Antivortex devices described in Chapter 10 will prevent this type of fluid motion. When selecting pumps for a low-g restart capability, the suction specific speed (S) is used as a comparison parameter between pumps for defining the appearance of cavitation surging, as follows:

$$S = \frac{N(\dot{m})^{1/2}}{(H_{sv})^{3/4}}$$

## GENERAL DYNAMICS | ASTRONAUTICS

where

- N = pump speed (rpm),
- $\dot{m}$  = pump flow (gpm),
- $H_{sv}$  = net positive suction head.

Higher values of S permit lower pump NPSH requirements and more reliable operation with low liquid levels and low tank pressures.

6.2.2.6 Pump Insulation. The immersed pump has no insulation problem. When the pump is not immersed, it can be placed in an evacuated box filled with powder insulation (see Chapter 5). Sealed, foamed-in-place polyurethane insulation is also adequate for reducing the heat leak into the pump casing.

6.2.3 TRANSFER AT ZERO G. When a space vehicle is put in orbit about a planet or is coasting in a transfer ellipse to another planet, the liquid hydrogen no longer remains settled in the bottom of the tank but flows over the walls as described in Chapter 12. To restart the engines, it is necessary to have the pump inlet covered with a sufficient depth of fluid to prevent the pump from cavitating upon initial startup. For pumps requiring high flow rates, the safest method for ensuring single phase flow is to accelerate the vehicle approximately 0.01g with settling rockets. For small rocket engines with low mass flow rate requirements, or for auxiliary power units that have to operate during zero g, there are other methods for transferring the fluid. These include:

1. Storing the hydrogen as cold high-pressure gas slightly above its critical temperature.
2. Expelling the fluid with positive-displacement devices such as pistons, bladders, and bellows.
3. Separating the gas phase from the liquid using centrifugal acceleration. This principle is used on the Centaur zero-g separator described in Section 12.3.2.
4. Using capillary tubes that would be filled by the all-wetting liquid hydrogen.

All four systems will function but some have inherent advantages over the others. Cold-gas hydrogen bottles ensure single-phase flow but incur a significant weight penalty due to the heavy tank wall required and smaller quantity of hydrogen that can be stored when compared to liquid storage. Positive-displacement bladders such as

## GENERAL DYNAMICS | ASTRONAUTICS

triple-ply 1/4-mil Mylar bags have been tested successfully in liquid hydrogen (Ref. 7). The Mylar withstood the flexing and folding required of this type of device. The system is lightweight but does not ensure single-phase flow of the liquid due to trapped gas pockets. For transfer at low rates, this may not be serious. Centrifugal separators are considerably more complicated than the cold-gas and bladder systems. They require dynamic seals in LH<sub>2</sub> and must be powered by an auxiliary unit or by the tank pressurization gas. Capillary tube transfer systems are limited by their low transfer rates.

In summary, for high mass rate of transfer, settling rockets appear to be the safest solution. Cold-gas storage and bladder devices appear promising for low-rate-of-transfer systems that operate at zero g.

### 6.3 NOMENCLATURE

A	internal cross-sectional area of the line
c	heat capacity
$\bar{c}$	mean heat capacity
$C_g$	mean heat capacity of gas phase per unit wall area ( $\bar{c}_{p,g} \bar{\rho} D$ ), (Btu/°R-ft. <sup>2</sup> )
$C_w$	mean heat capacity of wall per unit wall area ( $\bar{c}_{p,w} \bar{\rho}_w \delta$ ), (Btu/°R-ft. <sup>2</sup> )
D	internal diameter of container (line or tank)
f	friction factor
F	frequency
g	local gravitational acceleration (fps <sup>2</sup> )
H	average heat transfer coefficient between gas and wall (Btu/hr.-ft. <sup>2</sup> -°R)
$\Delta H$	latent heat of vaporization of LH <sub>2</sub>
$H_{sv}$	net positive suction head
k	thermal conductivity
$\bar{k}$	mean thermal conductivity
K	constant (~ 30 sec.)
$\ell$	partial transfer line length
L	total transfer line length



## GENERAL DYNAMICS | ASTRONAUTICS

$\dot{m}$	liquid hydrogen mass flow rate
$m$	mass
$\Delta m$	mass of pressurant gas required for discharge (lb.)
$M$	molecular weight of pressurant gas (lb./lb.-mole)
$N$	pump speed (rpm)
$P$	pressure
$q$	heat input to line
$Q_w$	heat transferred to tank wall if wall heats to temperature of inlet gas (Btu)
$R$	gas constant
$Re$	reynolds number
$S$	suction specific speed
$T$	absolute temperature
$\Delta T$	temperature difference
$\Delta T$ (Section 6.3.1)	temperature driving force for heat transfer ( $^{\circ}R$ )
$\Delta V$	volume change of gas phase during discharge (cu. ft.)
$\bar{w}$	time mean rate of mass flow of cooldown gas
$W$	$LH_2$ mass flow
$x$	thickness of equivalent slab
$X$	proportionality constant (see Figure 23)
$y$	length of tank discharged (ft.)

### 6.4 SUBSCRIPTS

1	refers to starting point on transfer line
2	refers to liquid or gas discharge point in transfer line
b	equivalent length of curved line
e	equivalent length
f	pipe friction

## GENERAL DYNAMICS | ASTRONAUTICS

g	gas
i	inlet gas
l	liquid hydrogen
m	cooldown mass
o	equivalent length of obstructions
p	constant pressure
v	constant volume
vp	vapor pressure
w	tank wall

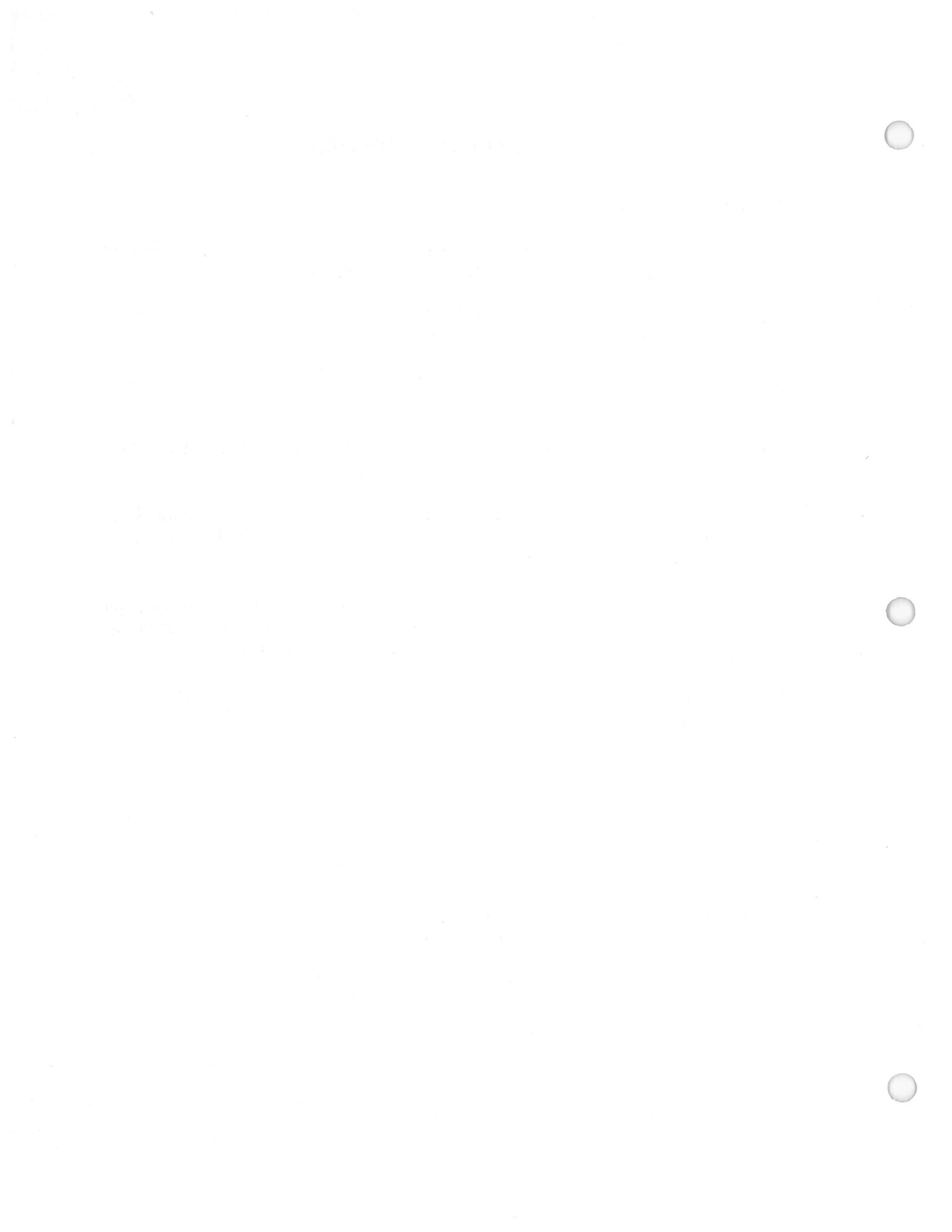
### 6.5 GREEK SYMBOLS

$\alpha$	thermal diffusivity of concentrated mass $\frac{\bar{k}}{\bar{\rho} \bar{c}_p}$
$\beta$	thermal coefficient of expansion of tank wall per °R
$\gamma$	$\frac{c_p}{c_v}$ of LH <sub>2</sub>
$\delta$	wall thickness (ft.)
$\epsilon$	angle subtended by line bend
$\Theta$	discharge time (hr.)
$\mu$	viscosity of gas (lb./ft.-sec.)
$\rho$	density
$\Sigma$	summation
$\tau$	cooldown time

## GENERAL DYNAMICS | ASTRONAUTICS

### REFERENCES

1. Problems in Cool-Down of Cryogenic Systems. J. C. Bronson, et al., *Advances in Cryogenic Engineering*, Vol. 7, Plenum Press, 1961, p. 202.
2. Single-Phase Flow Tests with Liquid Hydrogen. D. H. Pope, et al., *Advances in Cryogenic Engineering*, Vol. 5, Plenum Press, 1959, p. 444.
3. Storage, Transfer and Servicing Equipment for Liquid Hydrogen. B. M. Bailey, et al., WADC Tech. Report 59-386, July 1959, p. 248.
4. Chemical Engineer's Handbook. J. H. Perry, 3rd Ed., McGraw-Hill Book Co., Inc., N.Y., 1950, p. 390.
5. Gas Requirements in Pressurized Transfer of Liquid Hydrogen. D. F. Gluck and J. F. Kline, *Advances in Cryogenic Engineering*, Vol. 7, Plenum Press, 1961, p. 231.
6. An Analytical Method for Estimating Gas Requirements in the Pressurization and Transfer of Cryogenic Fluids. D. C. Bowersock Jr. and R. C. Reid, *Advances in Cryogenic Engineering*, Vol. 6, Plenum Press, 1960, pp. 261-271.
7. Expulsion Bladders for Cryogenic Fluids. B. J. Hunter, et al., *Advances in Cryogenic Engineering*, Vol. 7, Plenum Press, 1961, pp. 155-162.





## LIQUID HYDROGEN MEASUREMENTS

### 7.1 INTRODUCTION

Techniques for measuring the physical characteristics of liquid hydrogen are, in many ways, quite similar to other cryogenic fluids but have some significant differences. These differences are:

1. At LH<sub>2</sub> temperatures, the change in resistance of metals is low; consequently, many of the temperature-measuring resistive probes are not very sensitive in this range.
2. Liquid hydrogen's low density, 1/14 that of water, affects differential level sensors which rely on head pressures.
3. Liquid hydrogen's flammability in air dictates explosionproof design in electrical measuring probes. Special safety procedures are also required.
4. Hydrogen's high specific heat, 15 times that of air, affects the operation of the hot-wire liquid/gas probes.

### 7.2 TEMPERATURE MEASUREMENTS

Many temperature probes have been tested at Astronautics in an attempt to determine which device yields the most accurate temperature data. The results of these tests have shown platinum resistance thermometers to be the best transducers for field and flight temperature measurements (see Figure 32).

**7.2.1 PLATINUM RESISTANCE THERMOMETERS.** The main reasons for utilizing platinum resistance thermometers are:

1. Their stability.
2. The simple calibration requirements.
3. Their versatility. Some transducers may be utilized over a temperature range of 30° to 2,200°R or over any portion of this range.

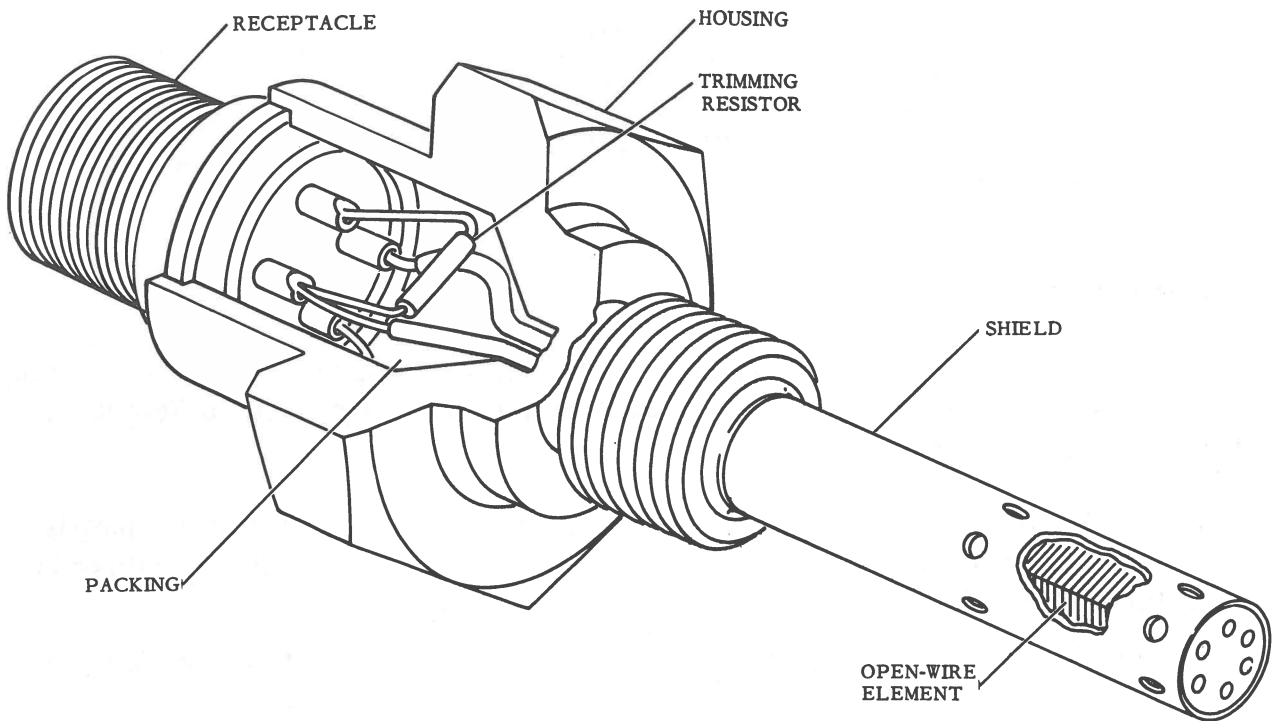


Figure 32. Platinum resistance thermometer.

4. The amount of information available from the National Bureau of Standards on the resistance vs. temperature characteristics of platinum. This is used in establishing calibration curves.
5. Ruggedness of existing element designs.
6. Relatively high output levels.

The methods used by Astronautics (for space vehicles and in the test labs) to measure LH<sub>2</sub> temperatures are outlined in the following paragraphs.

Platinum resistance thermometers are purchased from a reliable vendor. (Excellent results have been obtained with transducers from the Rosemount Engineering Co.). The Standards Laboratory measures the resistance of the transducers at several known temperatures. Liquid nitrogen, liquid oxygen, and ice temperatures are most commonly used. After the vendor's calibration has been validated, the transducers are placed in stock for issue.

## GENERAL DYNAMICS | ASTRONAUTICS

The temperature transducers which are used on production vehicles are manufactured in accordance with a specification control drawing. The transducer must have a specific base resistance at the low end of the desired range and a specific change in resistance over the total range. An example would be a transducer which has a base resistance of 500 ohms at 30°R and 600 ohms at 55°R.

The purpose of holding a specific resistance as well as resistance change over a specified range is to obtain basically interchangeable transducers. The 500-ohm base resistance is achieved by using an integral-series resistor in the transducer. For example, suppose the platinum element measures  $21 \pm 1$  ohms at 30°R and  $121 \pm 1$  ohms at 55°R. By adding a fixed-series resistor of 479 ohms, the resistance range is raised to the 500- and 600-ohm level.

The resistance bridge used for telemetering flight temperatures is illustrated in Figure 33. All temperature transducers on a given telemetering channel are continuously excited and an output voltage of the same magnitude for all measurements on one channel (approximately 110 mv), is continuously present on each commutator contact.

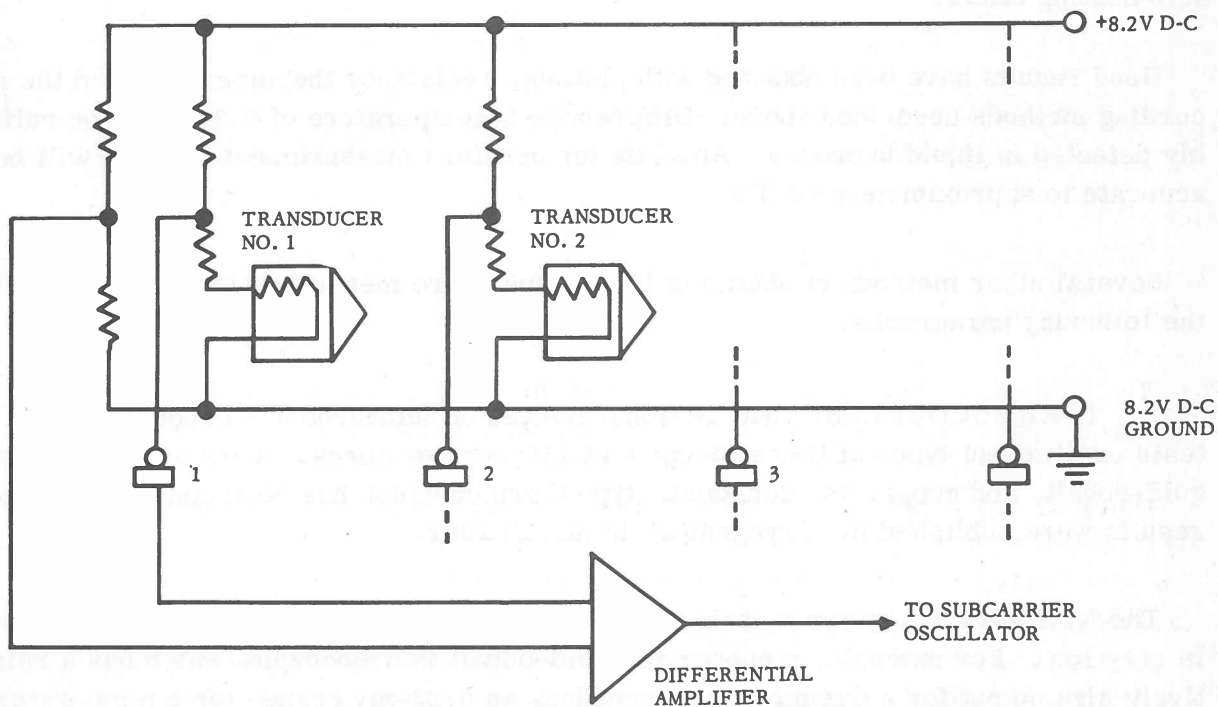


Figure 33. Typical flight vehicle telemetry temperature bridge.

## GENERAL DYNAMICS | ASTRONAUTICS

The bridge legs for each transducer are adjustable so that a variety of temperature ranges can be selected.

Many transducers are used on special engineering tests at Astronautics which do not utilize the standard space vehicle bridge circuit. It is more advantageous for the engineering test laboratories to use a general-purpose bridge circuit which may be used for many transducers and many ranges. This circuit, shown in Figure 34, is a three-wire system to minimize the errors due to the resistance changes of the lead wires. The fourth wire is used for calibration purposes. When switch  $S_1$  is actuated, the fourth wire is substituted for one of the leads connected to the transducer element and the decade box is substituted for the transducer. In this condition, the transducer is shorted and the decade box may be used to simulate the resistance change of the transducer. The padder resistor ( $R_{PAD}$ ) is used to limit the change in resistance of the bridge leg to 5% of the total leg resistance, thus ensuring good linearity. Any transducer which has a minimum resistance change of 10 ohms or a maximum change of 500 ohms may be used with this circuit. The voltage and fine balance controls have been eliminated in Figure 34 for the sake of clarity. The voltage is adjusted to produce 10 mv nominal output or until the current through the transducer element is 2 ma. A nominal 2-ma maximum transducer current has been established to minimize any self-heating effect.

Good results have been obtained with platinum resistance thermometers and the recording methods described above. Differences in temperature of  $0.1^\circ\text{F}$  may be reliably detected in liquid hydrogen. Absolute temperature measurements in  $\text{LH}_2$  will be accurate to approximately  $\pm 0.3^\circ\text{F}$ .

Several other methods of obtaining  $\text{LH}_2$  temperature measurements are outlined in the following paragraphs.

**7.2.2 THERMOCOUPLES.** The National Bureau of Standards has conducted many tests on different types of thermocouples at  $\text{LH}_2$  temperatures. Work with copper vs. gold-cobalt, and copper vs. constantan type thermocouples has been conducted. The results were published in "Cryogenics" in March 1961.

The NBS work has shown that the sensitivity of thermocouples at  $\text{LH}_2$  temperatures is very low. For example, a copper vs. gold-cobalt thermocouple (which has a relatively high output for a thermocouple) produces an 0.22-mv change for a temperature change of  $20^\circ\text{R}$  in  $\text{LH}_2$ . At normal room temperatures, a  $20^\circ\text{R}$  change would yield



GENERAL DYNAMICS | ASTRONAUTICS

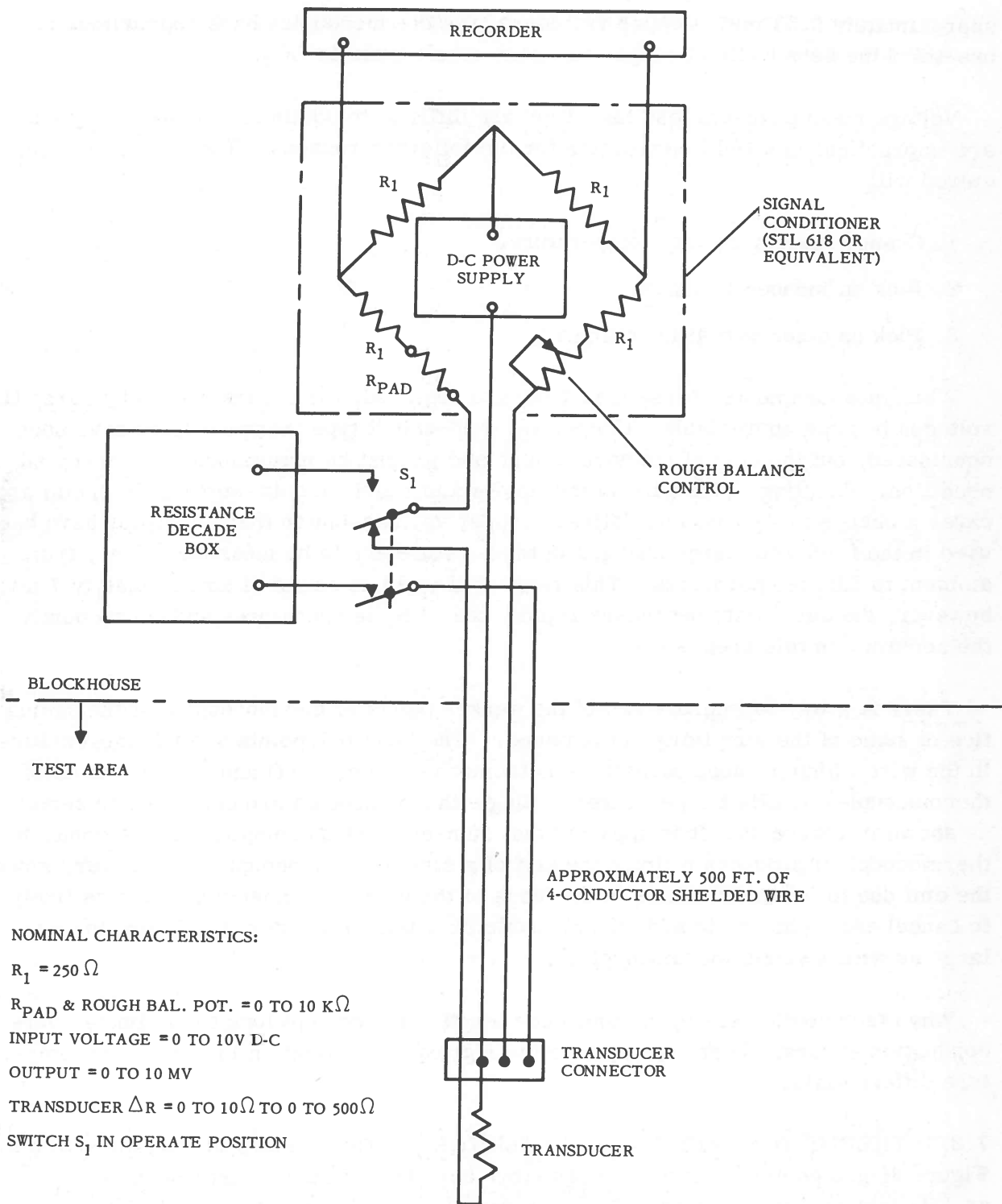


Figure 34. General-purpose bridge circuit for temperature measurements.

## GENERAL DYNAMICS | ASTRONAUTICS

approximately 0.53 mv. Copper vs. constantan thermocouples have approximately one-third the sensitivity of copper vs. gold-cobalt types in LH<sub>2</sub>.

Voltage measurements less than 1 mv are difficult to obtain in the laboratory and are impractical in a field installation for the following reasons. The long cables required will:

1. Change resistance with temperature.
2. Pick up induced voltages.
3. Pick up other parasitic voltages.

When measurements of less than 1 mv are required, the errors caused by parasitic voltages become appreciable. Copper vs. gold-cobalt type thermocouples have been considered, but the cost of the wire is high and it must be maintained in an annealed condition. Handling of the wire in the field would result in cold-working the metal and cause a change in its characteristics. Copper vs. constantan thermocouples have been used in the field when large changes in temperature are to be measured, i.e., from ambient to LH<sub>2</sub> temperatures. This range will yield an output of approximately 7 mv; however, the sensitivity decreases rapidly near LH<sub>2</sub> temperatures and consequently the accuracy in this area is poor.

There is a way to improve two of the weaker points of thermocouples at the sacrifice of some of the simplicity convenience. (The two weak points are inhomogeneities in the wire which produce parasitic electromotive forces (emf) and the low output of thermocouples at LH<sub>2</sub> temperatures.) Single thermocouples are connected in series as shown in Figure 35. It is apparent that an n-element thermopile (series-connected thermocouples) produces n times the emf of a simple thermocouple. Moreover, since the emf due to inhomogeneities in the leads of the various elements are just as likely to cancel each other as to add, the probable resultant emf error is only  $\sqrt{n}$  times as large as with a single thermocouple.

When thermopiles are used, the probe length must be kept long to minimize heat-conduction errors. Thermopiles have their greatest application in measuring temperature differentials.

**7.2.3 THERMISTORS AND CARBON RESISTORS.** Thermistors of the type shown in Figure 36 and commercial carbon resistors have been tested at Astronautics for use as LH<sub>2</sub> temperature sensors. These sensors have a high negative coefficient of resistance at LH<sub>2</sub> temperatures (resistance increases rapidly as temperature decreases).

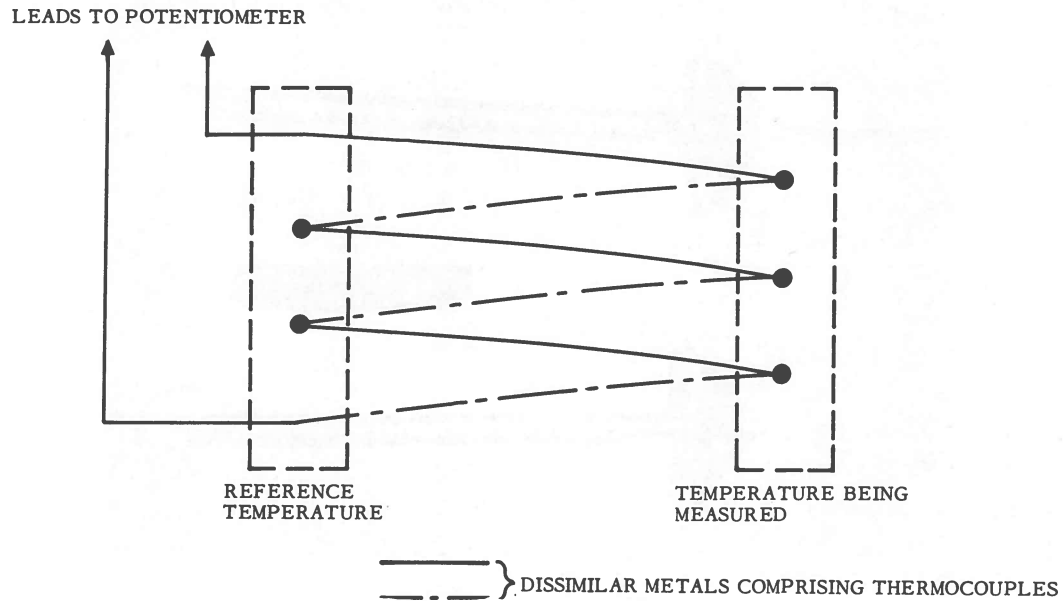


Figure 35. Thermopile.

Consequently, their output is low due to their limited power capabilities at LH<sub>2</sub> temperatures. In addition, the current through the sensor must be kept low to minimize the I<sup>2</sup>R self-heating effect. Increasing the sensor size minimizes self-heating but decreases the unit's temperature response rate (due to the increased mass).

Tests conducted at Astronautics indicated that carbon resistors and thermistors were not repeatable after being thermally shocked. If a sensor was kept at LH<sub>2</sub> temperatures, the resistance curve was found to repeat. However, if the sensor was warmed to room temperature between each run, it would not repeat. The repeatability of thermistors was better than that of carbon resistors, but thermistors of the same type and size exhibited large variations from one unit to another.

In order to accurately calibrate a thermistor in liquid hydrogen, it is necessary to place it in a cryostat and measure the temperature of LH<sub>2</sub> with a standard (platinum) thermometer while simultaneously measuring the resistance of the thermistor. The LH<sub>2</sub> temperature is changed by changing the vapor pressure. Such a calibration is quite complicated and costly and the calibration range is limited.

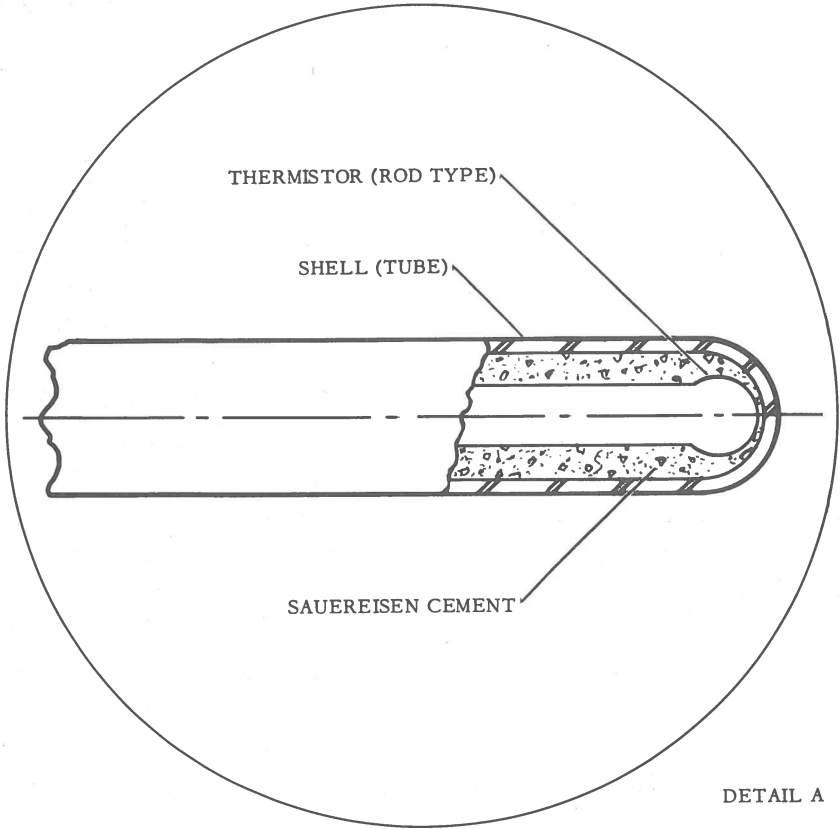
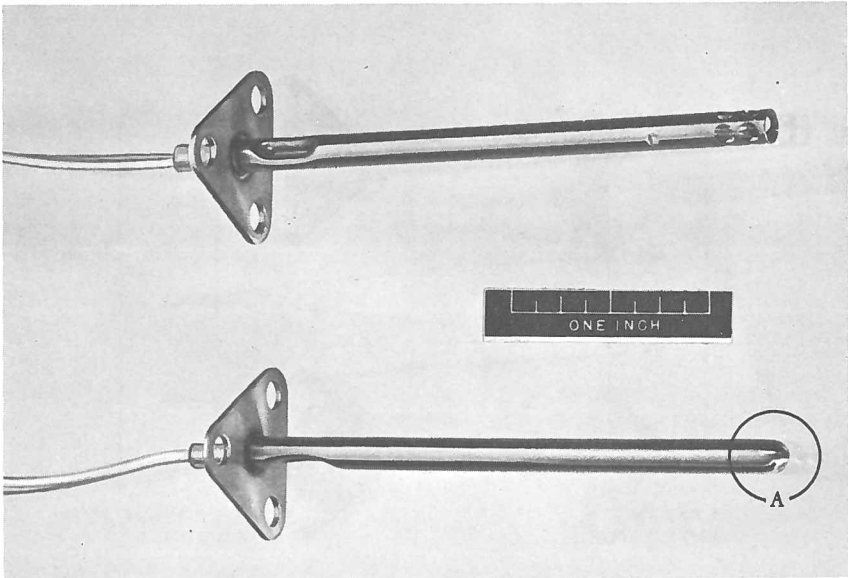


Figure 36. Typical thermistor probe.

## GENERAL DYNAMICS | ASTRONAUTICS

Carbon resistors appear to be pressure-sensitive; therefore, it is impractical to calibrate them in LH<sub>2</sub> by this method. This pressure sensitivity also makes their use in pressurized vessels (such as space vehicle tanks and ducts) unfeasible.

**7.2.4 GERMANIUM CRYSTALS.** Semiconductor temperature transducers using doped germanium crystals as sensing elements have been tested by NBS, Rutgers University, and other research facilities. Results have been promising. Repeatability near the helium boiling point was better than 0.001°K, and in the vicinity of the LH<sub>2</sub> boiling point, better than 0.05°K.

Existing sensors suffer from the disadvantage that they require laboratory treatment for installation as well as readout. Excitation current must also be limited to very low values.

Astronautics, in conjunction with the Radiation Research Corp., is developing a rugged immersion probe with a germanium element. The probe will be provided with an integral resistance bridge in its head so that an output voltage variation is obtained with temperature changes over a narrow range when excitation from a power supply is applied to the transducer. The new probes will be thoroughly tested by the vendor and by Astronautics after the completion of this design.

**7.2.5 GAS-PRESSURE THERMOMETERS.** Gas-pressure thermometers consist of a capillary tube (filled with helium) connected to a pressure transducer (see Figure 37). Since helium's behavior approaches that of a perfect gas and the small change in capillary volume with temperature is reasonably constant, the pressure change in the tube with temperature is nearly linear. Pressure transducers may be designed to yield high-output signals for small temperature changes.

The National Bureau of Standards has conducted experiments on these sensors with generally favorable results. Several manufacturers of rocket engines have reported similar findings. The main drawback to this type of device was found to be the slow response time (due to the mass of the tube). At present, only a few instrument manufacturers produce an LH<sub>2</sub> probe of this type.

### 7.3 PRESSURE MEASUREMENTS

Since frequency-response requirements for most LH<sub>2</sub> pressure measurements are low (10 cps or less), no problems are normally encountered in these measurements. A threaded boss is used on the duct or tank where the measurement must be taken. Tubing, at least 10 in. long, leads from the boss to the transducer. Any liquid hydrogen

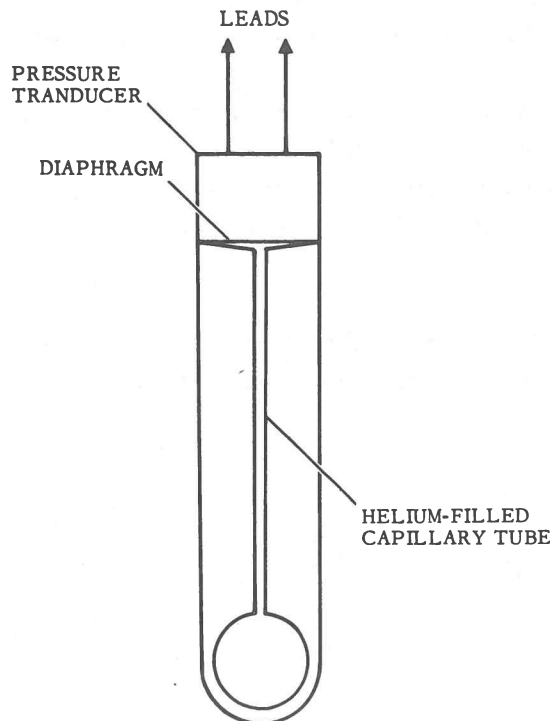


Figure 37. Gas-pressure temperature probe.

entering the tubing at the boss end boils rapidly and is gasified in the tubing. Transducer types commonly used are potentiometric pressure transducers utilizing pressure capsules or helical Bourdon tubes as sensing elements (see Figure 38).

For high-frequency response (0 to 800 cps) pressure measurements, such as in LH<sub>2</sub> pump ducts, the use of strain-gage pressure transducers of the type shown in Figure 39 was investigated. These transducers are normally installed directly into the duct so that LH<sub>2</sub> comes in physical contact with the sensing diaphragm. Earlier tests indicated that a small amount of residual water vapor (humidity) in the inlet port of the transducer can easily solidify and, hence, block the port. If the transducer is kept dry, and it has been temperature-compensated by the vendor to minimize inherent temperature errors in the LH<sub>2</sub> temperature region, it can be suitable for such pressure measurements.

Existing unbonded strain-gage transducers exhibit temperature gradient errors of 6% to 30% of full scale. This error is apparent whenever the transducer is exposed to

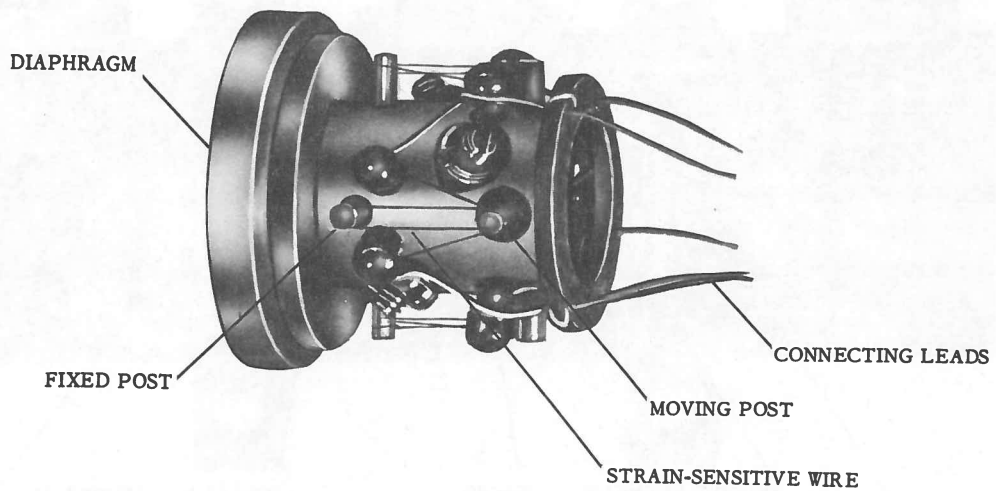
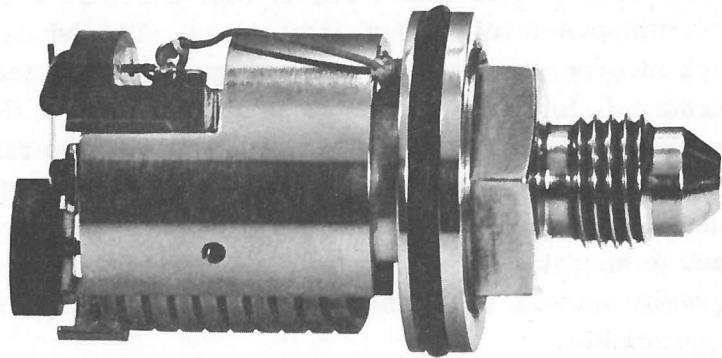


Figure 39. Strain-gage pressure transducer.

a step change in temperature. The error disappears after the entire internal portion of the transducer stabilizes at the new temperature level.

Difficulties are still encountered in reliable, accurate measurements of liquid level (head) measurements in LH<sub>2</sub> tanks where differential-pressure transducers are required to provide continuous-level (analog) indications. Transducers of the type shown in Figure 40, which incorporate a relative servo system, have yielded reasonably accurate measurements. Unfortunately, the transducer design for flight telemetry use has not proven too reliable for the following reasons. Since the range to be measured is normally 0 to 0.20 psia (equivalent to approximately 6 in. of water), available transducer types are usually not sufficiently sensitive, or evidence extremely high acceleration, vibration, and temperature errors. Even attitude errors (acceleration errors caused by earth gravity vectors not parallel to the plane of the sensing diaphragm or capsule) can be appreciable.

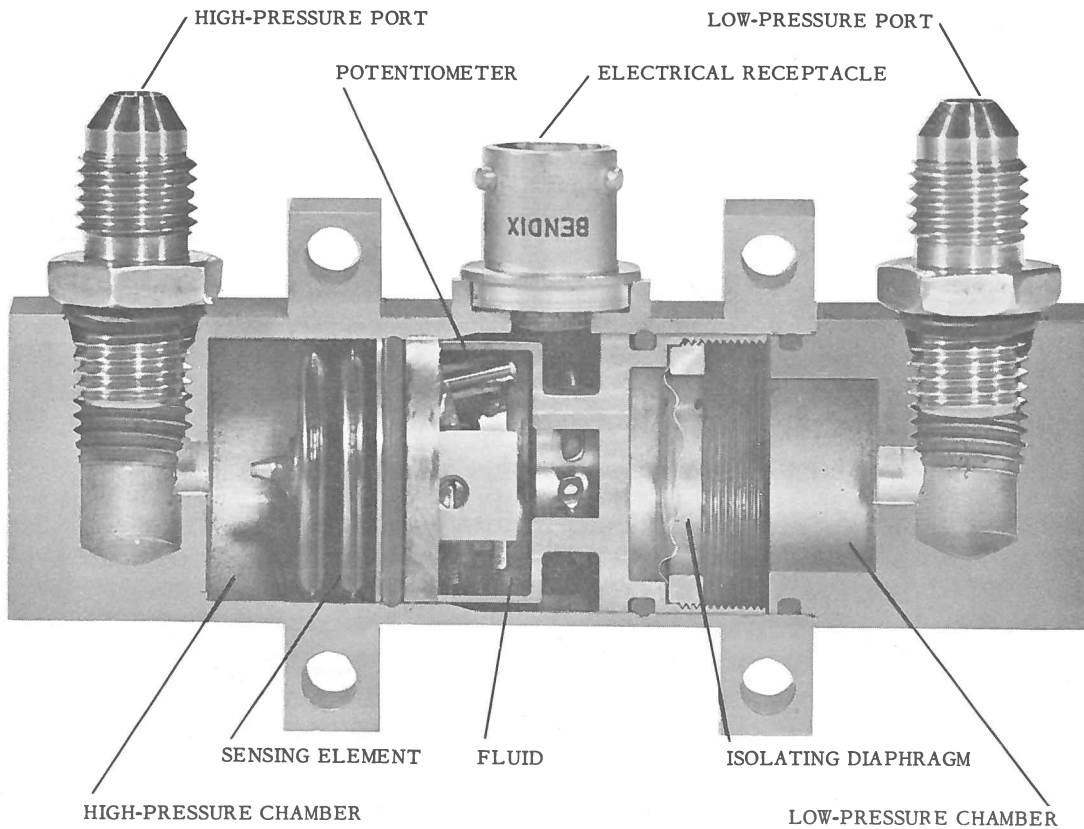


Figure 40. Typical differential pressure transducer.



## GENERAL DYNAMICS | ASTRONAUTICS

Astronautics has been directing design efforts of several vendors in the development of new differential-pressure transducers (mainly potentiometric and relative types) with increased sensitivity, that are less subject to acceleration effects.

### 7.4 FLOWMETERS

Turbine-type flowmeters have been almost exclusively utilized at Astronautics to measure  $LH_2$  flow (see Figure 41). These meters may be destroyed by overspeeding if a high gas flow precedes the liquid flow in a line. Care must be taken to slowly pre-chill the line prior to discharging large quantities of liquid in the line.

Some flowmeter manufacturers have recently released flowmeter designs with an integral magnetic rotor-braking system. As gaseous hydrogen passes through the flowmeter and the rotor speed increases, a signal is generated and amplified, which causes the current through the electromagnetic brake to increase. The brake retards the rotor in such a manner that it can never run at overspeed. Astronautics has evaluated one such flowmeter and preliminary results were quite promising.

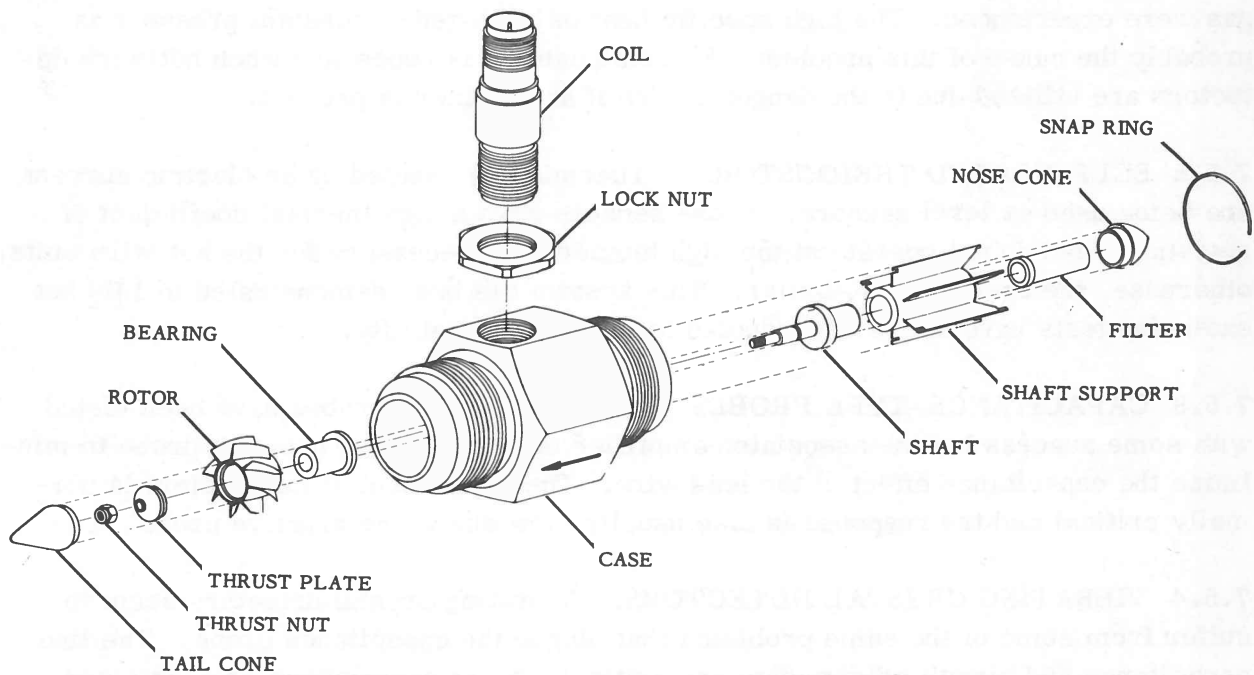


Figure 41. Typical turbine flowmeter.

## GENERAL DYNAMICS | ASTRONAUTICS

The turbine flowmeter is normally calibrated with water. The uncertainty of this calibration being applicable to LH<sub>2</sub> flow is approximately 2%. If greater accuracy than 2% is required, each flowmeter must receive an individual calibration using LH<sub>2</sub>. This was demonstrated by a series of tests performed by Astronautics in conjunction with Pratt & Whitney Aircraft.

Other types of flowmeters do not appear as useful in LH<sub>2</sub> measurements as turbine types. A strain-gage vane-deflection meter is being evaluated, but its operation in LH<sub>2</sub> is still doubtful.

### 7.5 LEVEL SENSORS

Many types of liquid level sensors are available and several have been tested at Astronautics to determine their usability in LH<sub>2</sub>. Some of the methods used for sensing liquid level are described in the following paragraphs.

**7.5.1 HOT-WIRE DETECTORS.** Since hot-wire level sensors worked well at Astronautics with liquid nitrogen and liquid oxygen, they were tested for use in LH<sub>2</sub>. It was found that the hot-wire detectors always operated well when first covered by the liquid but seldom operated correctly when uncovered. Long delays in indicating presence of gas were experienced. The high specific heat of hydrogen at constant pressure is probably the cause of this problem. Extreme caution is necessary when hot-wire detectors are utilized due to the danger of fire if an oxidizer is present.

**7.5.2 SELF-HEATED THERMISTORS.** Thermistors, heated by an electric current, are being used as level sensors. These sensors have a high thermal coefficient of resistance and do not operate at the high temperature necessary for the hot-wire units; otherwise, the operation is similar. This system has been demonstrated in LH<sub>2</sub> but extensive tests have not been conducted to prove its reliability.

**7.5.3 CAPACITANCE-TYPE PROBES.** Capacitance-type probes have been tested with some success but the associated amplifier must be located near the probe to minimize the capacitance effect of the lead wire. The adjustment of this system is normally critical and the response is also usually slow due to the massive probe.

**7.5.4 VIBRATING CRYSTAL DETECTORS.** Vibrating crystal detectors seem to suffer from some of the same problems that plague the capacitance probe. The line capacitance and circuit adjustments are critical. More success has been obtained with the vibrating crystal detectors, however, and the response of this type of system is normally fast. Some manufacturers have utilized very large lead wires to minimize

## GENERAL DYNAMICS | ASTRONAUTICS

capacitance effects and allow the amplifier to be installed in the blockhouse. This system is expensive relative to other methods.

**7.5.5 VIBRATING PADDLE DETECTORS.** Relatively good results have been obtained with vibrating paddle sensors (see Figure 42). This system uses a paddle mounted in a tank or duct excited by a 60-cycle or 400 cycle a-c voltage. The paddle has a natural frequency close to the frequency of the excitation voltage. When immersed in liquid, the vibration amplitude of the paddle is damped considerably. This amplitude is measured with a variable reluctance transducer.

These units have given good service but the types used were designed for the chemical industry and are too large for flight vehicle use.

**7.5.6 FLOAT SWITCHES.** Float switches in  $LH_2$  have been used at Astronautics without much success. If the float is made large enough and light enough to float in  $LH_2$ , the internal pressure in the tank is usually high enough to crush it. If the float was not crushed, it quite often jammed and did not operate. For these reasons, float switches are not being used at Astronautics.

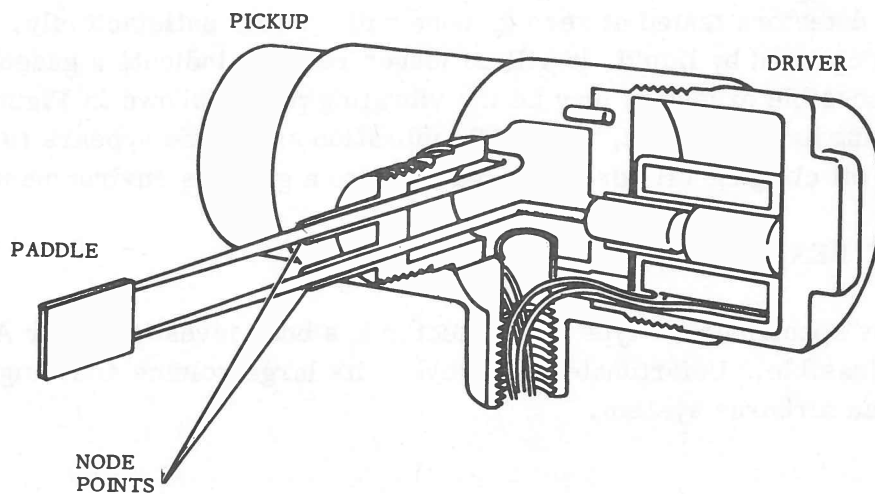


Figure 42. Vibrating paddle liquid-level sensor or liquid/gas detector.

7.5.7 DIFFERENTIAL PRESSURE TRANSDUCER. A differential pressure transducer has been used to measure liquid hydrogen head. It has two distinct advantages over point sensors:

1. It yields a continuous (analog) record of liquid level.
2. It measures liquid head rather than liquid level; consequently, the average density and mass of LH<sub>2</sub> left in the tank can be calculated.

A certain amount of "hash" will be present on the pressure records due to the LH<sub>2</sub> boiling out of the sensing lines.

7.5.8 ULTRASONIC LEVEL SENSOR SYSTEM. The application of magnetostrictive ultrasonic level probes, with associated oscillator-amplifier control units, seems promising. A system of this type has operated well in LN<sub>2</sub> and is currently undergoing evaluation in LH<sub>2</sub>.

## 7.6 LIQUID/GAS DETECTORS

Liquid/gas detectors are normally used as level sensors but are referred to as liquid/gas detectors when used in ducts or lines transporting the liquid or in space vehicle tanks for zero-g measurements. All the level sensors discussed in Section 7.5 may be used as liquid and gas detectors at 1g except differential pressure transducers and float switches. Sensors used in lines or ducts which have high velocity liquid flowing must be rugged. Hot-wire detectors are normally subject to damage in a high-velocity fluid. However, LH<sub>2</sub> does not normally cause problems of this sort due to its low density. Of the detectors tested at zero g, none will operate satisfactorily. Once the sensor has been covered by liquid, it will no longer reliably indicate a gaseous environment. One possible exception may be the vibrating paddle shown in Figure 42. Although no testing has been done, the paddle vibration amplitude appears to be large enough to shake off clinging LH<sub>2</sub> droplets and indicate a gaseous environment.

## 7.7 HYDROGEN LEAK DETECTORS

A hydrogen mass spectrometer-type leak detector has been investigated by Astronautics and found to be feasible. Unfortunately, however, its large volume and weight prohibit its use as an airborne system.

## 8

## PROPULSION SYSTEMS

Just as liquid oxygen is the workhorse of present liquid propulsion systems, liquid hydrogen will assume a predominant role in high-energy space vehicles and exotic propulsion systems. The reasons for this projected position are due essentially to hydrogen's low molecular weight, high-energy release when combined with suitable oxidizers, nontoxicity, noncorrosiveness, and excellent properties as a nozzle coolant. However, some of these advantages are mixed blessings. Its ease of ignition in air and oxygen over a wide flammability range is desirable for chemical combustion but presents a significant safety hazard. For nuclear systems, hydrogen's combustibility is completely undesirable. Hydrogen's low molecular weight also has its disadvantages in the form of liquid hydrogen's low density and low boiling point. Very large, and consequently heavy, tanks are needed to store sufficient quantities of liquid hydrogen; in addition, effective thermal insulation is needed to prevent excessive hydrogen boiloff.

The following four sections briefly summarize propulsion systems that presently use or contemplate using liquid hydrogen. The less familiar systems are discussed in greater detail. Table IX compares some significant characteristics of the propulsion systems described.

## 8.1 CHEMICAL PROPULSION

**8.1.1 HYDROGEN/OXYGEN SYSTEMS.** Saturn stages S-II and S-IV and the Centaur vehicle use this propellant combination. Centaur (see Figure 43) is in its early stages of flight testing. S-IV will be static-tested in the third quarter of 1962.

**8.1.2 HYDROGEN/FLUORINE SYSTEMS.** Considerable effort has been expended toward developing a hydrogen-fluorine engine due to the high specific impulse of such a system. However, fluorine's extreme reactivity with almost all materials plus the high toxicity of fluorine and hydrogen fluoride (the exhaust gas) has required a completely new technology to be developed. No flight tests have been attempted using this combination.

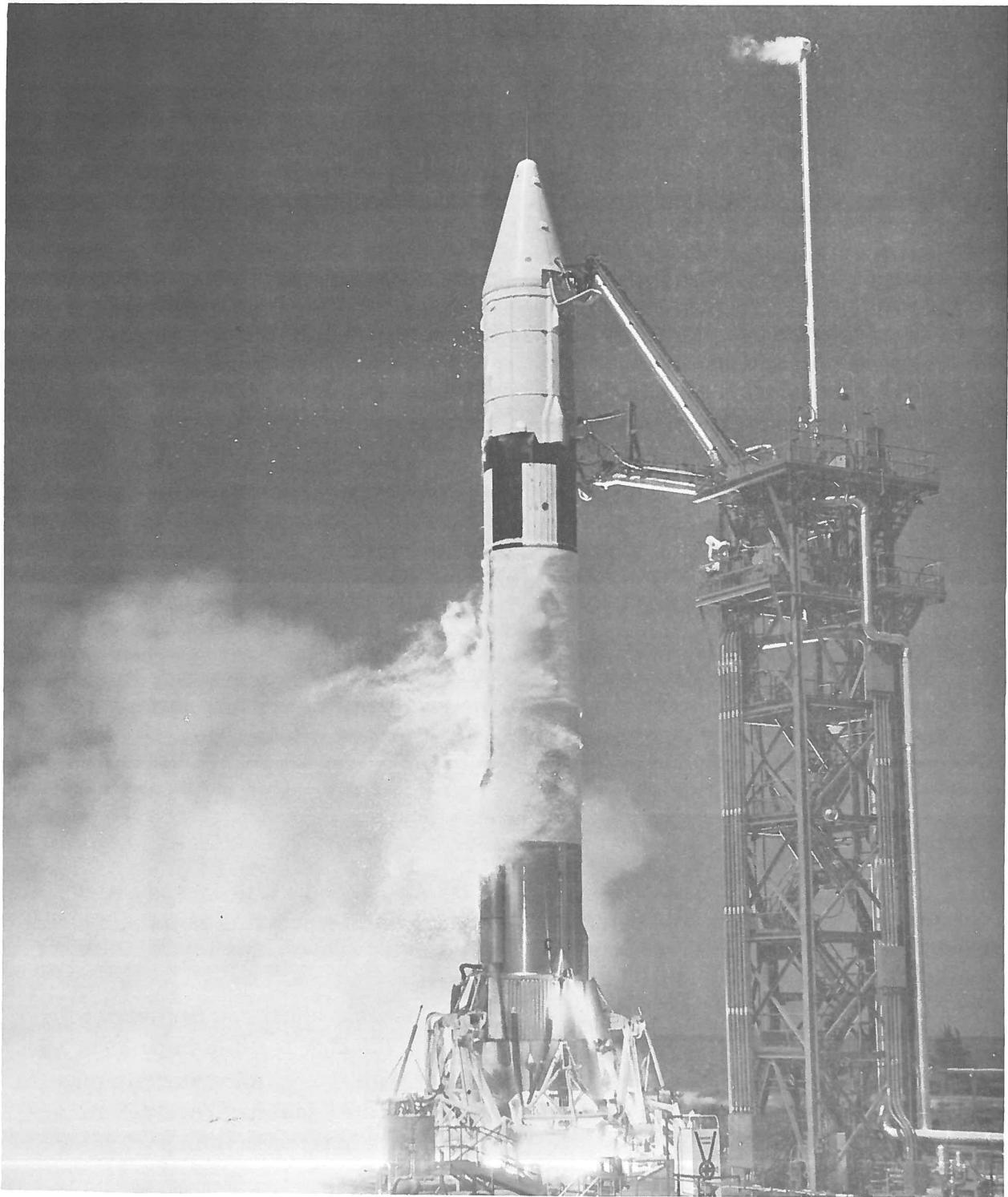


Figure 43. Centaur upper stage with Atlas booster just prior to liftoff.



GENERAL DYNAMICS | ASTRONAUTICS

Table IX. Propulsion methods using hydrogen.

	CHEMICAL PROPULSION		NUCLEAR PROPULSION			ELECTRIC PROPULSION		
	H <sub>2</sub> -O <sub>2</sub>	H <sub>2</sub> -F <sub>2</sub>	THERMAL REACTOR	FAST REACTOR	ATOMIC HYDROGEN RECOMBINATION	ELECTRIC-ARC-HEATED JET	ELECTRIC RESISTANCE HEATED JET	SOLAR HEATING
SPECIFIC IMPULSE (LB.-SEC./LB.)	364	373	765-820	950-1,050	1,200 (P CHAMBER = 1 ATM.) 2,000 (P CHAMBER = 10 <sup>-2</sup> ATM.)	1,400-2,000 (DEPEND- ING ON DESIGN)	1,100	400-500
CHAMBER TEMPERATURE (°R)	4,960 MAX.	5,560 MAX.	4,100-4,700	TO 5,400	5,400	~6,300	5,400	~1,980
SYSTEM SPECIFIC THRUST (LB. OF THRUST/LB. OF PROPELLANT SYSTEM HARDWARE)	50-80	50-80	~1		~0.1	0.005-0.05 (DEPEND- ING ON DESIGN & POWER SOURCE, β DECAY, REACTOR OR SOLAR)	~0.01	~0.05
ACCELERATION (THRUST/ WEIGHT)	1.2 - 1.5 (SURFACE)	1.2 - 1.5 (SURFACE)	0.3 - 1.2		~0.03	0.005 - 0.01	~0.005	~0.01
MANEUVERABILITY	EXCELLENT	EXCELLENT	EXCELLENT		FAIR	POOR	POOR	POOR
INITIAL INVESTMENT IN SPACEBORNE HARDWARE IN RELATION TO THRUST PRODUCED	LOW	LOW	FAIRLY LOW		FAIRLY HIGH	HIGH	HIGH	FAIRLY HIGH
PROPULSION SYSTEM MAINTAINABILITY & RELIABILITY	VERY LIMITED LIFE OF ENGINES & PUMPS		LONG LIFE, STRUCTURAL INTEGRITY OF REACTOR CORE MAY BE PROBLEM		LONGER LIFE THAN DIRECT HEAT TRANSFER DUE TO SLOW STARTUP	LONG LIFE, EROSION OF ELECTRODES A PROBLEM	LONG LIFE	LONG LIFE, PUMPS MAY BE PROBLEM
PROBABILITY OF EXTRA- TERRESTRIAL SUPPLY OF PROPELLANT	NONE	NONE	POSSIBLY SATURN MOON (TITAN) OR JUPITER MOONS		NONE (THRUST-TO- WEIGHT RATIO TOO LOW TO USE JUPITER MOONS)	NONE	NONE	NONE
POSSIBLE AREAS OF OPERATION	EARTH ASCENT, LUNAR TRANSFER, LUNAR LANDING, POSSIBLY MARS, VENUS TRANSFER		EARTH ASCENT, LUNAR TRANSFER, LUNAR LANDING, MARS, VENUS, JUPITER, SATURN TRANSFER		INTERPLANETARY	INTERPLANETARY	INTERPLANETARY	CISLUNAR

## 8.2 NUCLEAR PROPULSION

In contrast to bipropellant liquid systems where the heat of reaction of the oxidizer and fuel provides the kinetic energy necessary for thrust, a nuclear vehicle uses a monopropellant (liquid hydrogen) heated to high temperatures by a nuclear reactor.

The reactor-in-flight-test vehicle (initial flight date, 1967) uses this principle (see Figure 44). The Los Alamos Scientific Laboratory and Aerojet-General Corp. are developing the engine for this vehicle in the Kiwi test series. Successful engine tests have been conducted with gaseous hydrogen, and the first liquid-hydrogen full-power flow test has recently been conducted.

A typical flow chart of the propellant path from the rocket tank to the engine is shown in Figure 45. In this scheme, the enthalpy of the rocket nozzle is used to initially vaporize the fluid; the exhausted gas starts the turbopump and provides vehicle roll control. An auxiliary power unit for turbopump startup might be needed for multiple restarts in space.

At present, nuclear vehicles are only being considered as upper stages. In case there is a reactor malfunction, the stage can be dropped in the ocean a safe distance from the launch complex. If the Rift vehicle proves to be exceptionally safe and reliable, nuclear vehicles may also be considered as first-stage boosters for unmanned payloads. However, it should be pointed out that even if the nuclear vehicle works properly, fission products in the exhaust gas may heavily contaminate the launch area. For this reason it appears that only chemical stages will be used for first-stage boosters in the foreseeable future.

**8.2.1 THERMAL REACTOR.** A typical reactor core consists of a loading of uranium carbide, graphite, and binder. The channels in the reactor core, through which the hydrogen gas is heated, must be coated with a high-temperature material. This coating prevents reaction of the graphite and uranium with hydrogen at maximum core temperature.

The power level on this type of thermal reactor is controlled by rotating cylindrical drums of beryllium, covered on one side with a good neutron absorber such as boron (boron-aluminum alloy).

A beryllium reflector surrounding the uranium fuel keeps neutrons in the core.



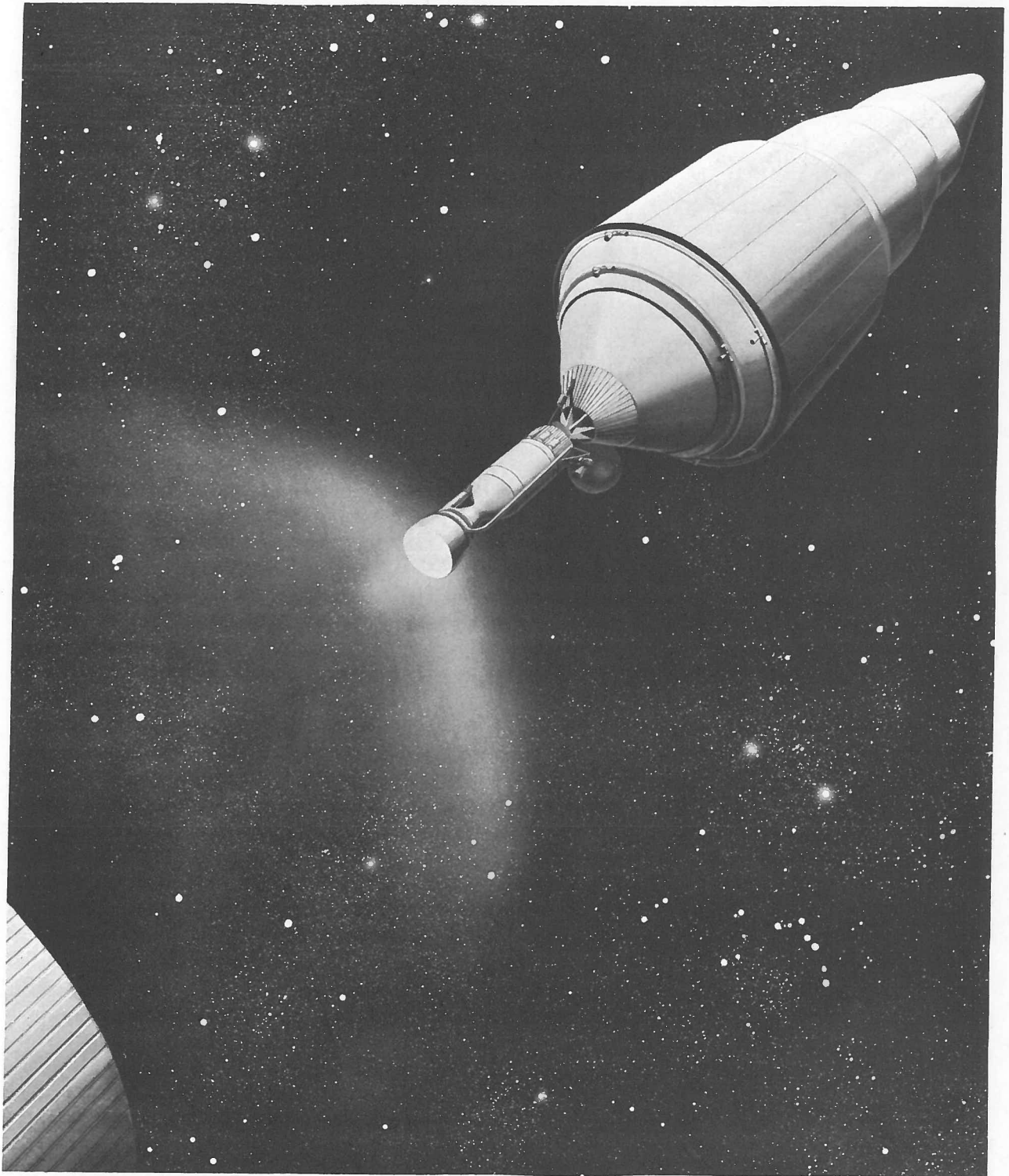


Figure 44. Proposed reactor-in-flight-test vehicle.

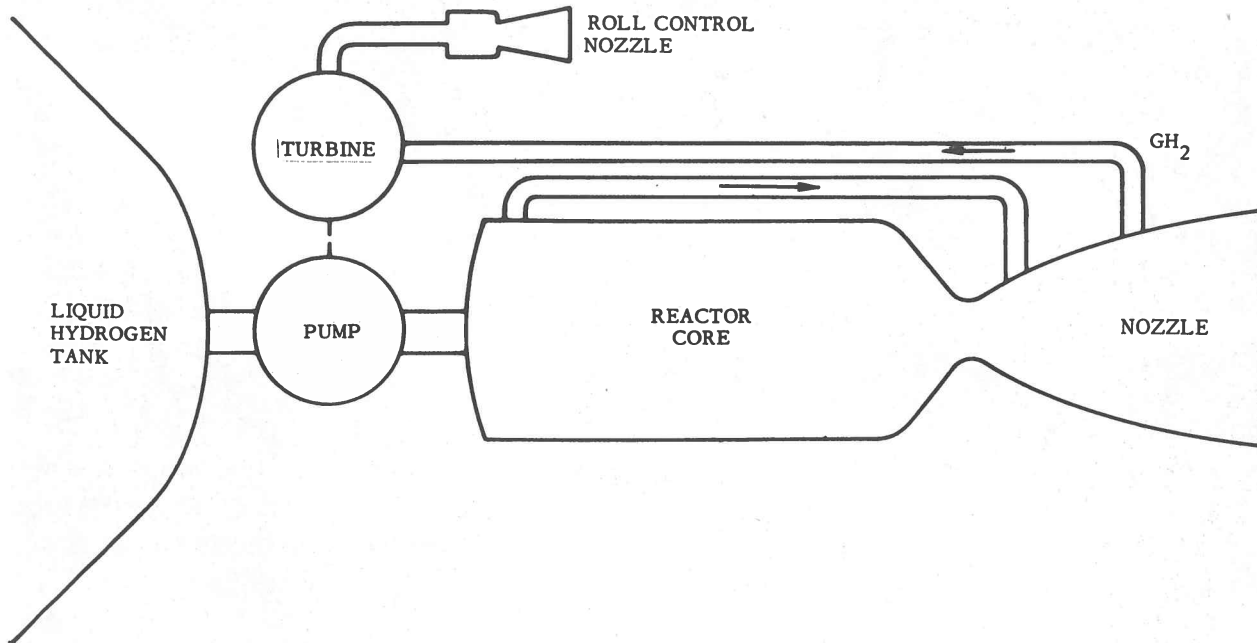


Figure 45. Typical liquid hydrogen flow for nuclear vehicle.

8. 2. 2 ADVANCED NUCLEAR ENGINE CONCEPTS. Two types of nuclear rocket engines which show promise for future application are the fast-reactor and reacting-propellant (low-pressure) engines. These designs offer potentially greater specific impulse and lower weight than presently conceived thermal, graphite nuclear-engine systems.

8. 2. 2. 1 Fast Reactor. Fast reactors utilize a higher proportion of high-energy (fast) neutrons to cause fission, in contrast to graphite-moderated reactors which use low-energy (thermal) neutrons to sustain a chain reaction. The higher specific impulse that can be obtained in fast-reactor systems, as compared to thermal, results from the higher reactor exit temperatures that can be obtained.

Since the goal of fast reactor design is to maintain and utilize high-energy neutrons, the amount of moderating material must be kept relatively small compared to thermal reactors, thus reducing reactor weight.

However, fast reactors have some disadvantages when compared to thermal systems: (1) The higher heat deposition rate in the fast reactor core must be dissipated more rapidly than in a thermal core in order to prevent the core materials from vaporizing; (2) the fast reactor power level is difficult to control using neutron

## GENERAL DYNAMICS | ASTRONAUTICS

absorbers since few elements are effective neutron poisons at fast-neutron energies. As a result, neutronic control of the reactor power level may have to use another method of control. A movable reflector (allowing more or less neutrons to escape the core) appears to be a feasible solution.

8.2.2.2 Reacting Propellant Concept. This concept, which has been under study by General Dynamics since 1960, is a variation of the fast reactor nuclear rocket engine in that the chamber pressure is kept low (on the order of 1 or 2 psia). At this pressure and a temperature of around 5,400°R, almost half of the hydrogen molecules are dissociated. As the atoms pass out the nozzle, some atoms recombine but the great majority do not. Addition of trace amounts of catalyst to the hydrogen stream increases the rate of recombination of the dissociated atoms many fold in the nozzle, thus adding the heat of recombination to the sensible enthalpy that is imparted to the gas in the reactor. Using appropriate catalysts, the reacting propellant concept can theoretically increase the specific impulse from approximately 1,050 sec. (maximum specific impulse for heat transfer nuclear rockets) to the range of 1,600 to 1,900 sec. Since this engine concept would normally be used for deep space missions using long firing times, the reactor core can be brought up to temperature gradually, alleviating many of the thermal shock problems encountered in higher thrust nuclear rockets.

With the support of Marshall Space Flight Center and Lewis Research Center, a development program is underway to measure the performance gain of reacting hydrogen in a nozzle test facility.

### 8.3 ELECTRIC PROPULSION SYSTEMS

During the past few years, electric propulsion systems have passed from the status of ideas which looked interesting but somewhat academic to the status of active research and development programs.

At first glance, the electric propulsion cycle looks tremendously cumbersome and roundabout. Nuclear or solar energy is first converted to heat, which in turn is converted into electrical energy, and this is used, either directly or indirectly, to accelerate the propellant rearward to produce thrust. In spite of these drawbacks, the electric propulsion cycle shows promise of minimizing initial weights and cost of future space missions beyond the moon.

The wide variety of methods possible for producing a propellant jet with electric power can be classified generally into three categories: (1) electrothermal jets,

(2) electrostatic jets, and (3) electromagnetic jets. Since hydrogen can be used only with electrothermal systems, the last two categories will not be discussed here.

8.3.1 ELECTROTHERMAL JETS. The principal devices in the first category are the electric-arc jets and the resistance-heated jet.

8.3.1.1 Electric-Arc Jet. The electric-arc jet heats hydrogen propellant to high temperatures (5,400° to 6,300°R) by passing it between an electric arc (see Figure 46). The pressure in the chamber is kept low (around 0.1 psia) to allow near-complete hydrogen dissociation, thus optimizing the specific impulse for a given power level.

Among the technical problems in application of electric-arc jets for propulsion are electrode erosion, nozzle cooling, and reducing the percentage of electric power which goes into heating the electrode, nozzle walls, and stabilizing resistors. To achieve high efficiency, most of this heat must be recovered by the propellant by means of regenerative cooling. However, if the heat picked up by the propellant from the nozzles and electrodes becomes a large part of the total heat added to the propellant, the coolant becomes so hot before it reaches the electric discharge that its cooling properties have been severely diminished. This means that for high efficiency, a limit is reached on the specific impulse that can be achieved before it becomes impossible to

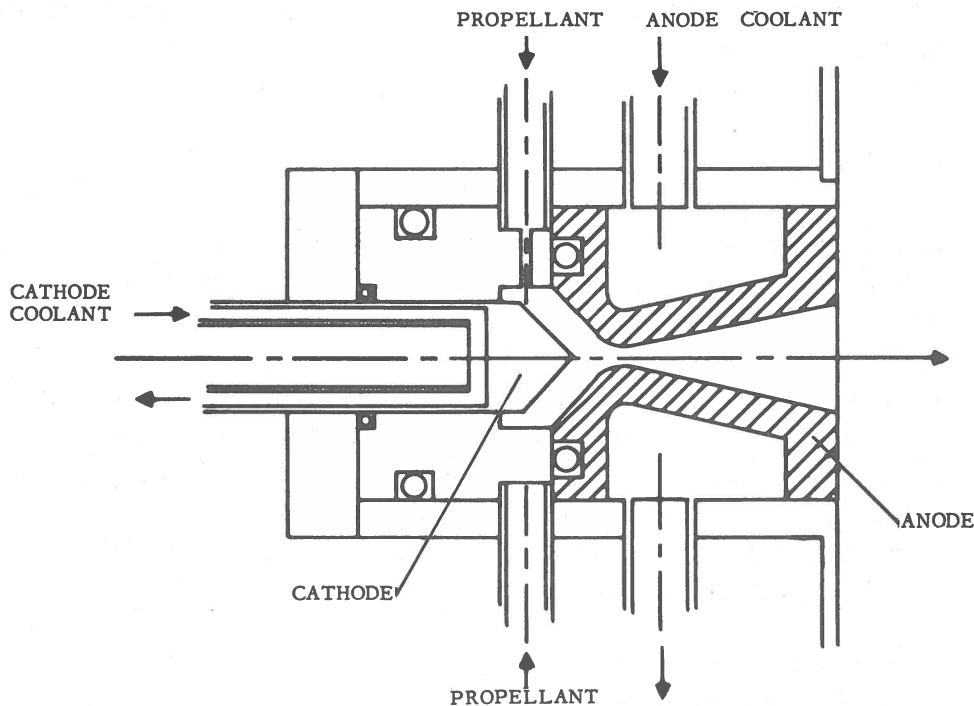


Figure 46. Electric arc-heated thrust device.

cool the surfaces with the propellant alone. When this limit is reached, either a radiator must be provided, with a secondary cooling loop, or the surfaces must be operated at sufficiently high temperatures that they produce adequate self-cooling.

For a typical arc-jet propulsion scheme, the specific impulse would range from 1,400 to 2,000 sec. The over-all efficiency of the system with turbogenerator equipment appears to be on the order of 0.1. Using the foregoing figures and making some additional assumptions, it would take 0.6 to 1.1 MW of power to produce 1 lb. of thrust.

Development contracts for propulsion applications have been awarded by NASA for a 30-kw and a 3-kw arc jet. The former may be used in conjunction with the Snap-8 power generator and the latter with Sunflower or Snap-2.

8.3.1.2 Electric Resistance-Heated Jet. The second electrothermal propulsion scheme, electric resistance-heated hydrogen jet, avoids many of the problems associated with electric-arc jets, in that no electrode erosion or arc heating of surfaces is involved (see Figure 47). The specific impulse is limited, however, to values attainable with hydrogen heated to the maximum temperature that the resistance-heated elements can tolerate. When tungsten in a porous or mesh form is used, this

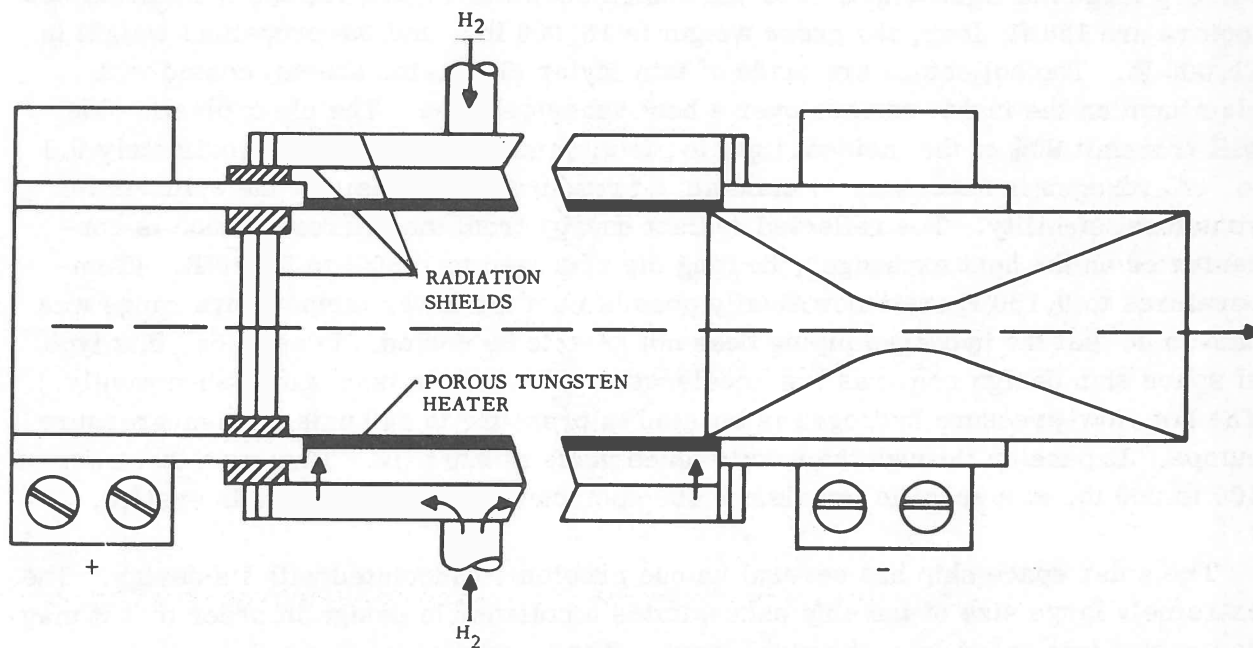


Figure 47. Electric resistance-heated thrust device.

maximum temperature is about 5,400°R, which produces a specific impulse of about 1,100 sec. Due to the fewer development problems involved, the resistance-heated jet may be a suitable alternative to the arc jet. A research program on this type of propulsion scheme has been studied by the NASA Lewis Research Center.

#### 8.4 SOLAR PROPULSION

Solar-powered propulsion is fundamentally the simplest scheme among nonchemical systems. It uses an existing energy source (the sun) in space in an efficient manner, by converting the radiant energy into heat.

The propulsion system consists of a liquid hydrogen storage tank, radiation collector, heat exchanger, and exhaust nozzle (see Figure 48). Pumps are required to circulate the hydrogen, but since the quantities involved are small (less than 1 lb.), the pumps are light, the horsepower requirement is low, and electrical high-speed drives appear practical. The necessity of concentrating the thinly spread solar energy requires the use of reflectors. (Near earth, the rate of radiant energy deposition is 442 Btu/hr. -ft<sup>2</sup>. This rate is proportional to the inverse square of the distance from the sun.)

A typical solar space ship would have the following characteristics: The ship would be very large but lightweight. For the design shown in Figure 49, the cylindrical collectors are 128 ft. long, the gross weight is 16,000 lb., and the propellant weight is 11,000 lb. The collectors are made of thin Mylar (0.001-in. sheets) coated with aluminum on the inside surface over a hemispherical area. The clear plastic side will transmit 90% of the incident light to the aluminized surface. Approximately 0.1 lb. of hydrogen is necessary to maintain a pressure of 0.01 psia in the cylinder for structural stability. The reflected radiant energy from the mirror surface is concentrated on the heat exchanger, heating the hydrogen to 1,800° to 2,000°R. (Temperatures to 9,100°R are theoretically possible but the lower temperature range was chosen so that the hydrogen piping does not have to be cooled. In addition, this type of space ship design requires low acceleration values as is discussed subsequently.) The hot, low-pressure hydrogen is boosted in pressure to 440 psia by high-pressure pumps. Expansion through the nozzle takes place at 220 psia. Thrust on the order of 100 to 200 lb. at a specific impulse of 450 sec. can be obtained with this system.

The solar space ship has several unique problems associated with its design. The extremely large size of the ship necessitates a collapsible design in order that it may be boosted into space by a chemical stage. The large size requires the vehicle



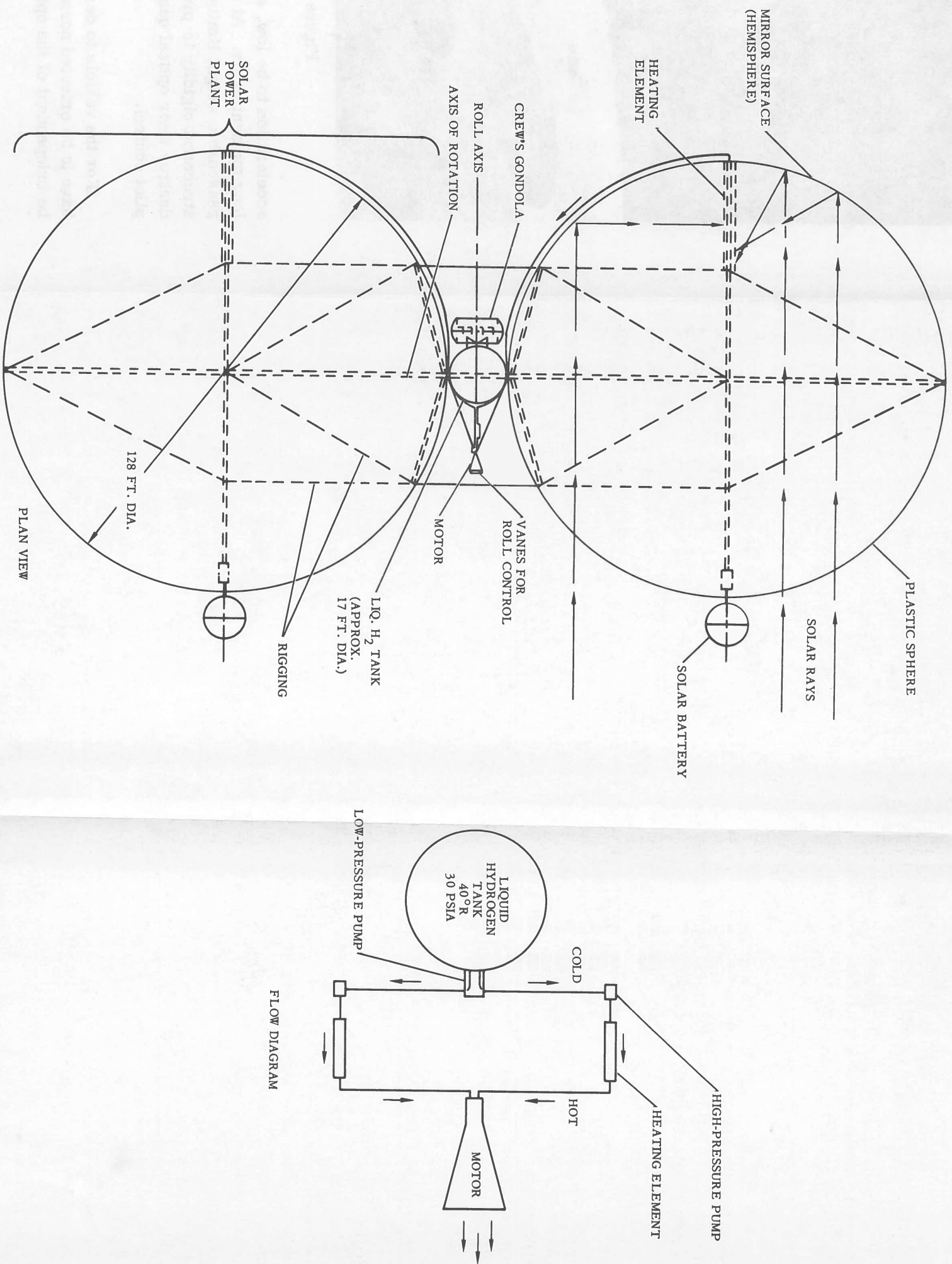


Figure 48. Solar-powered space ship prototype.

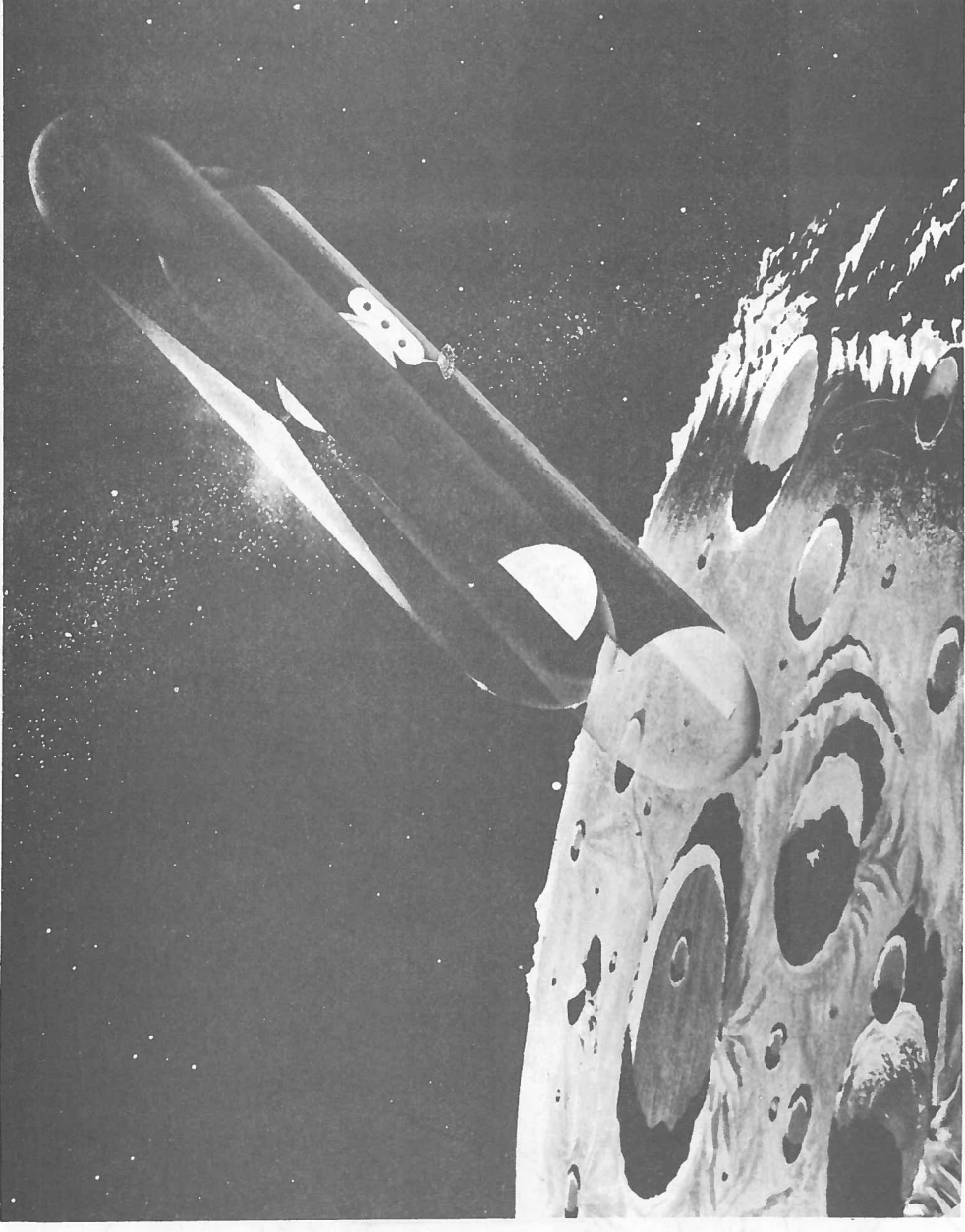


Figure 49. Artist's concept of solar-powered space ship.

acceleration to be low, approximately 0.01g, because the large collectors require long moment arms. At accelerations of 0.1 to 0.2g, it would not be possible, within reasonable weight limits for space vehicles of this size, to provide the necessary structural rigidity to prevent bending and distortion of the reflectors (which would destroy their optical quality). Structural rigidity is also needed for adequate auto-pilot control.

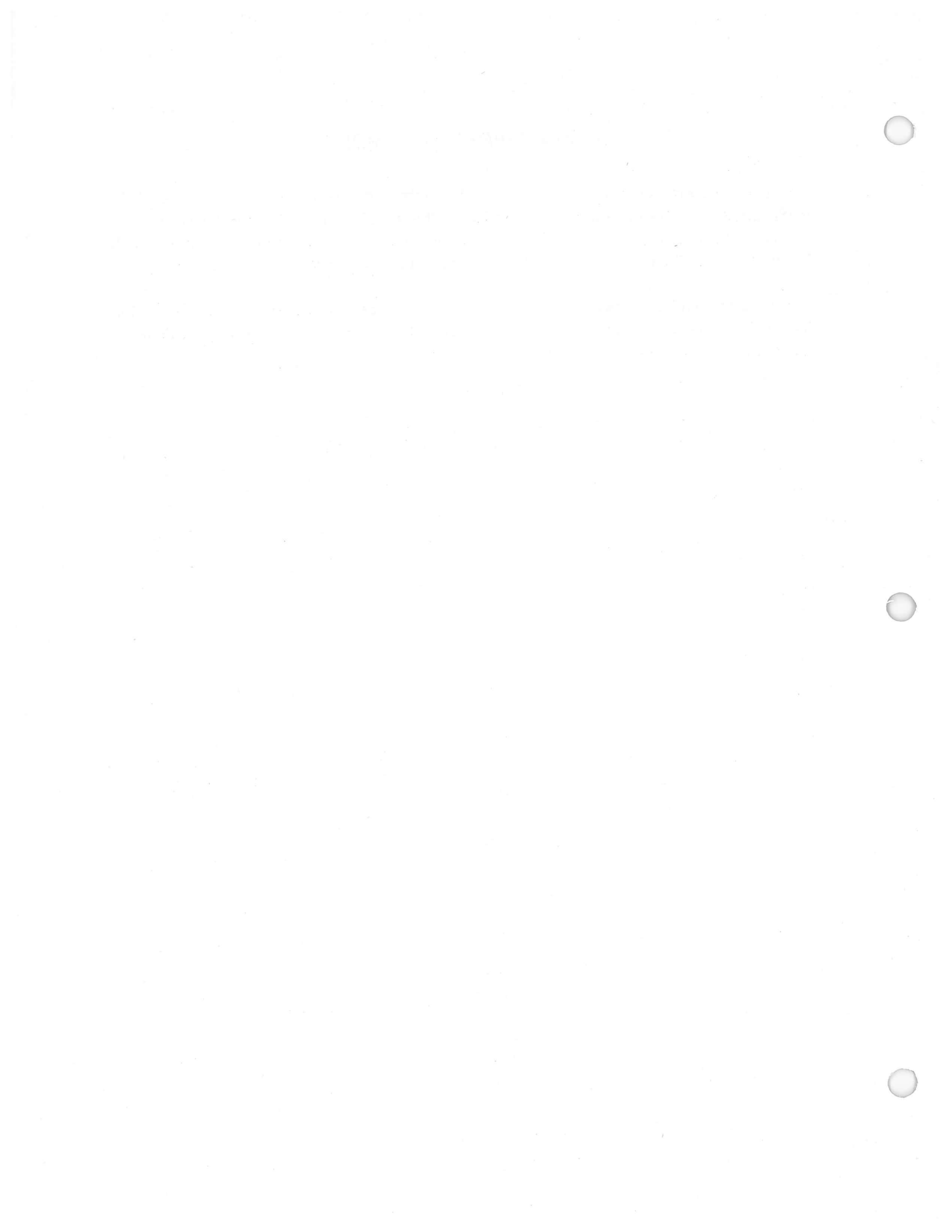
For the vehicle to derive maximum radiant energy from the sun, the reflectors have to be oriented normal to the sun's rays. This requires the thrust axis orientation be independent of the optical axis orientation.



## GENERAL DYNAMICS | ASTRONAUTICS

Other problem areas include meteoroid puncture of the reflector spheres and the operating life of the high-pressure pumps. The spheres may be able to maintain adequate rigidity by bleeding hydrogen gas into them to replace the gas lost through the punctures. The meteoroid hazard in space is discussed in Section 13.3.

If a solar-powered space ship is built, it will be restricted to cislunar operations due to its previously described operating characteristics. No contracts for solar space ship development have been let.



## 9

## SLOSHING

In writing the equation of motion for a missile or space vehicle, the problem of propellant sloshing is encountered. Due to the nature of the trajectory, sloshing motions may arise which rock the vehicle. These motions may be so phased with the resulting control forces as to drive the system unstable if the resultant forces are not properly compensated for. In early liquid-fueled missiles (e.g., V-2, Redstone) propellant sloshing was not thought to be a problem, and no means of slosh compensation was employed. The reason this problem did not appear for these vehicles was the fact that sufficient fluid damping was present due to the type of construction (internal rings and stringers) and small tank diameter (internal fluid damping varies inversely with tank diameter). This damping served to suppress fluid motions. Larger tanks are generally of cleaner internal construction and have little inherent fluid damping.

An obvious solution to the slosh problem lies in the insertion of baffles. However, baffle weight must be minimized on a launch vehicle; hence, before any slosh compensation scheme is studied, a means for treating the fluid's response in a vehicle is necessary.

### 9.1 MECHANICAL PENDULUM ANALOGY

**9.1.1 CYLINDRICAL TANK.** A hydrodynamic solution to the sloshing of fluids in a rigid-wall, cylindrical tank undergoing translation along its longitudinal axis and rotation about one of its perpendicular axes was derived by the Dynamics Group of Astronautics (Ref. 1). The hydrodynamic forces and moments about the base of the tank are determined for the oscillation of an incompressible, irrotational liquid. These equations are applicable to a vehicle which takes off vertically, pitches over in flight, but does not roll during the trajectory. For ease of handling, a mechanical analogy in the form of a pendulum or a spring mass is used. This analogy not only gives insight into the problem, but lends itself to a description of the liquid motion which is readily adapted for digital or analog computer simulations. Only the pendulum analogy is given here. Ref. 1 should be consulted for the spring mass analogy.

The forces and moments produced in a cylindrical tank of sloshing liquid can be represented by a fixed mass (liquid beneath the surface) and pendulum (sloshing liquid)

## GENERAL DYNAMICS | ASTRONAUTICS

as shown in Figure 50. The following pendulum-fixed mass equations for the first mode are exactly analogous to the hydrodynamic equations given in Ref. 1.

Force Perpendicular to the Longitudinal Axis

$$F = -s^2 x M_0 - s^2 \theta h_0 M_0 + \alpha_T \Gamma_{P_1} \quad (1)$$

Moment on Tank

$$M = -s^2 x M_0 h_0 - s^2 \theta \left( M_0 h_0^2 + I_0 \right) + M_1 h_1 \alpha_T \Gamma_{P_1} \quad (2)$$

The angle of the pendulum  $\Gamma_{P_1}$  with the longitudinal axis is given by:

$$\left( s^2 + \omega_1^2 \right) \Gamma_{P_1} = -\frac{1}{L_{P_1}} \left[ s^2 x + s^2 \theta \left( h_1 - L_{P_1} \right) \right] \quad (3)$$

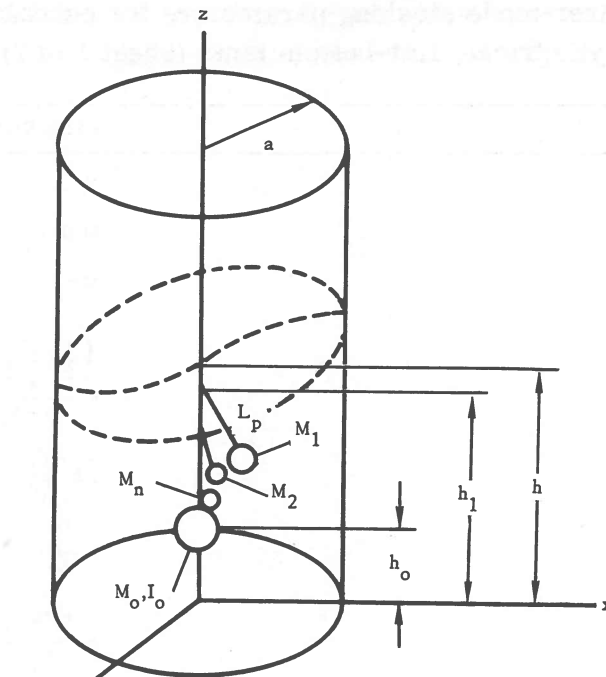
See Figure 50 for definition of symbols.

In these equations, the  $x$  and  $\theta$  terms describe the flight trajectory of the vehicle. Values for the other terms,  $M_0$ ,  $h_0$ ,  $I_0$ ,  $M_1$ ,  $h_1$ ,  $\omega_1$ , and  $L_p$  are obtained by the term-by-term comparison between the hydrodynamic equations and the pendulum-fixed mass analogy, as shown in Table X. For easy reference, these terms are also plotted as nondimensional parameters in Figure 51 as a function of the aspect ratio (fluid depth/tank radius).

Figure 50 illustrates the analogous pendulum-rigid mass system for the first three modes. Normally, only the first mode is considered in sloshing analyses because it has been shown analytically that the higher modes' contribution is not significant (Ref. 1). Another argument in support of disregarding the higher modes is the turbulent mixing noted during testing at high-frequency oscillations. This turbulence produces damping effects in the fluid.

9.1.2 CONICAL TANK. Ref. 2 gives equations for sloshing fluid in conical tanks. A mechanical analogy, in the form of a pendulum plus fixed mass, yielded identical results with perfect fluid hydrodynamic equations.

# GENERAL DYNAMICS | ASTRONAUTICS



- a TANK RADIUS
- $a_T$  LONGITUDINAL ACCELERATION
- $\Gamma_{P_1}$  ANGLE OF PENDULUM WITH TANK AXIS, FIRST MODE
- h DEPTH OF FLUID
- $h_o$  HEIGHT OF RIGID MASS CENTER OF GRAVITY ABOVE TANK BOTTOM
- $h_1, h_2$  HEIGHT OF SLOSHING ELEMENT ATTACH POINT ABOVE TANK BOTTOM
- $I_o$  MOMENT OF INERTIA, RIGID MASS
- $L_{P_1}$  LENGTH OF EQUIVALENT PENDULUM, FIRST MODE
- M TOTAL FLUID MASS
- $M_o$  FIXED FLUID MASS
- $M_1$  SLOSHING FLUID MASS, FIRST MODE
- n ORDERED NUMBER OF FLUID MODE
- $\omega_1$  FIRST FLUID MODE FREQUENCY
- s LAPLACE VARIABLE
- $\theta$  ANGLE OF ROTATION OF TANK AXIS IN FLIGHT
- x, y, z TANK COORDINATES

Figure 50. Tank model and coordinates for pendulum analogy.

# GENERAL DYNAMICS | ASTRONAUTICS

**Table X. First-mode sloshing parameters for pendulum analogy  
(cylindrical, flat-bottom tank) (sheet 1 of 2).**

MECHANICAL	HYDRODYNAMIC
$M_0 + M_1$	M
$M_0$	$M(1-A_1)$
$M_1$	$MA_1$
$h_0$	$\frac{\left(\frac{1}{2} + \frac{a^2}{4h^2} - B_1\right)}{(1-A_1)}$
$M_0 h_0^2 + I_0$	$Mh^2 \left(\frac{1}{3} + D_1 - B_1\right)$
$h_1$	$h \frac{B_1}{A_1}$
$L_p$	$h \frac{\coth K_1}{K_1}$
$\omega_1^2$	$\frac{\alpha T}{h} K_1 \tanh K_1$

NONDIMENSIONAL CONSTANTS, FIRST MODE

h/a	$K_1$	$\tanh K_1$	$\coth K_1$	$A_1$	$B_1$	$D_1$
0.00		0.0000	$\infty$		$\infty$	$\infty$
0.02		0.0368	27.174	0.8380	619.06	1237.8
0.10	0.185	0.1820	5.495	0.8290	24.77	49.2
0.20	0.368	0.3522	2.839	0.8025	6.20	12.1
0.30	0.554	0.5020	1.992	0.7624	2.80	5.2
0.50	0.921	0.7259	1.3776	0.6615	1.0335	1.764
0.60	1.108	0.8019	1.2470	0.6090	0.7430	1.177
0.70	1.290	0.8586	1.1647	0.5589	0.5716	0.8294
0.80	1.475	0.8999	1.1112	0.5126	0.4630	0.6088
1.00	1.841	0.9508	1.0517	0.4332	0.3390	0.3584
1.20	2.210	0.9761	1.0245	0.3706	0.2734	0.2294
1.40	2.578	0.9885	1.0116	0.3217	0.2336	0.1557
1.60	2.948	0.9945	1.0055	0.2832	0.2068	0.1104

# GENERAL DYNAMICS | ASTRONAUTICS

Table X. Sheet 2 of 2.

NONDIMENSIONAL CONSTANTS, FIRST MODE						
h/a	$K_1$	$\tanh K_1$	$\coth K_1$	$A_1$	$B_1$	$D_1$
1.80	3.311	0.9974	1.0013	0.2525	0.1872	0.0809
2.00	3.682	0.9987	1.0005	0.2275	0.1719	0.0610
2.25	4.140	0.9995	1.0002	0.2024	0.1566	0.0441
2.50	4.600	0.9998	1.0001	0.1822	0.1442	0.0329
3.00	5.519	0.9999	1.0001	0.1519	0.1248	0.0195
3.50	6.440	0.9999	1.0001	0.1302	0.1101	0.0124
4.00	7.360	0.9999	1.0001	0.1139	0.0985	0.00837
4.50	8.280	0.9999	1.0001	0.1012	0.0891	0.00590
5.00	9.200	1.0000	1.00000	0.0911	0.0812	0.00430
6.00	11.030	1.0000	1.00000	0.0759	0.0691	0.00249

## 9.2 DAMPING THE FLUID MOTION

9.2.1 WALL-WIPING ACTION. Quite often the inherent damping in the tank from wall-wiping action, while very low, is adequate for stability. The amount of wall wiping damping present is a function of such variables as the liquid's kinematic viscosity, tank surface roughness, tank diameter (crudely, the ratio of liquid mass to wall area), shape factors, and depth (proximity to tank bottom where the surface scrubbing action of waves increases the damping). The amount of damping present can only be obtained empirically. As a measure of the level of damping available from this source, the value obtained in slosh decay tests on water in smooth stainless steel cylindrical tanks of various sizes is:

$$S = \% \text{ of critical damping} = \frac{0.0038}{\text{tank diameter (ft.)}}$$

The Astronautics test setup used to obtain this value is shown in Figure 52. This relation holds as long as the water depth is at least one tank diameter.

While small, this inherent wall-wiping damping alone may prove adequate if the mass of sloshing fluid is small relative to the entire vehicle mass. Hence, its coupling with the vehicle is small. This situation is often found early in flight while a vehicle is still heavy. It also arises in the case of sloshing fluids of low density, such as liquid hydrogen.

GENERAL DYNAMICS | ASTRONAUTICS

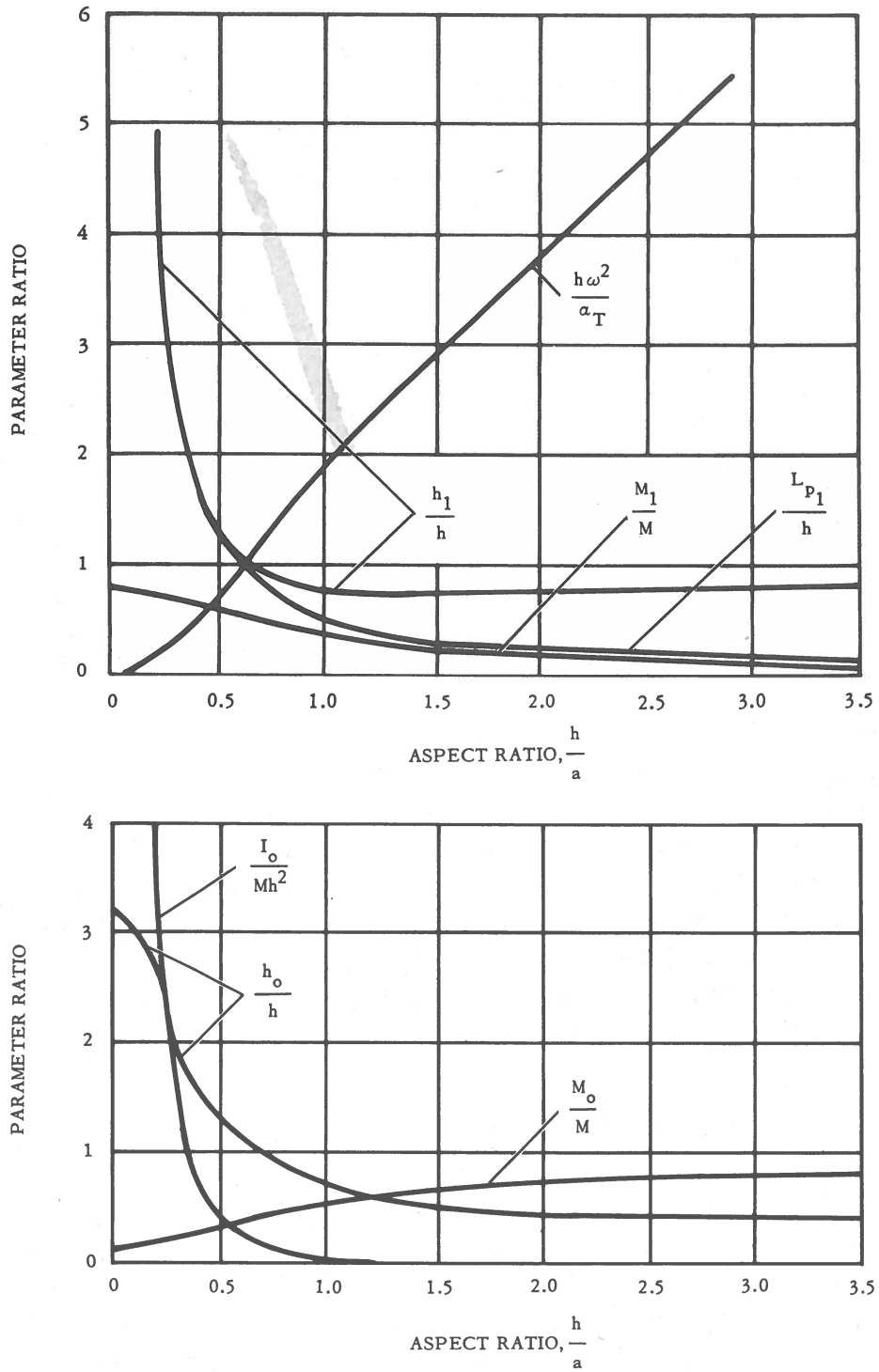


Figure 51. Nondimensional sloshing parameters for pendulum analogy; flat-bottomed cylindrical tank (first mode).



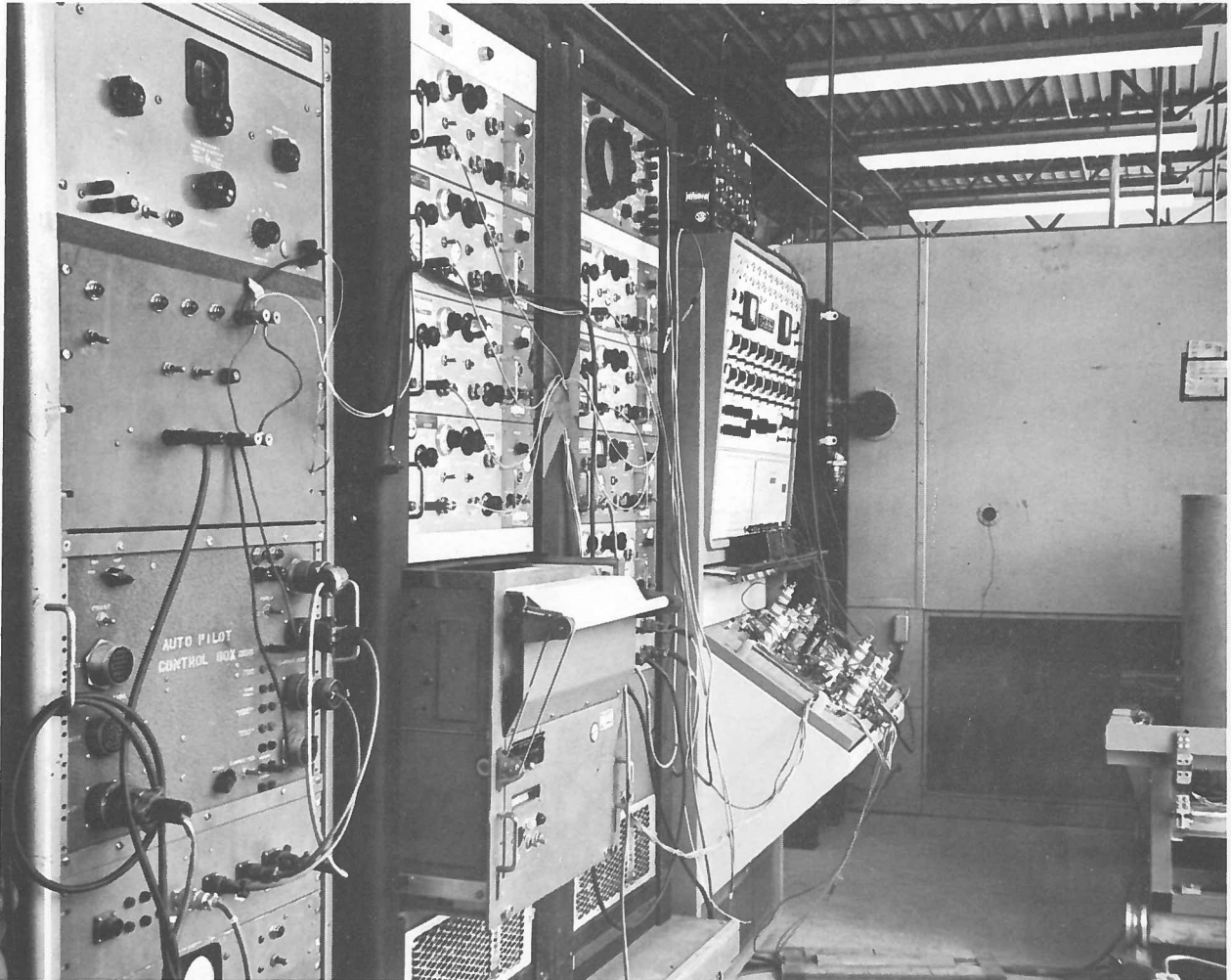


Figure 52. Slushing test setup at Astronautics.

9.2.2 BAFFLES. If it is found necessary to damp fluid motions in a large vehicle, mechanical baffles are added inside the tank. The most efficient baffling is obtained through the use of shelf-like projections for the following reasons:

1. The greatest fluid velocity in a tank of slushing liquid occurs near the wall.
2. The velocity is greatest at the fluid surface and is predominantly parallel to the tank axis.

Baffles totally out of the fluid as well as baffles deep in the fluid are ineffective, so a good baffle arrangement would consist of a series of annular rings as shown in Figure 53. Figure 54 shows a baffle arrangement used in model slushing tests.

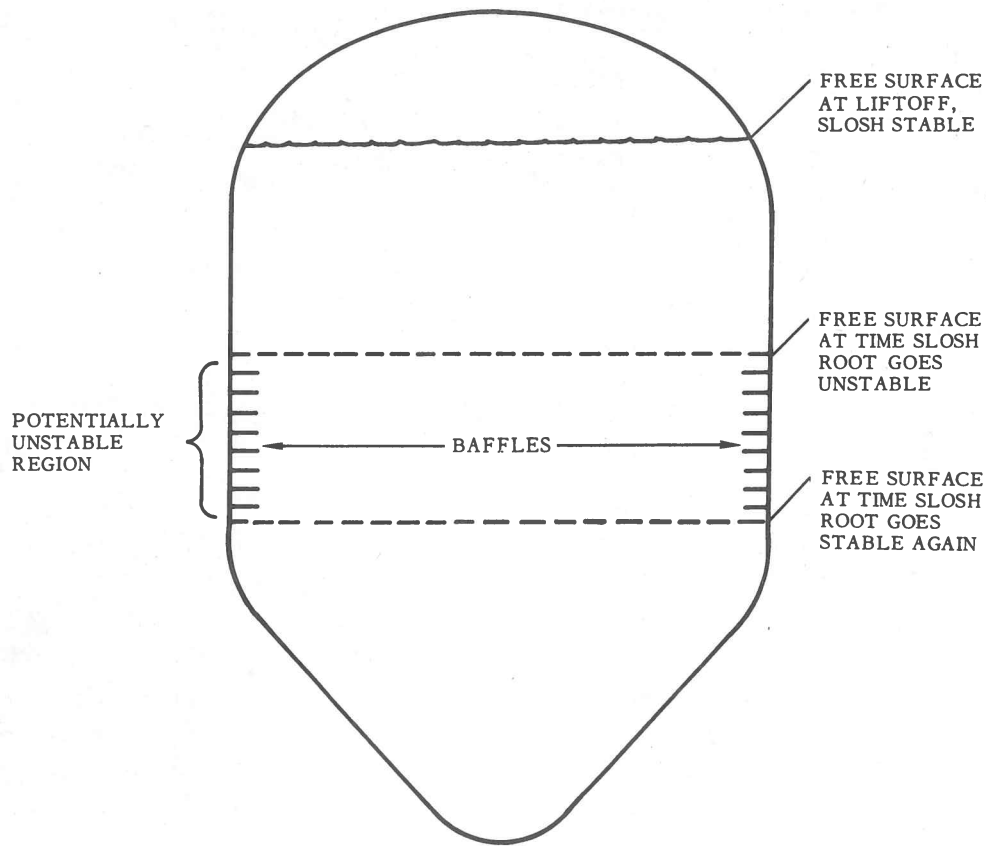


Figure 53. Typical baffle configuration.

From the preceding discussion it is clear that the designer needs information on baffle effectiveness as related to baffle width and depth below the free surface (to choose the baffle spacing). Semiempirical formulations of these properties have been derived which have proven satisfactory for design purposes. One such equation for cylindrical tanks is:

$$\gamma = 2.83 \left( \frac{A_{\text{baffle}}}{A_{\text{tank}}} \right)^{3/2} e^{-4.60 d/a} \left( \frac{j}{a} \right)^{1/2} \quad (4)$$

where:

$$\gamma = \text{damping ratio} = \frac{\sqrt{\omega^2 - \omega_d^2}}{\omega}$$

## GENERAL DYNAMICS | ASTRONAUTICS

$\omega$  = undamped fluid frequency,

$\omega_d$  = damped fluid frequency,

$d$  = depth of baffle under fluid free surface,

$a$  = tank radius,

$j$  = slosh height (see Figure 55),

$A$  = area.

This equation has been shown to be applicable for any ring submergence ( $d/a \geq 0$ ) and for ring widths corresponding to  $(A \text{ baffle}/A \text{ tank}) \leq 0.25$ . Measured damping ratios have fallen within  $\pm 30\%$  of the values predicated by this equation (Ref. 3). With Eq. 4, a study can be made of the optimum baffle width to baffle spacing, yielding the greatest damping for the least weight. A most significant characteristic of Eq. 4 is the fact that baffle damping is amplitude-dependent. It follows that before damping of fluid motion is possible, some sloshing is necessary. Thus, a limit-cycle oscillation is inevitable when mechanical baffles are used to contain the sloshing of an unstable liquid-propellant tank. The designer has to establish beforehand a limit cycle amplitude he will accept. Eq. 4 is then solved in an iterative (trial) manner to obtain the best baffle width and spacing that will meet his requirements.

### REFERENCES

1. Approximate Transfer Functions for Flexible-Booster-and-Autopilot Analysis. D. R. Lukens, A. F. Schmitt, and G. T. Broucek, WADD TR-61-93, April 1961, pp. A-13-A-20.
2. Propellant Sloshing in a Conical Tank Undergoing Arbitrary Forced Translational Motion. J. Harper, Astronautics Report ZU-7-089-TN, 2 January 1958.
3. Final Report on an Experimental Investigation of Sloshing. J. P. O'Neill, AFBMD-TR-60-52, 4 March 1960, p. 33.

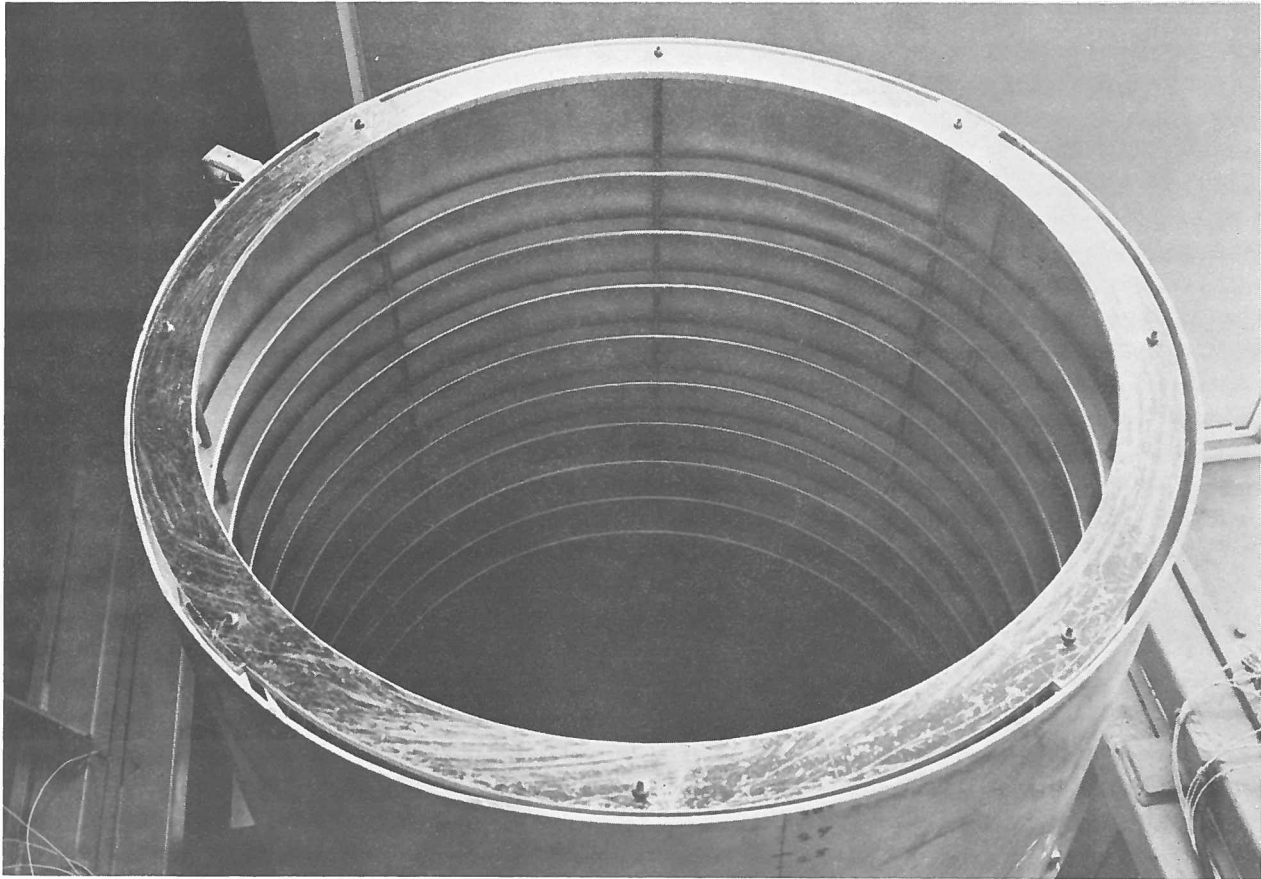


Figure 54. Annular ring baffles in a test tank.

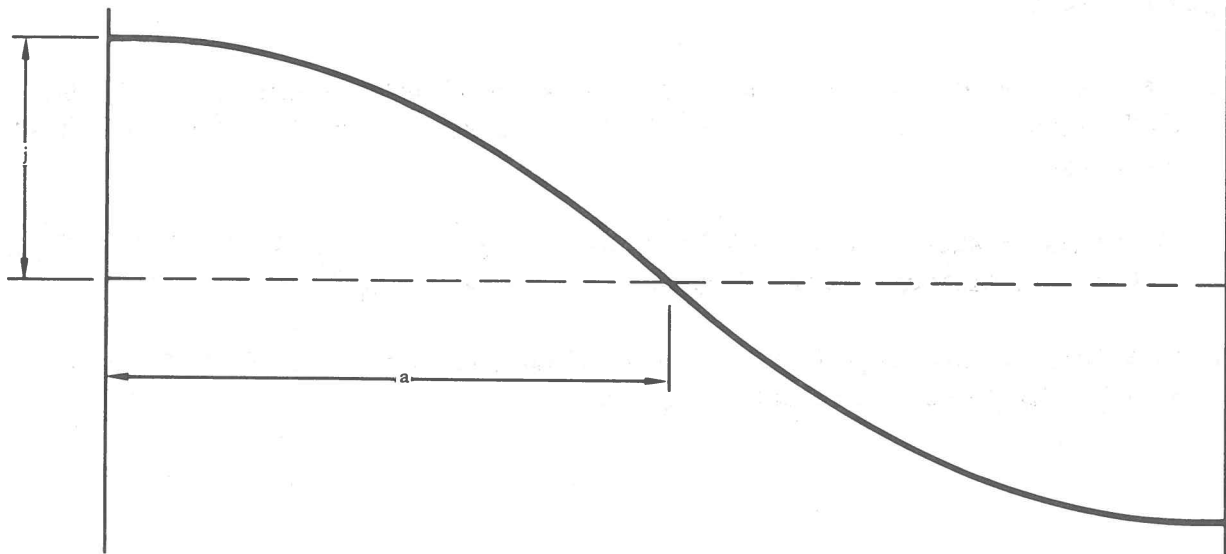


Figure 55. Slosh height definition.

# 10

## VORTEXING

The formation of a vortex core during the emptying process of a tub or funnel is a familiar sight to everyone. The reasons for the formation of such a core are not so familiar, and, in fact, the analysis for such a common occurrence falls into the class of problems known as nonsteady, free-boundary conditions. Such problems are difficult to solve because of the necessity for applying the boundary conditions at a boundary whose position is dependent upon the final solution. When complex shapes such as antivortex baffles and membranes are introduced in a launch vehicle tank to alter the vortex formation, an analytical solution to the problem becomes intractable, and the effect of the antivortex baffles must be resolved by experimentation.

Vortexing of liquid propellants has the disastrous effect of feeding a gas-liquid mixture to the turbopump when the vortex core reaches the pump inlet. Many ingenious designs have been tested and used to eliminate vortexing. Some of these tests have been run on full-scale mockups of the vehicle tank, as was the case for the Atlas. However, when tanks reach the size contemplated for the Saturn stages, it is economically desirable to run model tests and scale the results to full-size tanks.

### 10.1 SCALING MODEL TEST RESULTS

M. S. Plesset, a consultant to Astronautics, analyzed the similitudes of liquid motion in order to correlate experimental data obtained from model tests with the liquid motion of a prototype. The following model was used in his calculations. Consider a cylindrical container with a conical bottom and orifice at the cone apex. It is assumed the tank is vertical so that gravity is directed axially. Surface tension has been shown to have an insignificant effect on the discharge rate after the funnel has reached the orifice and on the liquid motion as the funnel is developing. (This is not true at very low  $g$  forces.)

The quantities which affect the vortex phenomena are as follows:

1. Independent Variable.  $t$  (time).
2. External Influences.  $p$  (pressure above ambient pressure over liquid),  
 $g$  (acceleration).

## GENERAL DYNAMICS | ASTRONAUTICS

3. Geometrical Parameters.  $R$  (tank radius),  $r_o$  (orifice radius),  $\beta$  (cone angle).
4. Fluid Properties.  $\rho$  (density of the fluid),  $\nu$  (viscosity of the fluid).
5. Flow Properties.  $h$  (height of liquid in tank at time  $t$ ),  $\gamma$  (depth of funnel depression below surface  $h$ ),  $U$  (average discharge velocity),  $\Gamma$  (average circular rotation rate of fluid).

Dimensional analysis gives the following relationships between dimensionless variables:

$$\frac{\gamma}{H} = f_1 \left( \sqrt{\frac{g}{H}} t, \frac{R}{r_o}, \frac{H}{r_o}, \beta, \frac{\gamma}{r_o \sqrt{gH}}, \frac{R \sqrt{gH}}{\nu} \right) \quad (1)$$

$$\frac{h}{H} = f_2 \text{ (same dimensionless variables as above),} \quad (2)$$

$$\frac{U}{\sqrt{2gH}} = f_3 \text{ (same dimensionless variables as above),} \quad (3)$$

where  $H$  = initial height of fluid. Eq. 1 gives the development of the funnel, Eq. 2 gives the instantaneous depth of the liquid, and Eq. 3 essentially determines the discharge coefficient.

Let the experimental model and prototype be geometrically similar, with magnification factor

$$n = \frac{\text{prototype linear dimension}}{\text{model linear dimension}}$$

Then the factors  $R/r_o$  and  $\beta$  remain constant. For model results to be directly applicable to a prediction of prototype flow, the similitude requirement is that the remaining nondimensional variables in  $f_1$ ,  $f_2$ , and  $f_3$  have the same value. Using a subscript,  $m$ , to refer to the model and no subscript to refer to the prototype, the following relations hold:

$$\frac{H}{r_o} = \frac{H_m}{r_{o_m}}, \quad \frac{H}{H_m} = \frac{r_o}{r_{o_m}} = n ;$$

## GENERAL DYNAMICS | ASTRONAUTICS

from

$$\sqrt{\frac{g}{H}} t = \sqrt{\frac{g_m}{H_m}} t_m,$$

$$\frac{t}{t_m} = \sqrt{\frac{H}{H_m}} \cdot \sqrt{\frac{g_m}{g}},$$

therefore,

$$\frac{t}{t_m} = n^{1/2} \sqrt{\frac{g_m}{g}}$$

The time scale of the prototype motion is thus  $n^{1/2} \sqrt{\frac{g_m}{g}}$  times that of the model motion

from

$$\frac{p}{\rho g H} = \frac{p_m}{\rho_m g_m H_m}$$

$$\frac{p}{p_m} = \left( \frac{H}{H_m} \right) \left( \frac{g \rho}{g_m \rho_m} \right)$$

therefore,

$$\frac{p}{p_m} = n \left( \frac{g \rho}{g_m \rho_m} \right).$$

This relation prescribes the excess tank pressure ratio.

## GENERAL DYNAMICS | ASTRONAUTICS

from

$$\frac{\Gamma}{r_o \sqrt{gH}} = \frac{\Gamma_m}{r_{o_m} \sqrt{g_m H_m}},$$

$$\frac{\Gamma}{\Gamma_m} = \frac{r_o \sqrt{gH}}{r_{o_m} \sqrt{g_m H_m}},$$

therefore,

$$\frac{\Gamma}{\Gamma_m} = n^{3/2} \sqrt{\frac{g}{g_m}}$$

The ratio of the average circular rotation rate of the fluid is prescribed by this equation. Finally, if it is required that the reynolds number have the same value, it follows that:

$$R \frac{\sqrt{gH}}{\nu} = \frac{R_m \sqrt{g_m H_m}}{\nu_m},$$

$$\frac{\nu}{\nu_m} = \frac{R}{R_m} \sqrt{\frac{H}{H_m}} \sqrt{\frac{g}{g_m}},$$

therefore

$$\frac{\nu}{\nu_m} = n^{3/2} \sqrt{\frac{g}{g_m}}.$$

Obviously, this last requirement cannot be met if the same liquid is used. Even if a different liquid is sought for the model tests, it is usually not possible to satisfy this condition for any reasonable value of  $n$ . For cryogenic fluids, the viscous effects are usually neglected in scaling test results.



## 10.2 ANTIVORTEX DESIGNS

Considerable experience has been gained by Astronautics in designing and testing anti-vortex baffles for the Atlas. The battleship tank facility at the Point Loma Test Site was utilized. Water was used to simulate the fuel in this full-scale mockup of the Atlas. One of the earlier designs consisted of a circular plate with a series of concentric holes located over the surface of the plate. The plate served the dual purpose of an antivortex baffle and a tank support for the thrust cone to prevent the tank from assuming an asymmetric shape due to thrust vectors (see Figure 56). Tests showed that the vortex core extended through the central holes of the plate and caused extensive bubble formation beneath the plate. A modified antivortex plate with two concentric rings of holes located at the periphery of the plate eliminated all vortexing and bubble formation beneath the plate (Figure 56).

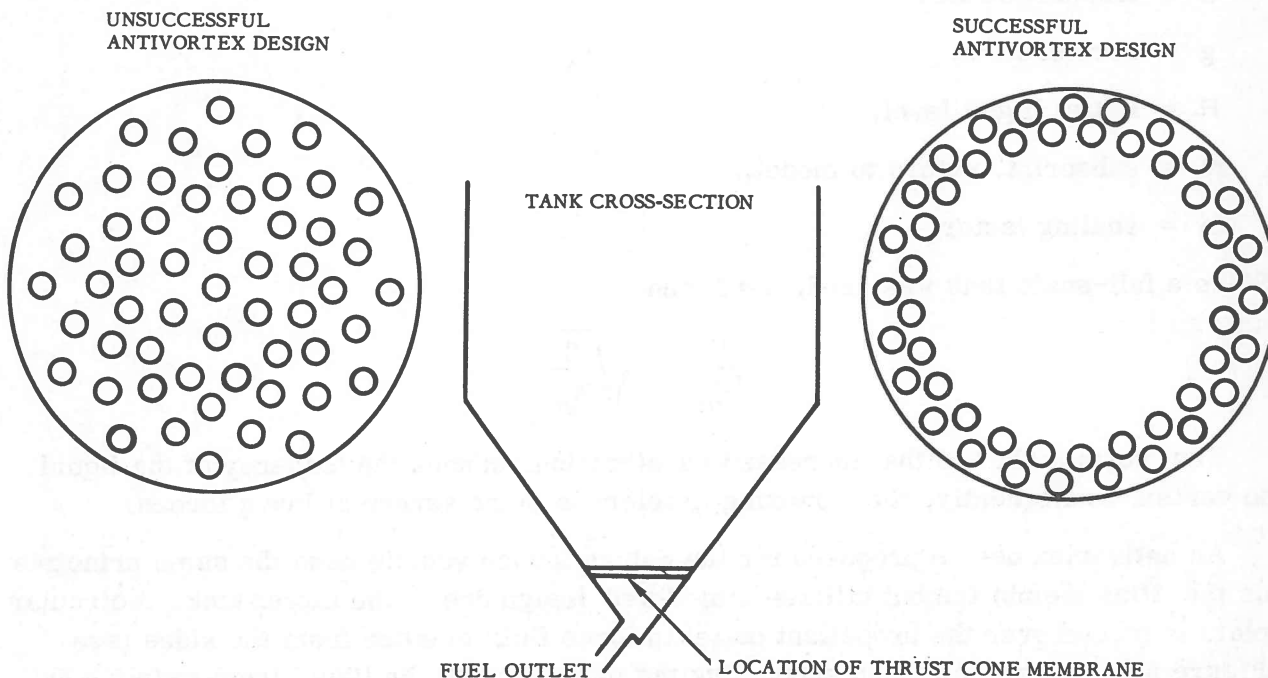


Figure 56. Atlas antivortex membranes.

## GENERAL DYNAMICS | ASTRONAUTICS

During these tests, the flow rates were varied to determine what effect different g forces had on the vortex formation. These rates were determined from the Froude number

$$\left( \frac{U}{\sqrt{gH}} \right)$$

$$\frac{U}{\sqrt{gH}} = \frac{U_m}{\sqrt{g_m H_m}}$$

$$\frac{U}{U_m} = \sqrt{\frac{g}{g_m}} \sqrt{\frac{H}{H_m}}$$

$$\frac{U}{U_m} = n^{1/2} \sqrt{\frac{g}{g_m}}$$

where

U = discharge rate,

g = acceleration,

H = initial liquid level,

m = subscript, refers to model,

n = scaling factor.

Since a full-scale tank was used,  $n = 1$  and

$$\frac{U}{U_m} = \sqrt{\frac{g}{g_m}}$$

Test results showed that increased acceleration reduces the tendency of the liquid to vortex; consequently, the vortexing problem is more severe at low g forces.

An antivortex device proposed for the Saturn launch vehicle uses the same principle as the Atlas membrane but utilizes a modified design due to the larger tank. A circular plate is placed over the propellant outlet to force fluid to enter from the sides (see Figure 57). Six radial vanes supporting the plate prevent the liquid from swirling as it enters the outlet.

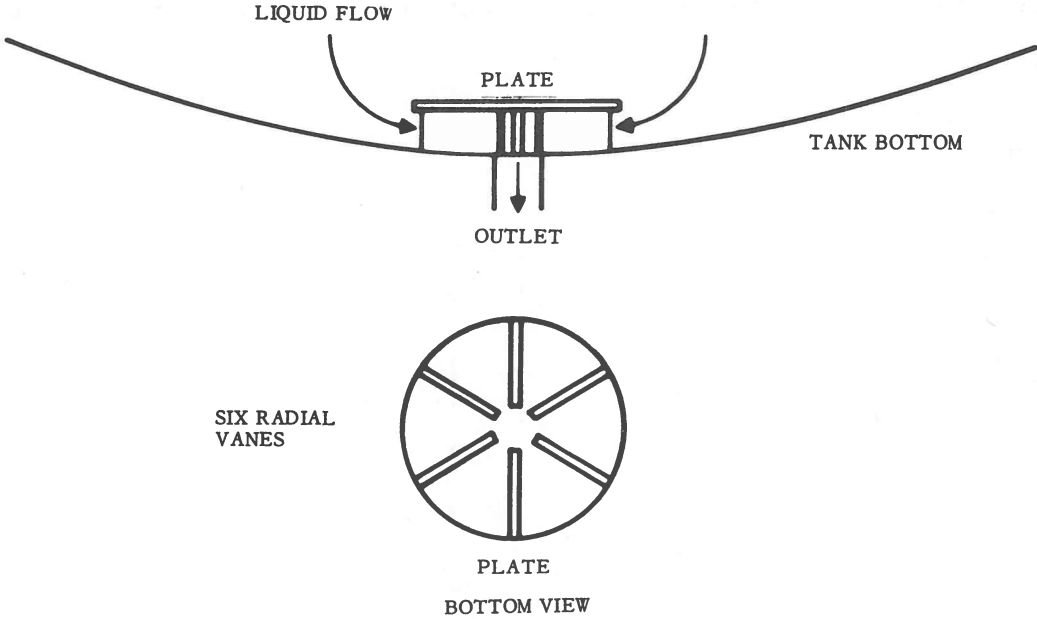


Figure 57. Proposed Saturn antivortex device.



# 11

## PROPELLANT HEATING

### 11.1 INTRODUCTION

Liquid hydrogen in a space vehicle is subjected to heating from external sources (aerodynamic heating, solar radiation, planetary radiation, and albedo) and onboard heat sources (heat-generating units such as the rocket nozzle or nuclear reactor--if used--plus the sensible enthalpy available in the vehicle mass including other propellants). Heat input into the propellant raises the fluid's temperature and, consequently, the vapor pressure. When the vapor pressure reaches the tank design limits, the hydrogen has to be subcooled using refrigeration equipment or gas has to be vented overboard. Either case represents a weight penalty to the vehicle. Due to the low heat of vaporization of liquid hydrogen, it is important that the heat-transfer rate into the fluid be calculated accurately prior to deciding on a vehicle's design. Once the heat contributions are known, tradeoff studies between the tank design pressure, insulation type and thickness, and refrigeration systems can be made. This section discusses the heat contributions from both the external environment and onboard sources.

### 11.2 ENVIRONMENTAL HEATING

11.2.1 GROUND HOLD. During ground hold, vented boiloff gas is replaced by topping the tank with liquid hydrogen just prior to liftoff. The major requirements during this period are to prevent excessive boiloff rates and prevent air condensation on the tank surface.

The hydrogen heat load derived from a sea-level atmosphere can be calculated as a function of the tank wall over-all conductivity. This is shown in Figure 58 for air. Conductivity values for different insulations are listed in Chapter 5. At higher thermal resistances the effect of the outside coefficient is secondary and therefore the heat rate can be used for all of the tank area except that exposed to another cryogenic tank. Mean value data for earth and solar radiation is also given in Figure 58 for daytime operation.

GENERAL DYNAMICS | ASTRONAUTICS

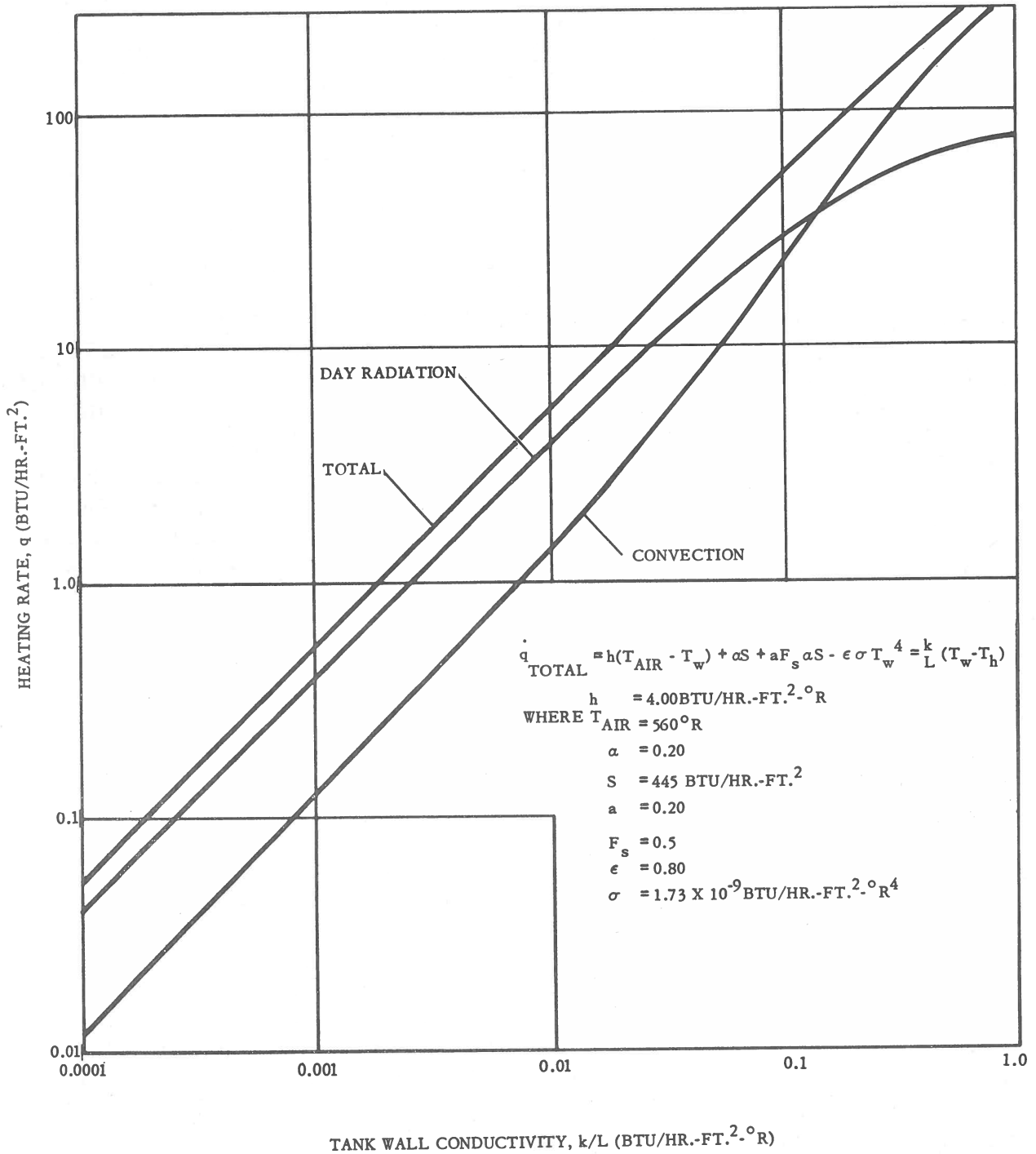


Figure 58. Ground heat load to hydrogen tank.

11. 2. 2 ASCENT AERODYNAMIC HEATING. Although aerodynamic heating rates are often sufficient to raise outside vehicle surface temperatures in certain locations to structural limits, the heating time period is of short duration and the over-all temperature difference across the tank wall to the hydrogen peaks at about twice its value on the ground or in space.

The aerodynamic heat transfer to the surface of a vehicle during flight in the atmosphere depends on the vehicle's shape as well as the flow field to which it is exposed. The so-called flat plate geometry has been investigated extensively and may be theoretically treated in a straightforward manner. A plane surface exposed to a flow field with a locally uniform velocity and flow direction fulfills the flat plate requirements. The flow velocity and, as a result, the pressure are also constant along the outer edge of the boundary layer. The boundary layer is specified such that it is thin enough to allow the pressure to be transmitted, without change, to the plate. In supersonic and hypersonic flow, the boundary layers are usually thick. As a consequence, the velocity and pressure vary along the outer edge of the boundary layer. The relations given below disregard these effects and assume locally constant pressure and temperature. However, the following equations yield heat-transfer calculations sufficiently accurate for design purposes when properties are evaluated at the reference enthalpy and inserted in the constant value expressions.

11. 2. 2. 1 Laminar Boundary Layers. The heat transferred ( $q$ ) from a laminar boundary layer to the wall is defined by the equation:

$$q = h (i_r - i_w), \text{ for variable specific heat}$$

where  $h$  = film coefficient of heat transfer ( $\frac{\text{lb.}}{\text{sec.} - \text{sq. ft.}}$ ),

$i_r$  = recovery enthalpy (defined by following equation) (Btu/lb.),

$i_w$  = enthalpy at wall temperature (Btu/lb.).

For variable specific heat, the recovery enthalpy,  $i_r$ , may be calculated from

$$i_r = i_s + \frac{rV^2}{2g}, \text{ with } i_s \text{ evaluated at stream conditions.}$$

## GENERAL DYNAMICS | ASTRONAUTICS

Where

$i_s$  = enthalpy at stream conditions,

$r$  = recovery factor,

$V$  = stream velocity,

$g$  = gravity constant.

The recovery factor  $r$  is calculated from the expression  $r = \sqrt{\text{Pr}^*}$

where

$\text{Pr}^*$  = prandtl number at reference enthalpy,  $i^*$ ,

and

$$i^* = 0.5 (i_s + i_w) + 0.11 r (\gamma - 1) M^2 i_s$$

where

$$\gamma = C_p / C_v \text{ of air}$$

$M$  = free-stream Mach number (Mach number of vehicle).

Since  $r$  also appears in the reference enthalpy equation, normally an arbitrary value (0.85 to 0.90) is chosen and the equations are solved by an iterative process until the answer converges.

The heat-transfer coefficient,  $h$ , is obtained from the Stanton number ( $St$ ) given by the equation

$$St = \frac{h}{\rho_a V}$$

where

$\rho_a$  = air density at the boundary layer edge,

$V$  = stream velocity.

The Stanton number may be obtained from the expression

$$St = \frac{c_f}{2} (\text{Pr}^*)^{-2/3}$$



## GENERAL DYNAMICS | ASTRONAUTICS

The skin friction coefficient ( $c_f$ ) is found from

$$c_f = 0.664 (\text{Re}^*)^{-1/2}$$

where  $\text{Re}$  = reynolds number at reference enthalpy,  $i^*$ .

11.2.2.2 Turbulent Boundary Layers. In the case of turbulent flow, the constant-property relations for the laminar boundary layer may be used when all the properties are evaluated at the reference enthalpy. Experimental data has shown that the recovery factor for turbulent boundary layers can be expressed by

$$r = (\text{Pr}^*)^{1/3}$$

and for reynolds numbers up to  $10^9$  the skin friction coefficient is given by

$$c_f = \frac{0.370}{(\log_{10} \text{Re})^{2.584}}$$

Further, the relation between stanton number and the skin friction coefficient is about the same for turbulent as well as laminar boundary layers, thus

$$\text{St} = \frac{0.185}{(\log_{10} \text{Re})^{2.584}} (\text{Pr}^*)^{-2/3}$$

The heat-transfer coefficient may then be calculated from the expression

$$\text{St} = \frac{h}{\rho_a V}$$

and the heat flux is again found from

$$q = h (i_r - i_w)$$

where the recovery enthalpy is expressed by

$$i_r = i_s + \frac{rV^2}{2g}$$

## GENERAL DYNAMICS | ASTRONAUTICS

The reference enthalpy at which fluid properties are evaluated is again given by

$$i^* = 0.5 (i_w + i_s) + 0.11 r(\gamma - 1) (M)^2 i_s$$

A digital computer program, assembly 2162, is in use which employs the above expressions to obtain heat transfer for both laminar and turbulent boundary layers.

**11.2.3 SPACE HEATING.** In order to thermally control space vehicles, it is necessary to know the magnitudes of the three external energy sources to which they are exposed: solar radiation, planetary radiation, and albedo.

For a transfer path from one planet to another, planetary radiation and albedo can be neglected once the vehicle is beyond three planet diameters from the surface. Consequently, the total heat flux will be almost entirely from solar radiation which varies as the square of the distance between the sun and the vehicle. (See Figure 59.) The quantity of this radiant flux that enters the LH<sub>2</sub> can be determined from Figure 60 if the incident solar flux and wall conductivity are known. The curves are plotted for

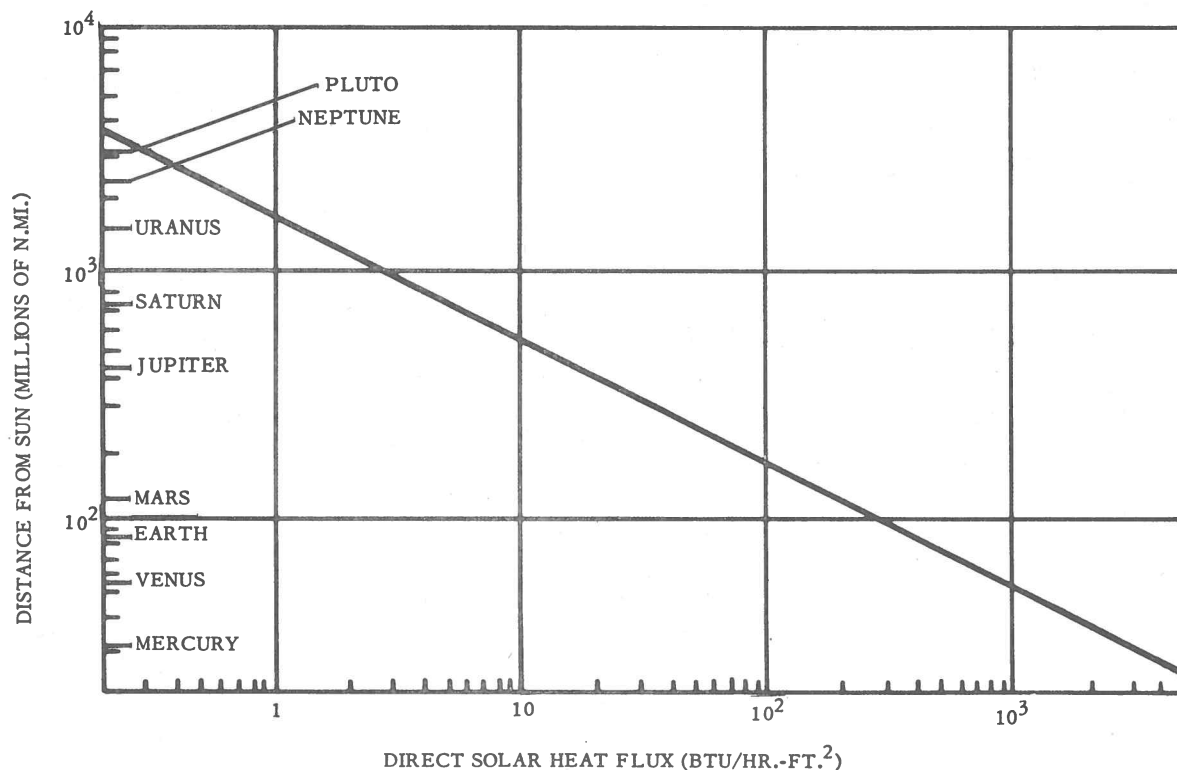


Figure 59. Variation of solar heat flux with distance to the sun.

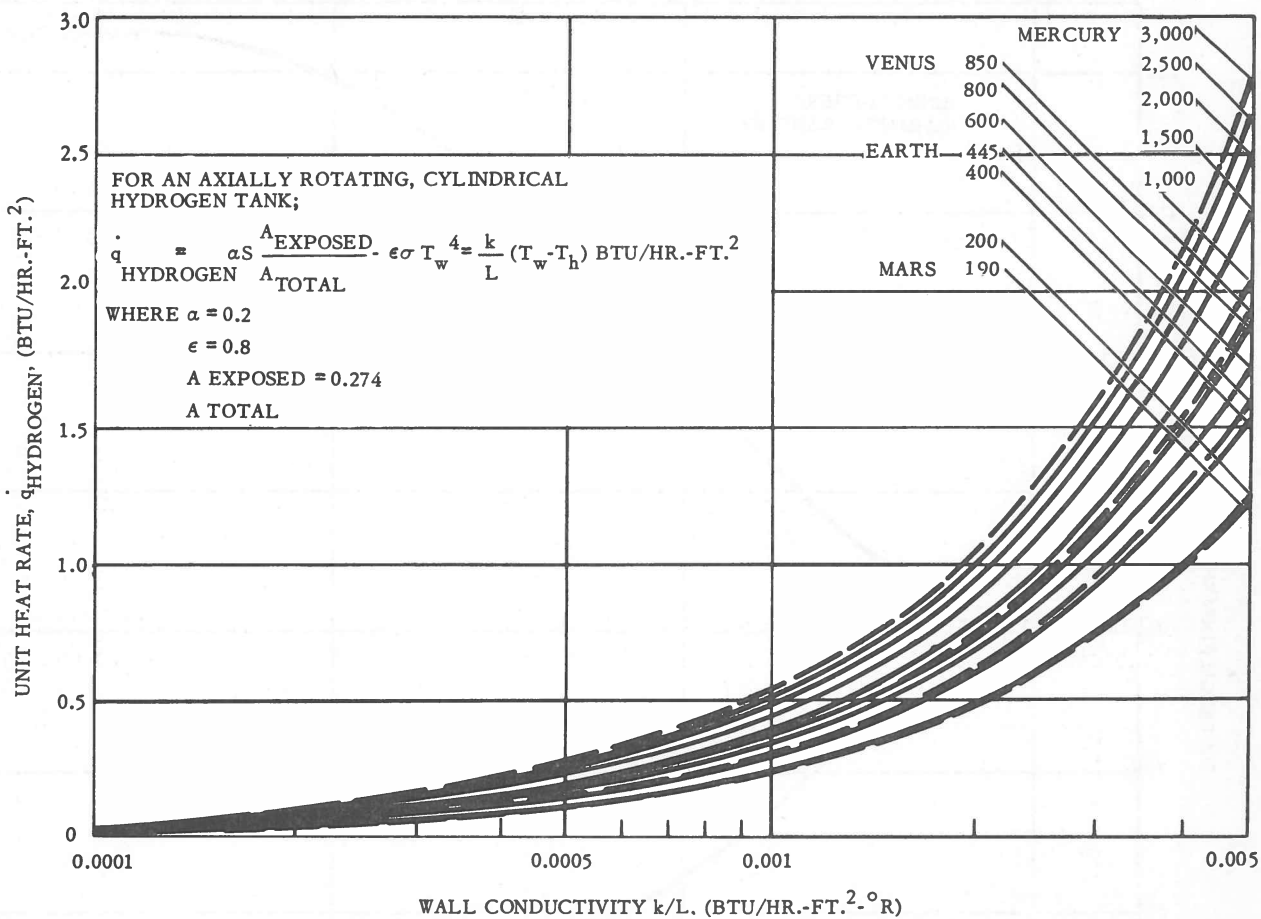


Figure 60. Unit heating rates in interplanetary space.

an axially rotating cylindrical tank with the broad side normal to the sun. This assumes an equilibrium temperature distribution over the surface. In order to sum the total heat flux entering the tank for an interplanetary trip, it is necessary to know the time rate of change of the vehicle's position with respect to the sun. Figure 61 gives the distance from the sun as a function of time for minimum-energy Hohmann transfers to Mars and Venus.

For orbiting vehicles, the relationship between the sun and the planet (in most cases, the earth) and the space vehicle's orbital position and spatial orientation are the main factors in computing the radiant heat flux from external energy sources. Direct solar radiation is the part of the external energy most easily determined, as it is usually independent of the altitude of the orbiting vehicle. Usually a satellite orbiting about a planet is exposed to a nearly constant value of solar heat flux, as its

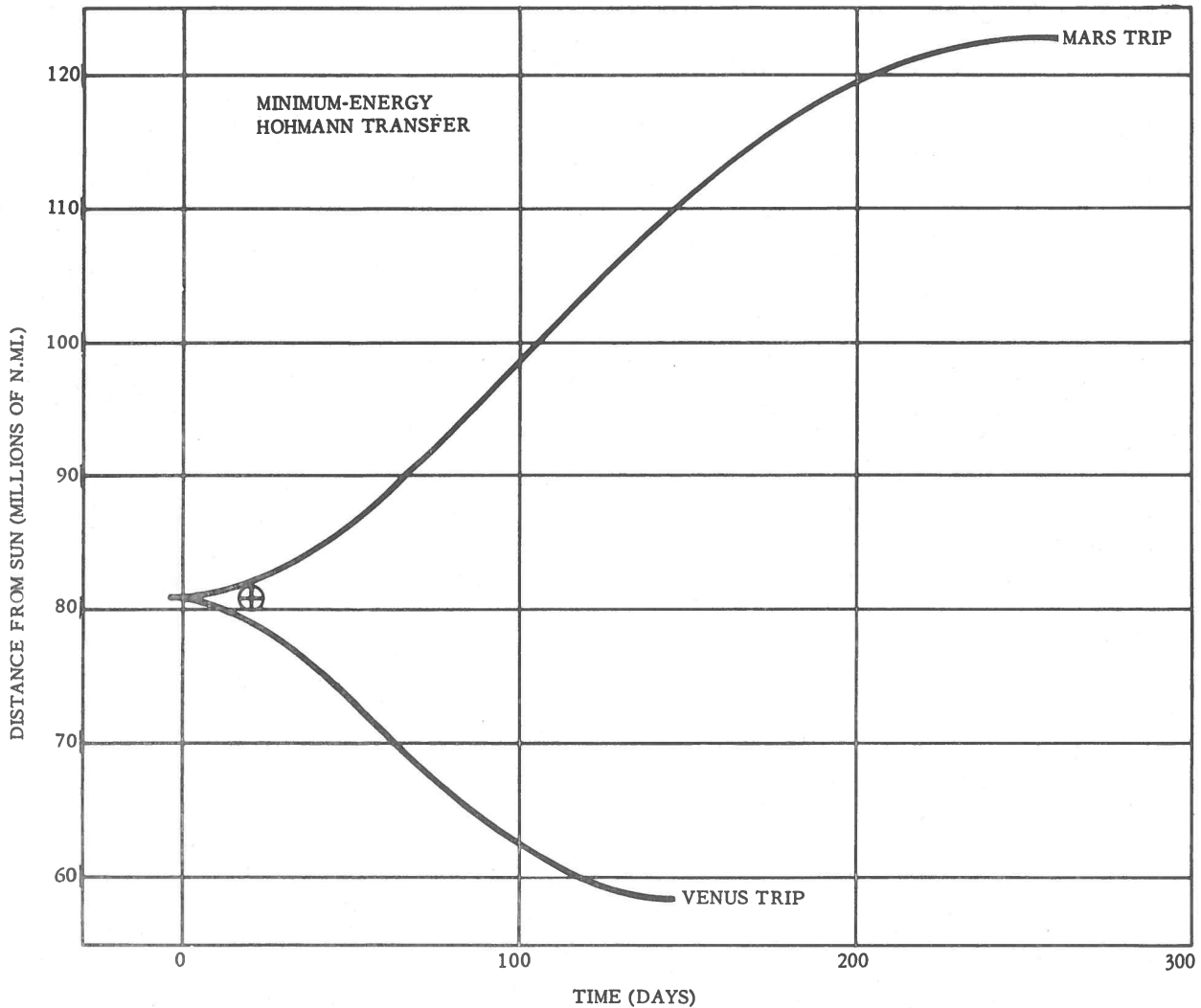


Figure 61. Distance from sun on typical interplanetary trajectories.

distance from the sun does not vary appreciably. The effective solar radiation incident upon any portion of a vehicle is a function only of the angle between the sun vector and a vector normal to any flat plate element by which any body may be approximated. The energy contributions from planetary albedo and thermal radiation can be expressed as a function of the vehicle's altitude and attitude.

The mathematical representations of solar radiation, planetary thermal radiation, and planetary albedo for orbiting vehicles follow.

## GENERAL DYNAMICS | ASTRONAUTICS

11.2.3.1 Solar Radiation. The direct solar radiation for an orbiting vehicle is given by:

$$q_{\text{solar}} = SA \cos (\vec{S}; N)$$

where

- $q_{\text{solar}}$  = incident energy from the sun (Btu/hr.),
- $S$  = solar constant (Btu/hr.-ft.<sup>2</sup>) (Figure 59),
- $A$  = area (sq. ft.),
- $\vec{S}$  = radius vector from the planet to the sun,
- $N$  = vector normal to a flat plate element,
- $(\vec{S}; N) = \Theta_3$  = the angle between the sun vector and a normal to a surface element (deg.).

Since both the solar constant ( $S$ ) and the element area are independent of time for an orbiting vehicle, it remains only to express the angle  $(\vec{S}; N)$ , or  $\Theta_3$ , as a function of time.

11.2.3.2 Planetary Thermal Radiation. The planetary thermal radiation to a flat plate is given by

$$q_{\text{thermal}} = F_t I_t A$$

where

- $q_{\text{thermal}}$  = incident planetary thermal radiation (Btu/hr.),
- $F_t$  = view factor for flat plate (nondimensional),
- $I$  = total energy rate emitted per planet unit area (Btu/hr.-sq. ft.),
- $I_t$  =  $(1-a) S/4$ , where  $S$  is the solar constant and  $a$  the planetary albedo constant,
- $A$  = area (sq. ft.),

## GENERAL DYNAMICS | ASTRONAUTICS

and where

$$F_t = \frac{1}{2\pi} \left[ \pi - 2 \sin^{-1} \frac{\sqrt{H^2 - R^2}}{H \sin \Theta_2} - \frac{1}{2\pi} \sin \left[ 2 \sin^{-1} \frac{\sqrt{H^2 - R^2}}{H \sin \Theta_2} \right] - \frac{R^2}{2H^2} \left[ 1 + \frac{2}{\pi} \sin^{-1} \frac{\sqrt{H^2 - R^2}}{R(-\tan \Theta_2)} + \frac{1}{\pi} \sin \left\{ 2 \sin^{-1} \frac{\sqrt{H^2 - R^2}}{R(-\tan \Theta_2)} \right\} \right] \right] \cos \Theta_2$$

or if

$$\Theta_2 < \tan^{-1} \frac{\sqrt{H^2 - R^2}}{R}$$

the expression for  $F_t$  reduces to simply

$$F_t = \frac{R^2}{H^2} \cos \Theta_2$$

In these expressions the definition of the newly introduced variables are,

$H$  = distance from center of planet to vehicle (n.mi.),

$\Theta_2$  = the angle between a normal to a surface element and radius vector from the planet to the vehicle, which is the same as the principal axis in the moving-vehicle system.

Figure 62 shows the geometrical relationships for planetary thermal radiation to a flat plate.

11.2.3.3 Planetary Albedo. The planetary albedo to a flat plate is given by

$$q_{\text{albedo}} = F_a a S A,$$

where

$q_{\text{albedo}}$  = incident planetary albedo (Btu/hr.),

$F_a$  = view factor for flat plate (nondimensional),

# GENERAL DYNAMICS | ASTRONAUTICS

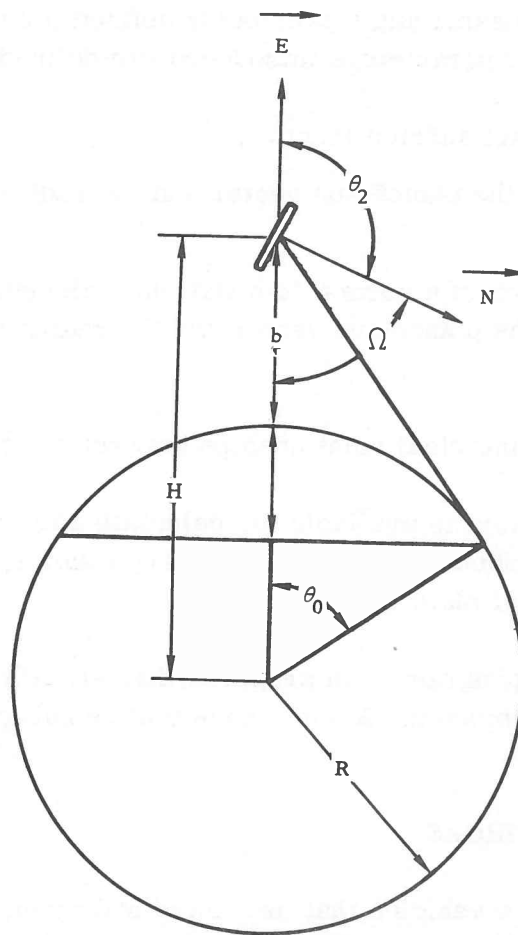


Figure 62. Geometry of planetary thermal radiation to a flat plate.

$S$  = solar constant (Btu/hr.-sq.ft.),

$A$  = area (sq.ft.)

and where

$$F_a = F_t(b, \Theta_2) \left\{ \left[ 0.86 + 0.14e^{-0.00022b} \right] \cos \left[ \Theta_1 - 0.0000417 (180 - \Theta_2)^3 \right] \right. \\ \left. \cos \phi_c \left( 1 - e^{-\frac{5.4b}{(180 - \Theta_2)}} \right) \right\}$$

## GENERAL DYNAMICS | ASTRONAUTICS

In this equation  $\Theta_2$  is the same angle previously defined for the case of planetary thermal radiation. The new parameters introduced are defined as follows:

$b$  = altitude above planet surface (n. mi.),

$\Theta_1$  = the angle between the planet-sun vector and the radius vector from the planet to the vehicle,

$\phi_c$  = the angle of rotation of a normal to a flat plate element, measured from a plane containing the planet-sun vector and the radius vector from the planet to the vehicle.

Figure 63 shows the geometrical relationships between the parameters.

A digital computer program is available for calculating the heat inputs from the three energy sources described herein for a cylinder, cone, sphere, ellipsoid hemisphere and, of course, a flat plate (see Ref. 1).

A configuration factors program is in progress that will allow the effect of shadowing by other bodies to be computed. A wide variety of geometrical shapes can be handled by this new program.

### 11.3 ONBOARD HEAT SOURCES

Looking at all types of space vehicles that use liquid hydrogen, there are essentially two ways heat can be transferred into the propellant from onboard power sources: (1) by solid conduction through the insulated walls and the through-connections, and (2) by volumetric heating of the propellant from a nuclear power source (reactor or radioisotopes).

**11.3.1 MISCELLANEOUS HEAT SOURCES.** Surface heat transfer at the tank wall from sources such as electronic equipment, gas generators, the engines, and the sensible enthalpy of the vehicle mass plus other propellants causes temperature stratification in the tank. The liquid hydrogen is warmed slightly at the walls, rises to the top, and forms a stratified layer. Excessive sloshing will prevent this layer from forming.

An estimate of the heat leak through plumbing connections, bosses, etc. can be made using Figure 64 if the "k" value and structural dimensions of the through-connection are known. Figure 65 shows a typical method for reducing the heat leak through a tank support. Once the total heat leak is known for all the through-connections, this value should be compared to the total heat leak through the insulation.



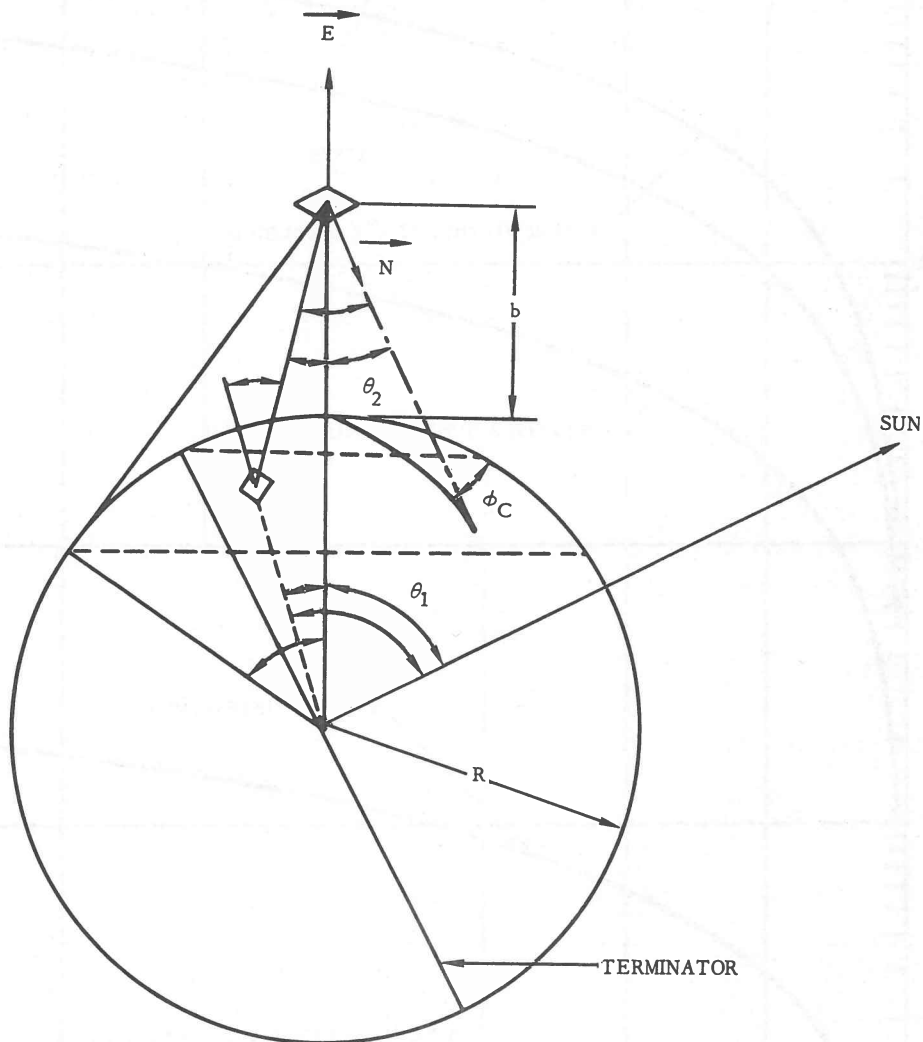


Figure 63. Geometry of planetary albedo to a flat plate.

This heat-leak ratio gives a good idea as to whether research and design efforts should be concentrated on improving the insulation or reducing the heat leak in the through-connections. Heat transferred between propellants at a common bulkhead can be significant and must be taken into account. Figure 66 gives the heat-transfer and hydrogen boiloff rate for a typical bulkhead between  $\text{LO}_2$  and  $\text{LH}_2$  tanks. Experience on Centaur has shown it is difficult to seal a welded vacuum-type bulkhead against hydrogen leakage; consequently, the heat-transfer rate is high. An electroformed bulkhead (one piece with no welds) is being tested, and results so far have been promising.

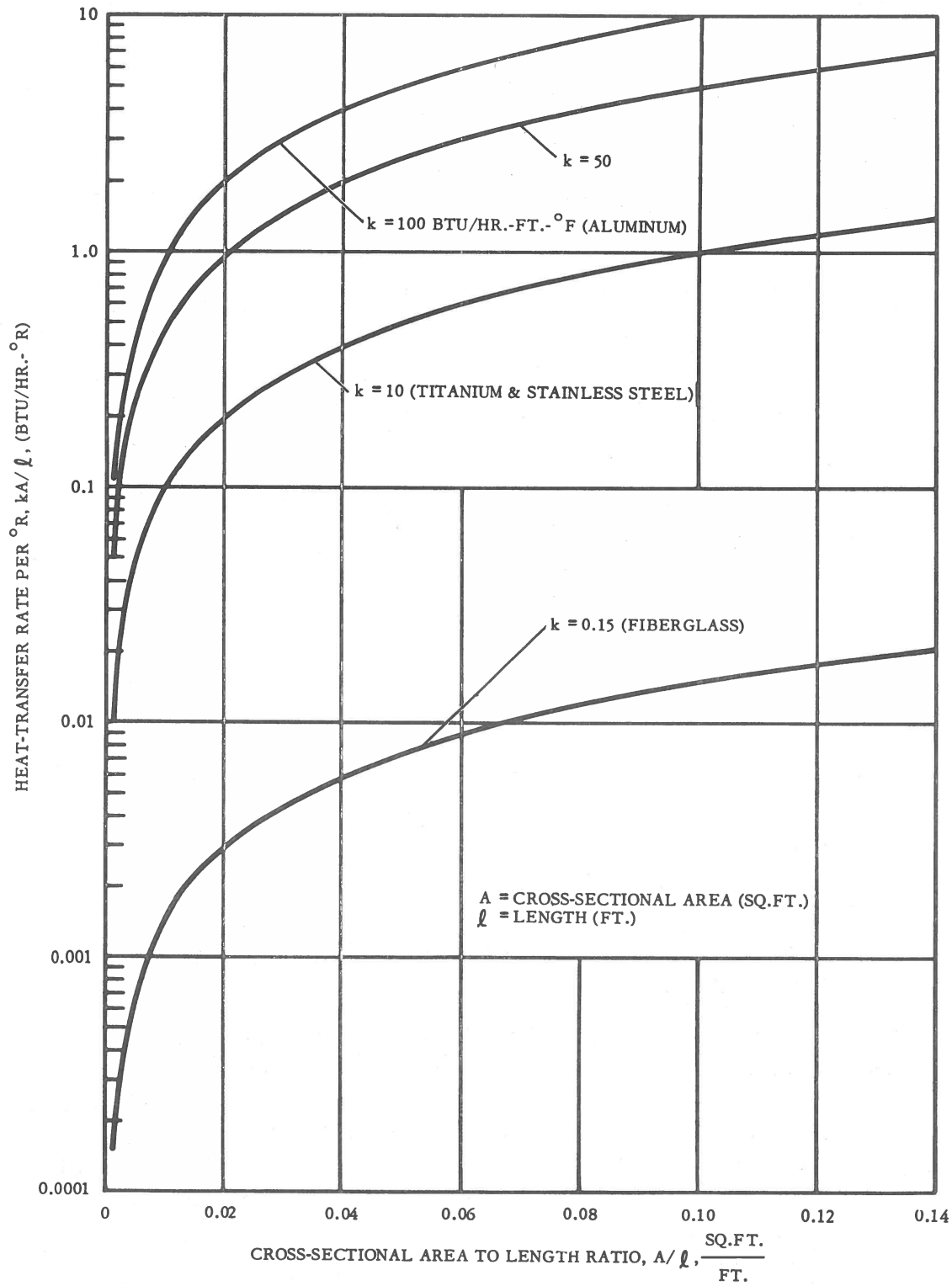


Figure 64. Through-connection heat-leak parameter.

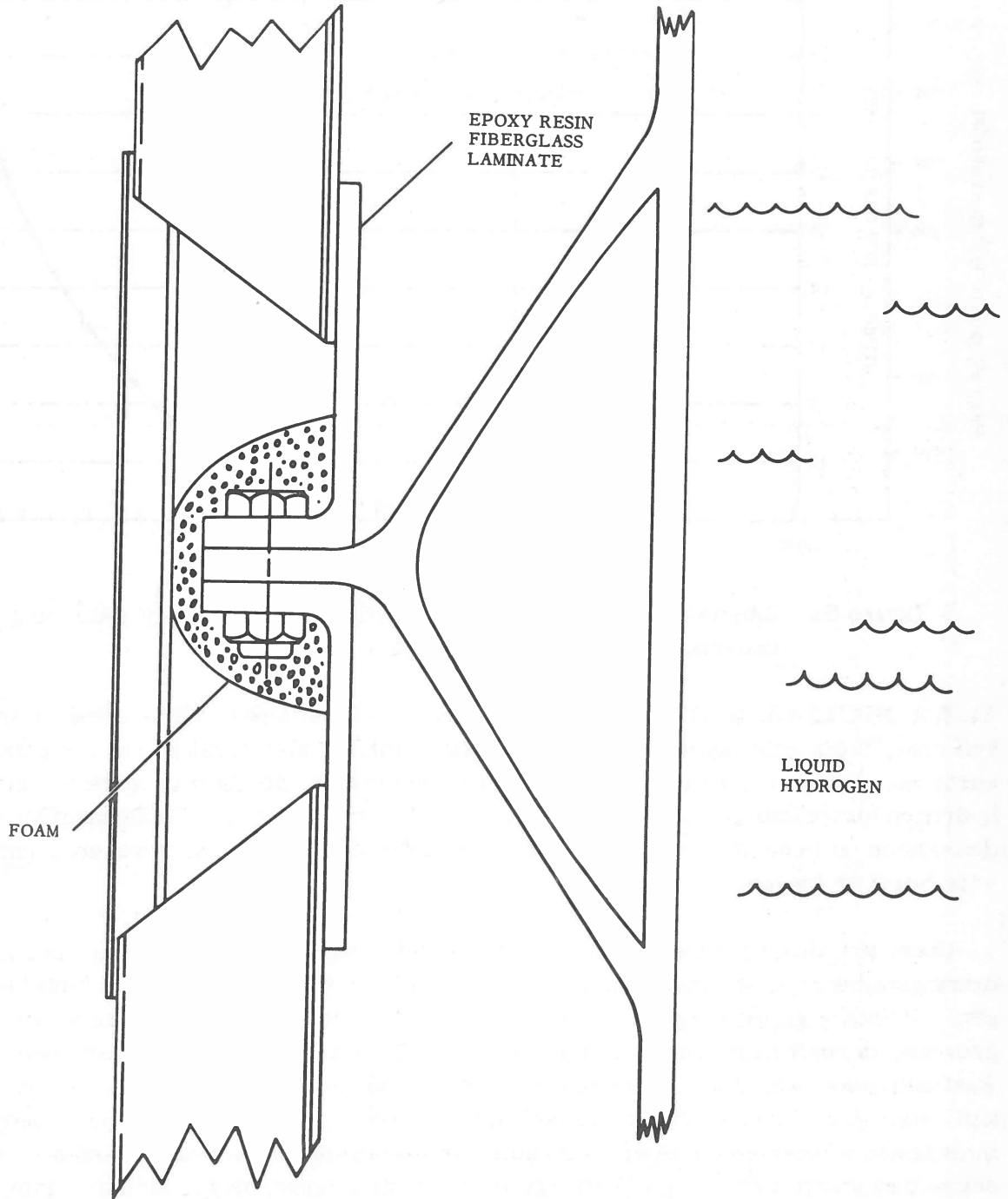


Figure 65. Typical hydrogen tank support.

## GENERAL DYNAMICS | ASTRONAUTICS

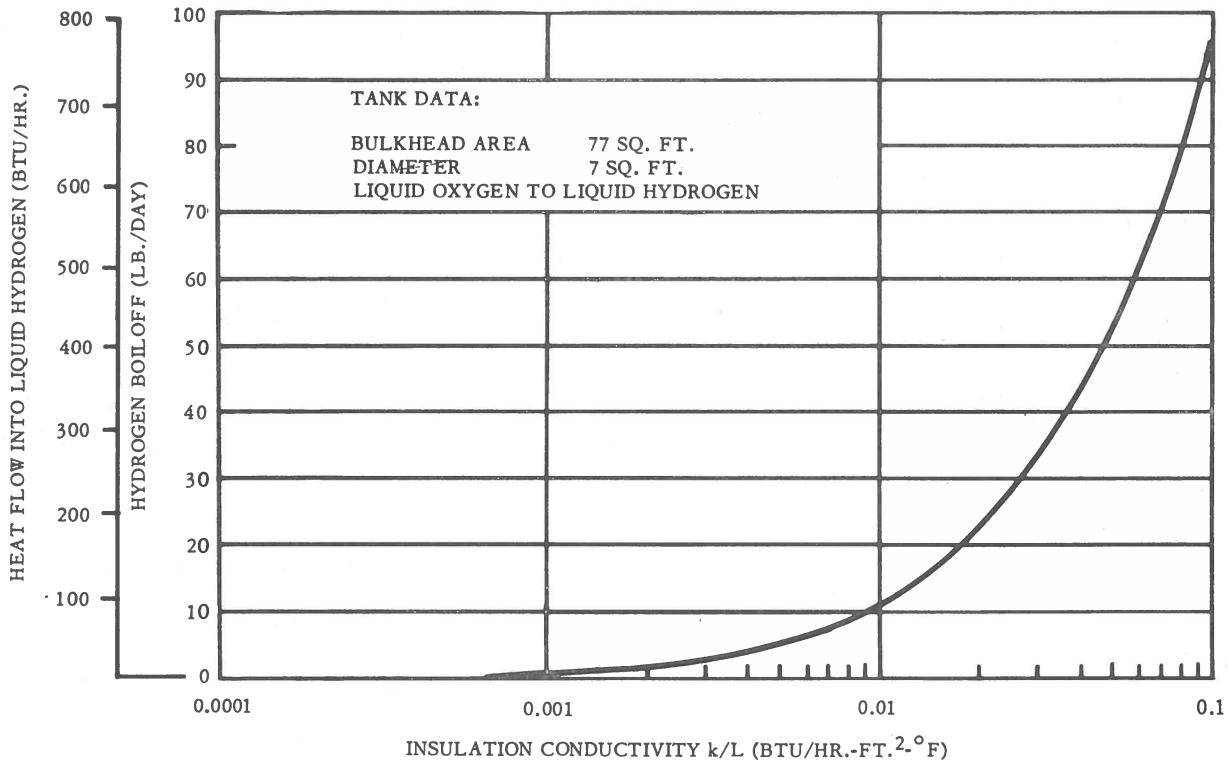


Figure 66. Intertank heat transfer as a function of conductivity (including convection and radiation in tank).

11.3.2 NUCLEAR HEAT SOURCES. Although radioisotopes will be used on space vehicles, their role appears to be limited to supplying electrical power for satellite systems. Reactors, on the other hand, will be used as the main propulsion unit on hydrogen-propelled vehicles due to their higher power density. Consequently, this discussion on propellant heating will be limited to the interaction of reactor radiations with liquid hydrogen.

There are three primary modes of propellant heating by reactor radiations: primary gamma ray, neutron, and secondary gamma ray interactions with liquid hydrogen. Primary gamma rays, which are produced in the reactor core during the fission process, deposit heat energy in materials by interactions with molecular electrons. Fast neutrons, which are produced in the core, deposit energy in materials by elastic and inelastic collisions with atomic nuclei. Secondary gamma rays are produced by the interaction of neutrons with atomic nuclei which results in gamma emission. These secondary gamma rays deposit energy in the same manner as the primary gamma rays. To determine the propellant temperature increase which will result from these modes of heat deposition, it is necessary to establish a heating model which describes

## GENERAL DYNAMICS | ASTRONAUTICS

actual conditions as closely as possible. From such a model a set of equations can be derived which will give the propellant temperature as a function of the parameters established by the model.

11.3.2.1 Baffled Tank Model. To increase the rate at which radiation induced heat would be removed from the tank, a unidirectional flow baffle has been proposed (see Figure 67). The baffle consists of a perforated plate designed to allow flow downward through the holes at a sufficiently high rate, approximately 1 fps, to prevent an upward flow of liquid hydrogen. Since approximately 95% of the radiation heating occurs in the bottom of a typical tank such as shown in Figure 67, most of the heated hydrogen is pulled through the pump before it has a chance to rise and form a stratified layer on top. Laboratory tests and flight tests have shown that the heat flux entering from the sides to a cryogenic fluid subjected to acceleration will be carried in lower-density liquid up the sides of the tank in a relatively narrow boundary layer on the inside surface. Since the baffled tank prevents about 95% of the radiation heated hydrogen from rising to the top, the final tank vapor pressure will be lower in a baffled tank than in a nonbaffled tank. To establish an equation for the propellant temperature increase at the tank outlet as a function of reactor operating time the following quantities are defined:

$M$  = mass of propellant below the baffle (lb.)

$\dot{m}$  = propellant flow rate through the baffle and pump (pps)

$q$  = rate at which radiation heat is deposited below the baffle (Btu/sec.)

$H(t)$  = heat content of propellant flowing through the baffle (Btu/lb.)

For the purpose of calculations,  $H(t)$  is set equal to 0 when  $t = 0$ .

$Q$  = accumulated instantaneous heat content below the baffle (Btu)

$\frac{dQ}{dt}$  = rate of change of heat content below the baffle with respect to time (Btu/sec.)

Based on these definitions, it can be seen that:

$\frac{\dot{m}Q}{M}$  = rate at which heat is removed from the tank bottom through the pump (Btu/sec.).

The rate of change of heat content below the baffle with respect to time is equal to the rate at which heat is deposited minus the rate at which it is removed; hence, the

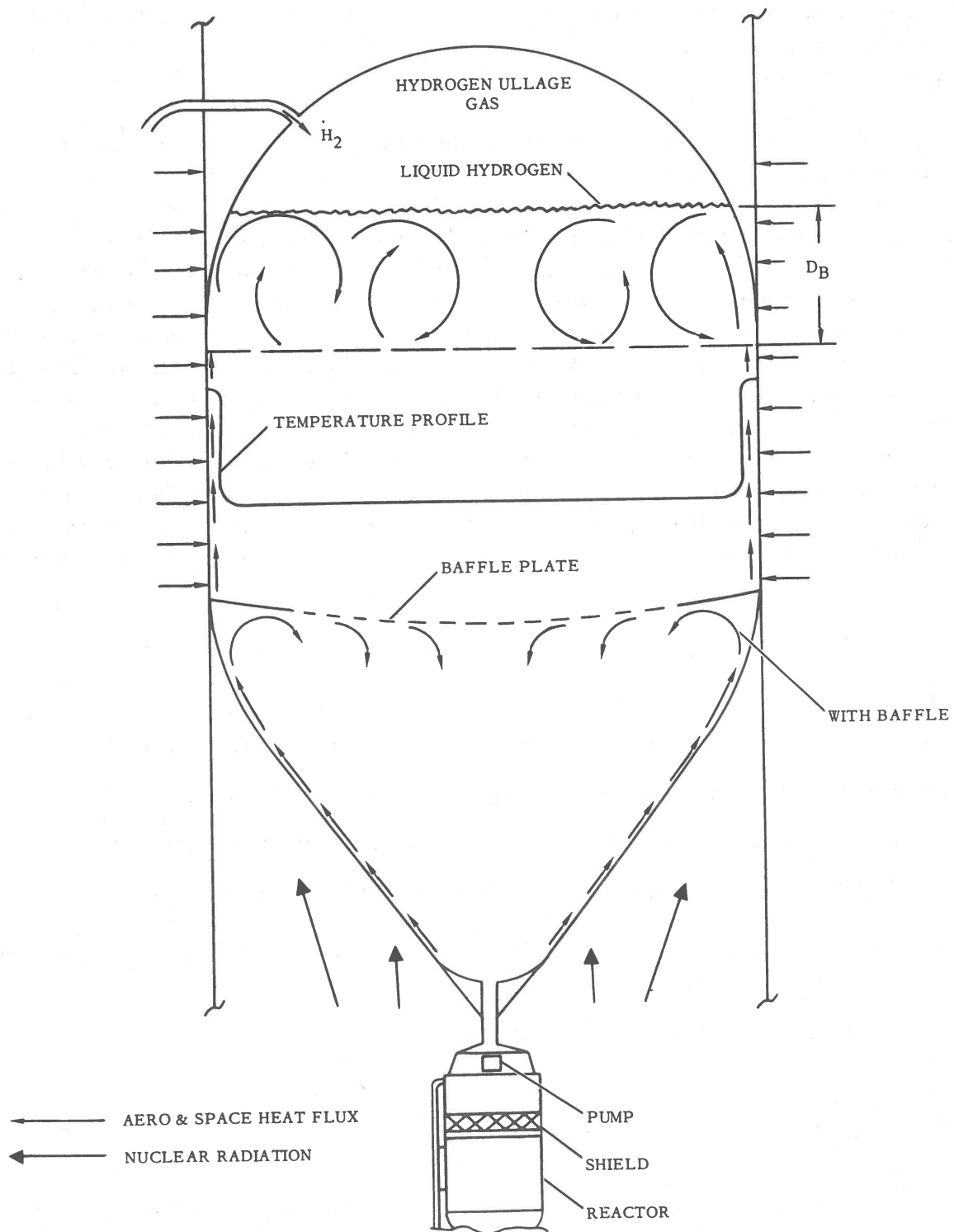


Figure 67. Hydrogen tank stratification model.

## GENERAL DYNAMICS | ASTRONAUTICS

heat balance equation is:

$$\frac{dQ}{dt} = \dot{m} H(t) + q - \frac{\dot{m}Q}{M} \quad (1)$$

This equation is valid for the operating time during which the propellant level is above the baffle. In this time interval, the quantities  $\dot{m}$ ,  $q$ , and  $M$  are constants. (Values for  $q$  can be calculated using the C-17 computer code developed by General Dynamics | Fort Worth. This code is described in the appendix to this chapter and covered in detail in Ref. 2.) Rearranging Eq. 1 gives:

$$\frac{dQ}{dt} + \frac{\dot{m}}{M} Q = q + \dot{m} H(t) \quad (2)$$

Utilizing an integrating factor and performing partial integration gives:

$$Q e^{\dot{m}/M t} = \frac{M}{\dot{m}} q e^{\dot{m}/M t} + \dot{m} \int H(t) e^{\dot{m}/M t} dt + \text{constant} \quad (3)$$

The heat content,  $H(t)$ , of the incoming fluid is not a simple function of time but is proportional to the propellant temperature rise. To simplify calculations, an approximation was made by assuming a constant value of  $H(t)$  over short periods of time when its average value could be taken with certainty. For purposes of calculation,  $H(t)$  is set equal to 0 when  $t = 0$ . The heat content remains zero until the warmer stratified propellant begins entering the baffle. At this time, the heat content of the propellant can be calculated using the following equation:

$$H(t) = C_P \Delta T_j \quad (4)$$

where

$C_P$  is the heat capacity of the fluid,

$\Delta T_j$  is the temperature increase above the initial temperature at the baffle plate in the time interval  $\Delta t_j$ .

## GENERAL DYNAMICS | ASTRONAUTICS

This temperature increase is a result of heating that takes place solely above the baffle plate. Substituting Eq. 4 into Eq. 3 and integrating gives:

$$Q \left( e^{\dot{m}/M t} \right) = \frac{M}{\dot{m}} (q) \left( e^{\dot{m}/M t} \right) + M C_p \left( \Delta T_j \right) \left( e^{\dot{m}/M \Delta t_j} \right) + \text{constant} \quad (5)$$

At the start of reactor operation  $t = 0$  and  $q = 0$ , hence:

$$\text{Constant} = - \left( \frac{M}{\dot{m}} \right) q - M C_p \left( \Delta T_j \right)$$

Substituting this quantity into Eq. 5, collecting terms, and dividing through by  $e^{\dot{m}/M t}$ , gives the accumulated instantaneous heat content below the baffle,

$$Q = \frac{M}{\dot{m}} q \left( 1 - e^{-\dot{m}/M t} \right) + M C_p \left( \Delta T_j \right) \left( 1 - e^{-\dot{m}/M \Delta t_j} \right) \quad (6)$$

Assuming complete mixing of the propellant below the baffle, the instantaneous heat content is directly proportional to the temperature increase below the baffle and is equated by:

$$Q = M C_p \Delta T$$

Substituting this into Eq. 6 and dividing through by  $M C_p$  gives the temperature increase as a function of time,

$$\Delta T = \frac{q}{\dot{m} C_p} \left( 1 - e^{-\dot{m}/M t} \right) + \Delta T_j \left( 1 - e^{-\dot{m}/M \Delta t_j} \right) \quad (7)$$

The values of  $\Delta T_j$  are obtained at times  $\Delta t_j$  as the stratified propellant passes through the baffle using the following method.

Since the temperature distribution in the Atlas liquid oxygen tank is known (Figure 68), an extrapolation to a liquid hydrogen flight tank has been proposed. In addition to the oxygen tank stratification data, the heat flux history, tank dimensions, and liquid flow rates must be known for each of the two tanks. (For the Atlas, tank diameter is 120 in.; LO<sub>2</sub> tank length is 480 in.; LO<sub>2</sub> flow rate during booster operation is 1,060 pps



GENERAL DYNAMICS | ASTRONAUTICS

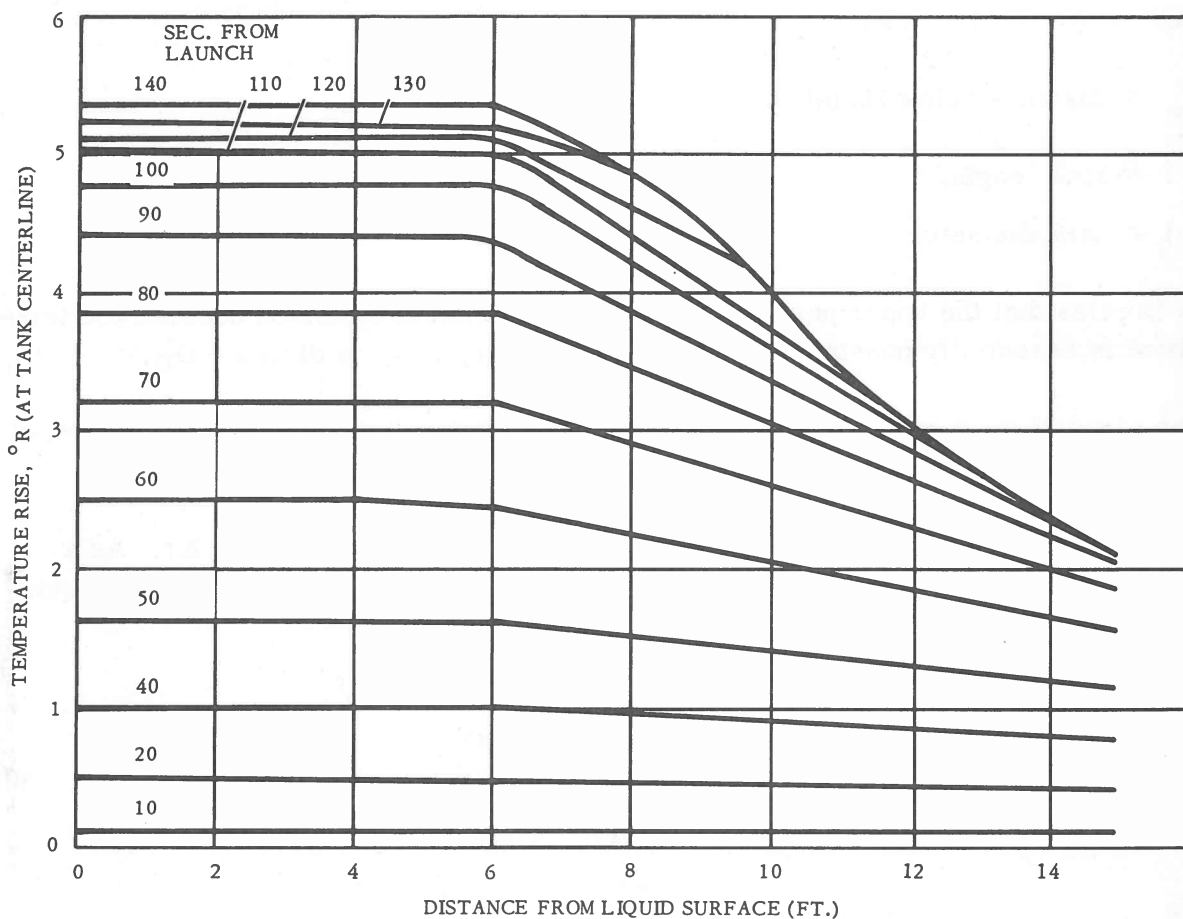


Figure 68. Liquid oxygen temperature stratification in Atlas missile 4-B.

and 160 pps during sustainer operation. The heat flux data for missile 4-B should be used.) It is assumed that all of the heat flux is carried by lower-density (higher-temperature) liquid up a relatively narrow boundary layer on the inside surfaces of the tank walls. With the baffle plate installed, more than 90% of the aerodynamic and space heat above the baffle comes from the tank side, and this tends to justify postulation of the boundary layer at the side. The inflection point on the temperature rise vs. distance curves (Figure 68) is extrapolated by:

$$(D_B)_{LH_2} = (D_B)_{LO_2} \frac{\left(\frac{1}{d}\right)_{LH_2}}{\left(\frac{1}{d}\right)_{LO_2}} \quad (8)$$

## GENERAL DYNAMICS | ASTRONAUTICS

where

$D_B$  = distance below liquid surface,

$l$  = tank length,

$d$  = tank diameter.

(This implies that the upper portion of the liquid is completely mixed because the temperature is essentially constant from the liquid surface down to distance  $D_B$ .)

The slope of the temperature curves from the inflection point down to the bottom of the tank can be determined for liquid oxygen from Figure 68.

The slope is primarily a function of heat input during the time interval  $\Delta t$ . As a first approximation, the slope for liquid hydrogen can be extrapolated from the liquid oxygen slope by:

$$\left( \frac{\Delta T_j}{\Delta D} \right)_{LH_2} = \left( \frac{\Delta T_j}{\Delta D} \right)_{LO_2} \frac{(\rho C_p)_{LO_2}}{(\rho C_p)_{LH_2}} \quad (9)$$

where

$\Delta T$  = temperature increment,

$\Delta D$  = distance increment,

$\rho$  = liquid density,

$C_p$  = specific heat at constant pressure.

This implies that the temperature of the boundary layer of liquid hydrogen increases by a factor of about 2.67 over that of liquid oxygen for the same heat input (see Ref. 3, Eq. 40).

The temperature rise vs. distance curve for each time increment is calculated with an iteration that equates the given heat flux to the integrated area under the temperature rise curve. A digital computer program is used at Astronautics.

## GENERAL DYNAMICS | ASTRONAUTICS

For times where the relative heat content of the fluid passing through the baffle is zero, such as when the reactor is restarted in orbit with no residual aerodynamic heat flux, Eq. 7 reduces to:

$$\Delta T = \frac{q}{\dot{m} C_p} \left( 1 - e^{-\dot{m}/M t} \right) \Bigg|_0^{t_b} \quad (10)$$

where  $t_b$  is the time between reactor startup and the time at which the propellant level reaches the baffle.

After the propellant level reaches the baffle the equations previously derived are no longer valid, since  $M$  and  $q$  are not constant and  $\dot{m}$  no longer represents the propellant flow rate through the baffle. An equation of different form was derived to give the additional propellant temperature increase after the propellant level reaches the baffle.

$$\Delta T = \frac{1}{\dot{m} C_p} \int_{h_b}^h \frac{Q(h)}{V(h)} \left( \frac{dV}{dh} \right) dh \quad (11)$$

This equation assumes complete mixing of the heat input between the time that the propellant level reaches the baffle and the time of reactor shutdown. The derivation of this equation and the explanation of terms is given in the following section.

**11.3.2.2 Complete Mixing Model.** For a tank without a unidirectional flow baffle, the heating model is difficult to establish accurately. This is primarily due to the lack of experimental data on radiation heat deposition in liquid hydrogen. However, due to liquid hydrogen's low viscosity and large density change with temperature, a complete mixing model may be close to the actual case. In the complete mixing model, instantaneous mixing of the radiation heat input occurs, resulting in a uniform propellant temperature at all times. There are primarily two factors which promote mixing of the heat input; propellant outflow and gravity-forced convection of the heated propellant. It should be noted that the tendency of the heated propellant in the tank bottom to rise may be overbalanced by the downflow of the propellant through the pump. This situation is similar to the baffled tank. Since most of the radiation heating is confined to the relatively small volume of the tank bottom, the heated propellant may be drawn out faster than is assumed by either model, hence the calculated temperature increase will be high.

## GENERAL DYNAMICS | ASTRONAUTICS

Utilizing cylindrical coordinates and angular symmetry, the following equation would apply for the complete mixing model:

$$Q(h) = m(h) C_p(T) \frac{dT}{dt} = \int_{V(h)} q(r, h) dV(r, h) \quad (12)$$

where

$Q(h)$  = integrated heating rate from tank bottom to height  $h$  (Btu/sec.),

$m(h)$  = mass of liquid from bottom of tank to height  $h$  (lb.),

$C_p(T)$  = propellant heat capacity at temperature  $T$  (Btu/lb.-°R),

$T$  = propellant temperature (°R),

$t$  = time (sec.),

$q(r, h)$  = volumetric heat input at  $(r, h)$  (Btu/cu.in.-sec.),

$dV(r, h)$  = incremental volume at  $(r, h)$ .

Let  $v(h)$  equal the downward linear velocity of the propellant surface and express the propellant mass in terms of its density and volume:

$$v(h) = \frac{dh}{dt} \text{ or } dt = \frac{dh}{v(h)} \quad (13)$$

$$m(h) = \rho(T) V(h) \quad (14)$$

Substituting Eq. 13 and 14 into Eq. 12 gives

$$Q(h) = V(h) v(h) \rho(T) C_p(T) \frac{dT}{dh} = \int_{V(h)} q(r, h) dV(r, h) \quad (15)$$

The total heat-generation rate  $Q(h)$  shown in Eq. 15 includes heating from neutron thermalization, secondary gamma rays from the  $(n, \gamma)$  reaction in hydrogen, and primary gammas from the reactor. These heating rates can be calculated as functions of position inside the tank using computer code C-17 developed by General Dynamics| Fort Worth. This code is described in the appendix and covered in detail in Ref. 2.

## GENERAL DYNAMICS | ASTRONAUTICS

The heat-generation rate as a function of  $h$  is calculated as follows:

$$q_j(h) = \int_{r=0}^{r(h)} q(r, h) 2\pi r \, dr = \sum_{i=1}^m q(r_i, h_j) 2\pi r_i \Delta r_i \quad (16)$$

where

$q_j(h)$  = integral of heating rate over cross-sectional area (Btu/in.-sec.),

$r$  = radial distance from tank centerline (in.),  $0 \leq r \leq r(h)$ ,

$h$  = distance along tank centerline from tank bottom (in.),

$r(h)$  = tank radius at height  $h$  (in.).

The  $q_j(h)$  values which are obtained in this manner are then plotted as a function of  $h$ . Then a value for  $Q(h)$  is obtained by summing  $q_j(h)$ :

$$Q(h) = \int_{h=0}^h q_j(h) \, dh = \sum_{j=0}^m q_j(h) \Delta h_j \quad (17)$$

Now that  $Q(h)$  can be calculated, Eq. 15 can be solved if values for  $\bar{v}(h)$  and  $dm(h)$  are known.

Since the mass flow rate ( $\dot{m}$ ) equals  $\frac{dm(h)}{dt}$  and  $dt = \frac{dh}{v(h)}$  (Eq. 13) then

$$\dot{m} = \frac{dm(h)}{dh/v(h)},$$

or

$$v(h) = \frac{\dot{m}}{dm(h)/dh} \quad (18)$$

$dm(h)$  is obtained by differentiating Eq. 14.

$$dm(h) = \rho(T) \, dV(h) + V(h) \, d\rho(T) \quad (19)$$

## GENERAL DYNAMICS | ASTRONAUTICS

Since  $\rho(T)$  changes a very small percentage over the temperature increase of interest it has been assumed that  $d\rho(T) = 0$ , giving:

$$dm(h) = \rho(T) dV(h) \quad (20)$$

Substituting these values of  $v(h)$  and  $dm(h)$  into Eq. 15 gives:

$$Q(h) = \frac{V(h) \dot{m} C_p(T) dT/dh}{dV(h)/dh} \quad (21)$$

Separation of variables and introduction of the integrals gives:

$$\dot{m} \int_{T_i}^{T_f} C_p(T) dT = \int_h^{h_c} \frac{Q(h)}{V(h)} \left( \frac{dV(h)}{dh} \right) dh \quad (22)$$

where

$T_f$  = final temperature of propellant ( $^{\circ}\text{R}$ ),

$T_i$  = initial temperature of propellant ( $^{\circ}\text{R}$ ),

$h$  = initial propellant height (in.),

$h_c$  = propellant height at reactor cutoff (in.).

Evaluation of Eq. 22 allows the determination of temperature,  $T$ , as a function of propellant height,  $h$ . This may be accomplished by graphical integration. For small temperature increments the heat capacity of liquid hydrogen can be considered constant, which allows a simplification of Eq. 22. This results in:

$$\Delta T = \frac{1}{\dot{m} C_p} \int_h^{h_c} \frac{Q(h)}{V(h)} \left( \frac{dV(h)}{dh} \right) dh \quad (23)$$

This equation has the same form as Eq. 11.

For larger variations in the propellant temperature the heat capacity can be assumed to be a linear function of  $T$ ,

$$C_p(T) = -1.52 + 0.1082T \quad (24)$$

## GENERAL DYNAMICS | ASTRONAUTICS

Substituting this equation into Eq. 22, integrating the left side, and rearranging terms yields:

$$T_f^2 - 28.1T_f + \left[ 28.1T_i - T_i^2 \right] = \frac{18.5}{\dot{m}} \int_h^h \frac{Q(h)}{V(h)} \left( \frac{dV(h)}{dh} \right) dh \quad (25)$$

### 11.4 NOMENCLATURE

a	albedo
A	area (sq.ft.)
A <sub>1, 2, ...</sub>	curve-fit coefficients
b	altitude above planet surface (n.mi.)
C <sub>0, 1, 2, 3, 4, ...</sub>	curve-fit coefficient
c <sub>f</sub>	skin friction coefficient
C <sub>p</sub>	heat capacity at constant pressure (Btu/lb.-°R)
C <sub>p</sub> (T)	propellant heat capacity at temperature T (Btu/lb.-°R)
C <sub>v</sub>	heat capacity at constant volume (Btu/lb.-°R)
d	tank diameter
D <sub>B</sub>	distance below liquid surface
ΔD	distance increment
E	eccentricity of ellipse (dimensionless)
F	effective attenuation for a particular source energy
F <sub>a</sub>	view factor for flat plate (nondimensional; planetary albedo)
F <sub>s</sub>	view factor for hydrogen tank on the earth's surface (nondimensional)
F <sub>t</sub>	view factor for flat plate (nondimensional; thermal radiation from planet)
g	gravitational constant
h	(Sections 11.2.1 and 11.2.2) film coefficient of heat transfer
h	(Section 11.3.2) distance along tank centerline from tank bottom (in.)

## GENERAL DYNAMICS | ASTRONAUTICS

$h_c$	propellant height at reactor cutoff (in.)
$H$	distance from center of planet to vehicle (n.mi.)
$H(t)$	heat content of propellant flowing through the baffle (Btu/sec.)
$i^*$	reference enthalpy
$i_r$	recovery enthalpy
$i_s$	enthalpy at stream conditions
$i_w$	enthalpy at wall temperature
$i_t$	$\frac{(1 - a)S}{4}$ , where $S$ is the solar constant and $a$ the planetary albedo constant
$k$	thermal conductivity
$l$	tank length or through-connection length
$L$	insulation thickness or thickness of material concerned
$LH_2$	liquid hydrogen
$LO_2$	liquid oxygen
$\dot{m}$	propellant mass flow rate through the baffle and pump (pps)
$m(h)$	mass of liquid from bottom of tank to height $h$ (lb.)
$M$	(Section 11.2.2) free-stream Mach number (Mach number of vehicle)
$M$	(Section 11.3.2) mass of propellant below the baffle (lb.)
$N$	vector normal to a flat plate element
$p(E, E_2, \mu r, M)$	function which represents that fraction of the source photons of energy $E$ which are degraded to final energy $E_2$ in penetration of $\mu r$ mean free paths of material
$P_r^*$	prandtl number at reference enthalpy, $i^*$
$q$	(Section 11.2.2) heat-transfer rate
$q$	(Section 11.3.2) rate at which radiation heat is deposited below the baffle (Btu/sec.)
$q(r, h)$	volumetric heat input at $r, h$ (Btu/cu.in.-sec.)



## GENERAL DYNAMICS | ASTRONAUTICS

$\dot{q}$	heat flux (Btu/hr.-ft. <sup>2</sup> or Btu/hr.)
$q_{\text{albedo}}$	incident planetary albedo (Btu/hr.)
$q_j(h)$	integral of heating rate over cross-sectional area (Btu/in.-sec.)
$q_{\text{solar}}$	incident energy from the sun
$q_{\text{thermal}}$	incident planetary thermal radiation (Btu/in.)
$Q$	accumulated instantaneous heat content below the baffle (Btu)
$Q(h)$	integrated heating rate from tank bottom to height $h$ (Btu/sec.)
$r$	(Section 11.2.2) recovery factor
$r$	(Section 11.3.2) radial distance from tank centerline (in.)
$r$	(Appendix) range in material necessary to degrade photon of energy $E$ to $E_2$ (g/sq.cm)
$R$	radius of planetary body (n.mi.)
$Re$	reynolds number
$Re^*$	reynolds number at reference enthalpy, $i^*$
$S$	solar constant (Btu/hr.-ft. <sup>2</sup> ; Figure 58)
$\vec{S}$	radius vector from the planet to the sun
$(\vec{S}; N)$	$\Theta_3$ equals the angle between the sun vector and a normal to a surface element (deg.)
$S_0(E)$	number of source photons/sec.-mev as a function of energy $E$
$S_0(E_2)$	number of source photons/sec.-mev at energy $E_2$
$S_1(E_2)$	total flux arriving at detector at an energy $E_2$
$St$	stanton number
$t$	time
$t_b$	time between reactor startup and when propellant level reaches the baffle
$\Delta t_j$	time interval
$T$	temperature
$T_{\text{air}}$	outside air temperature (°R)

## GENERAL DYNAMICS | ASTRONAUTICS

$T_f$	final temperature of propellant ( $^{\circ}\text{R}$ )
$T_h$	temperature of hydrogen ( $^{\circ}\text{R}$ )
$T_i$	initial temperature of propellant ( $^{\circ}\text{R}$ )
$\Delta T$	temperature increase
$\Delta T_j$	temperature increase above the initial temperature at the baffle plate in the time interval $\Delta t_j$
$T_w$	temperature wall exterior surface ( $^{\circ}\text{R}$ )
$v(h)$	downward linear velocity of the propellant surface
$V$	(Section 11.2.2) stream velocity
$V$	(Section 11.3.2) volume
$V(h)$	propellant volume at liquid level $h$
$dV(r, h)$	incremental volume at $r, h$
$Z$	effective atomic number of the material

### 11.5 GREEK SYMBOLS

$\alpha$	absorptivity
$\gamma$	$C_p/C_v$ of air
$\epsilon$	emissivity
$\Theta_1$	the angle between the planet-sun vector and the radius vector from the planet to the vehicle (deg.)
$\Theta_2$	angle between a normal to a surface element and radius vector from the planet to the vehicle, which is the same as the principal axis in the moving vehicle system (see Figure 59)
$\Theta_3$	the angle between the sun vector and a normal to a surface element (deg.)
$\mu$	mass absorption coefficient (sq.cm/gm)
$\mu_1$	linear absorption coefficient of material for gamma rays with energies $E$ and $E_2$ , respectively
$\rho$	liquid density

## GENERAL DYNAMICS | ASTRONAUTICS

$\rho_a$	air density at the boundary layer edge
$\sigma$	radiation constant, $1.73 \times 10^{-9}$ Btu/hr.-ft. <sup>2</sup> (°R) <sup>4</sup>
$\varphi_c$	angle of rotation of a normal to a flat plate, measured from the plane containing the planet-sun vector and the radius vector from the planet to the vehicle (deg.)
$\Omega$	angle between the unit vehicle-sun vector and an arbitrary reference vector in the pseudo-vehicle system (deg.)

### APPENDIX

C-17 CODE. The moments method as applied to this code involves the use of attenuation data obtained for various materials by the application of the spherical-harmonic method of approximating the Boltzmann equation. In this method the angular flux is expanded in terms of Legendre polynomials to obtain spatial moments. These moments are then used as the basis of a method of determining functions describing the spatial and energy dependence of point isotropic, monoenergetic sources penetrating infinite homogeneous media. The functions are then used to obtain values of the scattered-energy flux reaching a detector at various degraded energies, the detector being positioned at various mean free paths in the media. These values form curves of differential energy spectra and exist for a number of materials whose atomic numbers span the periodic table. To adapt this data to a generalized shielding program, the spectra have been curve-fitted and the coefficients included as input to the code.

Such spectral data are far more limited for neutrons than for gamma rays; therefore, Code C-17 makes the assumption that the attenuation of neutrons by any material may be represented by the attenuation of a fission spectrum through a material for which curve-fit coefficients exist (a "reference" material), provided the thickness of the material is replaced with an "equivalent" thickness.

These equivalent thicknesses (L) are used to compute effective attenuations by means of the equation:

$$F = \text{Exp.} - \left[ C_0 + C_1 (L) + C_2 (L)^2 + C_3 (L)^3 + C_4 (L)^4, \dots \right] \quad (1)$$

where F is the effective attenuation for a particular source energy and the C's are curve-fit coefficients for reference material attenuations.

## GENERAL DYNAMICS | ASTRONAUTICS

The last group of coefficients in each section contains the fast-neutron dose rate curve-fit coefficients. Spectral points and dose rates are obtained by multiplying Eq. 1 by the source intensity and dividing by  $4\pi R^2$ . Total dose rates are found by a histogram integration over energy.

For gamma ray penetration the differential energy spectra have been curve-fitted for initial gamma energies of 10, 9, 8, 7, 6, 5, 4, 3, 2, 1.375, 1, and 0.5 mev. The degraded energies are the same with the exception of 0.25 mev. The curve-fit takes the form:

$$\frac{F(L)}{\mu\rho L} = \text{Exp} - \left[ A_1 (\mu\rho L)^2 + A_2 (\mu\rho L) + A_3 (\mu\rho L)Z + A_4 Z + A_5 Z^2 + A_6 \right] \quad (2)$$

where

$A_1$  through  $A_6$  are the curve-fit coefficients,

$\mu$  is the mass absorption coefficient ( $\text{cm}^2/\text{gm}$ ),

$\rho$  is the density ( $\text{gm}/\text{cu. cm}$ ),

$L$  is the thickness of material concerned,

$Z$  is the effective atomic number of the material.

The gamma calculation is a repetitive use of the moments method spectral equation to compute the spectrum at the end of a segment in terms of the spectrum at the source end. The integration consists of a summation of the areas of histograms resulting from defining the integrand at the aforementioned gamma initial energies for the values of degraded energy. Thus, the total flux ( $S_1$ ) arriving at the detector at an energy  $E_2$  is given by the following equation:

$$S_1(E_2) = \frac{S_0(E_2)e^{-\mu_1 r}}{4\pi r^2} + \int_{E_2}^{\text{max } E} \frac{S_0(E)p(E, E_2, \mu r, M)dE}{4\pi r^2} \quad (3)$$

where

$S_0(E)$  is the number of source photons/sec.-mev as a function of energy  $E$ ,

$S_0(E_2)$  is the number of source photons/sec.-mev at energy  $E_2$ ,

## GENERAL DYNAMICS | ASTRONAUTICS

and  $\mu^1$  is the linear absorption coefficients of material for gamma rays with energies  $E$  and  $E_2$ , respectively,

$p(E, E_2, \mu r, M)$  is a function which represents that fraction of the source photons of energy  $E$  which are degraded to the final energy  $E_2$  in penetration of  $\mu r$  mean free paths of material,

$r$  is the range in material necessary to degrade photons of energy  $E$  to  $E_2$  (g/sq.cm).

**DISTRIBUTED SOURCE APPROXIMATION.** It is necessary to approximate the leakage from a distributed source by a set or sets of point sources. For this code, these point sources must be described in such a way that a summation of the leakages from these point sources will represent an integration over the volume containing them. It is also necessary to take into account the power distribution of the reactor core.

### REFERENCES

1. Space Vehicle Radiant Energy Program. H. E. Hogfors and R. S. Dummer, Astronautics Report ERR-AN-146.
2. Liquid Hydrogen in a Nuclear Environment. D. G. Abshier, Astronautics Report ERR-AN-150, pp. 6.1-6.110.
3. The Transient Thermal Response of a Step Pressurized Boiling Liquid Nitrogen System. Fenster, Van Wylen, and Clark, University of Michigan, UMRI Project 2646-14-T, Tech. Report 11, (Final Report).



# 12

## ZERO-GRAVITY BEHAVIOR

### 12.1 ZERO-GRAVITY AND SIMULATED ZERO-GRAVITY TESTING METHODS

**12.1.1 DROP TESTS.** Free-fall drop tests performed by Astronautics have provided about 2 sec. of zero-g testing time. The drop-test device consists of a test tower, winch, release mechanism, guide wires, drop capsule, and sand box (see Figure 69). The drop capsule contains the dewar configuration and liquid to be tested, along with a camera and associated test instrumentation. The pointed nose on the drop capsule reduces aerodynamic drag and provides a gradual deceleration when the capsule impacts in the sand.

A modification of the drop test has been used. Instead of elevating the capsule for a free-fall drop, the capsule is placed in a sand bucket and popped up into the air by accelerating a hydraulic cylinder that is attached to the capsule with cable and a section of flexible cord. The capsule is under zero-g conditions going up and coming down. Because of experimental difficulties, this testing method has been abandoned; only free-fall drop tests are being performed at Astronautics.

**12.1.2 AIRCRAFT TESTS.** Aircraft tests performed by Astronautics (Aerophysics and Instrumentation Design Groups) with the cooperation of the Aeronautical Systems Division of the Air Force in Dayton, Ohio, theoretically provided 25 to 35 sec. of zero-g testing time. A modified KC-135 aircraft was used.

The weightless condition was obtained by putting the aircraft through the following maneuvers. The aircraft descends in a shallow dive of  $5^\circ$  until Mach 0.87 is reached. The aircraft is then gradually pitched to an angle of climb of about  $45^\circ$ . The rate of pitch is based on maximum aircraft loading considerations. The aircraft follows a parabolic path until the initial Mach number is again attained. The aircraft is pulled out of the  $45^\circ$  dive at 2.5g, the maximum loading permissible on the aircraft (see Figure 70).

During the zero-g condition the pilot flies the aircraft "around" the test capsule, as shown in Figure 71, by means of accelerometer gages, a television monitor, and verbal commands from personnel stationed near the test capsule. During a good

## GENERAL DYNAMICS | ASTRONAUTICS

trajectory, the capsule is maintained in a zero-g condition for up to 14 sec., where the free-floating capsule does not strike the sides of the aircraft. When liquid hydrogen is tested, the test capsule is placed inside a large nitrogen-filled bag as a safety measure (see Figure 72).

**12.1.3 AEROBEE ROCKET TESTS.** Aerobee flights performed by the NASA Lewis Research Center, Cleveland, Ohio, provide up to 4 or 5 min. of zero-g testing time. Two Aerobee liquid-hydrogen zero-g tests were performed by NASA in the first half of 1961, followed by three shots with Astronautics hardware in the latter part of 1961 and the first half of 1962. Chronologically, the tests performed were: (1) General Dynamics| Electronics hot-wire liquid/gas detector, (2) liquid condensing test, and (3) unsymmetrical heating test. A sixth shot to evaluate the performance of a center vent tube was scheduled for June 1962.

**12.1.4 LIQUID/LIQUID MODEL TEST AT 1G.** Simple equilibrium configurations simulating the absence of gravity were experimentally determined by Plateau in 1873 by matching densities of two immiscible liquids. Using this technique to simulate steady-state zero-g conditions, the Instrumentation Design Group has constructed Plexiglas scale models of the Centaur liquid-hydrogen tank.

Two immiscible fluids were used. One fluid, representing the liquid hydrogen, consisted of Freon TF and Stoddard solvent. Distilled water was used to represent the gas ullage space. Since the Freon mixture readily wets the Plexiglas while the distilled water does not, the Freon flows around the sides of the "tank," and the distilled water forms a central "ullage" bubble (see Figure 73).

### 12.2 THE BEHAVIOR OF LIQUID HYDROGEN AT ZERO GRAVITY

**12.2.1 IDEALIZED CONFIGURATION OF LIQUID HYDROGEN AT ZERO GRAVITY WITH NO PERTURBATIONS.** Due to the ability of liquid hydrogen to "wet" most materials it contacts, the final configuration of liquid hydrogen under zero-g conditions consists of a central gas ullage bubble, with liquid hydrogen covering the walls of the container. The shape of the ullage bubble is dominated by surface tension effects and geometry.

Consider the case of liquid hydrogen in a closed tank with the shape of a body of revolution. If the contact angle between the liquid hydrogen and the tank wall is denoted by  $\theta$ , the surface energy per unit area of the hydrogen vapor to the tank wall



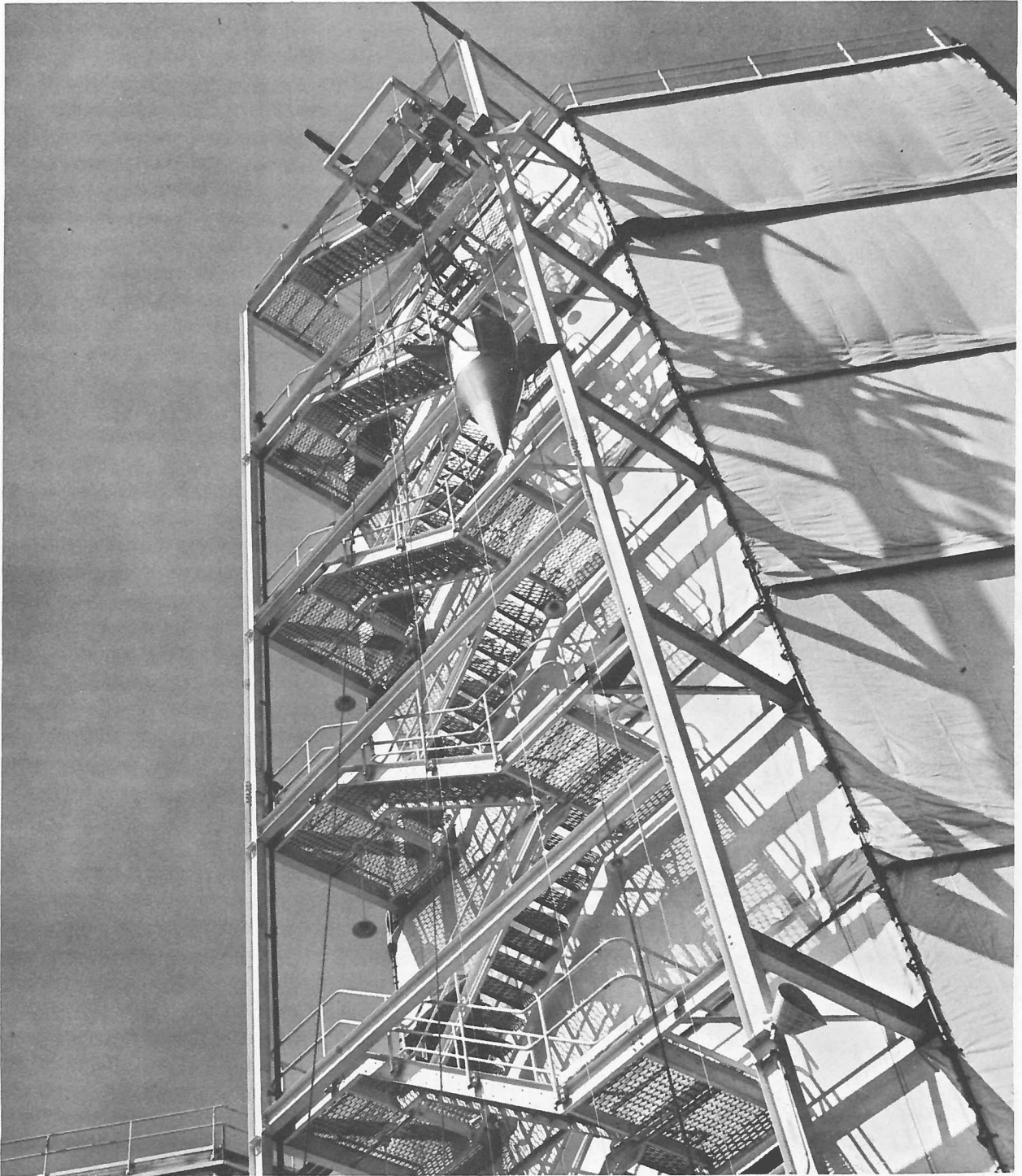


Figure 69. Astronautics' drop-test facilities for hydrogen zero-g test program.

GENERAL DYNAMICS | ASTRONAUTICS

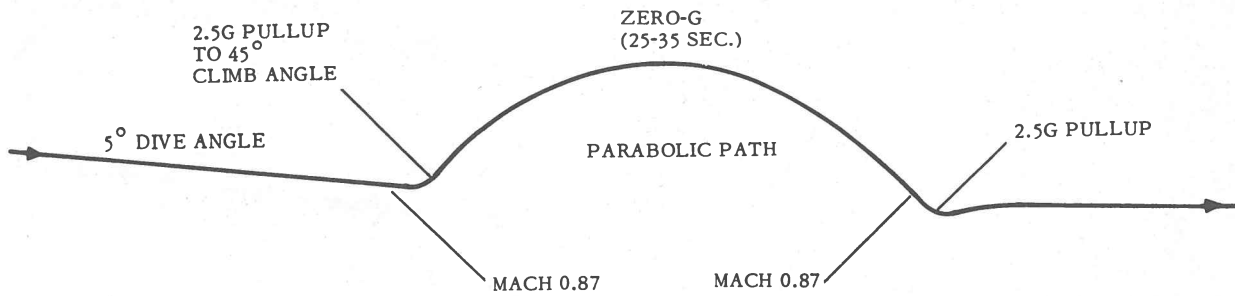


Figure 70. Aircraft zero-g trajectory.

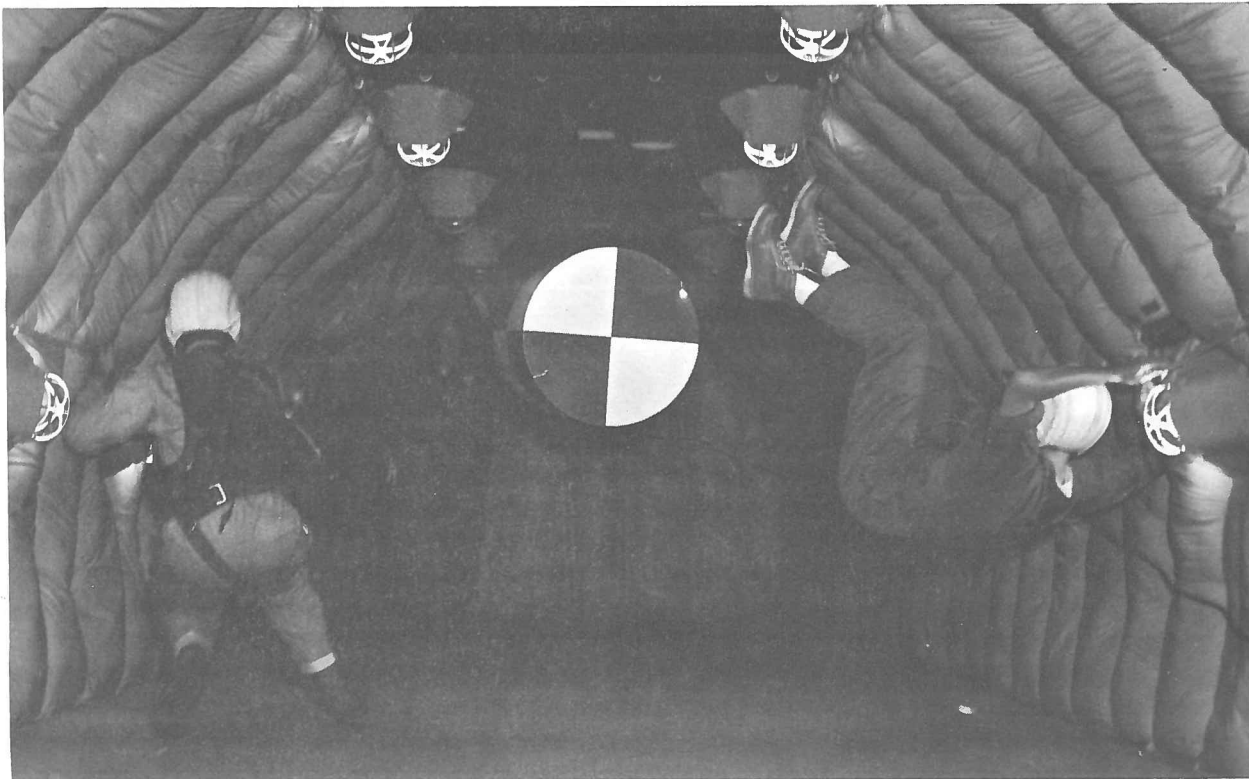


Figure 71. Free-floating test capsule and personnel during Astronautics zero-g aircraft tests.

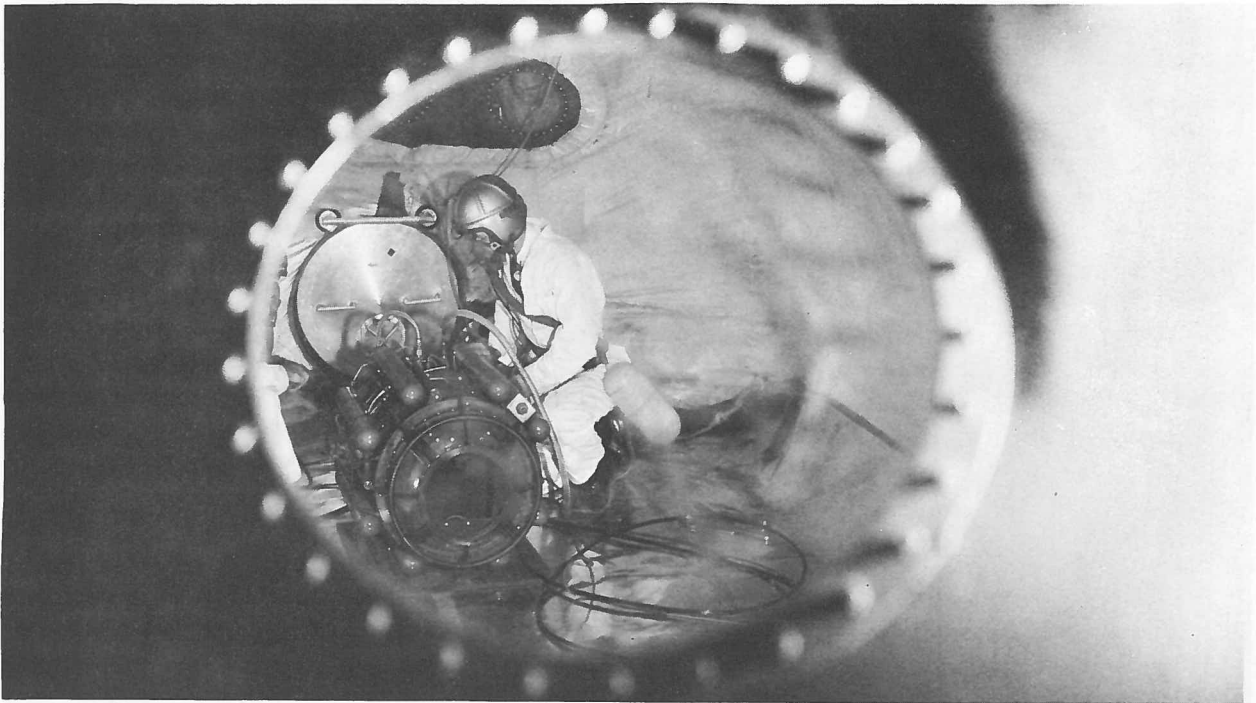


Figure 72. Test capsule and personnel viewed through a porthole of the nitrogen-filled bag, Astronautics aircraft zero-g tests.

by  $\gamma_{VW}$ , that of the liquid hydrogen to the tank wall by  $\gamma_{LW}$ , and that of liquid hydrogen to its vapor by  $\gamma_{LV}$ , it is known that the following relations holds.

$$\gamma_{VW} = \gamma_{LW} + \gamma_{LV} \cos \theta.$$

Since liquid hydrogen wets the wall ( $\theta = 0^\circ$ ,  $\cos \theta = 1$ ),

$$\gamma_{VW} > \gamma_{LW}$$

Therefore, to obtain the stable configuration of liquid hydrogen under zero gravity, the principle of minimum surface energy states that the total surface free energy for a stable configuration of the liquid is a minimum. As a result of this principle,  $\gamma_{VW}$  will be replaced by  $\gamma_{LW}$ , thereby minimizing the surface energy. This assumes there is sufficient liquid to wet the walls of the container. After this has been accomplished, the only remaining surface energy to be minimized is the surface energy between the liquid hydrogen and its vapor. The most effective way to do this is to have a vapor bubble in the "center" of the tank. This bubble should have a volume equal to the total volume of the vapor, and a shape with the smallest possible surface area, i. e., a sphere.

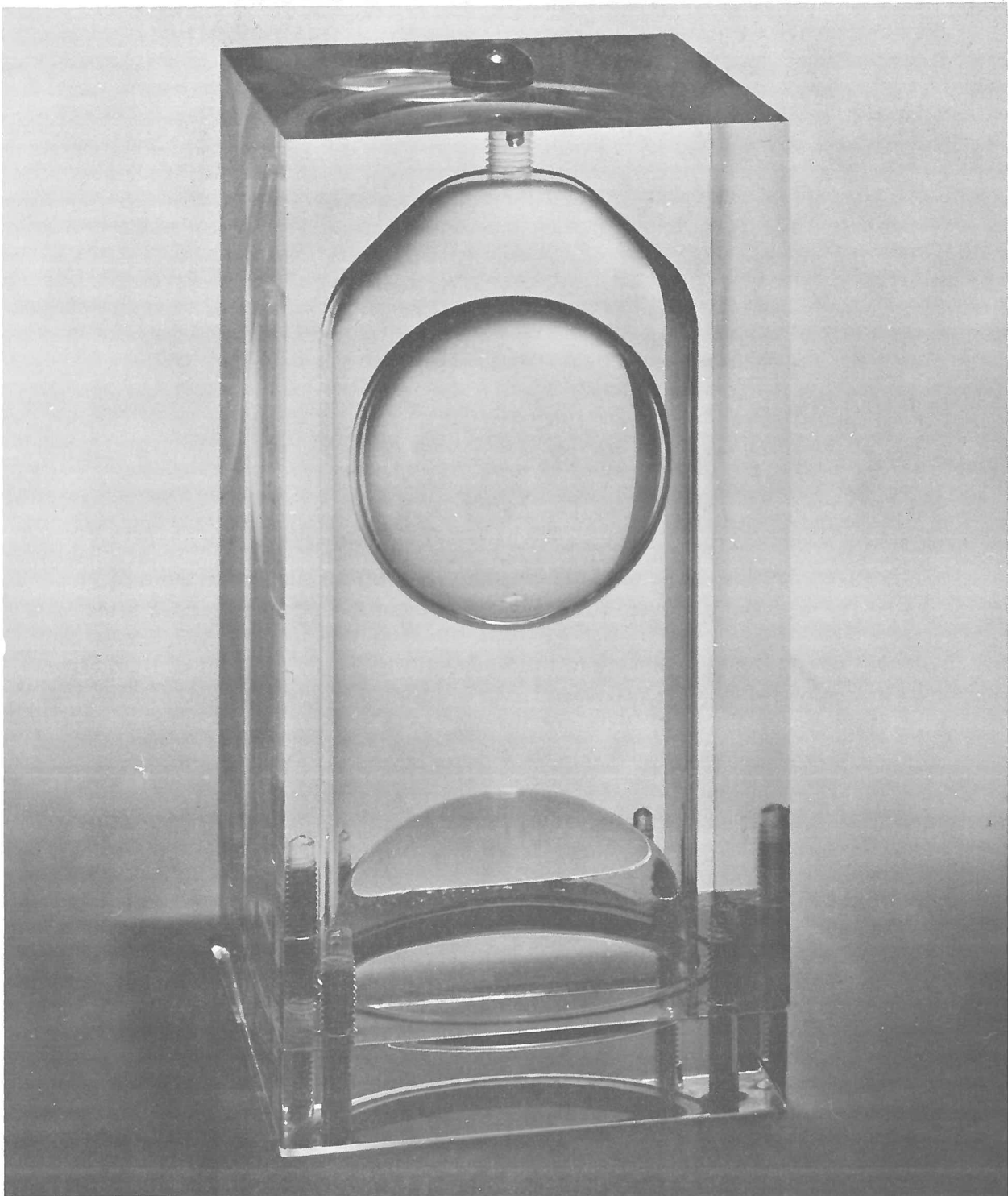


Figure 73. Centaur liquid/liquid model.

## GENERAL DYNAMICS | ASTRONAUTICS

Dr. Ta Li, formerly of the Space Physics Group of Astronautics, using the principle of minimum surface energy, mathematically derived the equation of a sphere as the most stable configuration for hydrogen vapor under zero gravity (Ref. 1). A remarkable consequence of his study is the revelation that the contact angle between a liquid and a solid is the same regardless of the magnitude of the gravitational field to which it is subjected. Results of liquid hydrogen drop tests, aircraft zero-g studies and liquid/liquid model tests have shown excellent agreement with Dr. Li's prediction.

When the volume of liquid hydrogen has dropped to a point where the spherical volume of the gas ullage space is larger than the smallest dimension of the tank, a sphere is no longer possible. Therefore, the largest sphere that can exist in a closed container is determined by:

$$V = 4/3\pi r^3$$

where

$2r$  = smallest dimension existing in the tank (the diameter of a cylindrical tank),

$V$  = volume of the gas ullage.

When the ullage gas space is larger than the volume shown above, the liquid will first wet the wall, then fill the cavities and form a central bubble, wherein the bulk liquid is distributed in such a manner that the surfaces backed by bulk liquid are of uniform curvature. Other surfaces will be film-wetted tank walls. The escaping tendency from the wetted tank walls will be adjusted by evaporation (thus reducing the thickness) to equal the escaping tendency from the curved surfaces. Thus, the escaping tendency of the surfaces exposed to the vapor volume will be uniform, and the pressure in the vapor will be uniform. If more than one configuration is possible, the one or ones with the smallest amount of liquid-vapor surface area will prevail. The bulk liquid surface will become tangent to the film wet surface in a transition region. The curvature of a bulk liquid surface will be greater than, or equal to, the curvature of any exposed film wet surface (otherwise the liquid will collect on the film wet surface).

The preceding statements describe the final or equilibrium configuration. However, if the space vehicle at engine cutoff is put into a zero-g state with no mechanical perturbations, the liquid surface will initially form an inverted hemisphere. The remaining tank walls will be covered with only a molecular layer of liquid hydrogen. Eventually, the liquid hydrogen will flow up the cylindrical tank walls and form another

## GENERAL DYNAMICS | ASTRONAUTICS

hemispherical cap at the forward bulkhead. Evaporation and condensation of the liquid will slowly increase the flow rate. Heat-transfer processes into the tank may keep the tank walls dry and prevent the final equilibrium shape from forming.

The zero-g configuration of liquid hydrogen in a typical tank is shown in Figure 74 as a function of the quantity of liquid hydrogen left in the tank. It has been estimated that for the Centaur vehicle it will take in the order of 200 sec. to form the initial hemispherical cap shown in Figure 74B. Liquid/liquid tests on model Centaur tanks confirm these general shapes (see Figure 73).

To determine the final configuration liquid hydrogen will assume under zero g in a tank of a given geometry, liquid/liquid tests must be run in a scale model of the tank. Scaling these results to a full-scale tank should be accurate, since Dr. Li has shown that a unique configuration of liquid is determined if the tank shape, contact angle, and vapor-to-tank volume ratio are given (Ref. 2).

### 12.2.2 LIQUID HYDROGEN BEHAVIOR AT ZERO GRAVITY WITH PERTURBATIONS

12.2.2.1 Effect of Complex Shapes. In Section 12.2.1 the configuration of liquid hydrogen at zero g was determined for a body of revolution. What happens to this configuration when complex shapes are placed inside the tank such as liquid/gas sensors, a probe support structure, or a center vent tube? Originally, it was felt that the all-wetting liquid hydrogen would creep over the surface of any protuberance much in the same way it covers the walls.

Using liquid/liquid models, it was observed that wires or small tubes could pierce the liquid/liquid interface with what seemed to be a finite pucker. Also, it was noticed that a wire loop pushed against the surface formed a depression which could be stretched into the ullage a short distance. Within a few diameters, the distorted surface necked down, became unstable, and pinched off.

C. K. Perkins of the Instrumentation Design Group, after observing these phenomena, mathematically analyzed the effect of a cylindrical center vent tube placed in the tank. Using some approximations, he derived an equation for the liquid/gas interface around the center vent (see Figure 75), as follows:

$$z = \cosh^{-1} r - \frac{r\sqrt{r^2 - 1}}{2(r_t + 1)} \quad (1)$$



# GENERAL DYNAMICS | ASTRONAUTICS

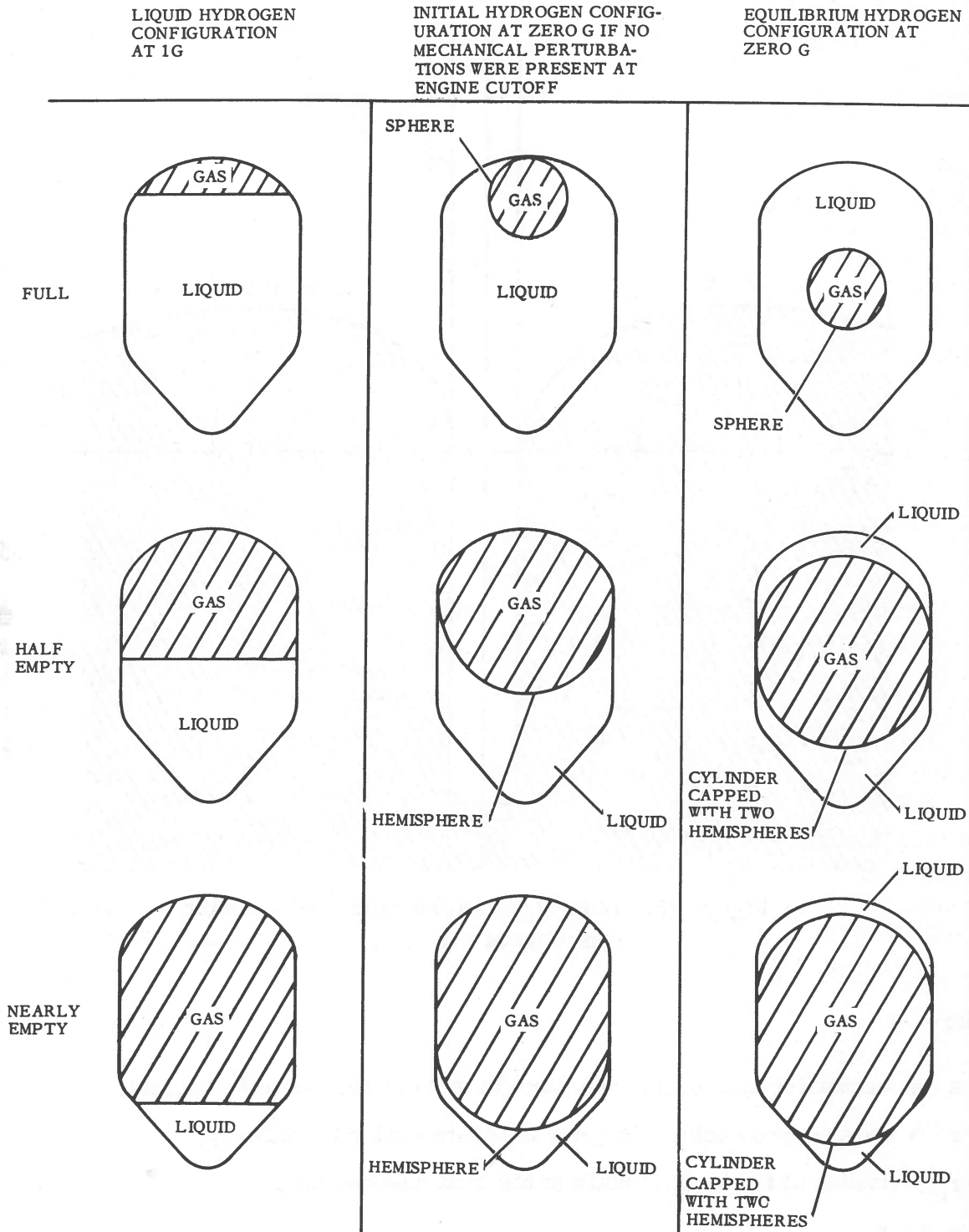


Figure 74. Configuration of liquid hydrogen at zero g for typical nuclear vehicle.

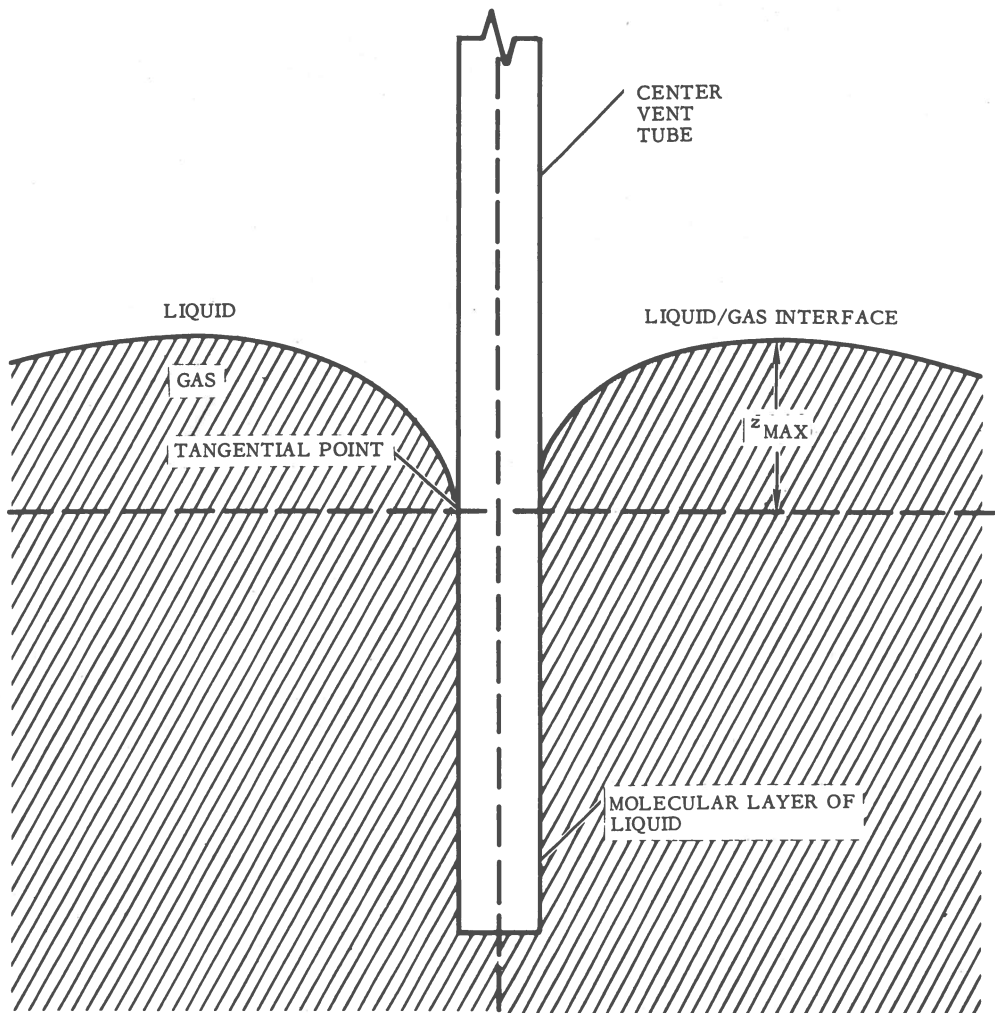


Figure 75. Liquid/gas interface around a center vent tube at zero g.

where

$z$  = centerline axis of the vent tube (in units of the vent tube radius),

$r$  = axis perpendicular to  $z$  (in units of the vent tube radius),

$r_t$  = radius of the tank (in units of the vent tube radius),

$r \ll r_t$ .



## GENERAL DYNAMICS | ASTRONAUTICS

Differentiating this equation with respect to  $r$ , setting  $\frac{dz}{dr} = 0$ , (the maximum point of the curve), solving for  $r$ , and substituting this value back into Eq. 1 gives the distance the liquid hydrogen has crept along the tube at equilibrium.

$$\frac{dz}{dr} = \frac{1}{(r^2 - 1)^{1/2}} - \frac{1}{2(r_t + 1)} \left[ \frac{r^2}{(r^2 - 1)^{1/2}} + (r^2 - 1)^{1/2} \right]$$

Setting  $\frac{dz}{dr} = 0$  and solving for  $r$  yields:

$$0 = \frac{1}{(r^2 - 1)^{1/2}} - \frac{1}{2(r_t + 1)} \left[ \frac{2r^2 - 1}{(r^2 - 1)^{1/2}} \right]$$

$$2r^2 - 1 = 2(r_t + 1)$$

$$r^2 = \frac{2r_t + 3}{2}$$

$$r = (r_t + 1.5)^{1/2}$$

Substituting this value of  $r$  in Eq. 1 yields:

$$z_{\max} = \cosh^{-1} (r_t + 1.5)^{1/2} - \frac{(r_t + 1.5)^{1/2} (r_t - 0.5)^{1/2}}{2(r_t + 1)} \quad (2)$$

where:

$z_{\max}$  = distance from the liquid hydrogen tangent point on the vent tube to the maximum point of the gas/liquid interface along the  $z$  axis (see Figure 75).

In his derivation,  $r$  and  $r_t$  are in units of the center vent radius; i. e., if the radius of the center vent tube is 2 in. and the radius of the tank is 180 in., all values of  $r$  and  $r_t$  are divided by two before substituting into the equations; therefore,  $r_t = 90$  units in this example.

## GENERAL DYNAMICS | ASTRONAUTICS

Solution of Eq. 2 for specific cases shows that a "small" tube passing through the liquid/gas interface causes little distortion of that surface. For example,  $z_{\max}$  is 2.8 in. for a 4-in. dia. tube inserted into a 360-in. tank. However, the equations do not describe the effect various structures within the tank have on positioning the ullage gas bubble.

Zero-g tests and liquid/liquid tests show the bubble is pushed away from internal structures within the tank, distorting the liquid/gas interface until a balancing pressure is produced. The larger the structure is the more effective it is in displacing the bubble.

General Dynamics | Electronics has developed a hot-wire liquid/gas sensor for use in liquid and gaseous hydrogen at zero g. The behavior of the sensor at zero g is well known and will be used on Centaur flights (Ref. 3).

12.2.2.2 Effect of Mechanical Disturbances. If, during zero g, the liquid hydrogen tank is mechanically disturbed by sun-seeking rockets, control rockets, or units aboard the vehicle, causing it to pitch, yaw, or roll, the liquid will be pushed away from the axis of rotation, and the large ullage bubble, plus any smaller bubbles, will be drawn toward the axis of rotation. The smaller bubbles will eventually coalesce into the main bubble under these conditions.

If, during the transition from powered to zero-g flight the liquid starts moving in the tank, the vapor bubble will oscillate through the following cycle (assuming there is enough liquid left in the tank for the vapor bubble to be spherical in shape):

1. Sphere.
2. Elongation (prolate spheroid).
3. Sphere.
4. Flattening (oblate spheroid).
5. Sphere.

The period of oscillation (T) and modulus of decay ( $\tau$ ) of the bubble are given by:

$$T = C_1 \sqrt{\frac{\rho}{\sigma}} D^3$$
$$\tau = C_2 \frac{\rho}{\mu} D^2,$$

## GENERAL DYNAMICS | ASTRONAUTICS

where

$T$  = period of oscillation,

$\tau$  = modulus of decay (time in which the amplitude of oscillation sinks to  $\frac{1}{e}$  of its original value),

$C_1$  = constant (0.641 for a sphere),

$\rho$  = density,

$\sigma$  = surface tension,

$D$  = characteristic linear dimension (diameter of a sphere),

$C_2$  = constant (0.0125 for a sphere),

$\mu$  = viscosity.

The values given for  $C_1$  and  $C_2$  apply only when the vapor bubble is oscillating in an infinite liquid medium. When there is not sufficient liquid hydrogen left in the tank for the gas ullage bubble to form a sphere during zero g, the constants  $C_1$  and  $C_2$  have to be determined empirically. Liquid/liquid tests at Astronautics have verified these two equations.

**12.2.2.3 Effect of Heat Transfer.** Heat is transferred at 1g between a solid and a liquid by conduction, gravity-forced convection, and forced convection due to bubble growth and rise.

At zero g, heat is transferred by forced convection or bubble dynamics and conduction. Some of the bubbles created by boiling will oscillate above the heated surface and some will be tangent to it. Coalescence will take place at an increased rate as the heating rate increases.

## GENERAL DYNAMICS | ASTRONAUTICS

Tests were run at Astronautics at both zero-g and 1g conditions to determine the heating rates necessary to initiate nucleate and film boiling in liquid hydrogen (Ref. 4). The results are shown in the following tabulation:

	ORDER-OF-MAGNITUDE HEATING RATES NECESSARY TO INITIATE NUCLEATE BOILING (BTU/HR. -FT. <sup>2</sup> )	ORDER-OF-MAGNITUDE HEATING RATES NECESSARY TO INITIATE FILM BOILING (BTU/HR. -FT. <sup>2</sup> )
Zero g (Closed-vent condition)	250	12,500
1g (Open-vent condition)	250 to 550	22,000 to 25,000

These heating rates were obtained with smooth surfaces; a roughened surface will lower these values somewhat. Due to the limited zero-g time available during aircraft tests, it was not possible to observe nucleate boiling at a lower heating rate than the value listed. The liquid hydrogen continuously rewetted the wall behind the bubbles during nucleate boiling.

After engine shutdown and propellant flow cutoff, a nuclear vehicle will be in a zero-g field. It is likely that the forward bulkhead of the hydrogen tank and portions of the tank wall will be covered by only a molecular layer of liquid hydrogen if there are no mechanical perturbations at engine shutdown. On restarting the engine, there is a good chance liquid hydrogen will contact the bare tank walls.

Tests were run at zero g to determine if vapor formation produced by liquid hydrogen striking a "warm" thin metal plate would violently force the liquid away from the wall. The action may be compared to dropping water on a hot skillet.

Analysis of film and recorder data showed conclusively that the impingement of liquid hydrogen against a relatively warm thin stainless steel plate--in the temperature range 100° to 300°R--results in no appreciable rejection or repulsion of the liquid (Ref. 5). Therefore, no additional complications need be feared from the eventuality of liquid hydrogen contacting a warm thin tank wall.

### 12.3 ZERO-GRAVITY LIQUID/GAS SEPARATORS

During zero g, liquid hydrogen will no longer remain settled in the bottom of the tank but will assume the configurations described in Section 12.2. If the vehicle is in a zero-g condition for a considerable length of time, heat transferred into the tank by solar radiation, albedo, and heat sources on the vehicle will raise the vapor pressure in the tank. When the vapor pressure reaches certain design limits, gas will have to be vented overboard. Preventing liquid hydrogen from being swept overboard with the vented gas is the unique problem encountered during zero g. An alternative to venting gas overboard is to provide refrigeration aboard the vehicle. The final choice between the two systems depends on reliability requirements and weight tradeoffs.

There have been two approaches at Astronautics to the problem of designing a liquid/gas separator for zero-g operation: static designs with no moving parts, and dynamic designs.

**12.3.1 STATIC SEPARATORS.** Originally, it was hoped that static separators could be designed that would separate liquid hydrogen from its vapor. Several different schemes were tested.

**12.3.1.1 Teflon-Covered Screens.** Two different geometries were tried, using Teflon-covered wire screens with 0.014-in. openings. Two cone-shaped screens, one mounted inside the other, were fastened over the vent hole. Another arrangement had two circular screens mounted in a tube, separated from each other by a distance of 3 in. It was hoped that liquid hydrogen would not wet the Teflon. In that event, a certain pressure differential would be required to overcome the surface tension effects and force liquid through the screen. Vapor could pass freely. However, tests using liquid nitrogen at zero g showed that the liquid passed readily through the screens. Additional testing has shown it is unlikely that any material will be found that will not be wetted by liquid hydrogen.

**12.3.1.2 Center Vent Tube.** Tests with Teflon-covered screens indicated it was not feasible to separate liquid from its vapor with static devices. However, since the configuration of the vapor bubble is known at zero g, the possibility of placing a simple vent tube in the vapor region was considered. In order for this venting arrangement to work successfully, five conditions must be met, as follows:

1. The end of the vent tube must be located inside the gas bubble at the time of venting.

## GENERAL DYNAMICS | ASTRONAUTICS

2. The gas ullage bubble must be large enough to prevent liquid hydrogen from accidentally entering the tube.
3. The venting rate must be low enough to prevent turbulent mixing of the liquid hydrogen.
4. Any mechanical perturbations at the time of venting must be of a low order to prevent liquid hydrogen from being sloshed into the vent tube.
5. Liquid hydrogen must not creep along the vent tube at such a high rate that the tube will fill with liquid.

Analytical studies on Centaur have shown that the liquid hydrogen will not be disturbed appreciably at the planned venting rates. The tank will be 30% full of liquid hydrogen at this time.

It has been shown in Section 12.2.2.1 that a tube passing through the liquid/gas interface would distort the interface only a matter of inches. The portion of the tube within the gas bubble would be covered only by a molecular layer of liquid hydrogen. If this molecular layer of liquid hydrogen flows along the outside of the vent tube into the tube, it is conceivable that it may become filled with liquid hydrogen, and a tube full of liquid hydrogen would be lost with each venting.

An estimate of the rate at which this tube will fill can be made. Evaporation and condensation processes may increase this calculated rate.

If it is assumed that the liquid hydrogen layer is three molecules thick ( $1 \times 10^{-8}$  cm), the vent tube has a diameter of 5 cm, and the liquid hydrogen flows at a rate of 10 cm/sec., the tube will fill at a rate of:

$$\pi (5 \text{ cm}) (1 \times 10^{-8} \text{ cm}) \frac{10 \text{ cm}}{\text{sec.}} \left( \frac{3,600 \text{ sec.}}{\text{hr.}} \right) = 6 \times 10^{-3} \text{ cu. cm/hr.}$$

If these assumptions are correct, the loss of liquid hydrogen from this source is negligible.

The results of liquid/liquid tests and drop tests have shown that a center vent has excellent potential as a venting device for Centaur. Rapid coalescence of the smaller vapor bubbles formed at the walls of the tank into the ullage will tend to maintain a large ullage bubble about the vent tube. Furthermore, surface evaporation may provide a major source of the boiling during venting. The results of model tests

## GENERAL DYNAMICS | ASTRONAUTICS

simulating the Centaur orientation sequence showed that the maneuver would cause considerable liquid rotation but probably would not cause liquid flow in the vicinity of the tube inlet (located near the tank center).

**12.3.2 DYNAMIC SEPARATORS.** Due to the failure of static separators to separate gas from liquid when immersed in liquid (the center vent works only when in gas), dynamic methods were investigated. After trying several schemes which included a rapidly rotating propeller placed over a vent hole to clear it of liquid, the final design for the Centaur utilized a rotating separator disc.

This disc consists of a circular flat plate with radially drilled holes, equally spaced, connected to a central hollow shaft. When this disc starts to spin, any liquid in these holes will be thrown out by centrifugal force. This rotating disc will vortex the liquid hydrogen, drawing the gas ullage bubble to it, thus allowing gas to vent through the holes.

A schematic drawing of the separator developed by Astronautics is shown in Figure 76 and a photograph of a test prototype is shown in Figure 77. The separator disc is connected directly to a velocity-compounded impulse turbine. When the gas pressure in the tank reaches a certain value, the control valve opens, allowing the hydrogen gas to flow to the turbine, starting to rotate it. Since the turbine is connected directly to the separator disc, the disc starts spinning, clearing the holes of liquid hydrogen and drawing the gas ullage bubble to it. Due to the differential pressure between the tank and the turbine housing (vented to free space), the hydrogen gas is cooled by its rapid expansion in the turbine. In order to take advantage of this cooling process, the expanded gas is passed through heat exchangers before being vented overboard. This heat-transfer process cools the gas in the tank, lowering the tank pressure, and consequently, the quantity of hydrogen vented. When the tank pressure drops to a preset value, the control valve closes.

There are two identical units in the zero-g separator, each containing a separator disc, control valve, turbine, and heat exchanger. The two separator discs counter-rotate to balance out their torques, preventing the vehicle from rolling during the zero-g period of the trajectory.

Astronautics' aircraft zero-g tests on a single disc separator mounted in liquid nitrogen proved the feasibility of this type of separator. During the test, the separator:

1. Expelled any liquid that was drawn in with the circulating vapor.
2. Expelled liquid that, due to external disturbances, would flow against the fluid expelled by the rotor.
3. Did not "draw in" liquid in the immediate vicinity of the rotor.

# GENERAL DYNAMICS | ASTRONAUTICS

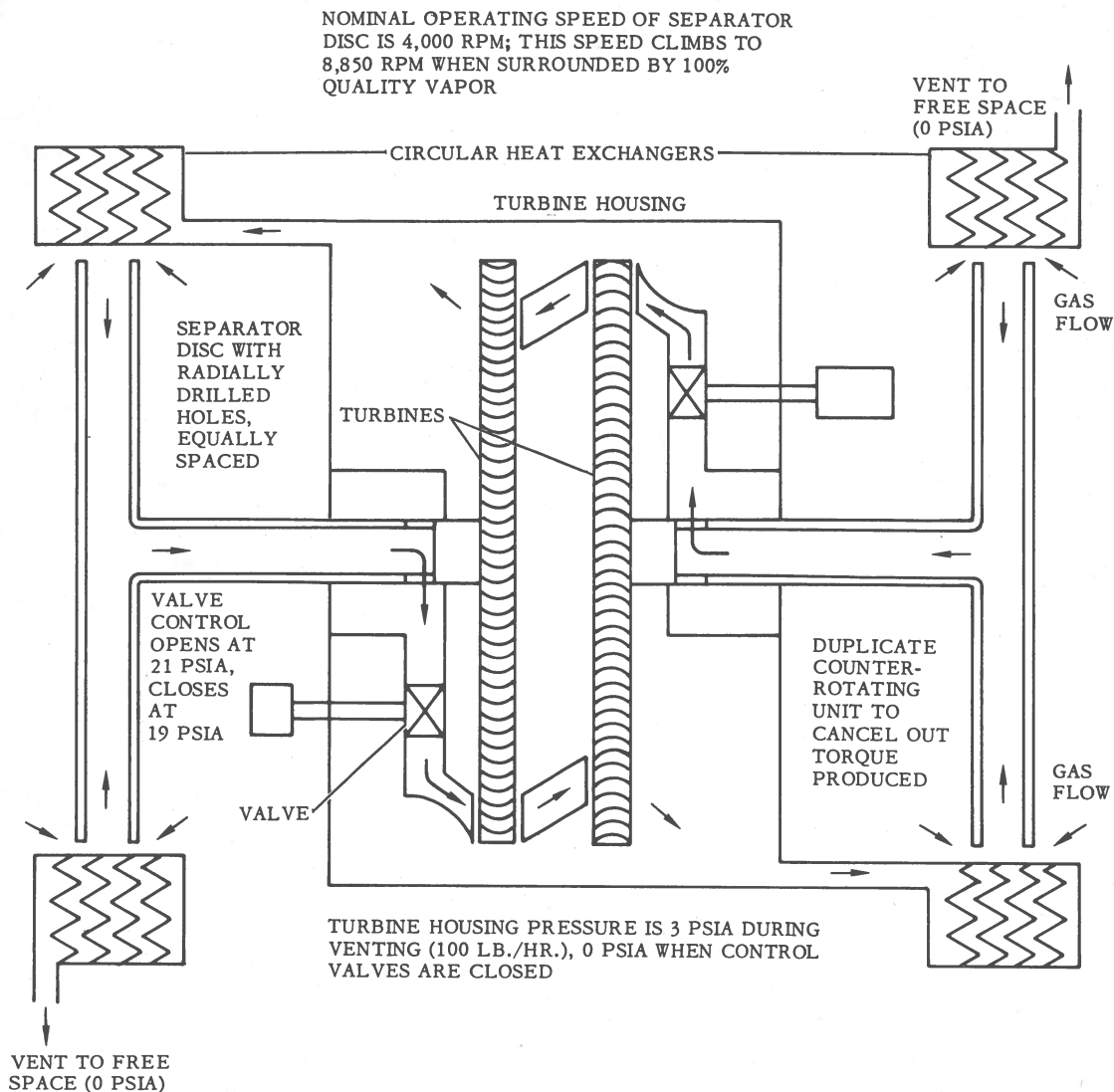


Figure 76. Schematic drawing of Centaur zero-g liquid/gas separator.

Flight certification tests at 1g have shown that the separator conforms to minimum requirements for actual flight. These tests included transport leakage, proof pressure, vibration, and abbreviated life tests.

Other tests were run at 1g to determine the operating characteristics of the separator in hydrogen vapor. With a temperature of 40°R, a pressure of 21 psia in



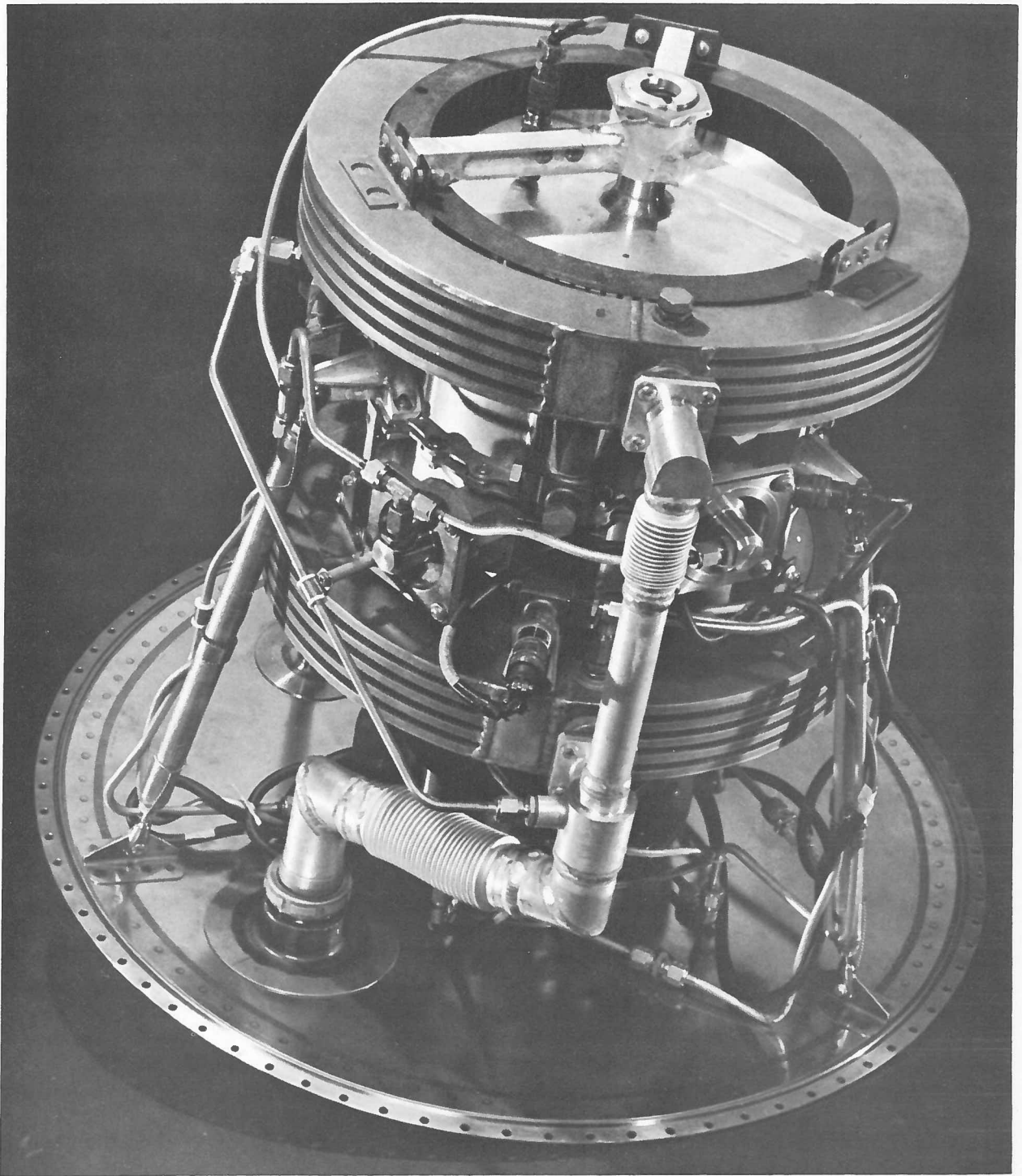


Figure 77. Test prototype of Centaur zero-g liquid/gas separator.

## GENERAL DYNAMICS | ASTRONAUTICS

the tank, and a mass flow rate of 100 lb./hr. through the separator, the pressure in the turbine housing was approximately 3 psia.

The specifications for the zero-g separator are given in Ref. 6.

### REFERENCES

1. Cryogenic Liquids in the Absence of Gravity. Ta Li, Astronautics Report, August 1961, pp. 11-13.
2. Ibid, p. 1.
3. March - May Progress Report for the Combined Laboratory and KC-135 Aircraft Zero-g Test Program. Astronautics Report AE61-0593, 22 June 1961, p. 19.
4. June - August Progress Report for the Combined Laboratory and KC-135 Aircraft Zero-g Test Program. Astronautics Report AE61-0871, 5 September 1961, pp. 3, 4, and 12.
5. March - May Progress Report for the Combined Laboratory and KC-135 Aircraft Zero-g Test Program. Astronautics Report AE61-0593, 22 June 1961, p. 25.
6. Separator - Zero G, Missileborne, Specification for. Astronautics Report 55-08129, 6 April 1960.

# 13

## SPACE STORAGE

The ability to store liquid hydrogen in space for planetary missions is essential in order to realize its performance potential in chemical and nuclear vehicles. To successfully accomplish this, heat influx into the tank must be reduced to an acceptable level and the tank must be protected against catastrophic meteoroid puncture. The design is further complicated by the air condensation problem prior to liftoff and structural integrity of insulation and meteoroid bumper systems during atmospheric ascent.

This discussion is divided into two sections: thermal protection and the meteoroid hazard. In one sense, this division is rather arbitrary since the meteoroid bumper and insulation system may be combined in a single design.

### 13.1 THERMAL PROTECTION

The following discussion is broken into two parts, the storage state of hydrogen and methods of thermal protection.

**13.1.1 STORAGE STATE.** To transport large quantities of hydrogen into space, it is necessary to store it in liquid form at various vapor pressures, as a solid/liquid "slush," or in solid form.

The most practical way to solidify the  $\text{LH}_2$  is to reduce the pressure over the fluid. Approximately 24% of a given quantity of  $\text{LH}_2$  at 1-atmosphere initial vapor pressure must be evaporated to solidify the rest. Due to unavoidable heat inputs, it does not appear practical to solidify the hydrogen completely on the ground. An alternative to this method consists of forming a slush prior to liftoff by lowering the vapor pressure, and then venting the tank once more when it is outside the atmosphere to complete the solidification. Storage of hydrogen as a solid has some additional advantages beside the longer storage time possible. No sloshing problems are encountered during in-flight accelerations and leakage from a meteoroid-punctured tank would be slow, allowing adequate time for repair.

## GENERAL DYNAMICS | ASTRONAUTICS

Due to the heat inputs into the tank, discussed in Chapter 11, the temperature of the stored hydrogen will rise with time; consequently the vapor pressure will increase. At some point in the mission, gas must either be vented overboard or reliquefied to reduce the tank pressure. (To vent at zero g, special vent devices such as a centrifugal liquid/gas separator or a center vent tube are needed; see Chapter 12 for a detailed examination of these devices.) No venting or reliquefaction is necessary if the tank is designed to withstand the contemplated pressure rise. Normally, however, this approach leads to excessively heavy tanks.

A discussion on active thermal protection (reliquefaction of the gas) and passive protection (insulation) follows.

### 13.1.2 THERMAL PROTECTION METHODS

13.1.2.1 Gas Reliquefaction. When very large hydrogen tanks and long space missions are contemplated, reliquefying the gas becomes more economical as to weight than increasing the insulation thickness. However, the added complexity and, consequently, reduced reliability, of this system compared to insulation must be considered along with weight considerations. Studies by the Malaker Laboratories indicate that a good-sized, flight-weight reliquefaction unit/power supply combination will weigh less than 5,000 lb. (see Table XI).

Table XI. Liquefaction unit weight.

LIQUEFACTION CAPACITY			
(LB./24 HR.)	50	150	300
TOTAL SHAFT POWER			
REQUIRED (EKW)	3.91	10.6	19.6
TOTAL WEIGHT OF LIQUEFACTION			
UNIT (LB.)	650	960	1190
TOTAL WEIGHT OF NUCLEAR ELECTRIC POWER SUPPLY PLUS RADIATOR FOR 30 EKW = 4,000 LB.			

13.1.2.2 Advanced Insulation Concepts. Flight-type insulations described in Section 5.2.3 are designed to reduce the heat load during ground hold, aerodynamic heating and for short times in space (hours) but are completely inadequate for long-term space storage. Of the insulations available, only laminar insulation reduces heat transfer to a point where storage of liquid hydrogen in space is practical for periods of days, weeks, or months. (Section 5.1.2 discusses the heat-transfer process through laminar insulation.)

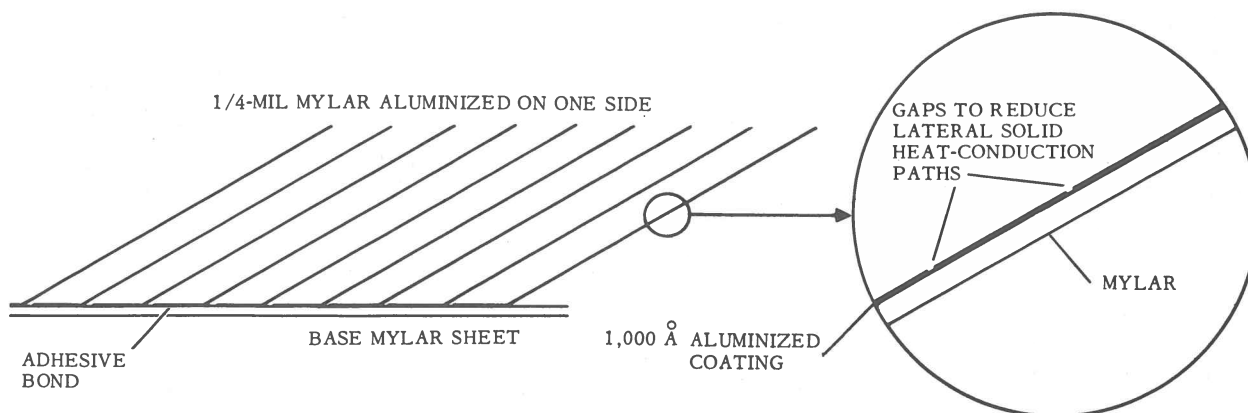
## GENERAL DYNAMICS | ASTRONAUTICS

There are several design problems associated with using laminar insulation on flight stages. These are:

1. Laminar insulation requires high vacuum to function properly ( $< 10^{-6}$  mm of Hg).
2. The individual sheets must be mechanically supported to withstand the acceleration and vibration flight environment.
3. Lateral conduction heat leaks and conduction heat leaks between touching sheets must be kept within certain limits.
4. The insulation should be capable of being installed on complex shapes.
5. The insulation must be protected from aerodynamic loads during atmospheric ascent.

The high vacuum requirement can be met in two ways. An evacuated double skin could be used on the LH<sub>2</sub> tank or the insulation could be allowed to outgas once the vehicle is outside the atmosphere. Judging from the difficulty encountered in evacuating the Centaur intermediate bulkhead, it appears that building a flight-weight, leak-tight, double-walled tank that goes from ambient to LH<sub>2</sub> temperatures is indeed a formidable task. Allowing the insulation to outgas in space appears a more feasible route to take at this time.

A design to allow rapid outgassing is shown in Figure 78. One edge of a thin ( $\sim 1/4$ -mil) Mylar sheet, aluminized on one side, is bonded to a base sheet, similar to shingles on a roof. This design allows gas trapped between the sheets to diffuse out rapidly. In addition, this type of support is sufficient to allow the insulation to withstand the acceleration and vibration loads imposed on it. Lateral conduction heat leaks are reduced by periodic breaks in the aluminized coating (Figure 78). Heat leaks between touching sheets are reduced by crinkling the Mylar to reduce contact points; this approach is used in NRC-2 insulation. This crinkling also allows the insulation to be installed on complex shapes such as spheres, cylinders, and ellipsoids. It is unlikely that this insulation would withstand aerodynamic loads imposed on it. However, since the tank also needs meteoroid protection (see Section 13.2), the bumper/energy-absorbing-core system can be used for this purpose. The energy-absorbing core material would serve the dual role of ground and atmospheric ascent insulation and meteoroid protection. Since the choice of bumper materials is not restricted by strength considerations (see Section 13.2.4), a porous material such as fiberglass sheet could be used to allow outgassing of the laminar insulation.



SHEETS ARE DRAWN AT AN ANGLE TO ILLUSTRATE ATTACHMENT METHOD. IN ACTUAL PRACTICE THEY WOULD LIE ON TOP OF EACH OTHER ALMOST PARALLEL TO THE BASE SHEET. THE SHEETS ARE CRINKLED TO REDUCE SOLID HEAT-CONDUCTION PATHS BETWEEN ADJOINING SHEETS.

Figure 78. Method for attaching laminar insulation to allow rapid outgassing in space.

The component parts necessary for a combined insulation-meteoroid protection system are shown in Figure 79. Two different combinations of these parts into an integral meteoroid/insulation protection system are shown in Figure 80, with the advantages and disadvantages of each combination listed. There are, of course, many other ways of combining the essential parts.

Due to the manufacturing complexity and significant weight penalty of the high-efficiency thermal/meteoroid protection system,  $LH_2$  storage will probably be divided into two separate tanks for prolonged space missions. One tank will have a minimum amount of insulation and no meteoroid bumper. Liquid hydrogen in this tank will be utilized early in the space mission and thus will not require the elaborate system.  $LH_2$  used later in the mission will be stored in the tank with high-efficiency thermal/meteoroid protection.

The two-tank system has another weight advantage that will help balance out the added weight of separate tanks. The tank used first can be emptied completely (fluid plus ullage gas) and ullage gas requirements for the second tank will be lower than for a single large tank. Consequently, a considerable weight saving in propellant required for long space missions is effected for large vehicles of the Saturn size.

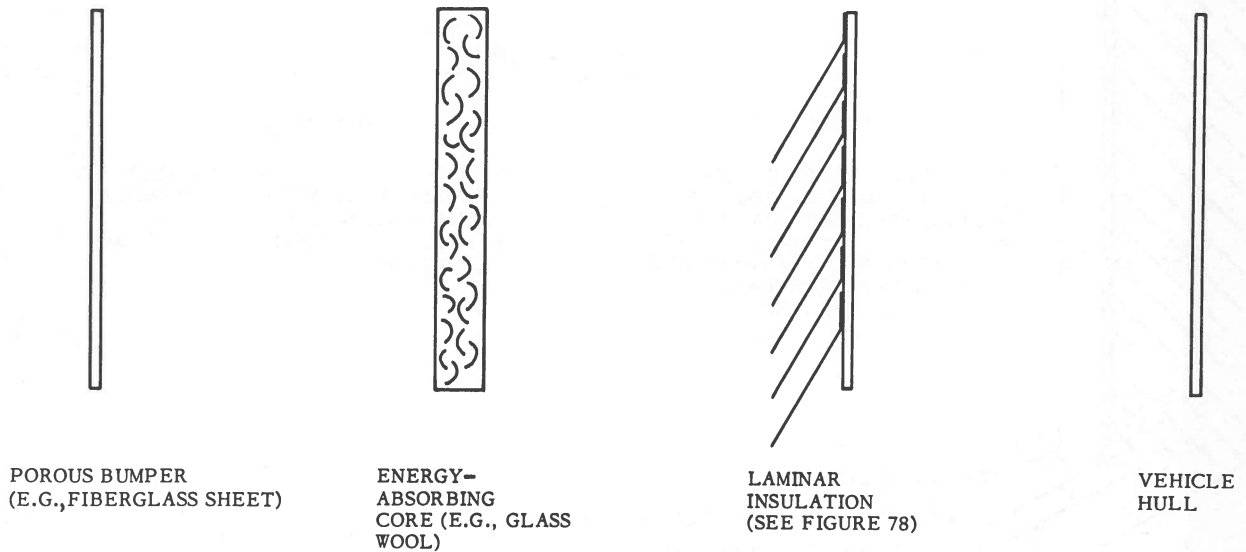


Figure 79. Component parts of thermal-meteoroid protection system.

### 13.2 METEOROID HAZARD

Among the many problems besetting a space-vehicle designer is that of protecting the vehicle from damage from the impact of meteoroids. These pieces of cosmic debris travel at high velocity and, on impact with a space vehicle, may puncture its thin-skinned, lightweight hull, even if the meteoroids are small. Fortunately, the number of meteoroids diminishes as their size increases so that the most likely damage to a vehicle is a small hole in the outer skin. They are numerous enough, however, that one must consider the possibility of a meteoroid large enough to rupture a hull extensively, thereby causing an explosive decompression, or to damage seriously the contents of a vehicle after piercing the skin. The chance of being struck increases, of course, with the size of the vehicle and the duration of the voyage. An indication of the possible seriousness of this hazard was obtained when fragments from the Atlas booster 109-D, which put the Mercury capsule Friendship 7 into orbit, exhibited extensive cratering apparently from hypervelocity impacts. (See Figure 81.) Preliminary data indicates that the booster orbited the earth four to six times before re-entering the atmosphere over South Africa.

The most straightforward method of protecting a vehicle from meteoroid penetration is to make the outer skin from a single sheet of material thick enough to resist penetration by the largest meteoroids that would be encountered on the voyage, taking into account the size of the vehicle, length of the flight, and maximum probability of

# GENERAL DYNAMICS | ASTRONAUTICS

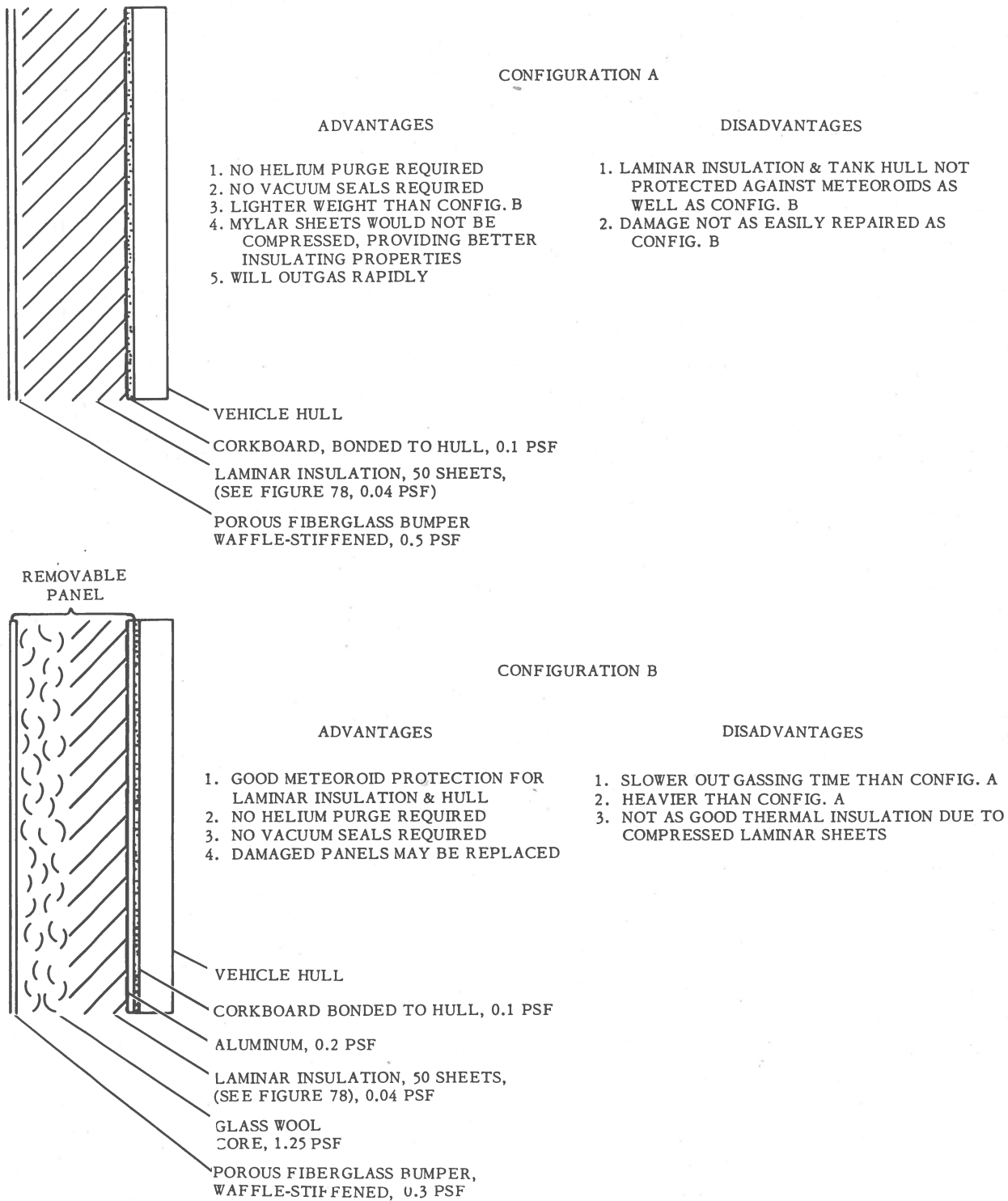


Figure 80. Typical thermal/meteoroid protection systems.



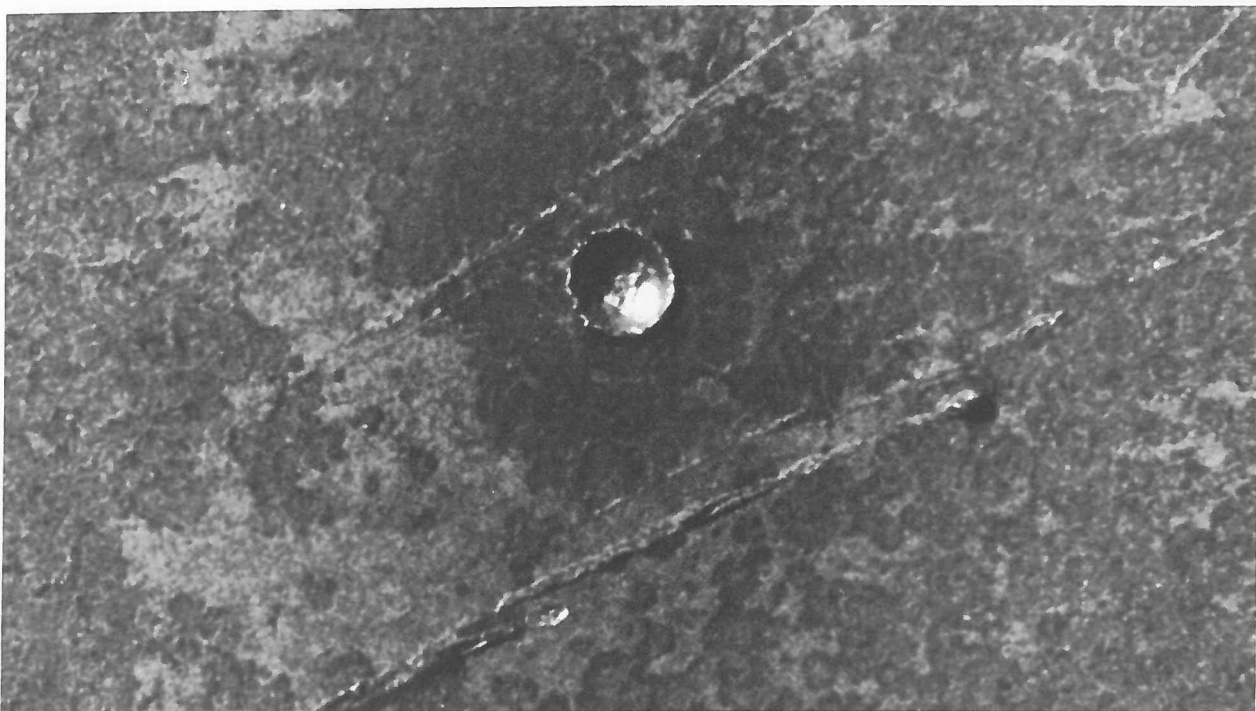


Figure 81. Closeup of typical crater on outside surface of Atlas 109-D fragment.

encounter allowed by the level of reasonable risk for the flight. This approach, however, results in a vehicle of unacceptably large weight.

A more sophisticated approach is to construct a double hull of sheets spaced apart. The value of this approach has been recognized for many years in the design of armor for military vehicles, although the application to spacecraft was first suggested by Dr. F. L. Whipple of the Harvard College Observatory. Whipple proposed that the spacecraft be surrounded by a thin outer shell spaced away from the main hull, which he called a meteor bumper. He suggested that a meteoroid would vaporize on impact with the bumper (along with vaporization of some of the bumper material) and its ability to penetrate the hull would thereby be sharply reduced. On the other hand, the meteoroid may possibly just be fragmented on impact with the bumper and not vaporize. If this is the case, the cloud of meteoroid and bumper fragments will diverge laterally with distance behind the bumper. (Experiments at Astronautics have shown this dispersion angle to be approximately  $60^\circ$ .) In this way, the kinetic energy of the meteoroid will not be concentrated in a single solid body but will be divided among the broken meteoroid and bumper fragments. The inner hull, because of the larger affected area, will be more resistant to penetration by the smaller, less potent particles (Figure 82).

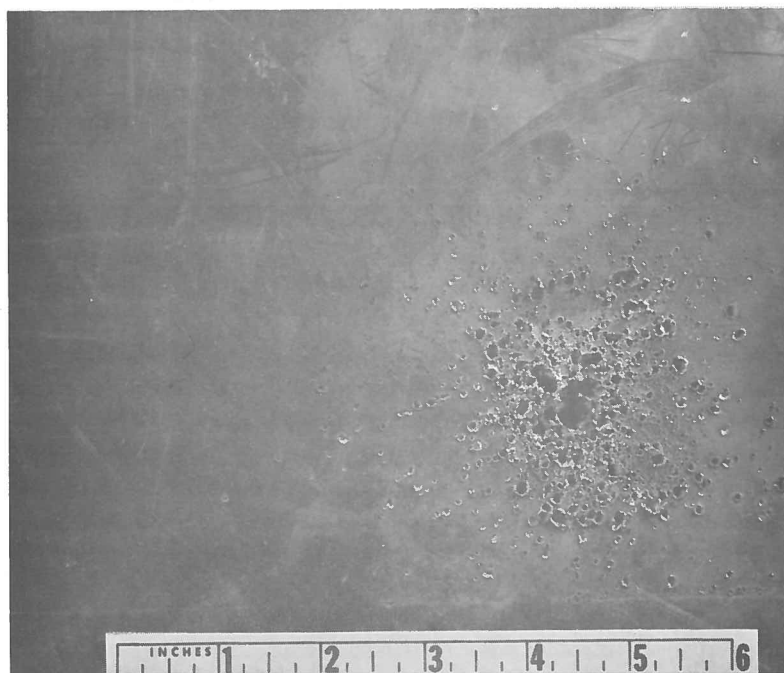
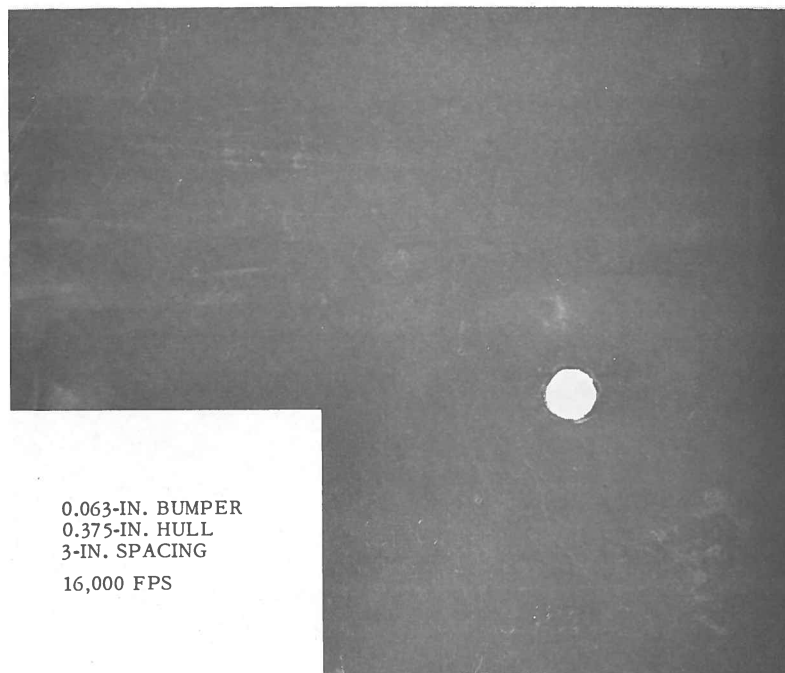


Figure 82. Aluminum bumper with 3-in. spacing.

## GENERAL DYNAMICS | ASTRONAUTICS

A refinement to this bumper concept that provides significantly improved protection with an over-all weight savings uses an energy-absorbing core material, such as glass wool, sandwiched between the bumper and the hull.

13.2.1 METEOROID ENVIRONMENT. The greatest certainty about the hazard to aerospace vehicles from meteoric particles is the great uncertainty in the predictions. Neither the number, mass, velocity, nor composition of the natural meteoric particles that constitute the local space environment is precisely known.

This problem is further complicated by the existence of meteor showers in addition to the sporadic background. These showers have been known to exceed the sporadic background by several orders of magnitude. Due to the variable nature of these showers, only the sporadic meteoroid flux can be considered here.

Whipple (Ref. 1) reports that more than 90% of photographed meteors have densities as low as 0.05 gm/cu. cm. Radio-radar observed meteors may have similar densities. This applies to meteors of mass roughly greater than  $10^{-4}$  gm, commonly referred to as dust balls. These dust balls may break up, however, producing smaller more conventional densities, perhaps more like those of silicate rocks. The asteroids may be the source of a large fraction of the meteoroid spectrum of smaller masses ( $<10^{-4}$  gm). Brown (Ref. 2 and 3) correlates the mass-frequency distribution of meteorites with that of the asteroids. The correlation is good. Meteorites range in density from 2.7 to 7.9 gm/cu. cm (stone-irons), the relative abundance being about 16 to 1, respectively. This would place the average density of asteroidal meteoroids at about 3 gm/cu. cm.

Geocentric velocities of meteors have been measured. Whipple (Ref. 1) calculates the average velocity of photographic meteors to be 28 km/sec. (A range of 11 to 72 km/sec. is possible in view of the fact that meteors are permanent members of the solar system.) From theoretical considerations, one would expect smaller meteoroids to have lower velocities. On this basis, Whipple constructed a table of velocity as a function of mass for meteoroids. This is plotted in Figure 83. This is probably the most reasonable velocity distribution for meteoroids which can be presently deduced. A conservative figure of 28 km/sec. may be used for all meteoroids.

Data on the flux of meteoroids has been obtained from visual, photographic, and radio-radar observations, and of late from counting devices on rockets and satellites. Data in the first category (i. e., visual, photographic, and radio-radar) yields meteor flux as a function of magnitude. It is then necessary to relate magnitude to the mass of the particle involved. To date no reliable relation exists. Whipple (Ref. 1)

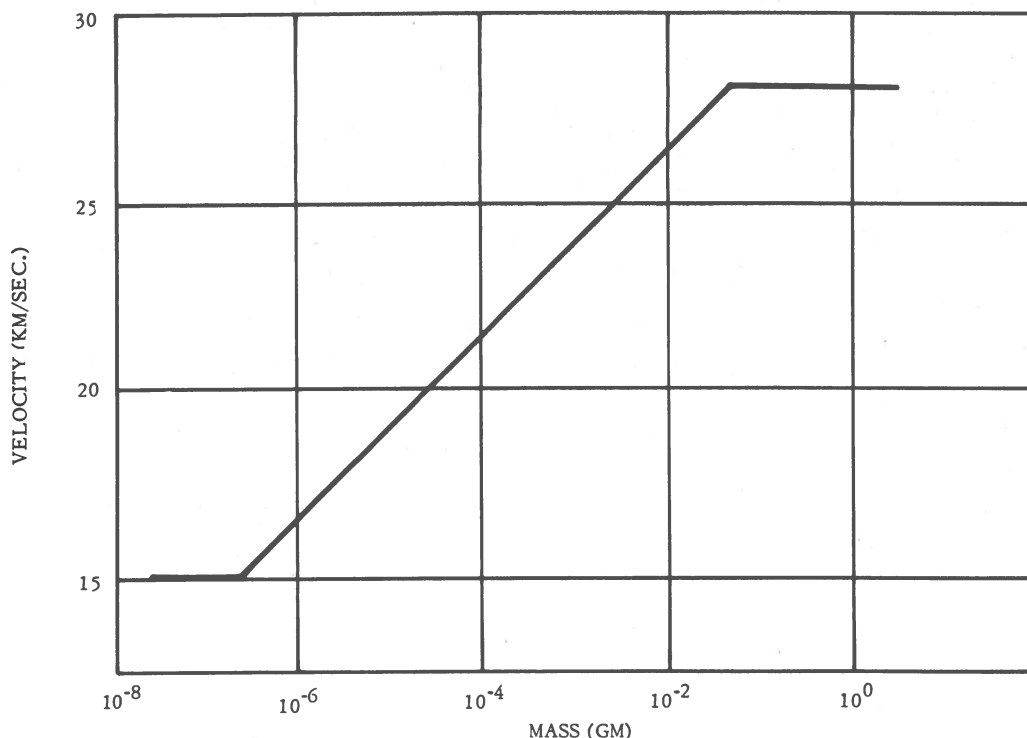


Figure 83. Mass-velocity distribution of meteoroids.

assigned a value of 25 gm to a zero magnitude meteor, while Watson (Ref. 4) chose the value 0.25 gm. On these bases, two curves are obtained of the flux of meteoroids of mass equal to and greater than mass  $m$ , as a function of mass. These have been extrapolated to particles of smaller mass (see Figure 84). These two estimates can perhaps be taken as bounds on the sporadic meteoroid environment in the mass range from  $10^{-4}$  to 1 gram.

A nearly complete list of in situ rocket and satellite measurements has been compiled and the most significant measurements are presented in Figure 84. They are listed in order of decreasing significance, the solid symbols representing the most significant measurements. The points plotted are based on an assumed velocity of 15 km/sec. since satellite sensors respond to momentum. \* The data has not been corrected for earth-shielding, as is sometimes the custom, since while in the earth's

\* Russian sensors reportedly respond to the kinetic energy of the impacting particle.

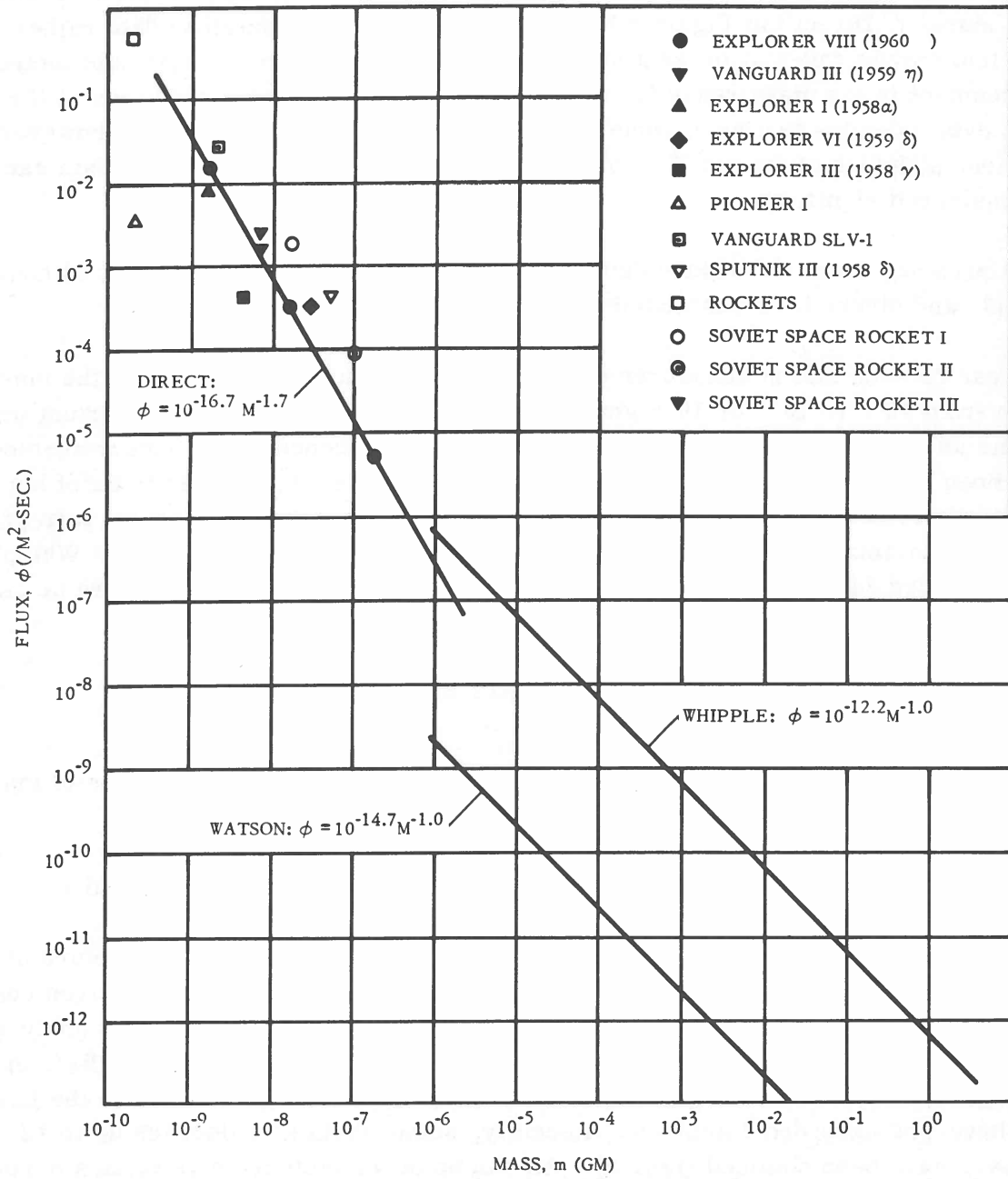


Figure 84. Meteoroid flux.

vicinity, a vehicle will see the shielded flux and there are theoretical indications that meteoroid flux decreases with increasing altitude. The most significant measurements have reportedly been taken on the Explorer VIII satellite, where measurements were made in three momentum ranges. The three Explorer VIII points fall on a good straight line, marked "Direct" in Figure 84 which also fits the other satellite data rather well. This line may be taken at present as the best representation of the sporadic meteoroid environment in the mass range from  $10^{-9}$  to  $10^{-6}$  gm. A closer inspection of the satellite data indicates that no altitude dependence of the flux is discernible; however, the mean altitudes of the satellite orbits vary only 800 km and the rocket data cannot be considered significant.

At present, then, no altitude dependence can be deduced experimentally although Whipple and others have postulated this dependence analytically.

It can be seen that no measurements of meteoroid flux are available in the mass range from  $10^{-6}$  to  $10^{-4}$  or  $10^{-3}$  gm. This is unfortunately the most important mass regime as far as propellant losses due to puncture are concerned. Sensor surfaces have been very small in the past due to the weight limitation, and had to be of high sensitivity to record a significant number of hits. Consequently, a conservative mass-flux relation must be used until better data is available. It is believed that Whipple's curve (Figure 84) represents such a relation. Meteoroid flux will therefore be assumed to follow the law

$$\phi = 10^{-12.2} m^{-1.0} \quad (1)$$

where  $m$  is the meteoroid mass in grams, and  $\phi$  is the number of particles of mass greater than and equal to  $m$  per square meter per second.

A more complete discussion of meteoroid flux is given in Ref. 5, 6, and 7.

**13.2.2 HOLE AREA DUE TO METEOROID PUNCTURE.** Meteoroid puncture of a thin skin involves a hypervelocity impact process which has, of late, received considerable experimental and theoretical attention. Excellent compilations and analyses of experimental and theoretical work are presented by Herrmann and Jones (Ref. 8) and Rolsten, Hunt, and Wellnitz (Ref. 7). Until recently, velocities attained in the laboratory have not exceeded 6 km/sec. Recently, some shots at velocities up to 12 km/sec. have been obtained (Ref. 9). As can be seen, meteoroid velocities have barely been approached in the laboratory. Extrapolation of experimental data taken

## GENERAL DYNAMICS | ASTRONAUTICS

at low velocities to the much higher meteoroid velocities is strictly invalid since the physical process involved is different. At hypervelocities, strength effects are negligible during part of the impact process since the pressures involved far exceed the material strength.

Theoretical work by Bjork (Ref. 10) gives the depth of penetration (d) for a hydrodynamic impact of iron on iron and aluminum on aluminum numerically in the inviscid, adiabatic approximation. He obtained the relations:

$$\begin{aligned} \text{Al on Al: } d &= 1.09 (mv)^{1/3} \\ \text{Fe on Fe: } d &= 0.606 (mv)^{1/3} \end{aligned} \tag{2}$$

where m is the meteoroid mass in gm, and v is the meteoroid velocity in km/sec. Bjork recently suggested that the penetration in a given target material by projectiles of different materials but the same mass and velocity is proportional to the initial interface velocity on impact. Herrmann and Jones (Ref. 8) show the initial interface velocities  $v^*$  for impacts of dissimilar materials are given with a maximum error of about 20% for most materials by

$$v^* = \frac{1}{2} \left( \frac{\rho_p}{\rho_t} \right)^{1/3} v \tag{3}$$

for projectile velocities v above 3 km/sec., where  $\rho_p$  and  $\rho_t$  are projectile and target densities, respectively. Eq. 2 can therefore be modified for different projectile materials to yield

$$d = 1.09 \left( \frac{\rho_p}{\rho_{Al}} \right)^{1/3} (mv)^{1/3} \tag{4}$$

for impacts on aluminum targets, and

$$d = 0.606 \left( \frac{\rho_p}{\rho_{Fe}} \right)^{1/3} (mv)^{1/3} \tag{5}$$

for impacts on iron targets.

## GENERAL DYNAMICS | ASTRONAUTICS

It has been observed (Ref. 8) that if a projectile will penetrate a semi-infinite target to a depth of  $d$ , it would puncture a thin plate of thickness  $1.5 d$ . Therefore, in terms of plate thickness, Eq. 4 and 5 become

$$t_{Al} = 1.64 \left( \frac{\rho_p}{\rho_{Al}} \right)^{1/3} (mv)^{1/3} \quad (6)$$

$$t_{Fe} = 0.908 \left( \frac{\rho_p}{\rho_{Fe}} \right)^{1/3} (mv)^{1/3} \quad (7)$$

Eq. 6 and 7 may be combined with Eq. 1 to yield the flux of meteoroids which will puncture a thin vehicle skin of thickness  $t$ . This will be called, after Bjork, the penetrating flux  $\psi$ . Given a skin thickness,  $t$ , and taking velocities from Figure 83 or assuming a meteoroid velocity of 28 km/sec., Eq. 6 and 7 yield the size of the smallest mass meteoroids which will puncture the skin.

This is called the threshold mass ( $m_{th}$ ). All meteoroids of mass greater than  $m_{th}$  will likewise puncture the skin. Using velocities from Figure 83 and meteoroid density  $\rho_m = \rho_p = 3$  gm/cu. cm,  $m_{th}$  was calculated as a function of skin thickness for both steel and aluminum skins and appears in Figure 85. It is seen that meteoroids of mass as low as  $10^{-6}$  gm may be important in contributing to propellant losses, depending on skin thickness.

If it is assumed that the hole produced by a meteoroid impact is of constant diameter throughout its depth (the diameter being equal to the entrance diameter produced by the meteoroid), and the depth of penetration  $p$  given in Eq. 4 and 5 is also the radius of the hole, then the area of a hole produced by a meteoroid of mass  $m$  is given by:

$$a(m) = \pi p^2 = \pi C^2 \left( \frac{\rho_m}{\rho_{Al \text{ or } Fe}} \right)^{2/3} \left[ m v(m) \right]^{2/3} \quad (8)$$

where  $C = 1.09$  for aluminum targets,  $C = 0.606$  for steel targets, and  $\rho_m$  is the meteoroid density. For  $\rho_m = 3$ , Eq. 8 is quite accurate for meteoroids of mass near the threshold mass, since the ratios of skin thickness to diameter of threshold meteoroid (assuming a spherical meteoroid) are 6 and 2.33, for aluminum and steel



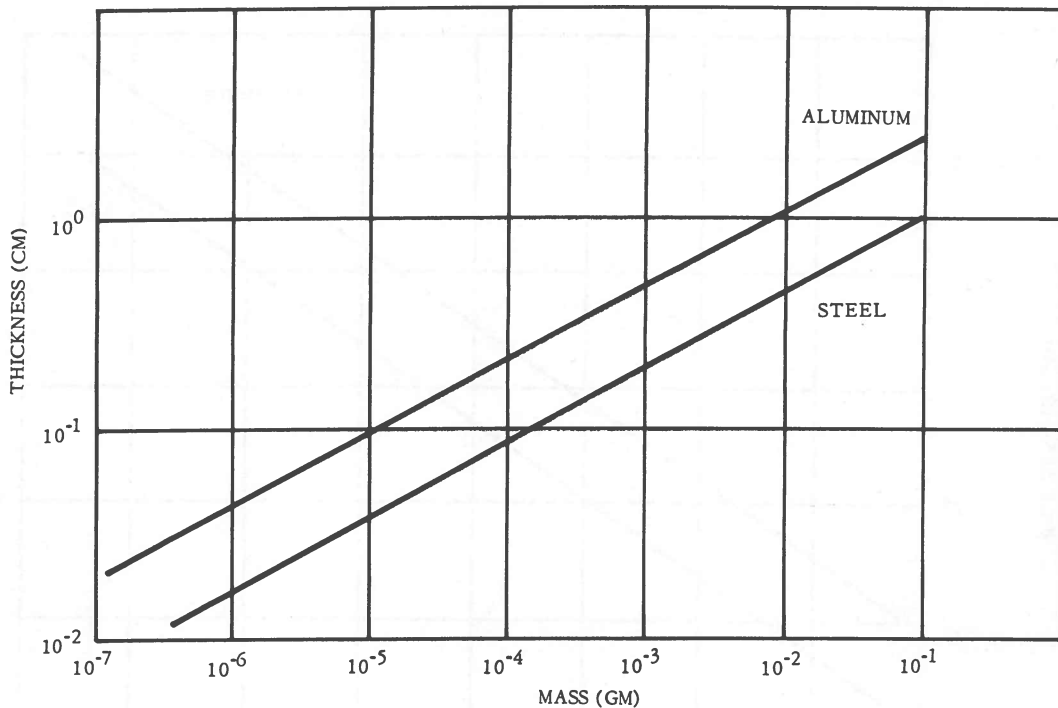


Figure 85. Skin thickness vs. threshold meteoroid mass.

targets, respectively. For meteoroids of mass greater than the threshold mass, Eq. 8 will overestimate the actual area, the overestimate increasing as mass increases. This is due to the fact that the radius of a crater produced by a given projectile in a semi-infinite target is greater than the radius of a hole produced by the same projectile in a thin plate. Since the significance (i. e., number) of meteoroids decreases with increasing mass above the threshold mass, the error introduced by using Eq. 8 for all meteoroids will not be substantial. At any rate, Eq. 8 gives a conservative estimate of area.

Hole area vs. meteoroid mass for both aluminum and steel is given in Figure 86.

13.2.3 PROPELLANT FLOW FROM A PUNCTURED TANK. If the vehicle is assumed to be coasting in space, Bernoulli flow from a reservoir at zero g into a vacuum is applicable. The exhaust velocity is therefore given by

$$v_e = \left( \frac{2P}{\rho_f} \right)^{1/2} \quad (9)$$

# GENERAL DYNAMICS | ASTRONAUTICS

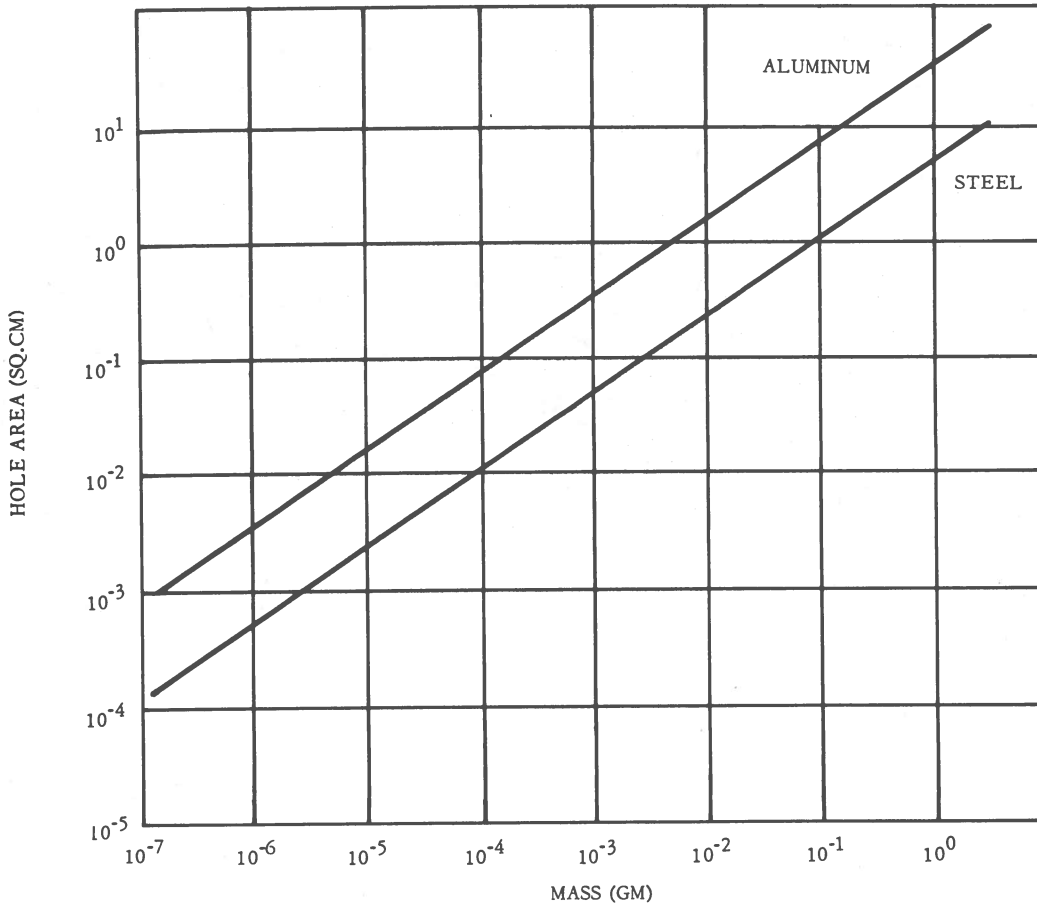


Figure 86. Hole area vs. meteoroid mass.

where  $P$  is the tank pressure and  $\rho_f$  the fuel density. The flow rate is therefore

$$Q = r a \left( \frac{2P}{\rho_f} \right)^{1/2} \tag{10}$$

where  $r$  is an orifice coefficient and  $a$  the area. The mass flow is

$$Q_w = r a \left( \frac{2P}{\rho_f} \right)^{1/2} \tag{11}$$

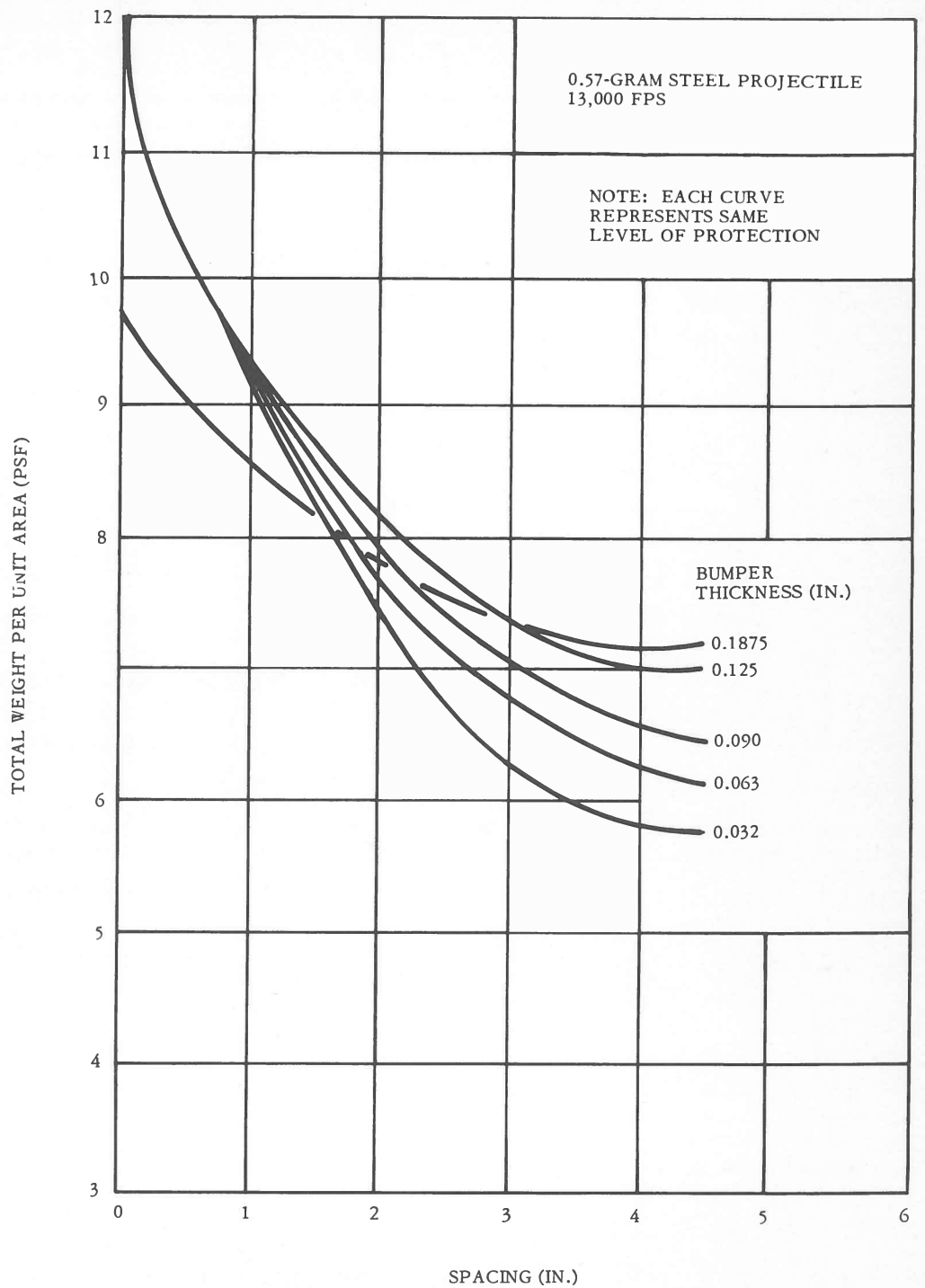


Figure 88. Effectiveness of bumper spacing and bumper thickness.

2. When the space between the bumper and target is less than approximately 0.25 in., a thin bumper may be extensively damaged from material erupted or splashed back from the crater (see Figure 89).

Work by Funkhouser (Ref. 11) and Olshaker (Ref. 12) determined the dependence of the total penetration on the distance between the bumper and target (see Figure 90). The spacing of the bumper in front of the target surface was varied: (1) from zero to 6 in. with a constant aluminum bumper thickness of 0.031 in., and projectile mass and velocity of 0.0183 gram and 12,000 fps, respectively and (2) from 0.25 to 1.49 in. with a constant lead bumper thickness of 0.054 in., and projectile mass and a velocity of 0.188 grams and 8,366 fps, respectively. There is a rapid decrease in total penetration in aluminum from zero spacing to a spacing of 2 in.; with greater distances the total penetration is almost constant. The decrease in total penetration in lead with a 0.50-in. spacing is even more pronounced than with aluminum.

13.2.4.3 Energy-Absorbing Core Materials. Energy-absorbing core materials have been shown to significantly improve a bumper system's resistance to penetration with an over-all weight saving.

A good core material must have moderate compressive and shear strength, low density, directionality of mechanical properties and low ablation rates. In addition,

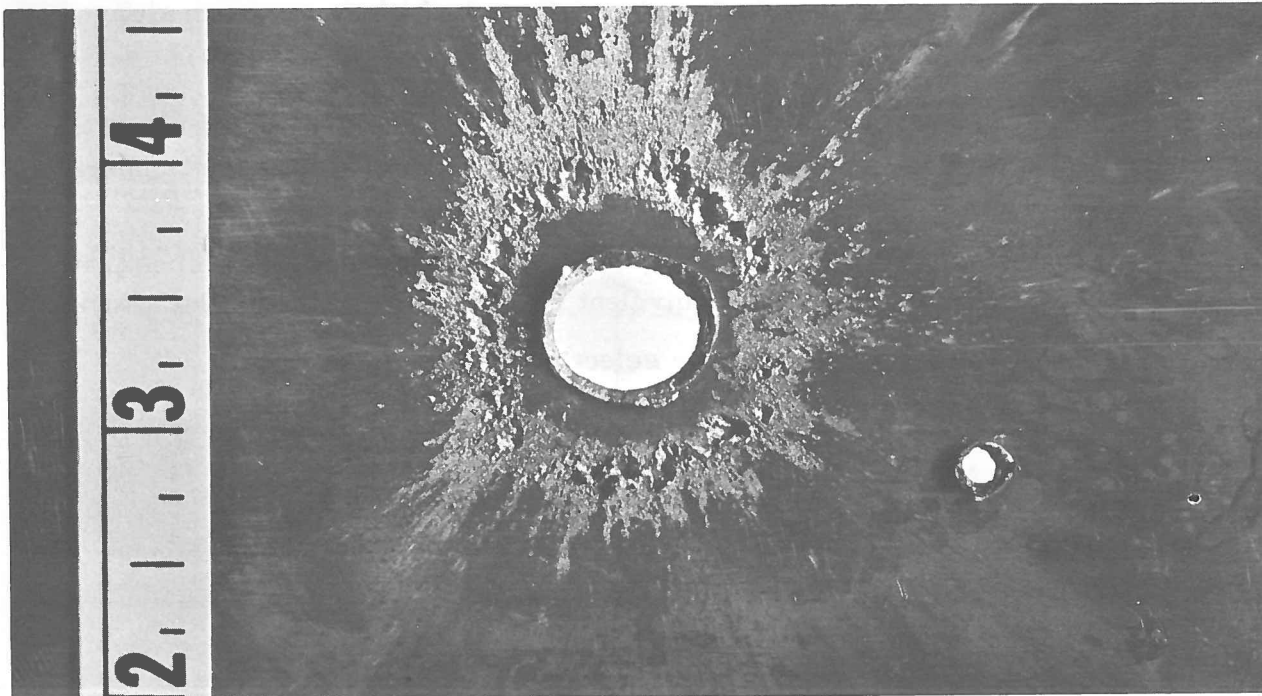


Figure 89. Reverse side of bumper spaced 0.25 in. from hull plate.

When dealing with  $LH_2$ , the question may be raised whether the liquid might not freeze while expanding through the hole, thus temporarily plugging the hole and decreasing the effective flow rate. Experience at Astronautics has shown that liquid hydrogen escaping through a small hole will plug momentarily, then the solid hydrogen will break loose and the flow will resume. Whether this intermittent flow occurs depends on the tank pressure and size of the hole.

13.2.4 METEOROID BUMPERS. Due to the meteoroid hazard, discussed previously, experimental work has been conducted to determine the most effective meteoroid bumper system. Some of these results are discussed in the following sections on bumper materials, bumper spacing, and energy-absorbing core materials.

13.2.4.1 Bumper Materials. The effectiveness of the thin meteoroid bumper depends on its mass. The thin bumper need not possess strength or toughness since the impact and shear processes are fluid above approximately 8,000 fps. Work done by Astronautics (Ref. 7) has shown that bumpers of aluminum alloy (6061-T6), magnesium-lithium alloy (LA-141), plate glass, and stainless steel (301) are equally effective on the basis of total weight per unit panel area. Total weight includes the weight of both the bumper and the aluminum (6061-T6) vehicle hull. Pertinent test data is shown in Figure 87. It can be seen that test panels with a mass and spacing in the area: (1) above the upper curve are not perforated or cracked; (2) between the two curves may or may not be perforated or cracked; and (3) below the bottom curve are always perforated or cracked. Thus it can be concluded that:

1. The degree of brittleness or ductility does not appear to be an important property of the bumper since plate glass, aluminum, and Mg-Li alloy bumpers function equally well.
  2. Thin stainless steel and moderately thick aluminum plates, as well as plate glass and aluminum plates of equivalent mass, function in a similar manner.
  3. The mass concept permits a wide selection of materials.
- 13.2.4.2 Bumper Spacing. Experimental work by Astronautics (Ref. 7) with aluminum bumpers and aluminum targets has shown that:
1. Less total weight (bumper plus target) is required for (1) thicker bumpers at small separation distances and (2) thinner bumpers with increasing distance of separation (see Figure 88).

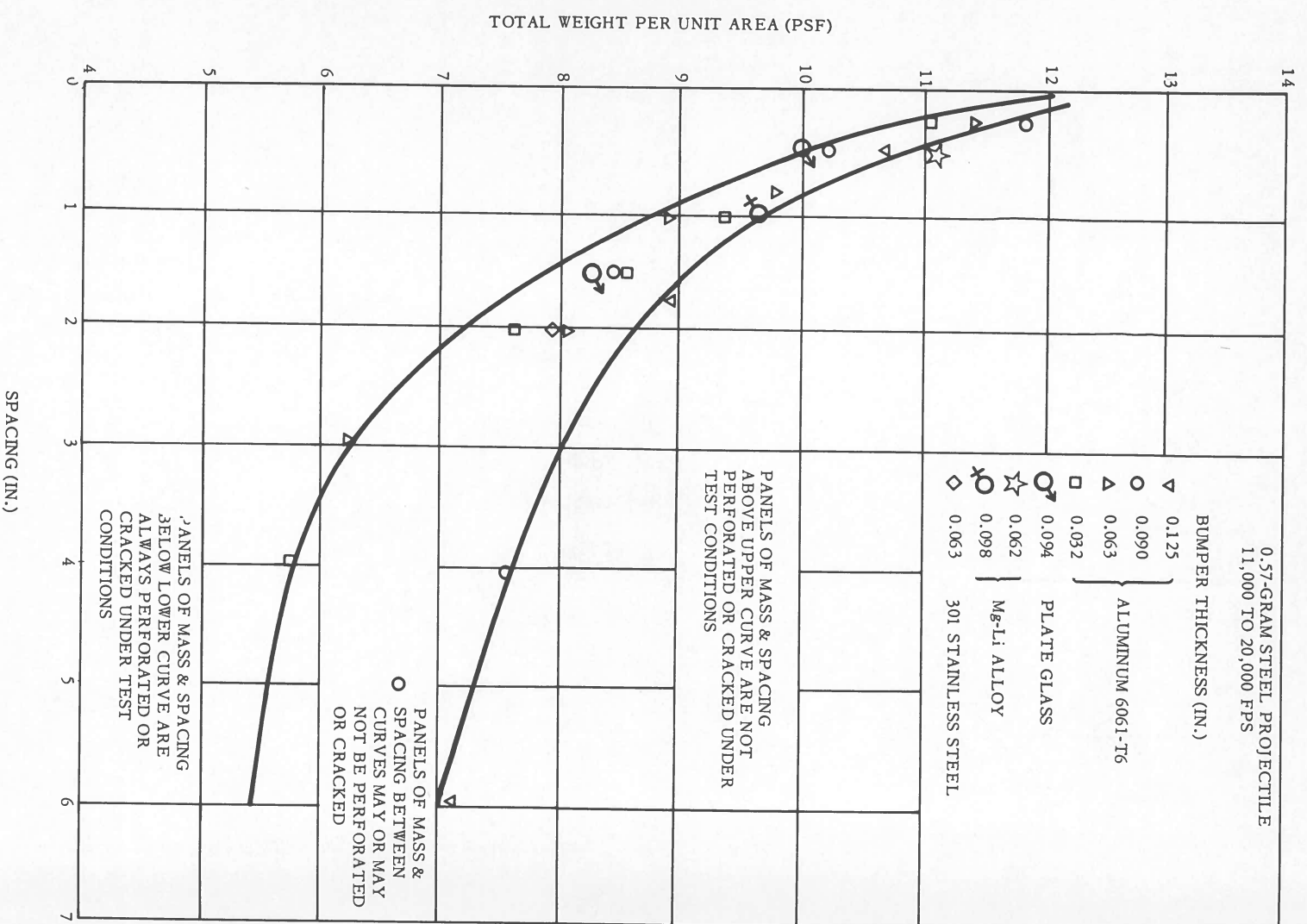


Figure 87. Effectiveness of different bumper materials.

2. When the space between the bumper and target is less than approximately 0.25 in., a thin bumper may be extensively damaged from material erupted or splashed back from the crater (see Figure 89).

Work by Funkhouser (Ref. 11) and Olshaker (Ref. 12) determined the dependence of the total penetration on the distance between the bumper and target (see Figure 90). The spacing of the bumper in front of the target surface was varied: (1) from zero to 6 in. with a constant aluminum bumper thickness of 0.031 in., and projectile mass and velocity of 0.0183 gram and 12,000 fps, respectively and (2) from 0.25 to 1.49 in. with a constant lead bumper thickness of 0.054 in., and projectile mass and a velocity of 0.188 grams and 8,366 fps, respectively. There is a rapid decrease in total penetration in aluminum from zero spacing to a spacing of 2 in.; with greater distances the total penetration is almost constant. The decrease in total penetration in lead with a 0.50-in. spacing is even more pronounced than with aluminum.

13.2.4.3 Energy-Absorbing Core Materials. Energy-absorbing core materials have been shown to significantly improve a bumper system's resistance to penetration with an over-all weight saving.

A good core material must have moderate compressive and shear strength, low density, directionality of mechanical properties and low ablation rates. In addition,

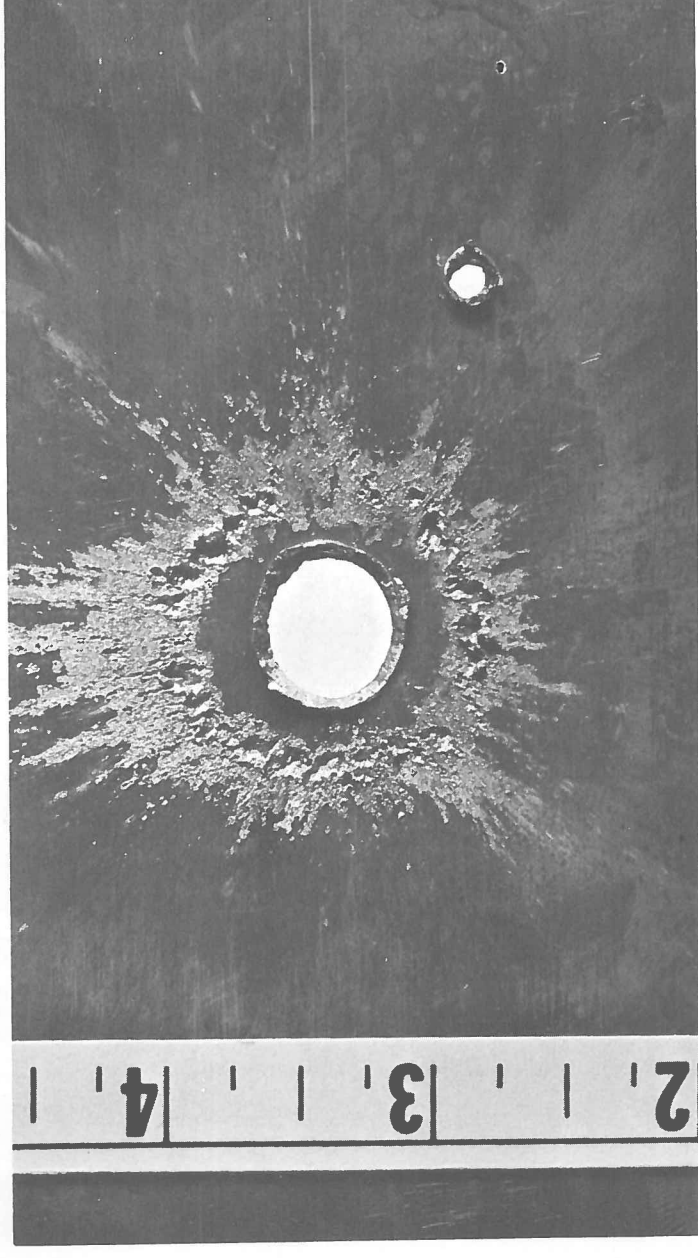


Figure 89. Reverse side of bumper spaced 0.25 in. from hull plate.

GENERAL DYNAMICS | ASTRONAUTICS

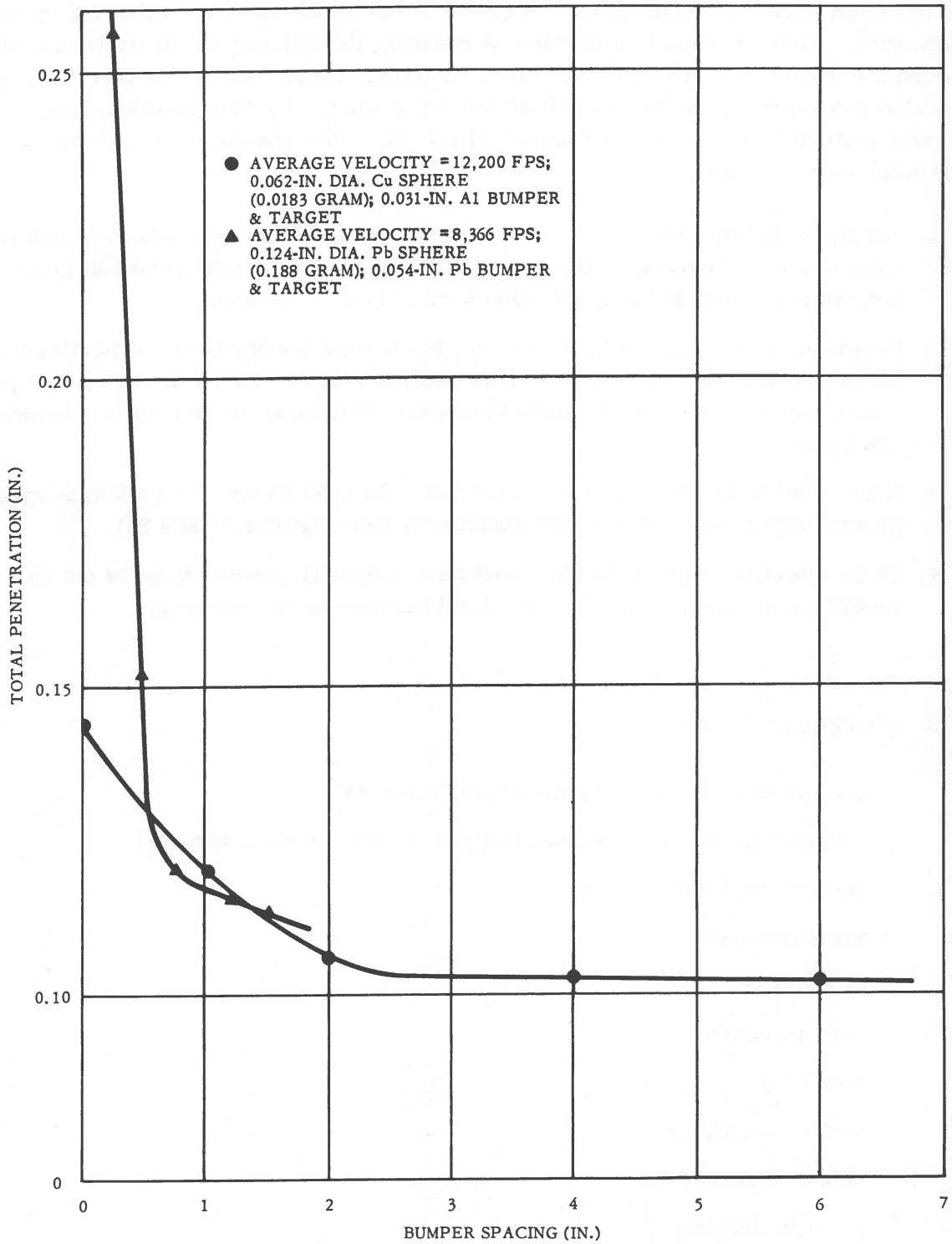


Figure 90. Dependence of total penetration on bumper spacing.

## GENERAL DYNAMICS | ASTRONAUTICS

the material must not measurably contribute to the shock cone or to the fast-moving fragments. Also, it should be capable of reducing the velocity of all particles moving toward the main tank. Thermal stability, moderate toughness, and a uniform texture are also desirable. Results of preliminary experiments by Astronautics (Ref. 7) with 10 core materials are shown in Figures 91 and 92. The results of this study can be summarized as follows:

1. Organics (foams, adhesives, etc.) are not suitable as core materials due to excessive gas formation. However, since these experiments were run in air, the volume of gas formed may be considerably less in vacuum.
2. Honeycomb cores are not satisfactory since they confine both the particles and the gas formed during impact. This confinement increases the particle's penetrating power. Figure 93 shows the extensive damage occurring to a honeycomb core.
3. Glass wool is an effective core material. Both NASA and Astronautics experimental programs confirm this conclusion (see Figures 91 and 94).
4. To be effective, core material must have a density greater than 10 pcf but should not exceed 30 to 40% of the total bumper-core-hull weight.

### 13.3 NOMENCLATURE

a	area of hole produced by meteoroid (sq. cm)
c	constant (1.09 for aluminum targets 0.606 for steel targets)
d	depth of penetration (cm)
m	mass (grams)
p	probability
P	tank pressure
Q	flow rate
r	orifice coefficient
t	skin thickness (cm)
v	velocity (km/sec.)



# GENERAL DYNAMICS | ASTRONAUTICS

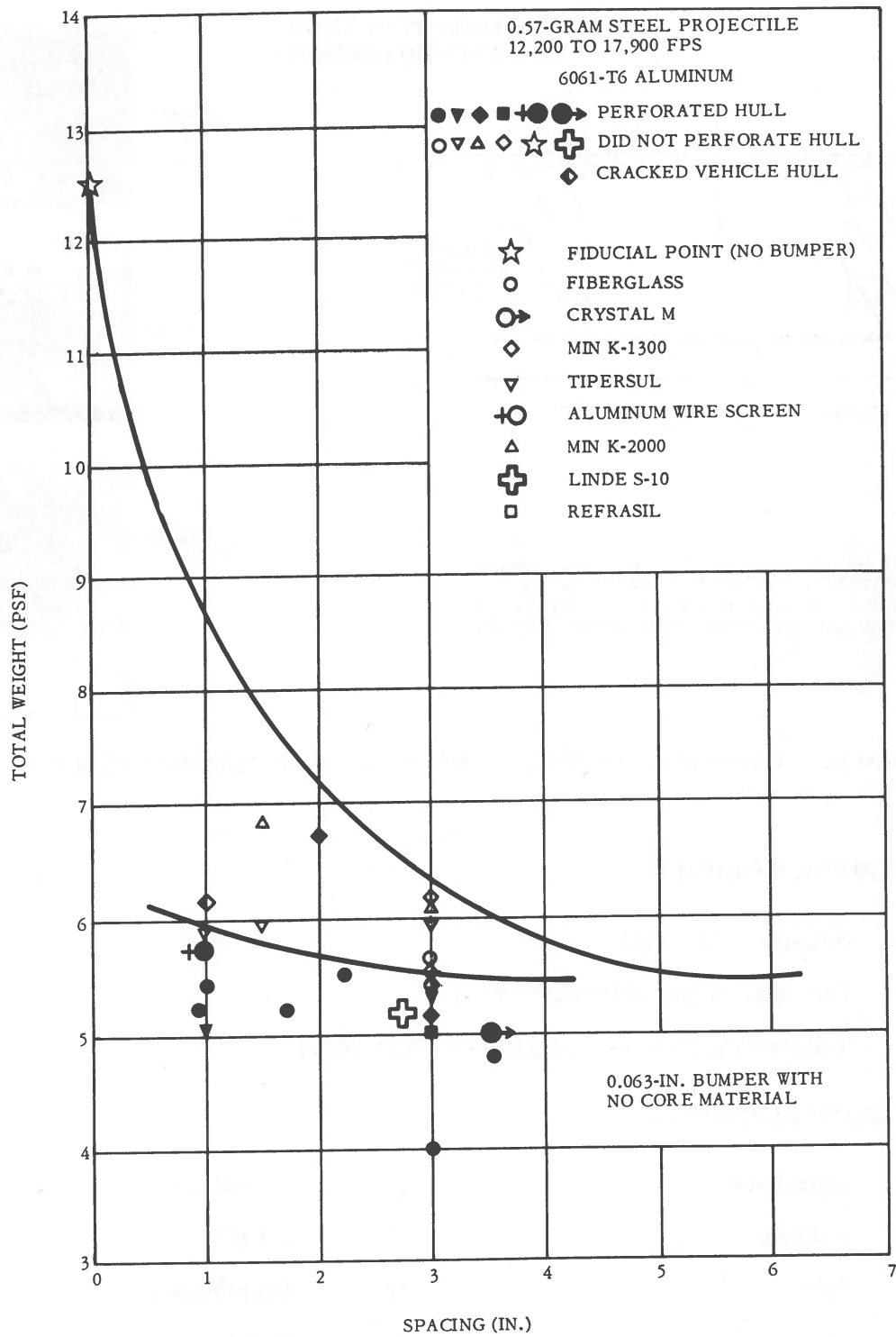
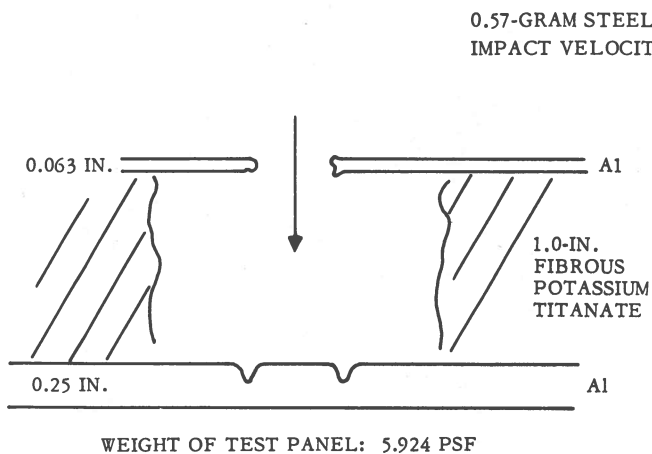


Figure 91. Effectiveness of 10 core materials.

# GENERAL DYNAMICS | ASTRONAUTICS



BUMPER FRAGMENTED PROJECTILE; LOW DENSITY CORE MATERIAL SLOWED DOWN FRAGMENTS & ALLOWED ENERGY RELEASED TO ACT Laterally; ONLY THE LARGEST FRAGMENTS FORMED CRATERS IN VEHICLE HULL

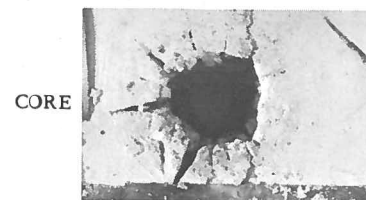
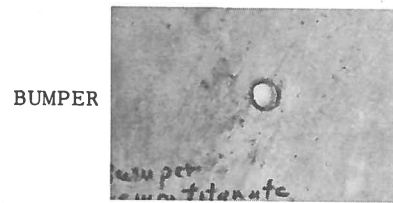


Figure 92. Experiment showing the advantage of energy-absorbing core material.

## 13.4 GREEK SYMBOLS

- $\rho$  density (g/cu. cm)  
 $\phi$  flux (no. of particles/m<sup>2</sup> sec.)  
 $\psi$  penetrating flux (no. of particles/m<sup>2</sup> sec.)

## 13.5 SUBSCRIPTS

- |    |           |    |            |
|----|-----------|----|------------|
| Al | aluminum  | p  | projectile |
| e  | exhaust   | t  | target     |
| f  | fuel      | th | threshold  |
| Fe | iron      | w  | mass       |
| m  | meteoroid |    |            |



GENERAL DYNAMICS | ASTRONAUTICS

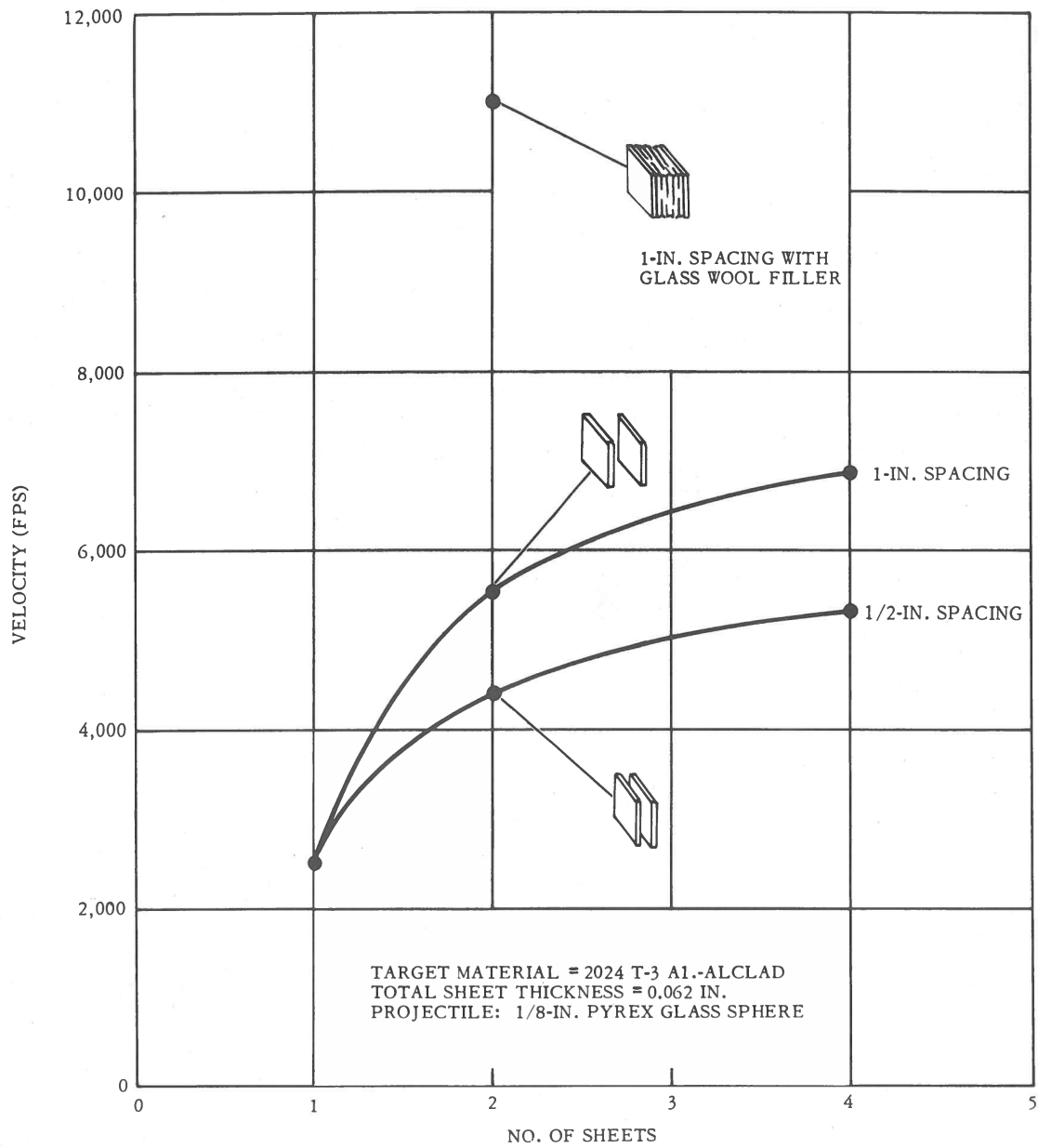


Figure 94. Variation of target ballistic limit as a function of number of sheets and core material.

## GENERAL DYNAMICS | ASTRONAUTICS

### REFERENCES

1. The Meteoritic Risk to Space Vehicles. F. L. Whipple, *Vistas in Astronautics*, 1958.
2. The Density of Mass Distribution of Meteoritic Bodies in the Neighborhood of the Earth's Orbit. Harison Brown, *J. Geophys. Research*, Vol. 65, June 1960, p. 1, 679.
3. Addendum: The Density and Mass Distribution of Meteoritic Bodies in the Neighborhood of the Earth's Orbit. Harrison Brown, *J. Geophys. Research*, Vol. 66, April 1961, p. 1, 316.
4. *Between the Planets*. F. G. Watson, Ch. 7, Harvard University Press, 1956.
5. Fuel Losses on a Typical 6.2 Hour Centaur Mission Due to Meteoroid Puncture. A. H. Jazwinski, *Astronautics Report AE61-1042*, August 1961.
6. Meteoroid Puncture of Space Vehicles with Application to Fuel Losses on the Centaur. A. H. Jazwinski, *Astronautics*, to be published.
7. Study of Principles of Meteoroid Protection. R. F. Rolsten, et al., *Astronautics Report AE62-0413*, April 1962.
8. Survey of Hypervelocity Impact Information. W. Herrmann and A. H. Jones, *MIT ASRL Report 99-1*, September 1961.
9. Effects of Meteoroid Impact on Space Vehicles. R. L. Eichelberger and J. W. Gehring, *BRL Report 1155*, December 1961.
10. Effects of Meteoroid Impact on Steel and Aluminum in Space. R. L. Bjork, *10th International Astronautical Congress*, London, 1959.
11. A Preliminary Investigation of the Effects of Bumpers as a Means of Reducing Projectile Penetration. J. O. Funkhouser, *NASA TN-D-726*, 1961.
12. Experimental Investigation in Lead of the Whipple Meteor Bumpers. A. E. Olshaker Jr., *J. Appl. Phy.*, Vol. 31, No. 12, 1960, pp. 2, 118-2, 120.



# 14

## PROPERTIES

This chapter summarizes some of the properties of hydrogen. If the accuracy of the data was listed in the literature, it is included in the graphs or tables. The convention of subscripting numbers whose accuracy is in doubt is used in this section. In some cases, more than one source was used to compile the data on a single property. This sometimes causes a slight discrepancy in the values listed.

NASA has requested the use of standard hydrogen data for certain properties due to the discrepancies found in the literature. This data is identified by the notation, "NASA-recommended value."

All the information is referenced, and a reference list is included at the end of the chapter. Many of the values listed were taken from extensive tables. The original source of information should be consulted if more detailed information is needed. The data throughout this book has been transposed into engineering units, as far as was practicable. Most of the original data was in the metric system. Any special information relating to a specific graph or table is included on that graph or table.

Liquid hydrogen produced commercially is essentially parahydrogen. Therefore, para values (100% p-H<sub>2</sub>) or equilibrium values (99.79% p-H<sub>2</sub>) should be used for the liquid hydrogen data. On some of the data listed, the ortho/para composition was not specified in the literature.

Definitions of terms, symbols, and abbreviations used are listed at the end of the chapter. Conversion factors for converting from engineering units to the metric system are also included.

### 14.1 DEFINITION OF TERMS

Absolute zero is the temperature at which a gas would show no pressure if the general law for gases would hold for all temperatures. It is equal to -273.16°C, 0°K, -459.69°F, and 0°R.

## GENERAL DYNAMICS | ASTRONAUTICS

Absorption coefficient ( $\mu$ ) is defined by the equation for the exponential attenuation of x-rays or gamma rays in matter.

$$I = I_0 e^{-\mu d}$$

Where

$I_0$  = incident photon intensity,

$I$  = transmitted photon intensity,

$d$  = absorber thickness.

Barn =  $10^{-24}$   $\text{cm}^2$  (see cross-section definition).

Boiling point is the temperature at which the vapor pressure of the liquid equals the externally applied pressure.

Compton scattering or the Compton effect is the name for a process whereby an incident photon transfers only a part of its energy to an electron during an interaction. The photon is not only degraded in energy but is also deflected from its original path.

Critical pressure is the pressure under which a substance may exist as a gas in equilibrium with the liquid at the critical temperature.

Critical temperature is that temperature above which a gas cannot be liquefied by pressure.

Cross-section is a measure of the probability of a particular process, such as the absorption or scattering of an incident particle or the activation of a nuclide.

Dielectric constant of a medium is defined by  $\epsilon$  in the equation

$$F = \frac{QQ^1}{\epsilon r^2}$$

where  $F$  is the force of attraction between two charges  $Q$  and  $Q^1$  separated by a distance  $r$  in a uniform medium.



## GENERAL DYNAMICS | ASTRONAUTICS

Dissociation constant for gases equals the product of the partial pressures of the dissociated atoms or molecules at equilibrium divided by the partial pressure of the undissociated gas, with each partial pressure raised to that power which is the coefficient of the substance in the dissociation equation.

Enthalpy is a thermodynamic quantity. It is equal to the sum of the internal energy of a system plus the product of the pressure-volume work done on the system.

Entropy is the capacity factor for isothermally unavailable energy. The increase in the entropy of a body during an infinitesimal stage of a reversible process is equal to the infinitesimal amount of heat absorbed divided by the absolute temperature of the body.

Free energy is a thermodynamic function defined by the equation:

$$F = H - TS$$

where

F = free energy,

T = absolute temperature,

S = entropy,

H = enthalpy.

Fusion temperature is the temperature at which the solid and liquid phases of a substance are in equilibrium.

Half life is the time lapse during which a radioactive mass decays to one-half its original intensity.

Heat capacity is that quantity of heat required to increase the temperature of a system or substance one degree of temperature.

Heat content (see enthalpy definition).

Isotopic masses in this compilation include the mass of the nucleus and the extra-nuclear electrons. The scale used is the physical atomic weight scale in which the mass of an atom of  $O^{16}$  is assigned a mass of exactly 16.00000 units.

## GENERAL DYNAMICS | ASTRONAUTICS

Latent heat of fusion is the amount of heat necessary to liquefy a unit mass of solid without a change in temperature.

Latent heat of vaporization is the amount of heat necessary to vaporize a unit mass of liquid without a change in temperature.

Mole is a mass numerically equal to the atomic weight of a substance.

Molecular weight is the sum of the atomic weights of all the atoms in a molecule.

Normal hydrogen contain 25% parahydrogen and 75% orthohydrogen.

Orthohydrogen. Each nucleus of the diatomic hydrogen molecule has a mechanical momentum characterized as nuclear spin. Molecules in which the spins of the two nuclei are parallel are called orthohydrogen.

Pair production is the name for a process which involves the creation of a positron-electron pair by a photon of at least 1.02 mev in the strong electric field near an atomic nucleus.

Parahydrogen. Each nucleus of the diatomic hydrogen molecule has a mechanical momentum characterized as nuclear spin. Molecules in which the spin of the two nuclei are antiparallel are called parahydrogen.

Photoelectric effect is the name for a process in which a photon of energy,  $h\nu$ , ejects a bound electron from an atom or molecule and imparts to it an energy of  $h\nu - b$  where  $b$  is the energy with which the electron was bound. The photon disappears completely in the process.

Prandtl number is the viscosity times the heat capacity divided by the thermal conductivity ( $\eta C_p/k$ ). It is a dimensionless number.

Refractive index is the ratio of the velocity of light in vacuum to its velocity in a given substance.

Saturated refers to the liquid phase and vapor phase of a substance in temperature equilibrium.

Surface tension of a liquid is the force per unit length on the surface of a liquid which opposes the expansion of the surface area.

## GENERAL DYNAMICS | ASTRONAUTICS

Thermal conductivity is the time rate of transfer of heat by conduction, through a unit thickness, across a unit area for a unit difference of temperature.

Triple point is the temperature at which the solid, liquid, and gas phases of a single substance are in equilibrium.

Vapor pressure is the pressure exerted when a solid or liquid is in equilibrium with its own vapor. The vapor pressure is relatively unaffected by the external pressure.

Virial equation of state relates pressure, volume, and temperature of a real liquid or gas.

Viscosity is a measure of the resistance of fluids to a change of form.

### 14.2 DEFINITION OF SYMBOLS AND ABBREVIATIONS

atm.	atmosphere
Å	Angstrom ( $10^{-8}$ cm)
Btu	British thermal unit
cm	centimeter
C <sub>p</sub>	heat capacity at constant pressure
C <sub>p</sub> <sup>o</sup>	heat capacity at constant pressure of an ideal gas
C <sub>s</sub>	heat capacity at saturation vapor pressure
C <sub>v</sub>	heat capacity at constant volume
E	energy
E <sub>0</sub> <sup>o</sup>	internal energy of an ideal gas at absolute zero
e-H <sub>2</sub>	equilibrium hydrogen (99.79% para)
ev	electron volt
F	free energy of an ideal gas, a thermodynamic function
g	gram
H, h	enthalpy, a thermodynamic function

## GENERAL DYNAMICS | ASTRONAUTICS

$H^\circ$	enthalpy of an ideal gas, a thermodynamic function
${}_1H^1$	isotope of hydrogen, mass 1
${}_1H^2$	deuterium
K	dissociation constant
$^\circ K$	degrees, kelvin
k	thermal conductivity
$L_v$	latent heat of vaporization
mb	millibarns
mev	million electron volts
n	neutron
n- $H_2$	normal hydrogen (25% para)
$N_{Pr}$	prandtl number
o- $H_2$	orthohydrogen
P	pressure
p- $H_2$	parahydrogen
psia	pounds per square inch, absolute
R	gas constant
$^\circ R$	degrees, rankine
S, s	entropy, a thermodynamic function
STP	standard temperature (491.7 $^\circ R$ or 32 $^\circ F$ ) and pressure (14.7 psia)
T	absolute temperature
$t^{1/2}$	half life of a radioactive species
V	volume
x	unit length
Z	compressibility factor
$\gamma$	gamma rays
$\epsilon$	dielectric constant

## GENERAL DYNAMICS | ASTRONAUTICS

$\mu$	gamma ray absorption coefficient
$\eta$	viscosity
$\rho$	density
$\sigma$	cross-section

### 14.3 PHYSICAL CONSTANTS AND MISCELLANEOUS INFORMATION

The molecular weight of hydrogen is 2.01600 (chemical scale), 2.01654 (physical scale) (Ref. 1).

The triple points of hydrogen are shown in Table XII (Ref. 2). Table XIII lists the critical constants for hydrogen. Table XIV presents the boiling points of normal and equilibrium hydrogen (Ref. 2).

The fusion temperature of hydrogen is 25.13°R and 13.96°K at 0.99 psia (Ref. 2).

Table XV (Ref. 4) presents data concerning the compressibility of solid hydrogen as a function of pressure. Table XVI gives data concerning its expansivity as a function of temperature. Figures 95, 96, and 97 are graphical presentations of compressibility data. Table XVII gives the virial equation of state.

Figures 98 through 111 and Tables XVIII and XIX present additional data on the physical properties of hydrogen.

For the dissociation of hydrogen (see Figure 112 and 113),  $\text{H}_2 \rightleftharpoons 2\text{H}$ , the equilibrium constant is:

$$K_{\text{H}_2} = \frac{P_{\text{H}}^2}{P_{\text{H}_2}}$$

where

$P_{\text{H}}$  = partial pressure of the dissociated hydrogen,

$P_{\text{H}_2}$  = partial pressure of the undissociated hydrogen.

Table XX (Ref. 2) lists data on hydrogen dissociation with increasing temperature.

# GENERAL DYNAMICS | ASTRONAUTICS

## Table XII. Hydrogen triple points.

	NORMAL HYDROGEN (n-H <sub>2</sub> )	EQUILIBRIUM-HYDROGEN (e-H <sub>2</sub> )
TEMPERATURE (°R)	25.12 <sub>3</sub> *	24.86 <sub>3</sub>
(°K)	13.95 <sub>7</sub>	13.81 <sub>3</sub>
PRESSURE (PSIA)	1.044	1.021
(ATM.)	0.07105	0.0694 <sub>7</sub>

\*ACCURACIES BEYOND FIRMLY ACCEPTED VALUES

## Table XIII. Critical constants.

	n-H <sub>2</sub> (Ref. 2)	e-H <sub>2</sub> (Ref. 3)
TEMPERATURE (°R)	59.74	59.3 <sub>57</sub>
(°K)	33.19	32.9 <sub>76</sub>
PRESSURE (PSIA)	190.8	187. <sub>51</sub>
(ATM)	12.98	12.7 <sub>59</sub>
VOLUME (CU. FT./LB.)	0.5320	0.510
(CU. CM/G)	33.21	31.8
DENSITY (LB./CU. FT.)	1.880	1.960
(G/CU. CM)	0.03011	0.0314

## Table XIV. Boiling point at 14.696 psia.

	n-H <sub>2</sub>	e-H <sub>2</sub>
TEMPERATURE (°R)	36.70 <sub>2</sub>	36.49 <sub>1</sub>
(°K)	20.39 <sub>0</sub>	20.27 <sub>3</sub>

GENERAL DYNAMICS | ASTRONAUTICS

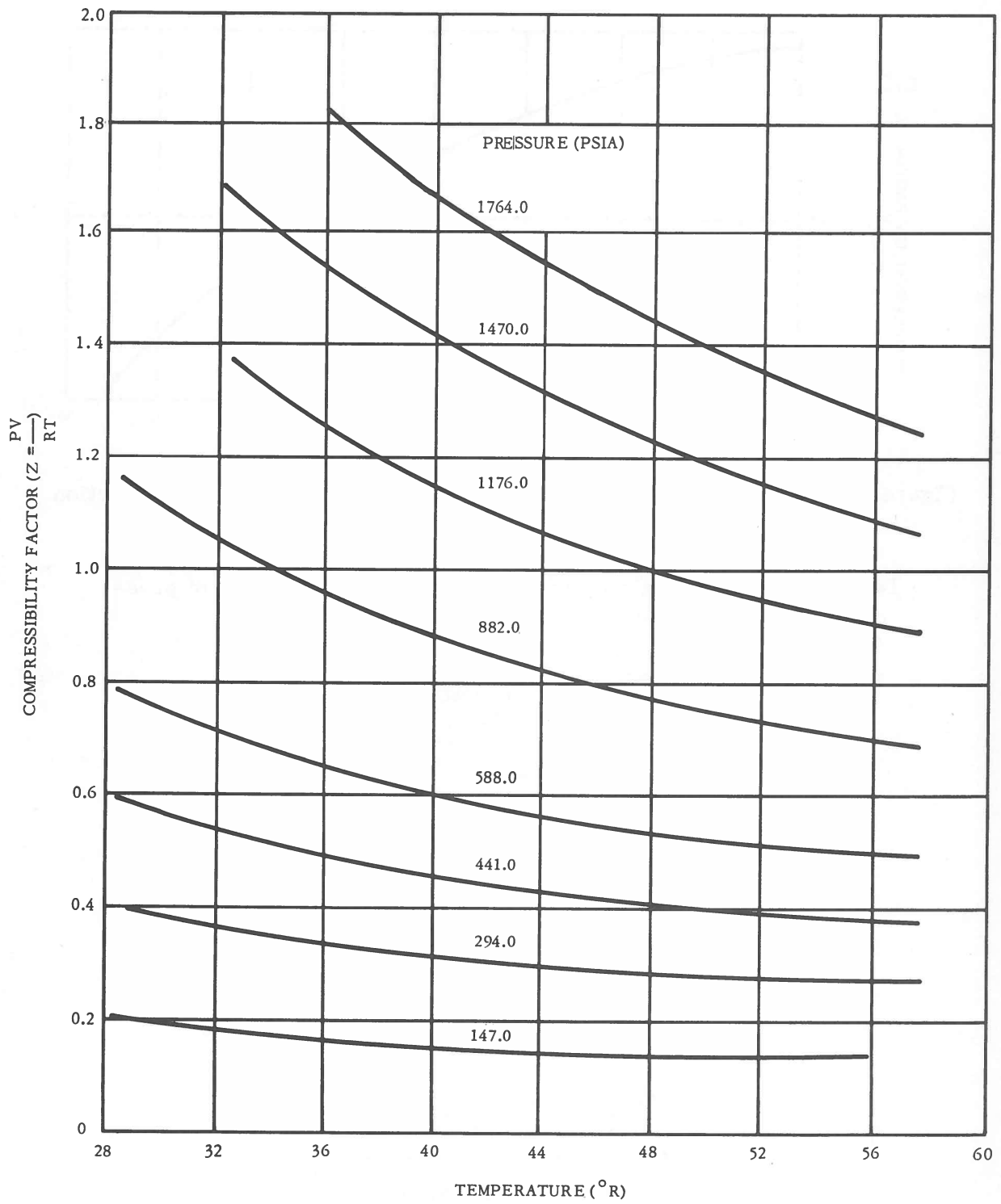


Figure 95. Compressibility factor for liquid hydrogen as a function of temperature.

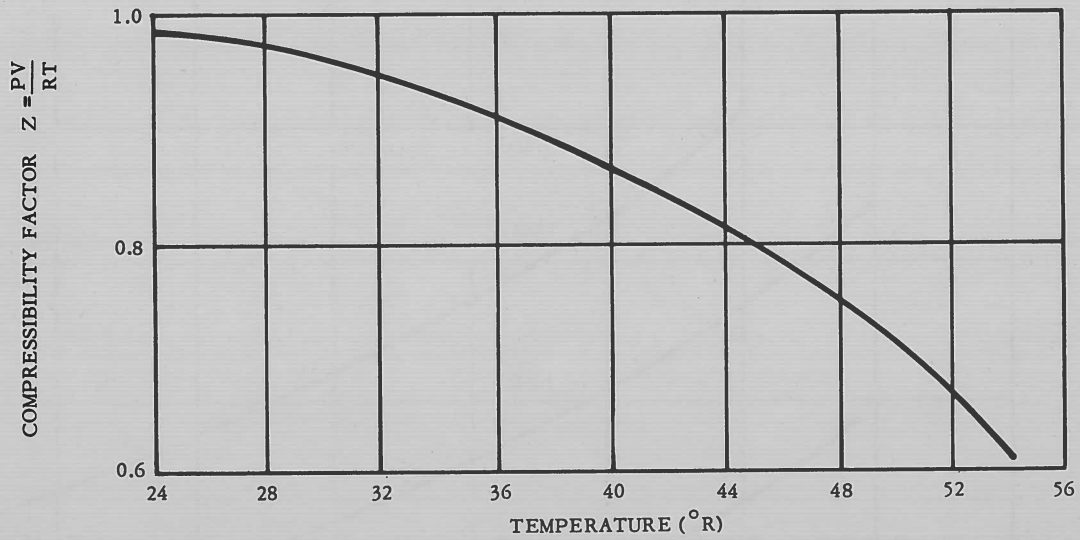


Figure 96. Compressibility factor for saturated hydrogen vapor as a function of temperature.

Table XV. Compressibility of solid hydrogen as a function of pressure at 7.6°R.

PRESSURE (PSIA)	COMPRESSIBILITY $\frac{1}{V} \left( \frac{dV}{dP} \right)_T, (\text{PSIA})^{-1}$
0	$(0.48 \pm 0.11) \times 10^{-4}$
1,422	$0.22 \times 10^{-4}$

Table XVI. Expansivity of solid hydrogen as a function of temperature.

TEMPERATURE (°R)	EXPANSIVITY $\frac{1}{V} \left( \frac{dV}{dT} \right)_P, (^\circ\text{R})^{-1}$
7.6	$0.13 \times 10^{-2}$
19.8	$0.28 \times 10^{-2}$



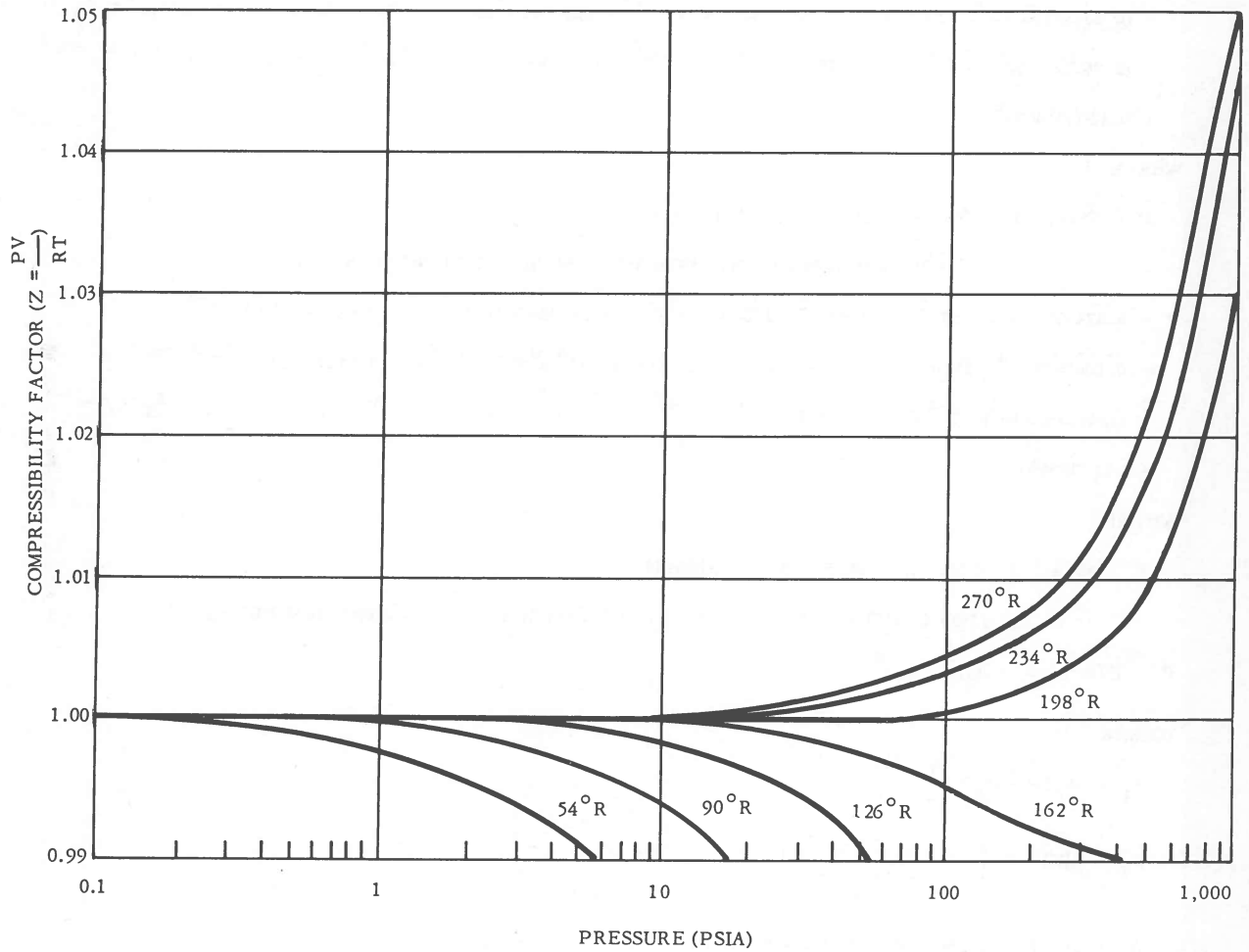


Figure 97. Compressibility factor for gaseous hydrogen as a function of temperature and pressure.

# GENERAL DYNAMICS | ASTRONAUTICS

## Table XVII. The virial equations of state.

### NASA-RECOMMENDED EQUATIONS

(FOR COMPRESSED LH<sub>2</sub> FROM 36° TO 59°R AND UP TO 5,100 PSIA; REF. 7);

$$\begin{aligned}
 P = & (5.3248178)T\rho + (2.696798)T\rho^2 - (328.36904)\rho^2 - (8033.93)\rho^2 T^{-1} + (274351.2)\rho^2 T^{-2} - (8.58400 \times 10^7)\rho^2 T^{-4} \\
 & - (0.43157596)T\rho^3 + (59.540726)\rho^3 + (0.046379694)T\rho^4 + (1.530941 \times 10^5)\rho^3 T^{-2} e^{-A\rho^2} + (4.664626 \times 10^6)\rho^3 T^{-3} e^{-A\rho^2} \\
 & - (2.26713 \times 10^8)\rho^3 T^{-4} e^{-A\rho^2} - 7891.15 \rho^5 T^{-2} e^{-A\rho^2} - (6.92328 \times 10^5)\rho^5 T^{-3} e^{-A\rho^2} + (2.31173 \times 10^7)\rho^5 T^{-4} e^{-A\rho^2} \\
 & + 0.130264609\rho^6 \dots
 \end{aligned}$$

WHERE

$$P = \text{PSIA}, \quad T = \text{°R}, \quad \rho = \text{PCF}, \quad A = 0.1136468.$$

(FOR COMPRESSED GH<sub>2</sub> FROM 36° TO 540°R 1 UP TO 5,100 PSIA; REF. 7);

$$\begin{aligned}
 P = & 5.3248T\rho + 0.8725T\rho^2 - 119.948\rho^2 - 12085.94\rho^2 T^{-1} + (3.47926 \times 10^5)\rho^2 T^{-2} - (9.81604 \times 10^7)\rho^2 T^{-4} \\
 & + 0.1067811T\rho^3 + 19.0299\rho^3 + 0.0078447T\rho^4 - 2.552649 \times 10^5 \rho^3 T^{-2} e^{-A\rho^2} + (4.359427 \times 10^7)\rho^3 T^{-3} e^{-A\rho^2} \\
 & - (1.49538 \times 10^8)\rho^3 T^{-4} e^{-A\rho^2} + 5807.28 \rho^5 T^{-2} e^{-A\rho^2} - (1.829817 \times 10^6)\rho^5 T^{-3} e^{-A\rho^2} + (7.14137 \times 10^7)\rho^5 T^{-4} e^{-A\rho^2} \\
 & + 0.19433549\rho^6 \dots
 \end{aligned}$$

WHERE

$$P = \text{PSIA}, \quad T = \text{°R}, \quad \rho = \text{PCF}, \quad A = 0.1136468.$$

(FOR COMPRESSED GH<sub>2</sub> FROM 540° TO 2,600°R AND UP TO 3,000 PSIA; REF 8);

$$P = RT\rho + A_1\rho^2 + A_2\rho^3 + A_3\rho^6$$

WHERE

$$\begin{aligned}
 A_1 = & B_0 RT - A_0 + \frac{C_0}{T^2} + \frac{D_0}{T^4} \\
 A_2 = & bRT - a + \left( \frac{c}{T^2} + \frac{\delta}{T^4} \right) \left( \frac{1 + \gamma\rho^2}{e^{\gamma\rho^2}} \right)
 \end{aligned}$$

$$A_3 = a\alpha, \quad P = \text{ATM}, \quad R = \text{GAS CONSTANT (0.362216)}, \quad T = \text{°R}, \quad \rho = \text{PCF}$$

### VALUES OF THE VIRIAL COEFFICIENTS

$$A_0 = 113.74$$

$$b = 0.06449$$

$$B_0 = 0.14594$$

$$c = 1284.9 \times 10^3$$

$$C_0 = 1477.6 \times 10^3$$

$$\alpha = 0.049396$$

$$D_0 = -46,687 \times 10^5$$

$$\delta = -36.429 \times 10^8$$

$$a = 64.484$$

$$\gamma = 0.41040$$

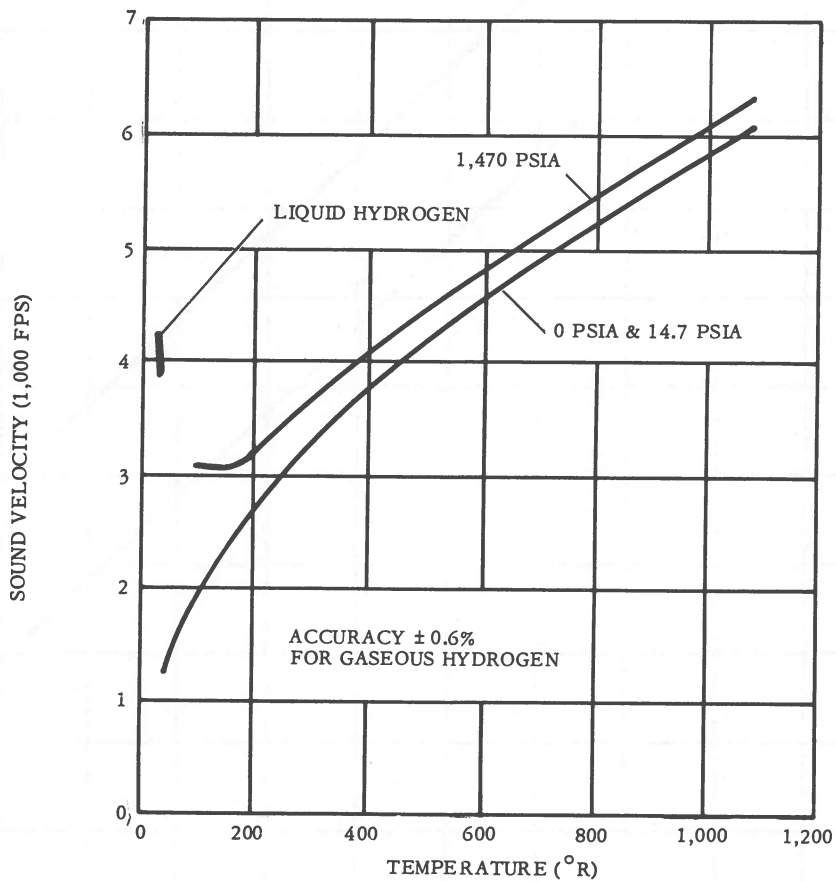


Figure 98. Sound velocity in hydrogen as a function of temperature and pressure.

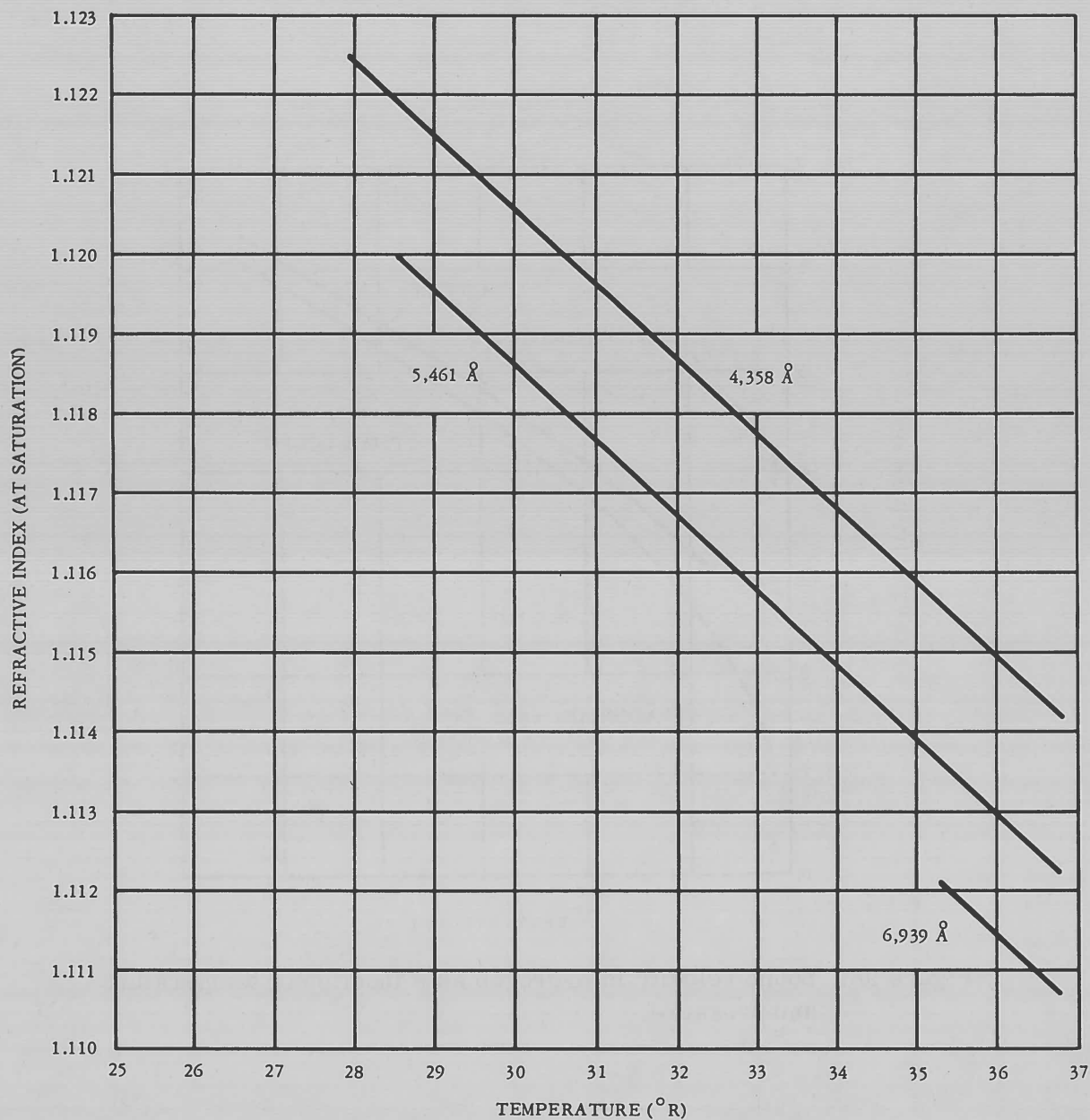


Figure 99. Refractive index of liquid normal hydrogen as a function of temperature.

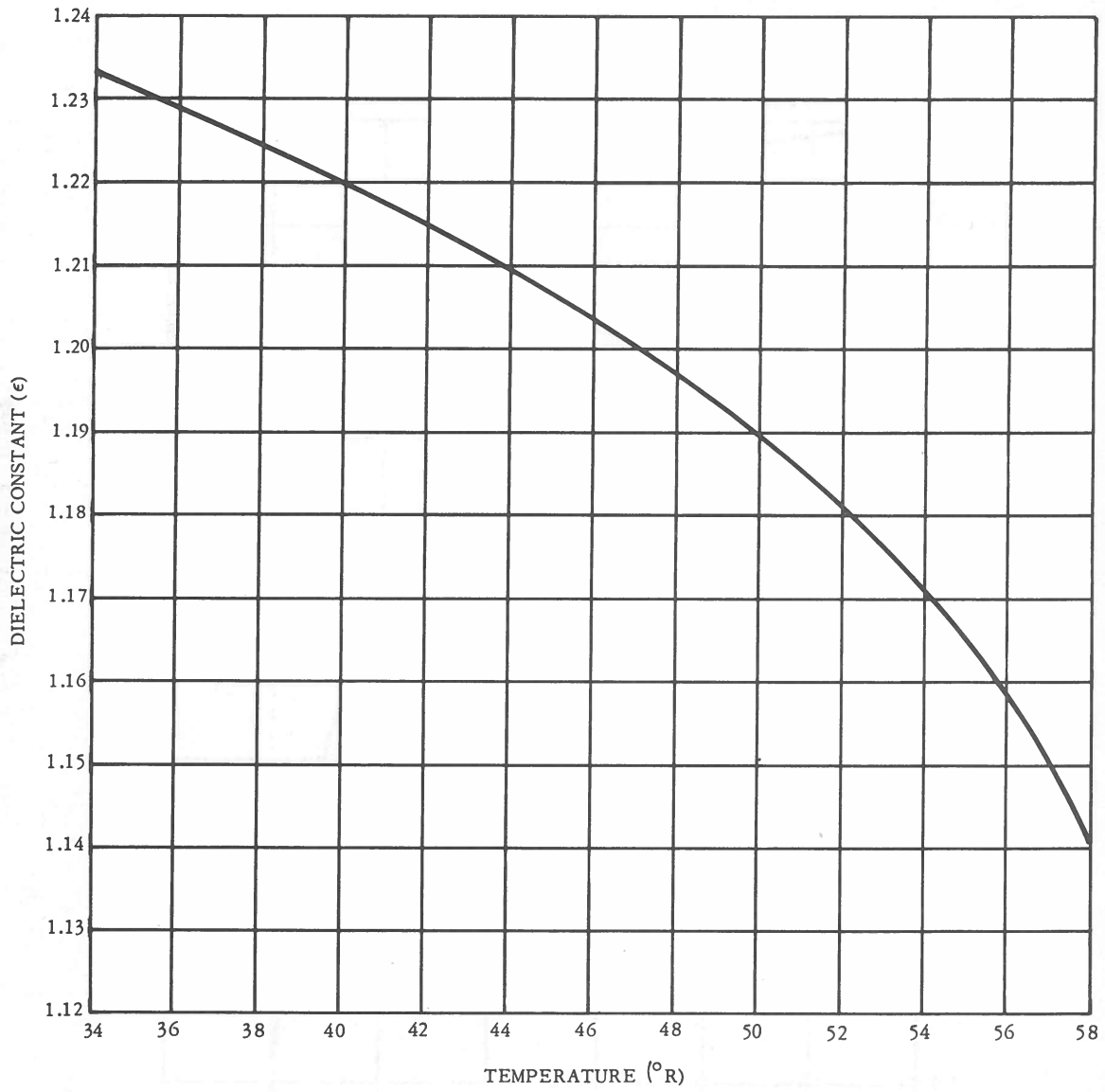


Figure 100. Dielectric constant of saturated liquid parahydrogen as a function of temperature (NASA-recommended values).

# GENERAL DYNAMICS | ASTRONAUTICS

FOR n-H<sub>2</sub> 25.1 < °R < 36.7

$$\rho(\text{PCF}) = \frac{1}{0.19663 - 3.5335 \times 10^{-4}T + 3.1184 \times 10^{-5}T^2}$$

FOR p-H<sub>2</sub> 24.9 < °R < 36.5

$$\rho(\text{PCF}) = \frac{1}{0.19786 - 3.9198 \times 10^{-4}T + 3.2135 \times 10^{-5}T^2}$$

WHERE T = °R

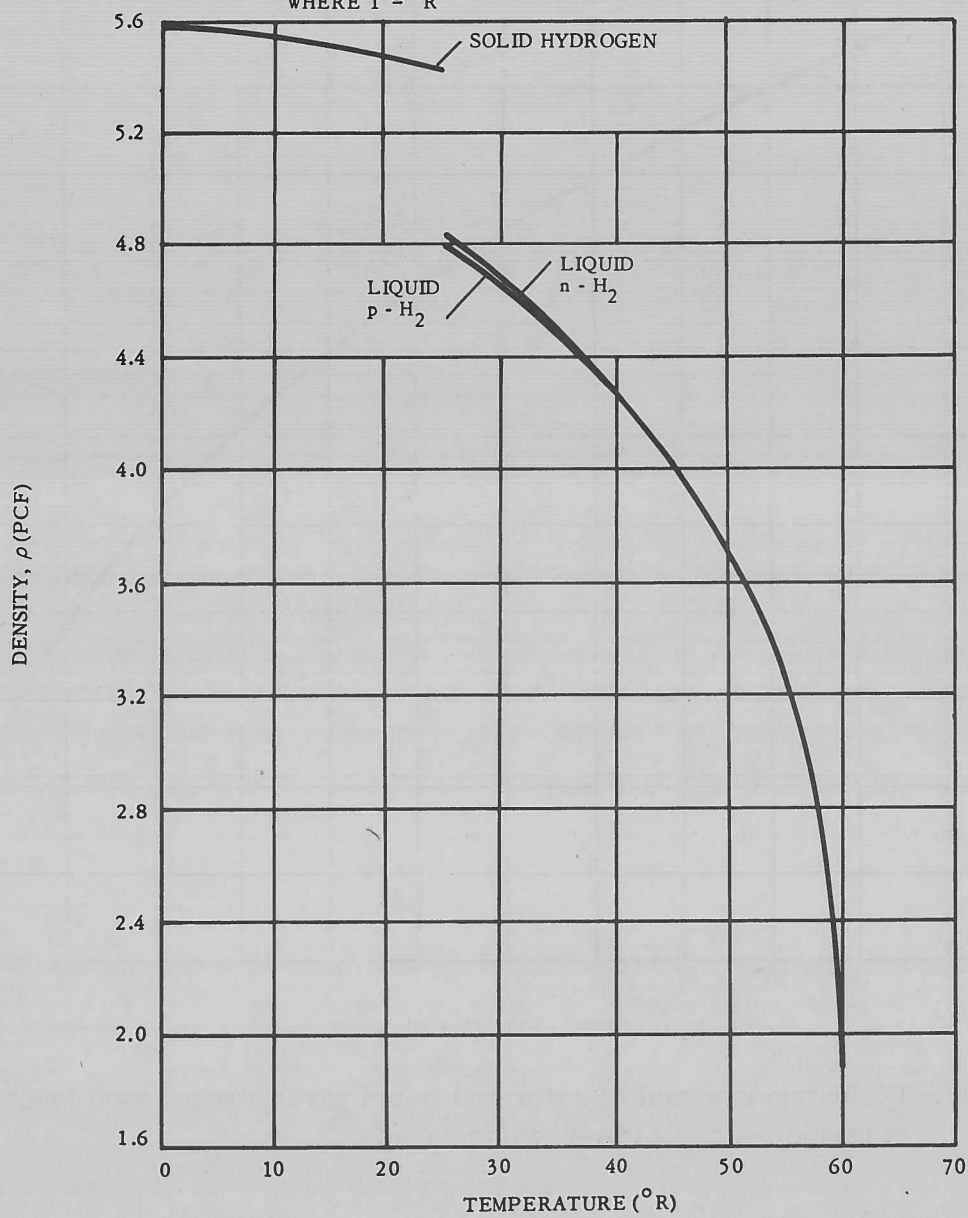


Figure 101. Density of solid and liquid hydrogen as a function of temperature.

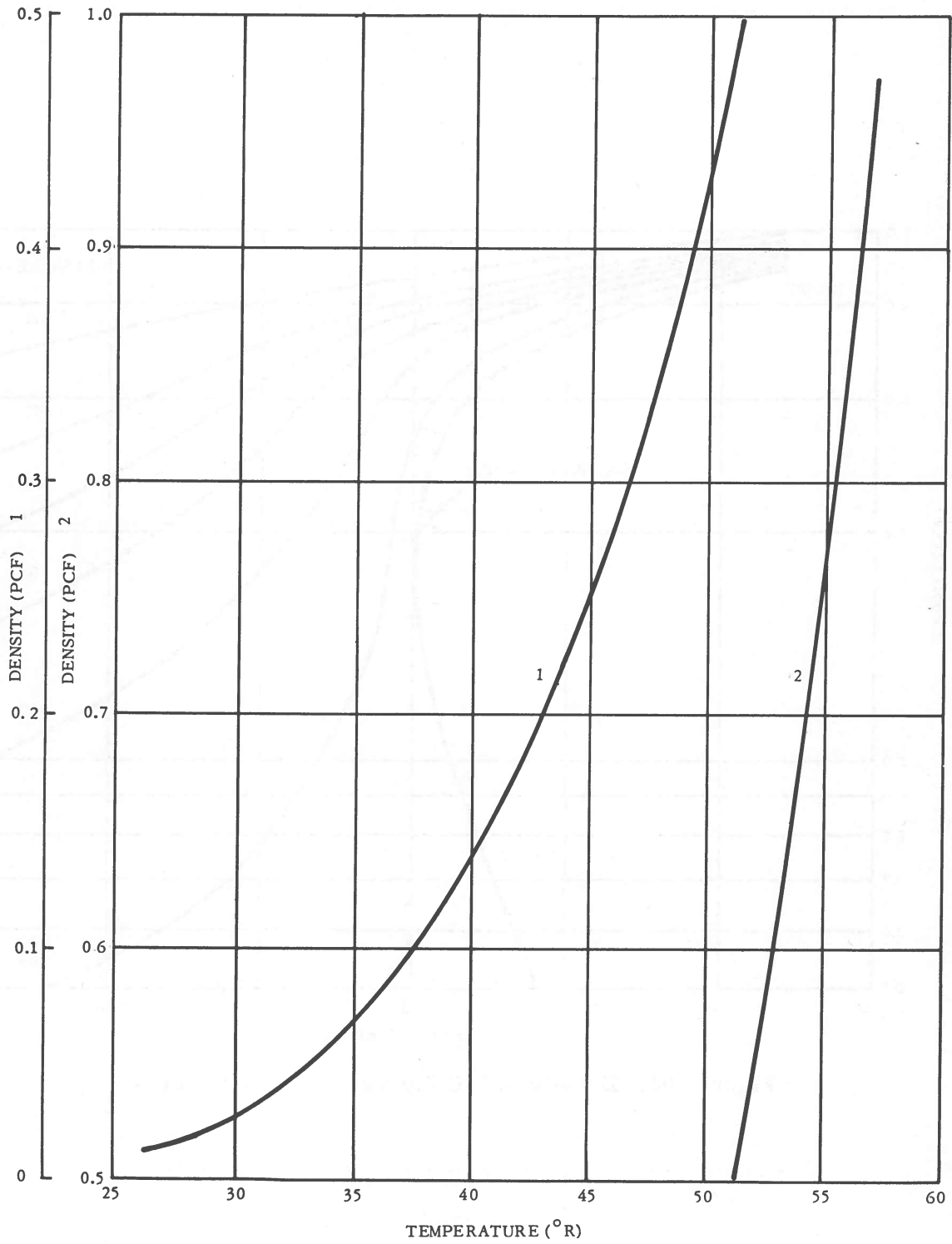


Figure 102. Saturated vapor density of e-H<sub>2</sub> as a function of temperature.

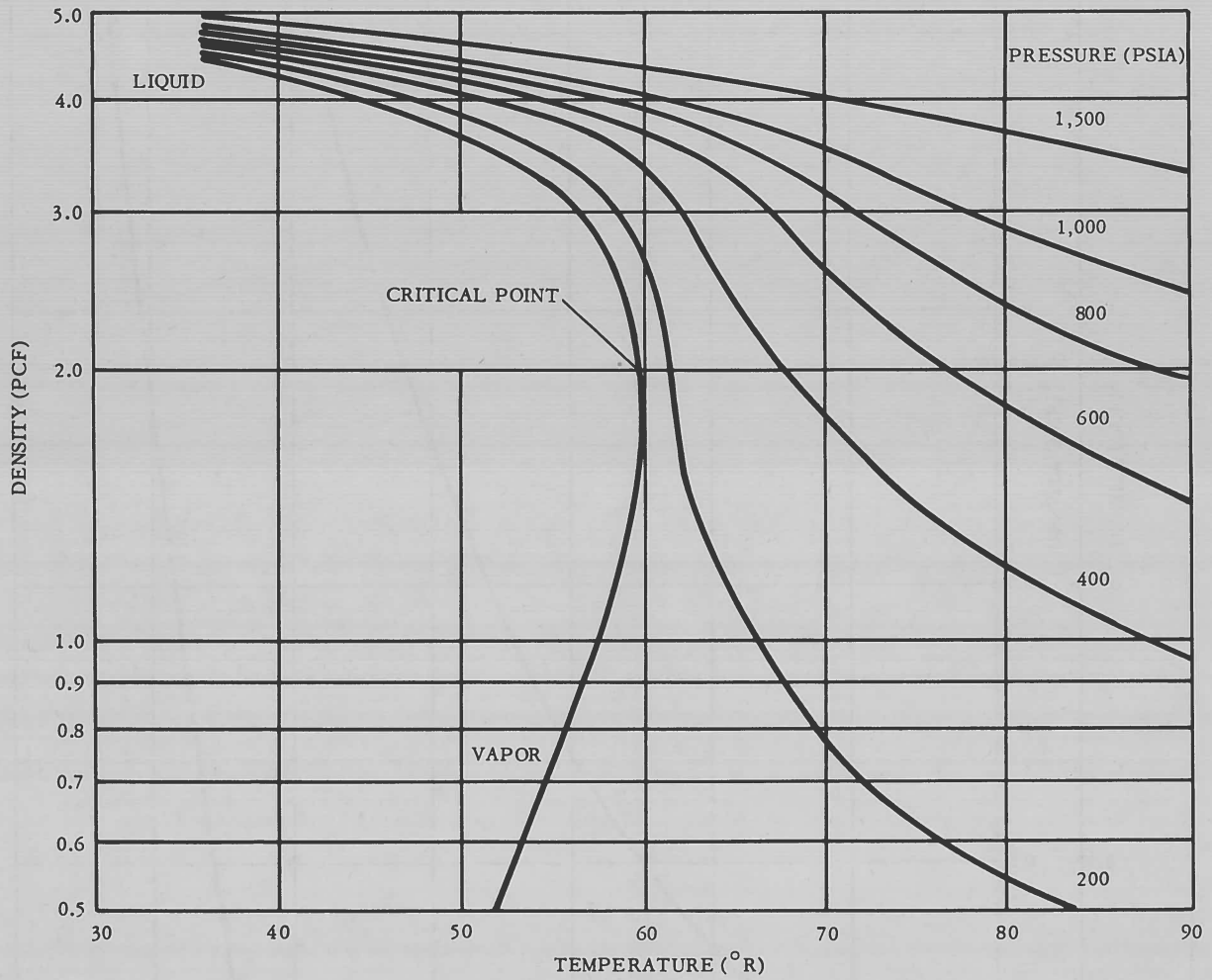


Figure 103. Density of hydrogen at low temperatures.



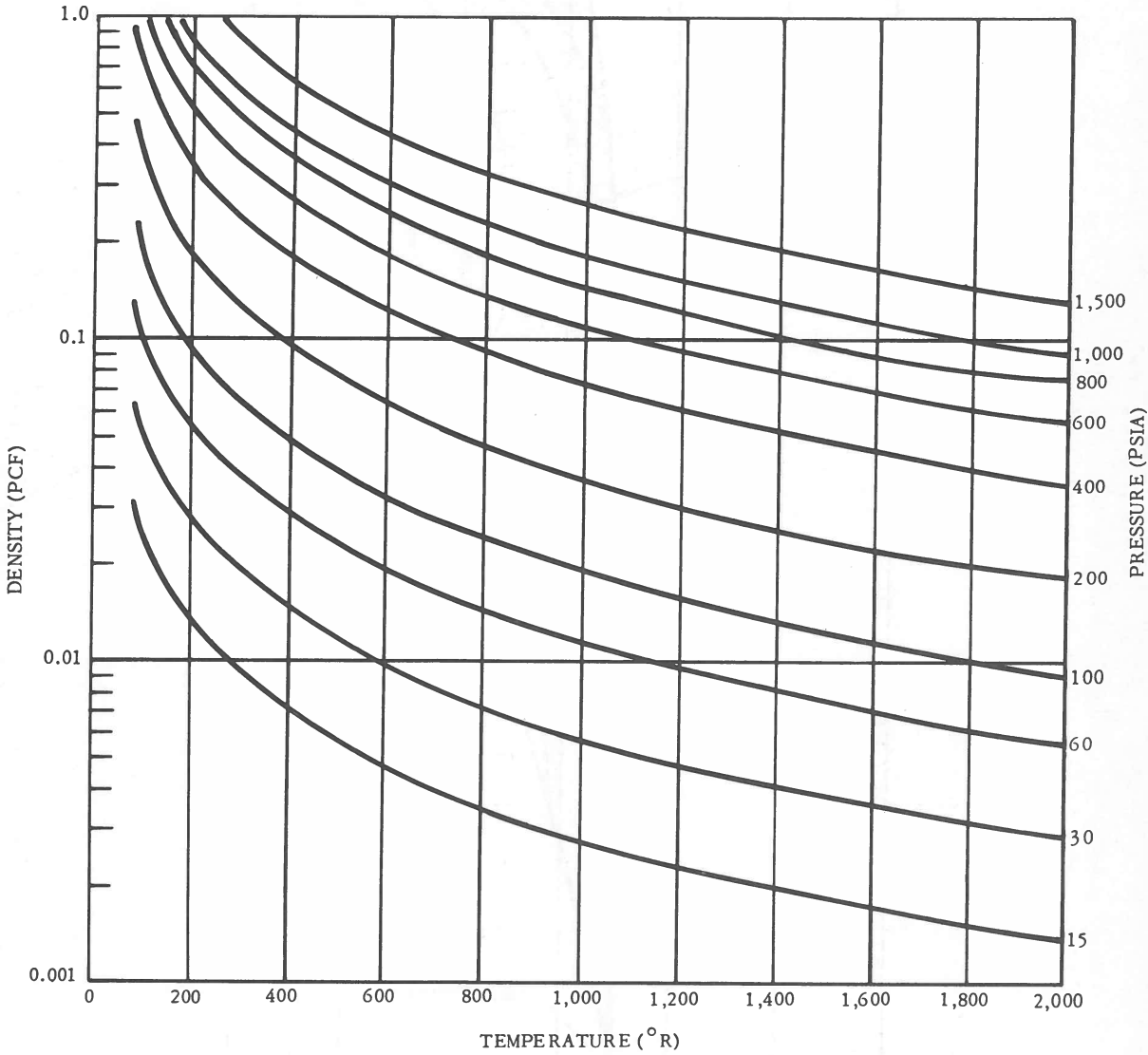


Figure 104. Density of gaseous hydrogen at high temperatures.

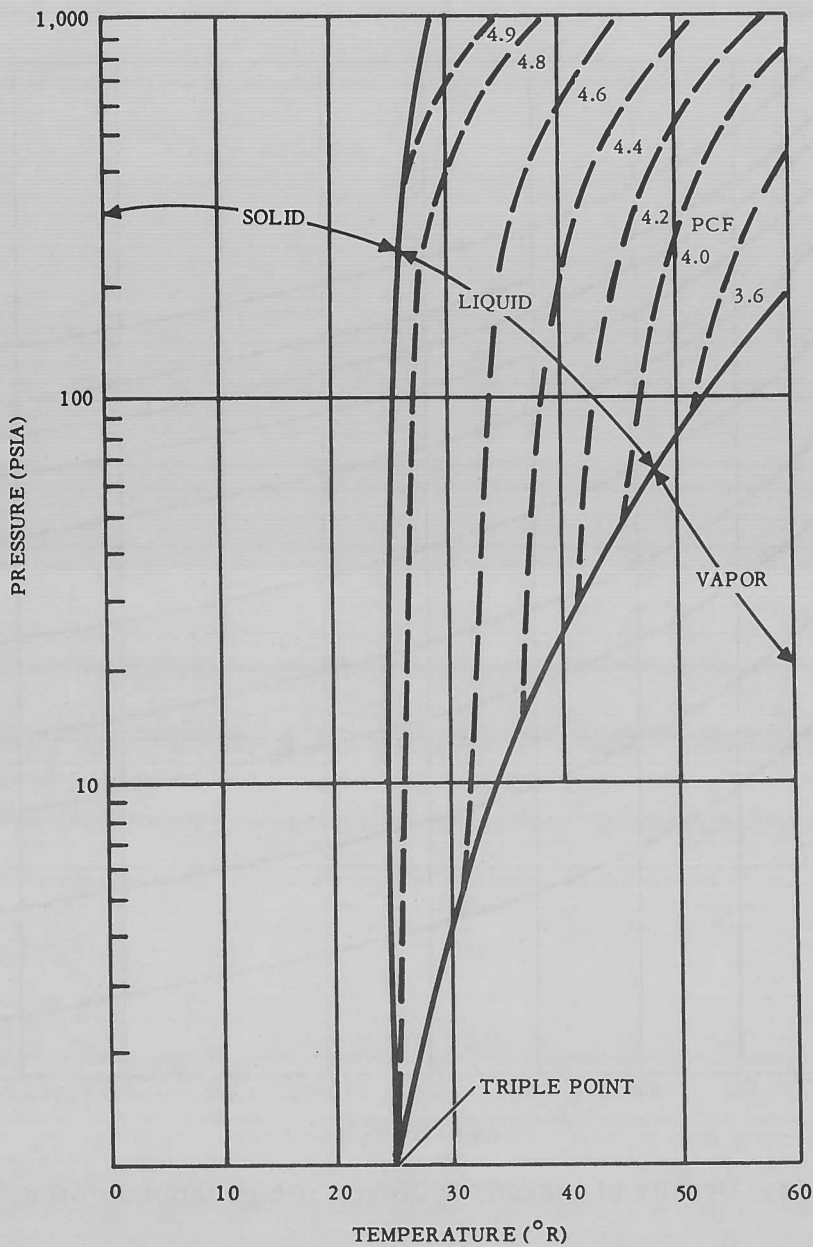
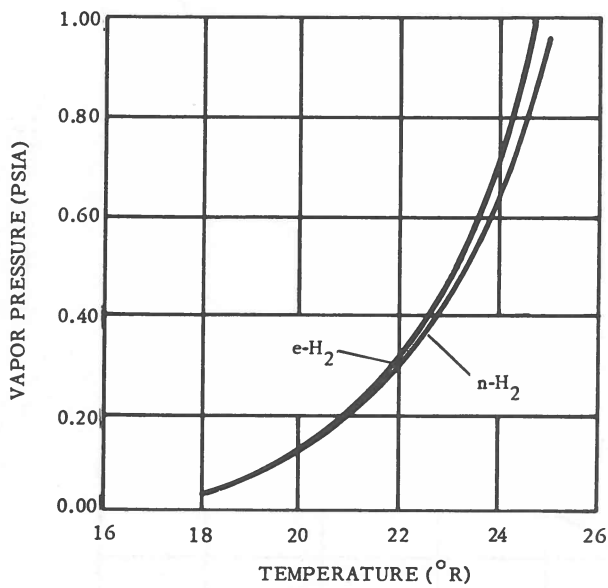


Figure 105. Hydrogen phase changes as a function of temperature and pressure.



FOR SOLID e-H<sub>2</sub>:  $\text{LOG}_{10}P = 2.91075 - \frac{84.6310}{T} + 0.02019T$

FOR SOLID n-H<sub>2</sub>:  $\text{LOG}_{10}P = 2.85125 - \frac{84.9706}{T} + 0.02188T$

WHERE: P = PSIA  
T = °R

Figure 106. Vapor pressure of solid hydrogen as a function of temperature.

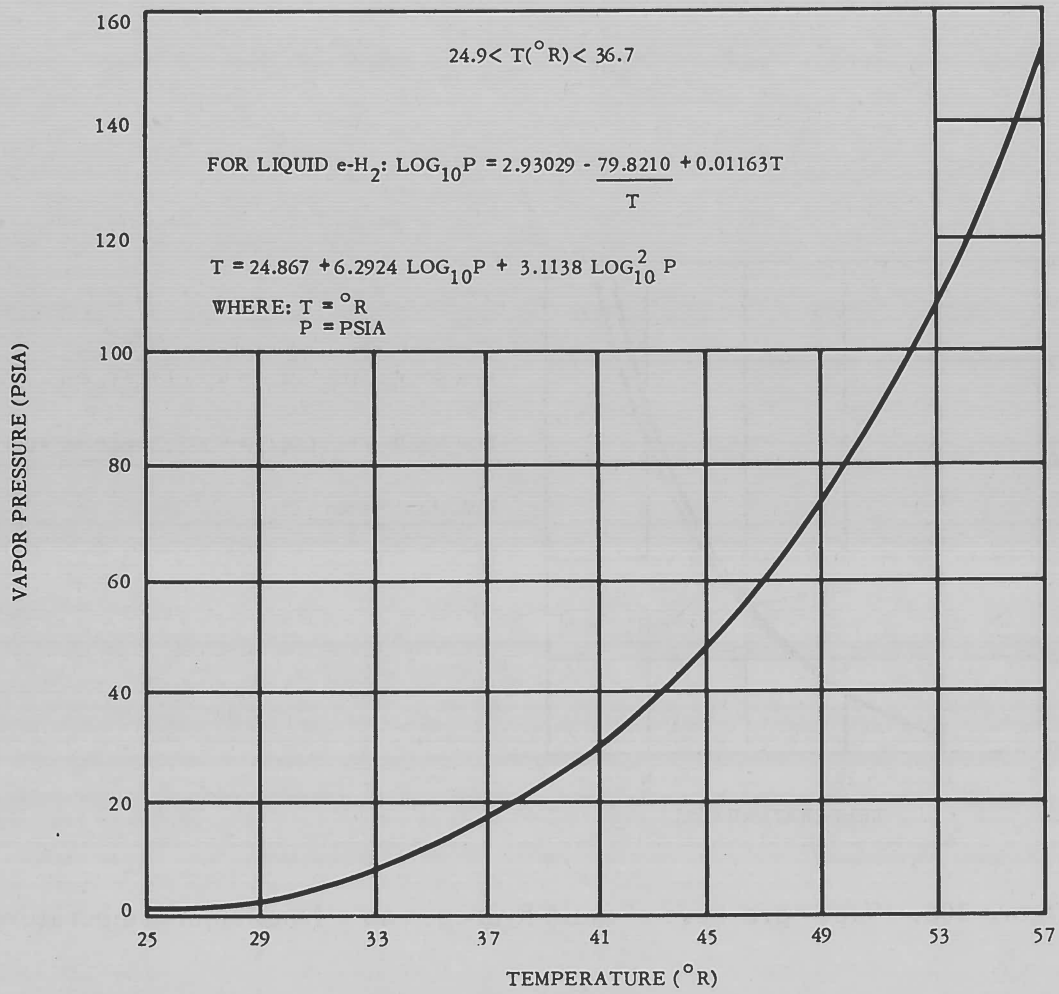


Figure 107. Vapor pressure of liquid equilibrium hydrogen as a function of temperature.

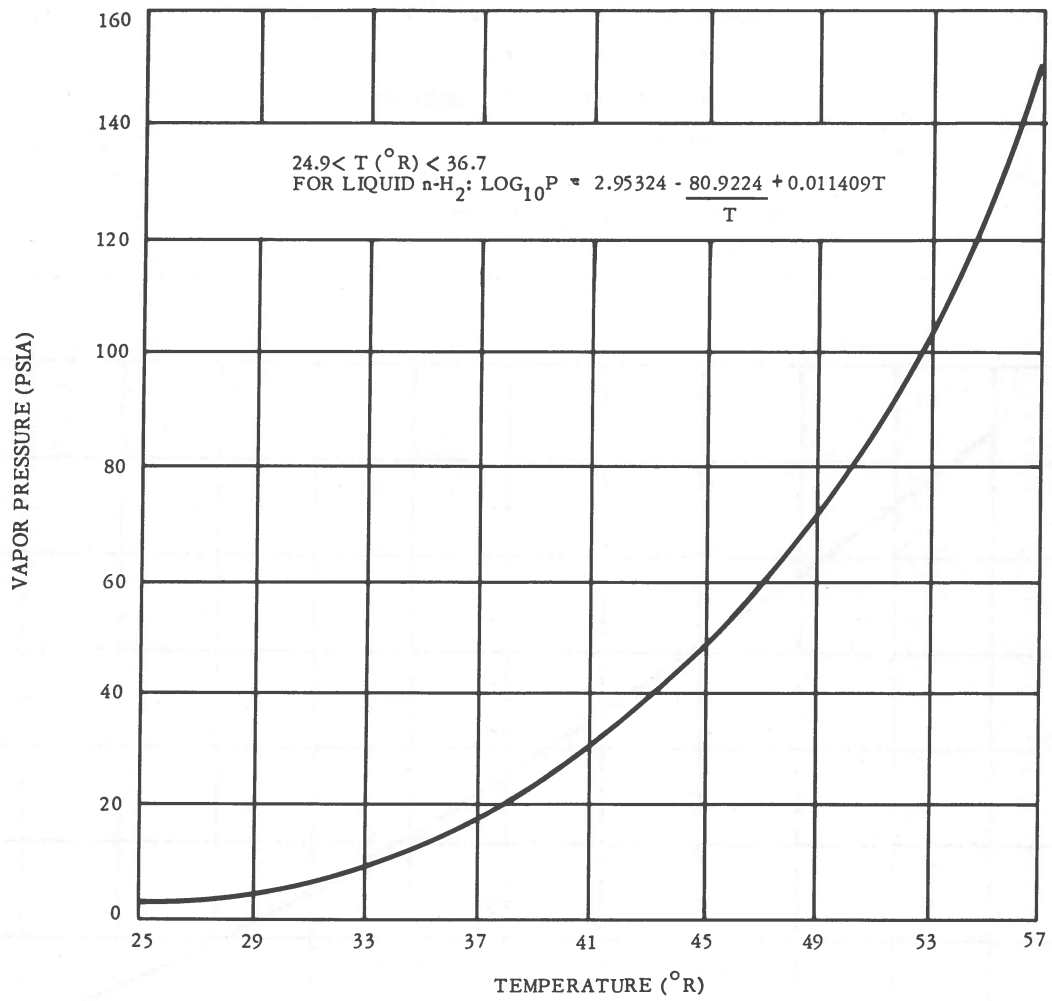


Figure 108. Vapor pressure of liquid normal hydrogen as a function of temperature.

# GENERAL DYNAMICS | ASTRONAUTICS

$$4.8 > \rho > 1.94$$

$$\begin{aligned} \mu &= \bar{\mu} - 1.69 \times 10^{-7} + 2.3886 \times 10^{-19} e^{6.4074\rho} \\ &\quad + 4.977 \times 10^{-7} \rho - 4.626 \times 10^{-8} \rho^2 + 1.8014 \times 10^{-8} \rho^4 \\ \bar{\mu} &= 1.41449 \times 10^{-7} + 1.782 \times 10^{-8} T - 2.06908 \times 10^{-11} T^2 \\ &\quad + 1.86397 \times 10^{-14} T^3 - 8.1916 \times 10^{-18} T^4 + 1.356 \times 10^{-21} T^5 \end{aligned}$$

WHERE  $\mu$  = LB./FT.-SEC.

$\bar{\mu}$  = LB./FT.-SEC. AT 1 ATMOSPHERE

$\rho$  = PCF

$T$  = °R

(NASA-RECOMMENDED EQUATIONS)

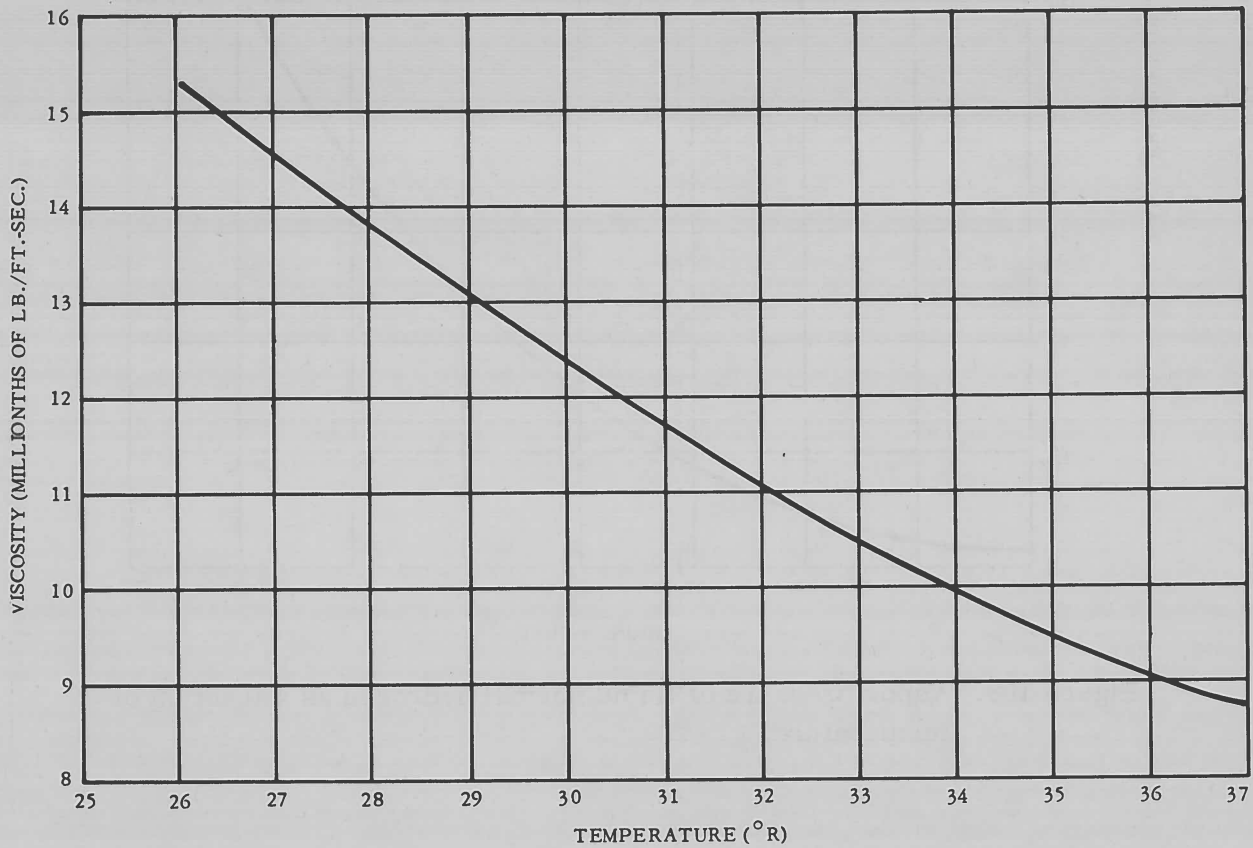


Figure 109. Viscosity of liquid hydrogen as a function of temperature.

2300 > T > 0  
4.5 > ρ > 0

$$\mu = \mu^* + [1.814 + 5.016 \rho + 23.191 \rho^2 - 2.207 \rho^3 + 0.487 \rho^4] 10^{-8}$$

$$\mu^* = 1.41449 \times 10^{-7} + 1.782 \times 10^{-8} T - 2.06908 \times 10^{-11} T^2$$

$$+ 1.86397 \times 10^{-14} T^3 - 8.1916 \times 10^{-18} T^4 + 1.356 \times 10^{-21} T^5$$

WHERE  $\mu = \text{LB./FT.-SEC.}$

$\mu^* = \text{LB./FT.-SEC. AT 1 ATM.}$

$\rho = \text{PCF}$

$T = ^\circ\text{R}$

(NASA-RECOMMENDED EQUATIONS)

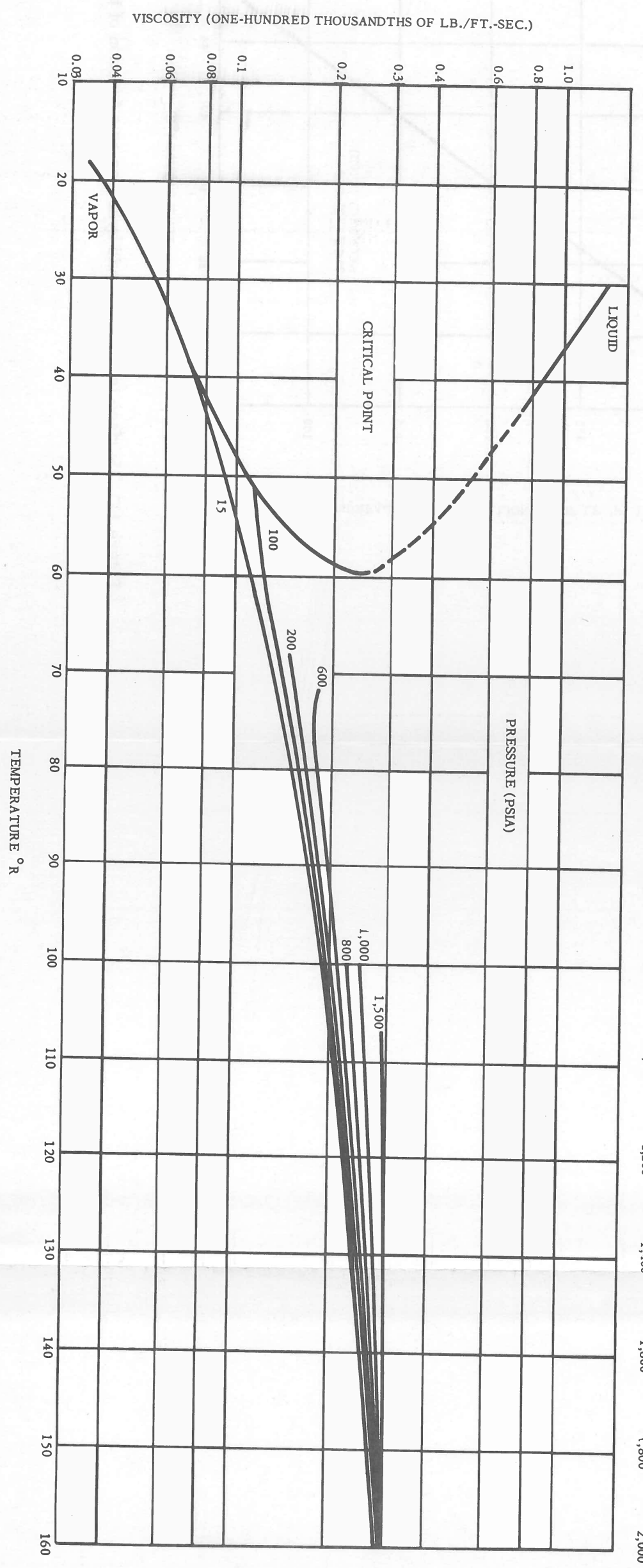
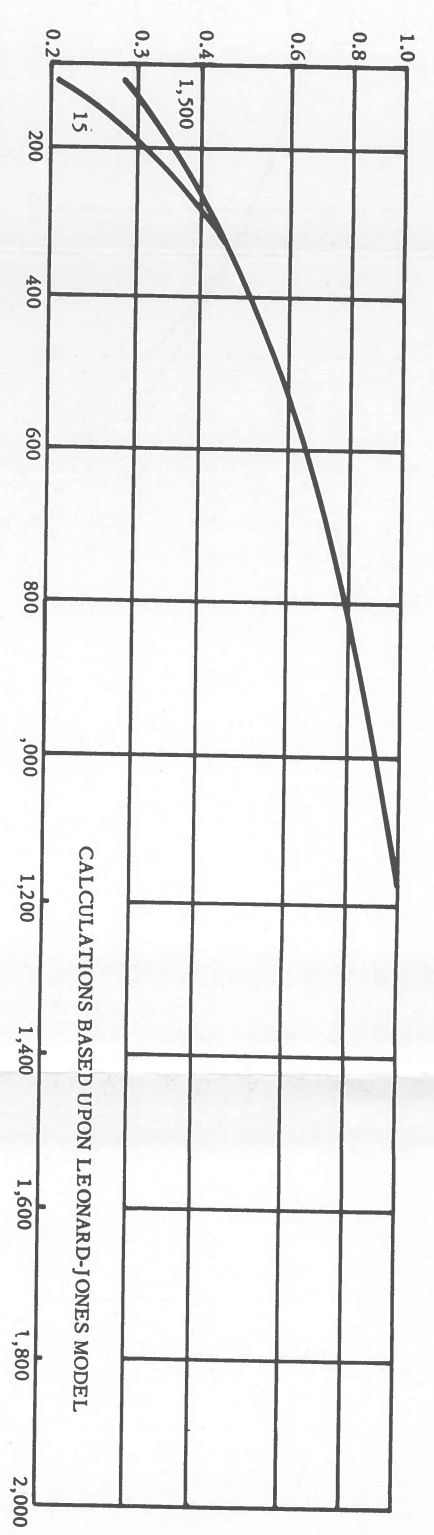


Figure 110. Viscosity of hydrogen.

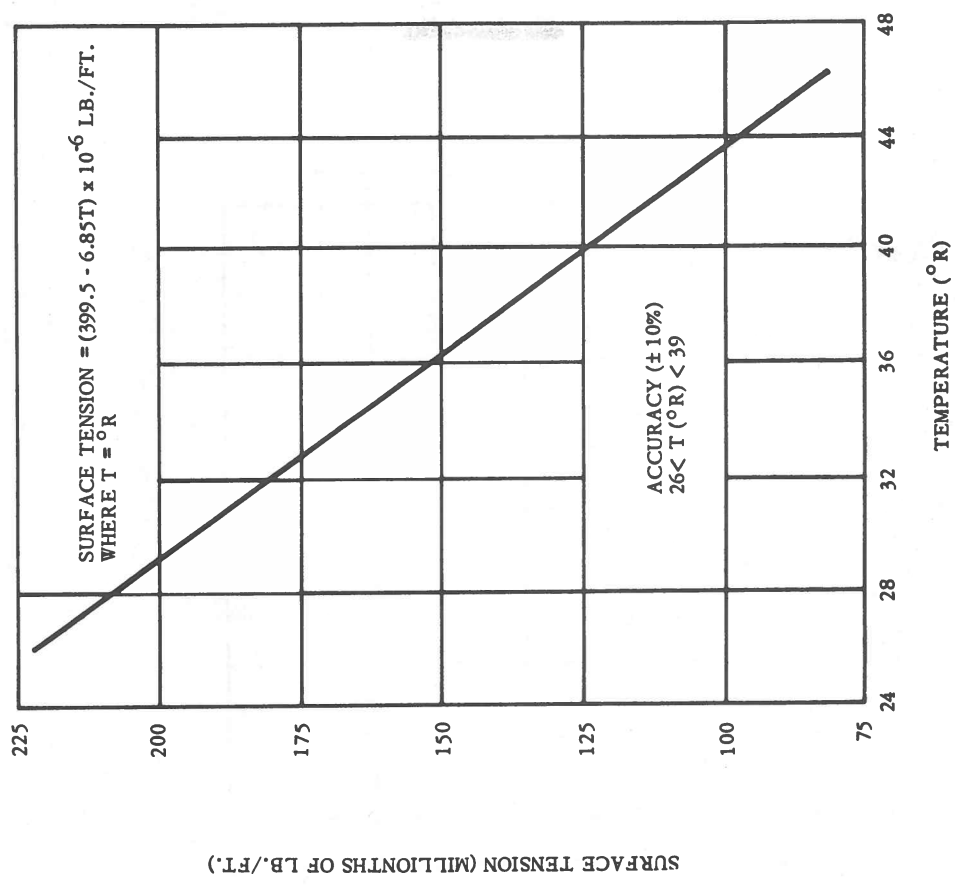


Figure 111. Surface tension of liquid hydrogen as a function of temperature.



# GENERAL DYNAMICS | ASTRONAUTICS

**Table XVIII. Sound velocity in ideal gaseous normal hydrogen as a function of temperature.**

TEMPERATURE (°R)	VELOCITY (FPS)	TEMPERATURE (°R)	VELOCITY (FPS)
36	1,216	100.8	2,032
39.6	1,276	104.4	2,067
43.2	1,332	108	2,102
46.8	1,387	117	2,184
50.4	1,439	126	2,262
54.0	1,490	135	2,335
57.6	1,539	144	2,405
61.2	1,586	153	2,471
64.8	1,632	162	2,534
68.4	1,677	171	2,594
72	1,720	180	2,651
75.6	1,763	270	3,147
79.2	1,804	360	3,573
82.8	1,844	450	3,963
86.4	1,884	540	4,324
90	1,922	720	4,984
93.6	1,960	900	5,568
97.2	1,996	1,080	6,096

NOTE: NASA-RECOMMENDED VALUES; REF. 11.

# GENERAL DYNAMICS | ASTRONAUTICS

**Table XIX. Dielectric constant of liquid parahydrogen as a function of temperature and pressure.**

PRESSURE (PSIA)	TEMPERATURE (°R)											
	36	38	40	42	44	46	48	50	52	54	56	58
15	1.2294											
20	1.2296	1.2249										
30	1.2299	1.2253	1.2203									
40	1.2302	1.2257	1.2207	1.2152								
50	1.2305	1.2260	1.2211	1.2157	1.2097							
60	1.2308	1.2263	1.2215	1.2161	1.2102	1.2036						
70	1.2311	1.2267	1.2218	1.2166	1.2108	1.2043	1.1969					
80	1.2314	1.2271	1.2222	1.2170	1.2113	1.2050	1.1977					
90	1.2318	1.2274	1.2226	1.2175	1.2118	1.2056	1.1984	1.1901				
100	1.2321	1.2277	1.2229	1.2179	1.2123	1.2062	1.1992	1.1910	1.1811			
120	1.2327	1.2284	1.2237	1.2187	1.2132	1.2073	1.2005	1.1928	1.1836	1.1710		
140	1.2332	1.2290	1.2244	1.2195	1.2142	1.2083	1.2018	1.1945	1.1858	1.1745		
160	1.2338	1.2297	1.2251	1.2203	1.2151	1.2093	1.2030	1.1960	1.1877	1.1774	1.1635	
180	1.2344	1.2303	1.2259	1.2211	1.2159	1.2103	1.2043	1.1974	1.1896	1.1800	1.1678	
200	1.2349	1.2309	1.2265	1.2218	1.2168	1.2114	1.2055	1.1988	1.1913	1.1824	1.1714	
250	1.2363	1.2323	1.2281	1.2237	1.2189	1.2137	1.2081	1.2019	1.1951	1.1873	1.1782	1.1671
300	1.2376	1.2338	1.2297	1.2254	1.2208	1.2158	1.2105	1.2048	1.1984	1.1915	1.1835	1.1742
350	1.2389	1.2352	1.2312	1.2271	1.2226	1.2178	1.2128	1.2073	1.2014	1.1951	1.1879	1.1797
400	1.2401	1.2365	1.2327	1.2286	1.2243	1.2197	1.2149	1.2097	1.2042	1.1982	1.1917	1.1843
450	1.2413	1.2377	1.2340	1.2301	1.2259	1.2215	1.2169	1.2119	1.2067	1.2010	1.1950	1.1882
500	1.2425	1.2390	1.2354	1.2315	1.2275	1.2233	1.2188	1.2140	1.2090	1.2036	1.1979	1.1918
600	1.2448	1.2414	1.2380	1.2343	1.2304	1.2264	1.2222	1.2178	1.2131	1.2082	1.2031	1.1977
700	1.2469	1.2437	1.2404	1.2368	1.2331	1.2293	1.2254	1.2212	1.2169	1.2124	1.2076	1.2026
800	1.2489	1.2458	1.2426	1.2392	1.2358	1.2321	1.2284	1.2244	1.2203	1.2160	1.2116	1.2070
900	1.2508	1.2478	1.2448	1.2415	1.2382	1.2346	1.2311	1.2273	1.2235	1.2194	1.2152	1.2109
1,000	1.2526	1.2497	1.2468	1.2437	1.2405	1.2370	1.2336	1.2300	1.2263	1.2225	1.2186	1.2145
1,250	1.2570	1.2544	1.2516	1.2487	1.2456	1.2425	1.2394	1.2361	1.2328	1.2293	1.2259	1.2222
1,500	1.2610	1.2585	1.2559	1.2532	1.2504	1.2476	1.2446	1.2416	1.2385	1.2353	1.2321	1.2288
1,750	1.2648	1.2623	1.2599	1.2573	1.2546	1.2520	1.2492	1.2464	1.2435	1.2406	1.2376	1.2345
2,000	1.2682	1.2659	1.2636	1.2612	1.2586	1.2561	1.2534	1.2508	1.2481	1.2454	1.2425	1.2396
2,500	1.2744	1.2724	1.2703	1.2680	1.2658	1.2635	1.2612	1.2588	1.2563	1.2537	1.2512	1.2487
3,000	1.2802	1.2783	1.2763	1.2743	1.2721	1.2700	1.2679	1.2656	1.2633	1.2610	1.2588	1.2564
3,500		1.2837	1.2817	1.2799	1.2779	1.2759	1.2738	1.2718	1.2697	1.2676	1.2653	1.2632
4,000			1.2867	1.2851	1.2832	1.2812	1.2793	1.2775	1.2754	1.2735	1.2713	1.2693
4,500				1.2899	1.2881	1.2862	1.2844	1.2826	1.2807	1.2789	1.2769	1.2749
5,000				1.2943	1.2925	1.2909	1.2892	1.2874	1.2855	1.2839	1.2820	1.2802

**NOTES:**

1. VALUES BELOW THE STEPPED LINE REPRESENT AN EXTRAPOLATION OF  $\rho$  WITH DENSITY.
2. NASA-RECOMMENDED VALUES.
3. SEE REF. 13.

GENERAL DYNAMICS | ASTRONAUTICS

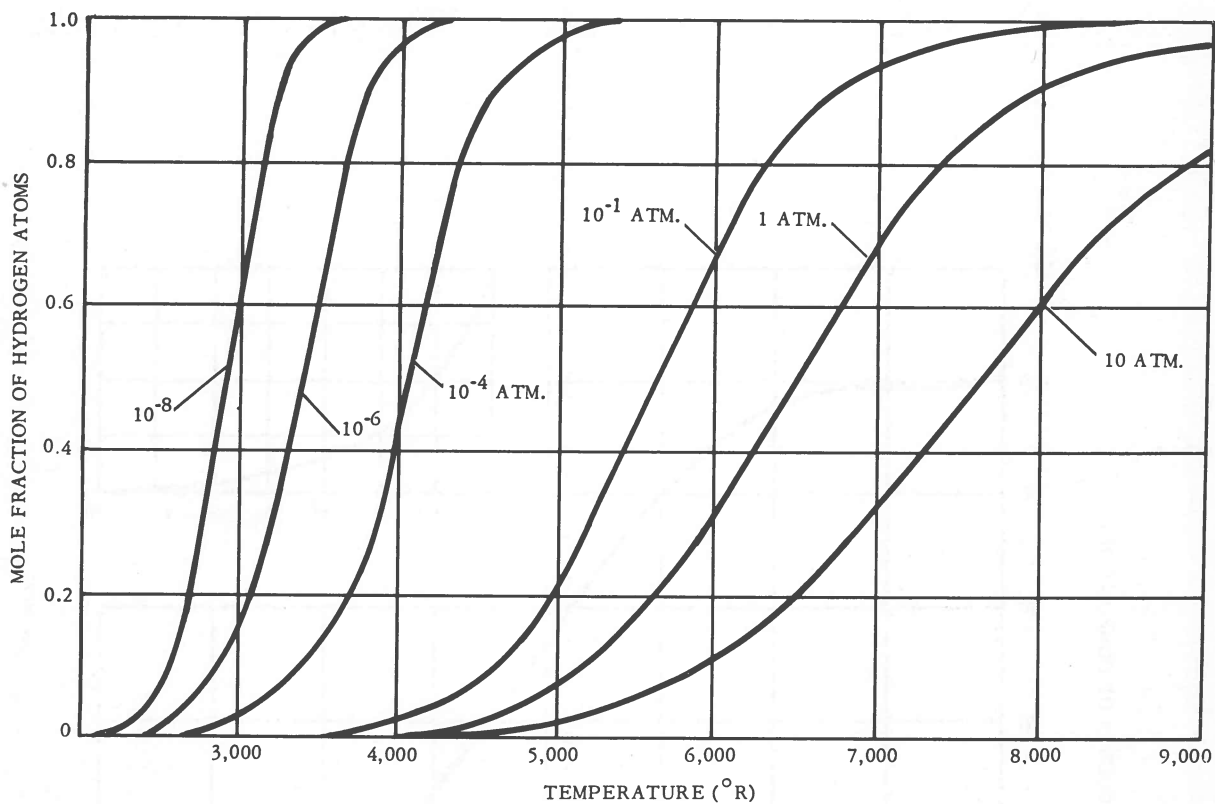


Figure 112. Hydrogen dissociation as a function of temperature and pressure.

Table XX. Dissociation of hydrogen molecules as a function of temperature at a pressure of one atmosphere.

TEMPERATURE (°R)	DISSOCIATION CONSTANT	
	$K_{H_2}$ (ATM)	FRACTION DISSOCIATED
540	$18.39 \times 10^{-72}$	$21.44 \times 10^{-37}$
900	$4.939 \times 10^{-41}$	$3.514 \times 10^{-21}$
1,800	$5.174 \times 10^{-18}$	$1.137 \times 10^{-9}$
2,700	$3.100 \times 10^{-10}$	$8.675 \times 10^{-6}$
3,600	$2.641 \times 10^{-6}$	$8.125 \times 10^{-4}$
5,400	$2.480 \times 10^{-2}$	0.07850
7,200	2.5236	0.6220
9,000	41.038	0.9546

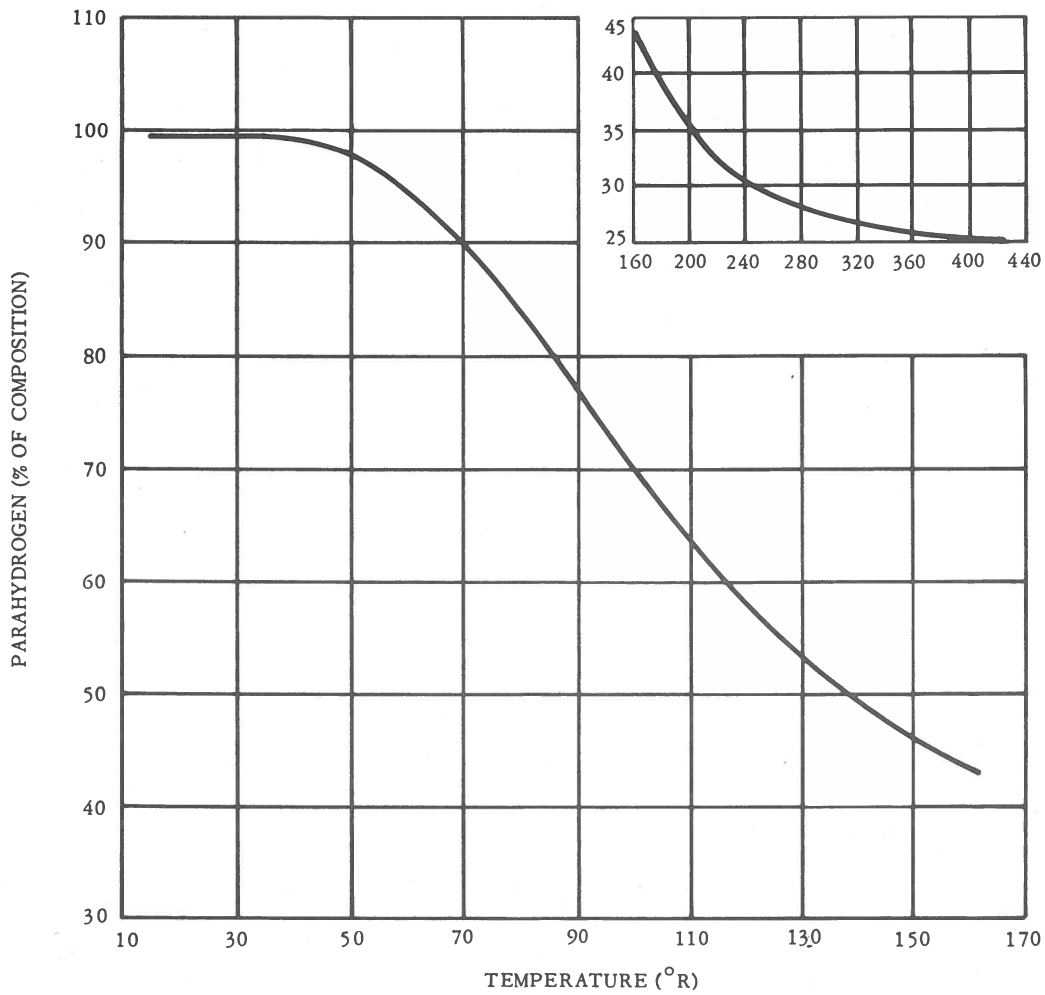


Figure 113. Orthohydrogen/parahydrogen composition at equilibrium as a function of temperature.

# GENERAL DYNAMICS | ASTRONAUTICS

## 14.4 THERMAL PROPERTIES

Thermal properties of hydrogen are presented in Tables XXI (Ref. 2), XXII, and XXIII (Ref. 20), and in Figures 114 through 133.

Table XXI. Heat of dissociation of hydrogen for the reaction  $H_2 \rightleftharpoons 2H$ .

TEMPERATURE (°R)	p-H <sub>2</sub> (BTU/LB.)	o-H <sub>2</sub> (BTU/LB.)	n-H <sub>2</sub> (BTU/LB.)
0	92,172	91,869	91,945
536.7	93,022	93,006	93,009

Table XXII. Latent heat of fusion of solid hydrogen.

	HEAT OF FUSION (BTU/LB.)	TEMPERATURE (°R)	PRESSURE (PSIA)
n-H <sub>2</sub>	25.0	25.12	1.044 (Ref. 2)
p-H <sub>2</sub>	25.0 <sub>8</sub>	24.92	1.020 (Ref. 19)

# GENERAL DYNAMICS | ASTRONAUTICS

**Table XXIII. Equations for computing thermal conductivity of normal parahydrogen.**

NORMAL HYDROGEN (1280 > T > 0)

$$k_n = k_n^* + 4.45096 \times 10^{-4} + 4.272438 \times 10^{-3} \rho + 7.6126 \times 10^{-2} \rho^2 - 1.14346 \times 10^{-1} \rho^3 + 7.8859 \times 10^{-2} \rho^4 - 2.9826 \times 10^{-2} \rho^5 + 6.4055 \times 10^{-3} \rho^6 - 7.3610 \times 10^{-4} \rho^7 + 3.5245 \times 10^{-5} \rho^8$$

$$k_n^* = 2.42596 \times 10^{-4} T - 1.10712 \times 10^{-7} T^2 + 5.1766 \times 10^{-11} T^3 - 9.6663 \times 10^{-15} T^4 + 5.9265 \times 10^{-19} T^5$$

WHERE

$$k_n = \frac{\text{BTU} - \text{FT.}}{\text{FT.}^2 - \text{HR.} - ^\circ\text{R}} \quad \rho = \text{PCF} \quad T = ^\circ\text{R}$$

$$k_n^* = \frac{\text{BTU} - \text{FT.}}{\text{FT.}^2 - \text{HR.} - ^\circ\text{R}} \quad \text{AT 1 ATM.} \quad n = \text{NORMAL HYDROGEN}$$

PARAHYDROGEN (1280 > T > 0)

$$\frac{k_p}{k_n} = 1 + 0.19457 e^{-\left(\frac{0.556T - 169.78}{6958.5}\right)} - \left\{ 0.19457 e^{-\left(\frac{0.556T - 169.78}{6958.5}\right)} \left[ -1.3606 + 4.4522 \times 10^{-3} T - \frac{(0.556T - 169.78)^2}{615667} \right] \right\}$$

WHERE

p = PARAHYDROGEN

T = °R

NORMAL & PARAHYDROGEN (2700 > T > 1280)

USE A LINEAR EXTRAPOLATION BETWEEN THE PREVIOUS EQUATIONS & THE FOLLOWING EQUATIONS.

NORMAL & PARAHYDROGEN (9000 > T > 2700)

$$k = A_1 e^{-\frac{1}{2} \left(\frac{T - A_3}{A_2}\right)^2} + A_4 + A_5 T$$

WHERE

$$k = \frac{\text{BTU} - \text{FT.}}{\text{FT.}^2 - \text{HR.} - ^\circ\text{R}} \quad T = ^\circ\text{R}$$

VALUE OF CONSTANTS A<sub>1</sub> THROUGH A<sub>5</sub> AS A FUNCTION OF PRESSURE

PRESSURE (ATM.)	A <sub>1</sub>	A <sub>2</sub>	A <sub>3</sub>	A <sub>4</sub>	A <sub>5</sub>
0.1	6.56275	434.85	3233	7.687580 × 10 <sup>-2</sup>	1.0527 × 10 <sup>-4</sup>
0.5	5.8332	500.57	3556	8.82935 × 10 <sup>-3</sup>	1.2858 × 10 <sup>-4</sup>
1.0	5.47613	532.07	3716	-3.98893 × 10 <sup>-2</sup>	1.4503 × 10 <sup>-4</sup>
2.0	5.15876	587.36	3902	-1.05226 × 10 <sup>-2</sup>	1.3378 × 10 <sup>-4</sup>
10.0	4.524739	732.61	4386	6.69821 × 10 <sup>-2</sup>	1.0611 × 10 <sup>-4</sup>
50.0	3.86798	932.3	5001	9.99047 × 10 <sup>-2</sup>	9.378 × 10 <sup>-5</sup>
100.0	3.51094	1013.9	5268	9.95902 × 10 <sup>-2</sup>	9.39 × 10 <sup>-5</sup>

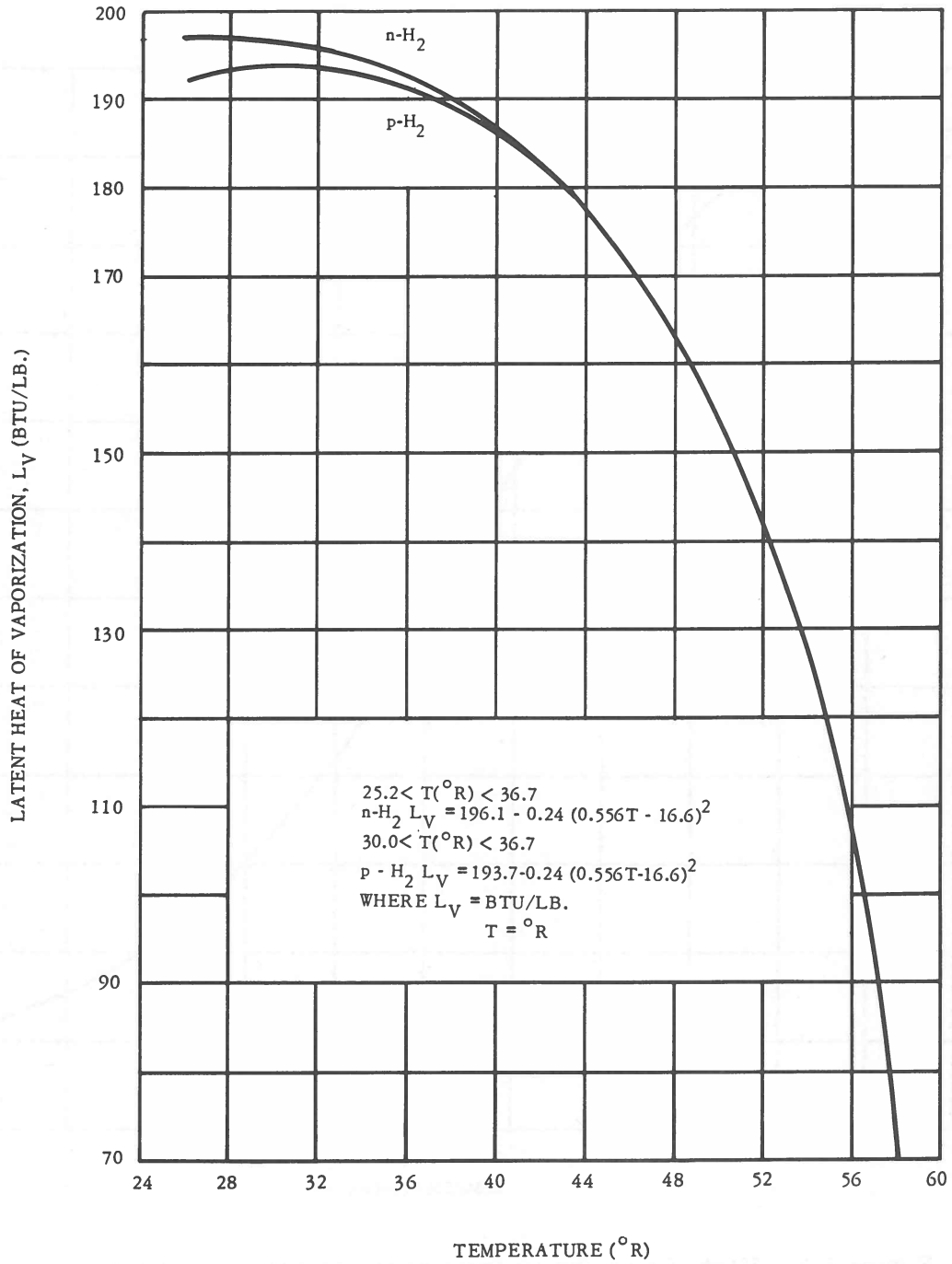


Figure 114. Latent heat of vaporization of liquid hydrogen as a function of temperature.

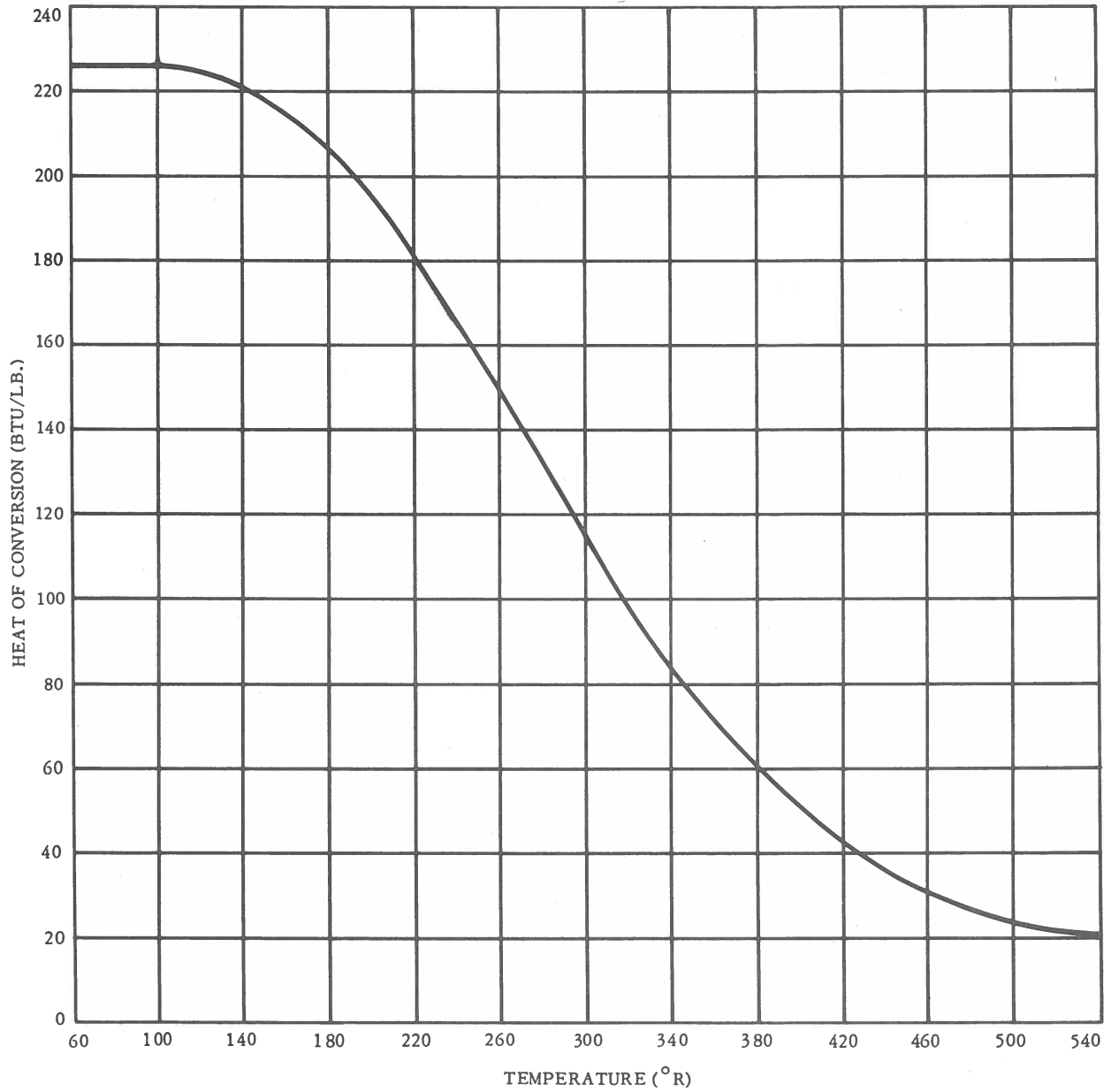


Figure 115. Heat of conversion from normal hydrogen to parahydrogen.



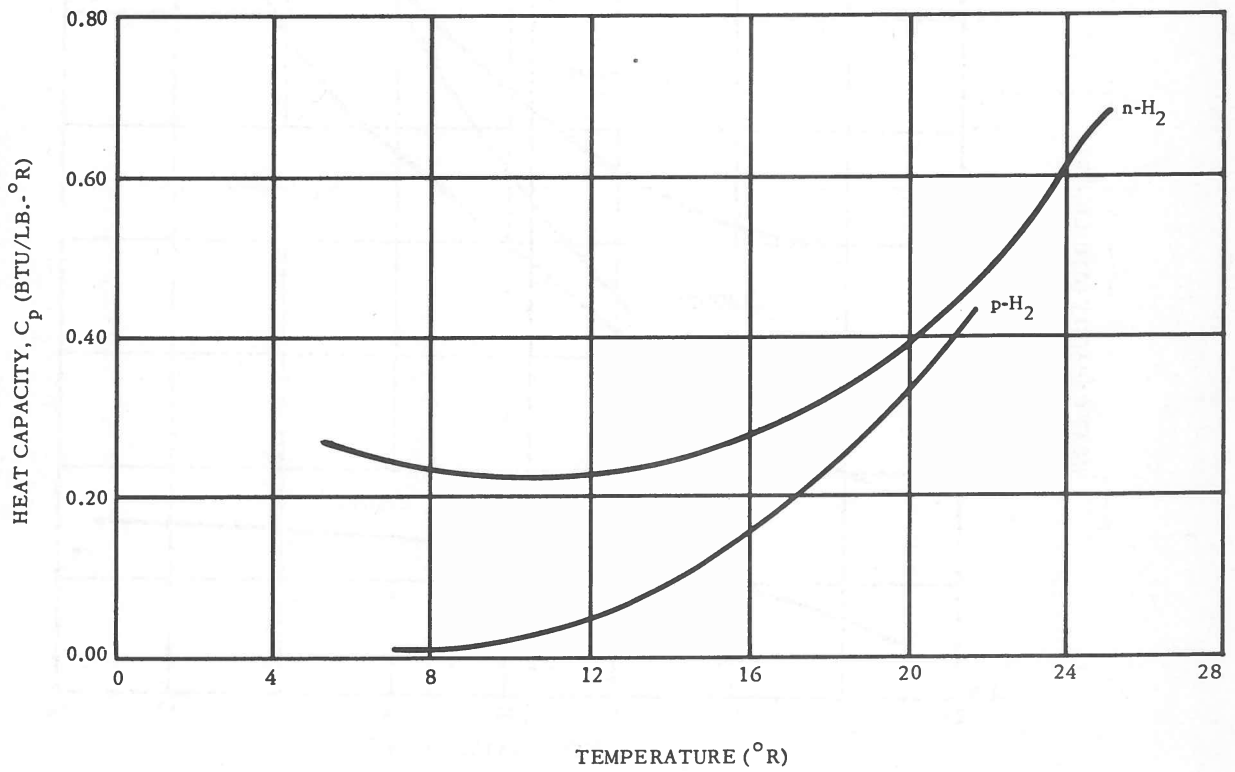


Figure 116. Heat capacity of solid hydrogen as a function of temperature.

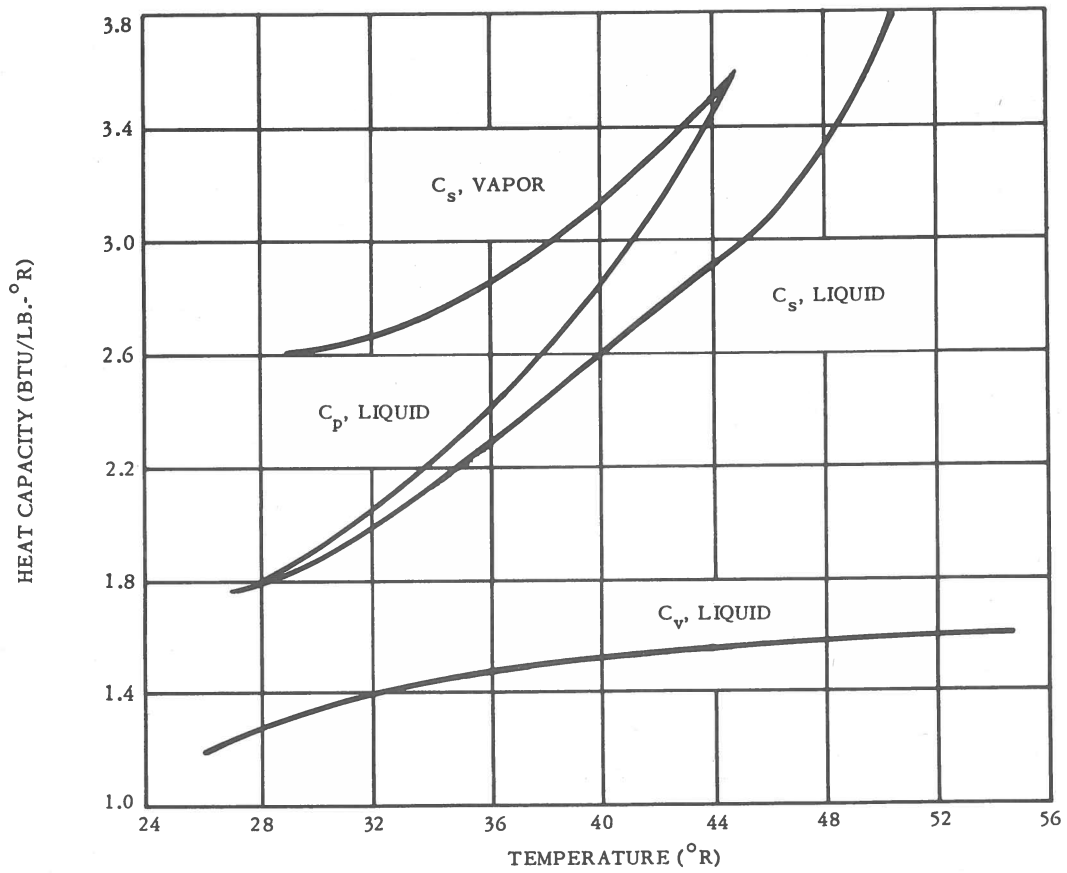


Figure 117. Heat capacity of liquid hydrogen and saturated vapor as a function of temperature.

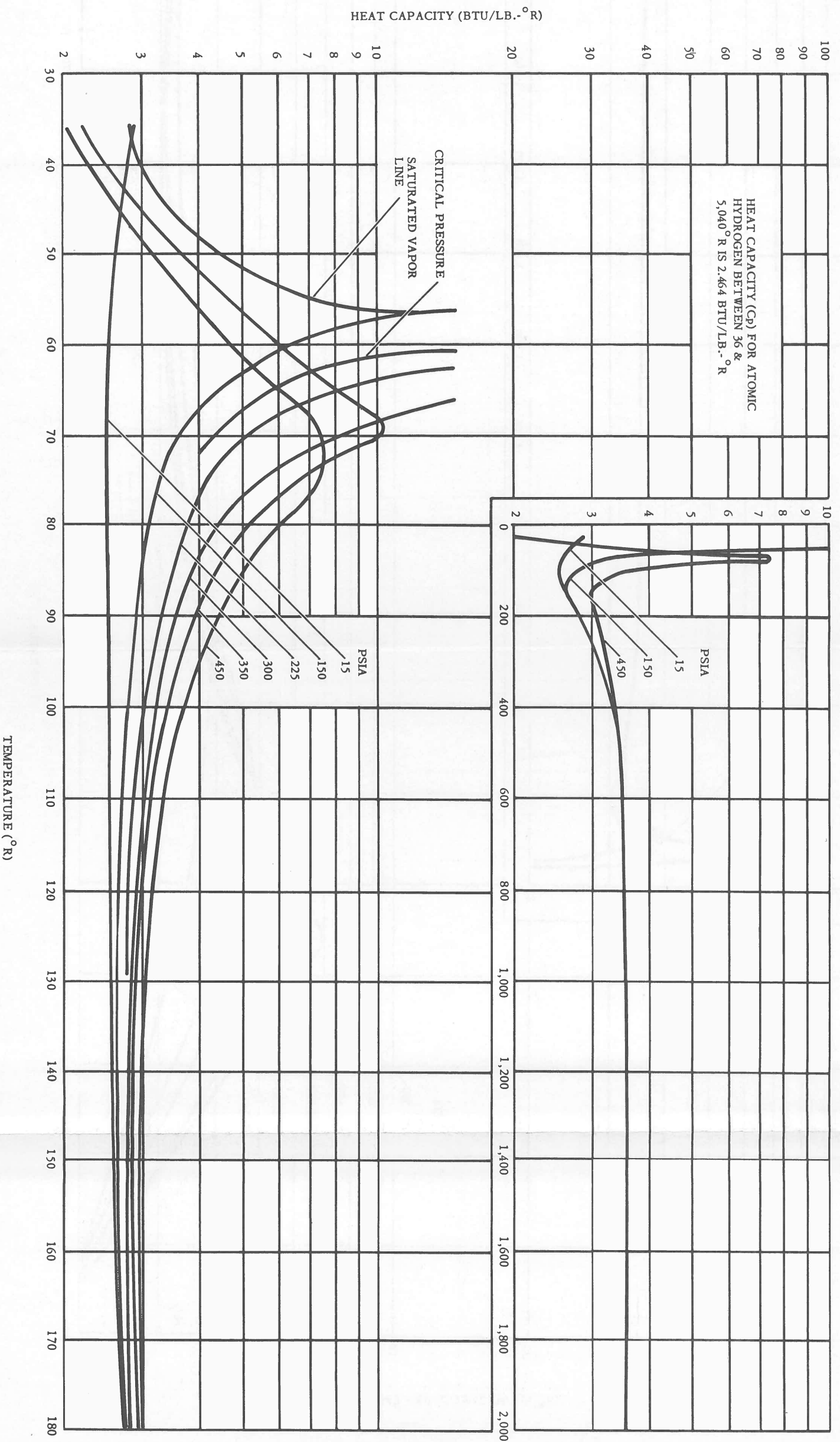


Figure 118. Heat capacity of hydrogen at low pressure, C<sub>p</sub>.

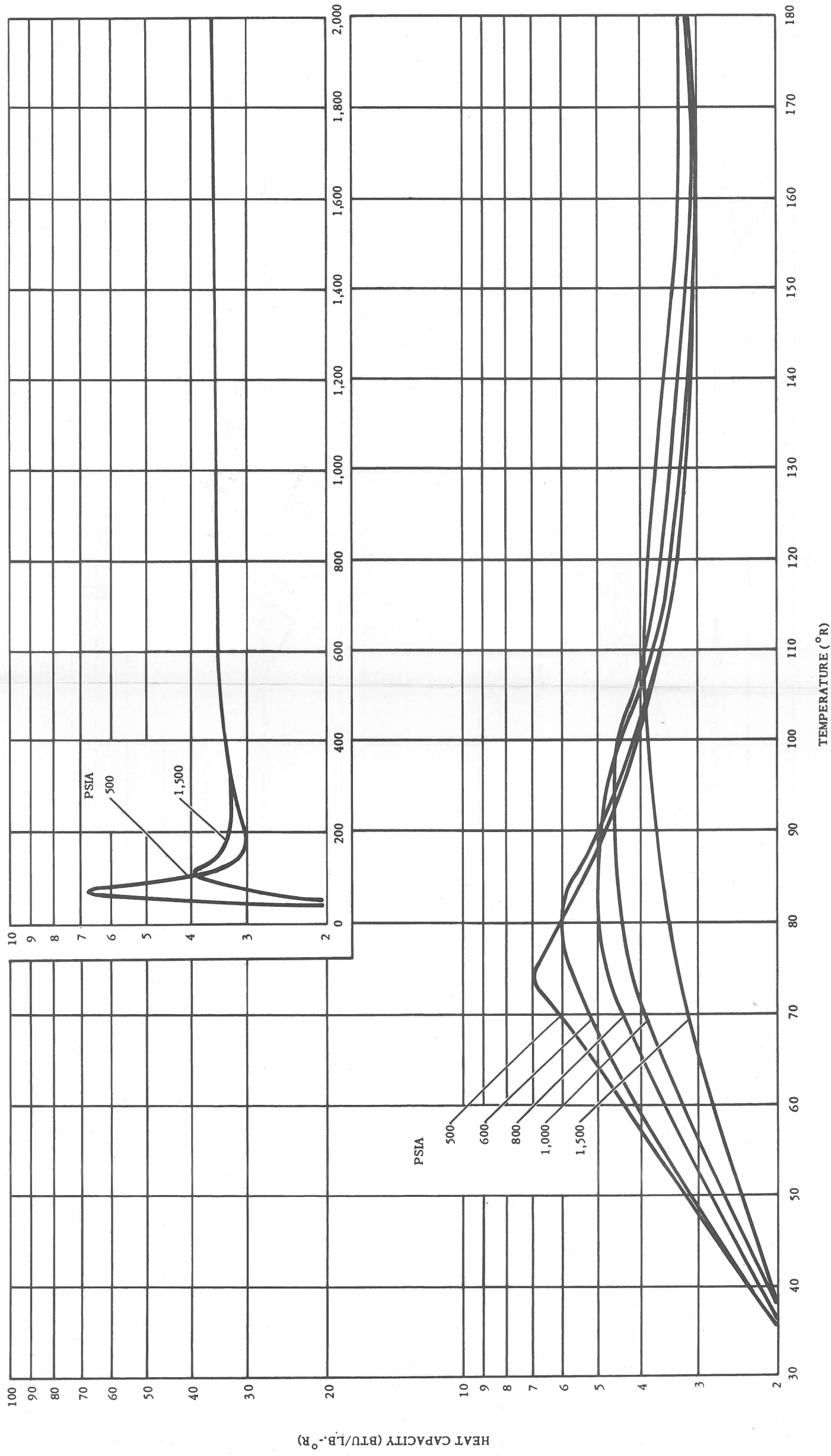


Figure 119. Heat capacity of hydrogen at high pressure,  $C_p$ .

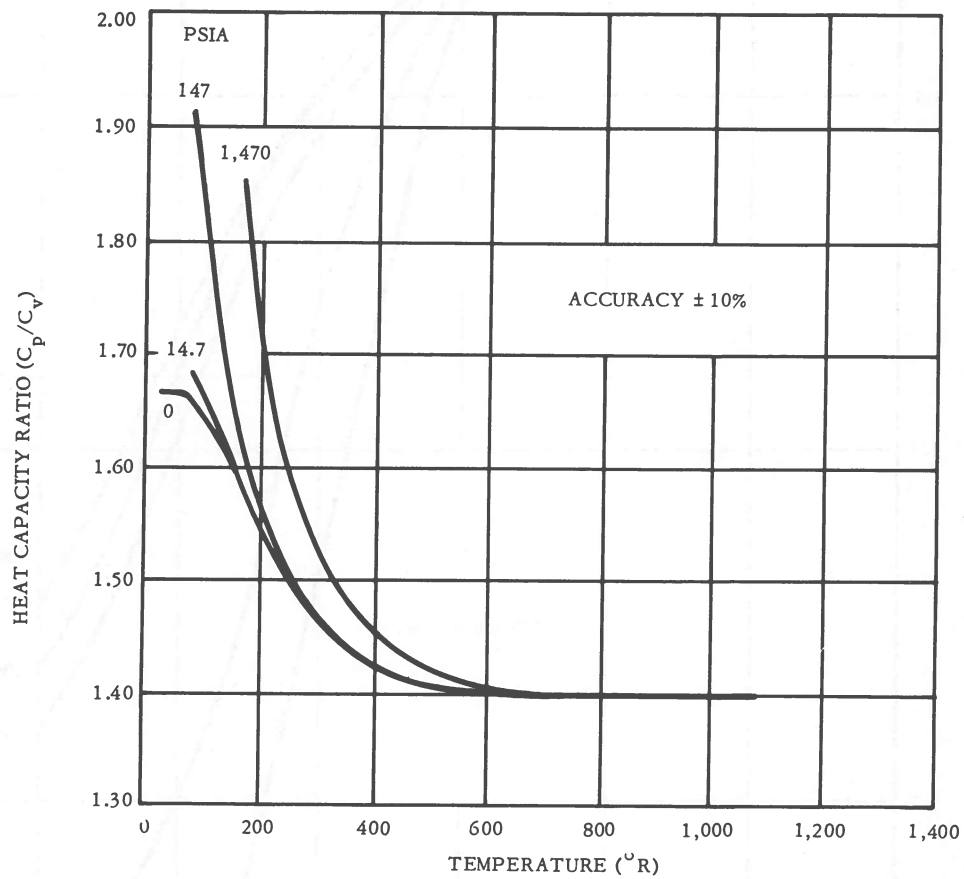


Figure 120. Heat capacity ratio ( $C_p/C_v$ ) of hydrogen as a function of temperature and pressure,  $C_p/C_v > 1.4$ .

GENERAL DYNAMICS | ASTRONAUTICS

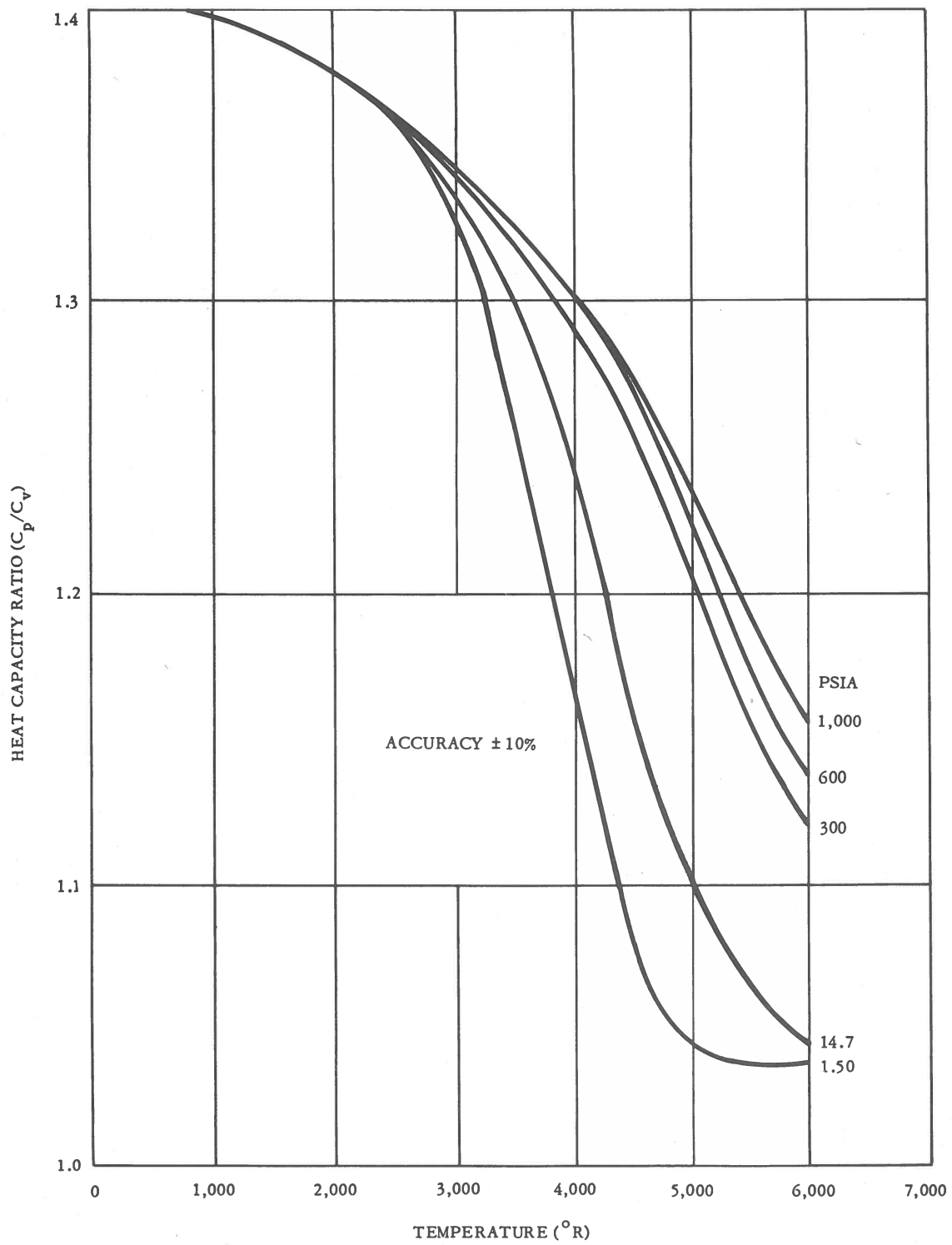


Figure 121. Heat capacity ratio ( $C_p/C_v$ ) of hydrogen as a function of temperature and pressure,  $C_p/C_v < 1.4$ .

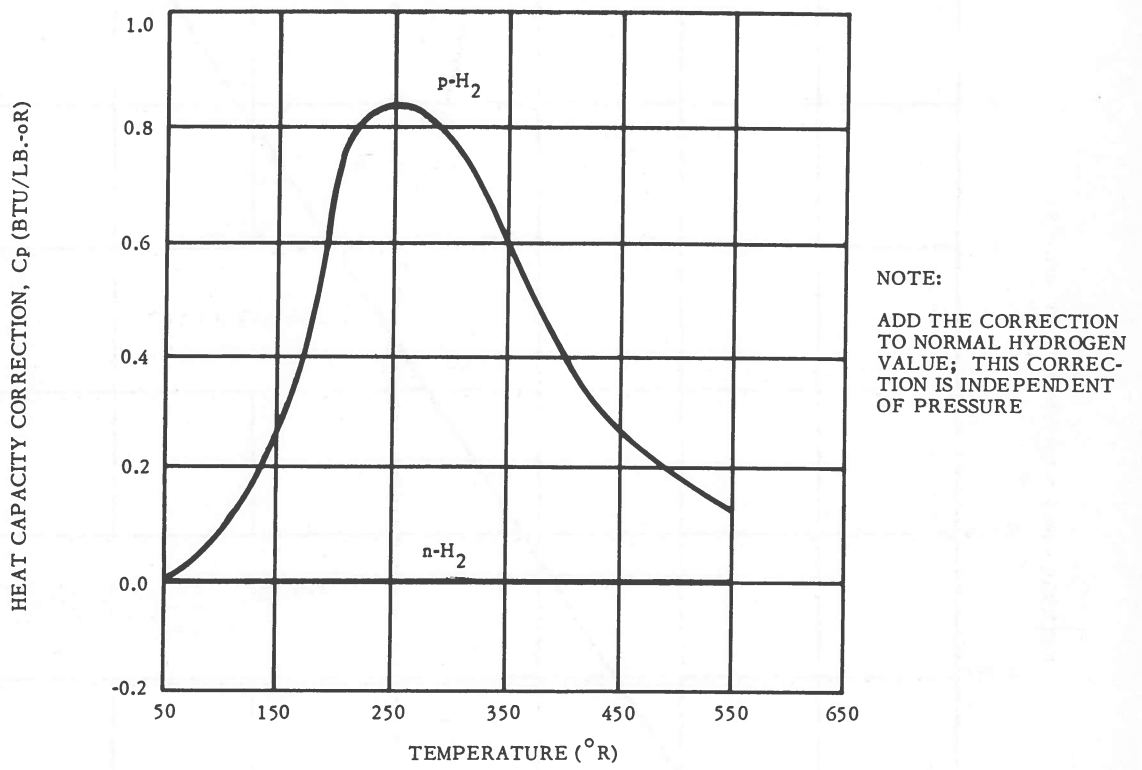


Figure 122. Heat capacity correction from normal hydrogen to parahydrogen.

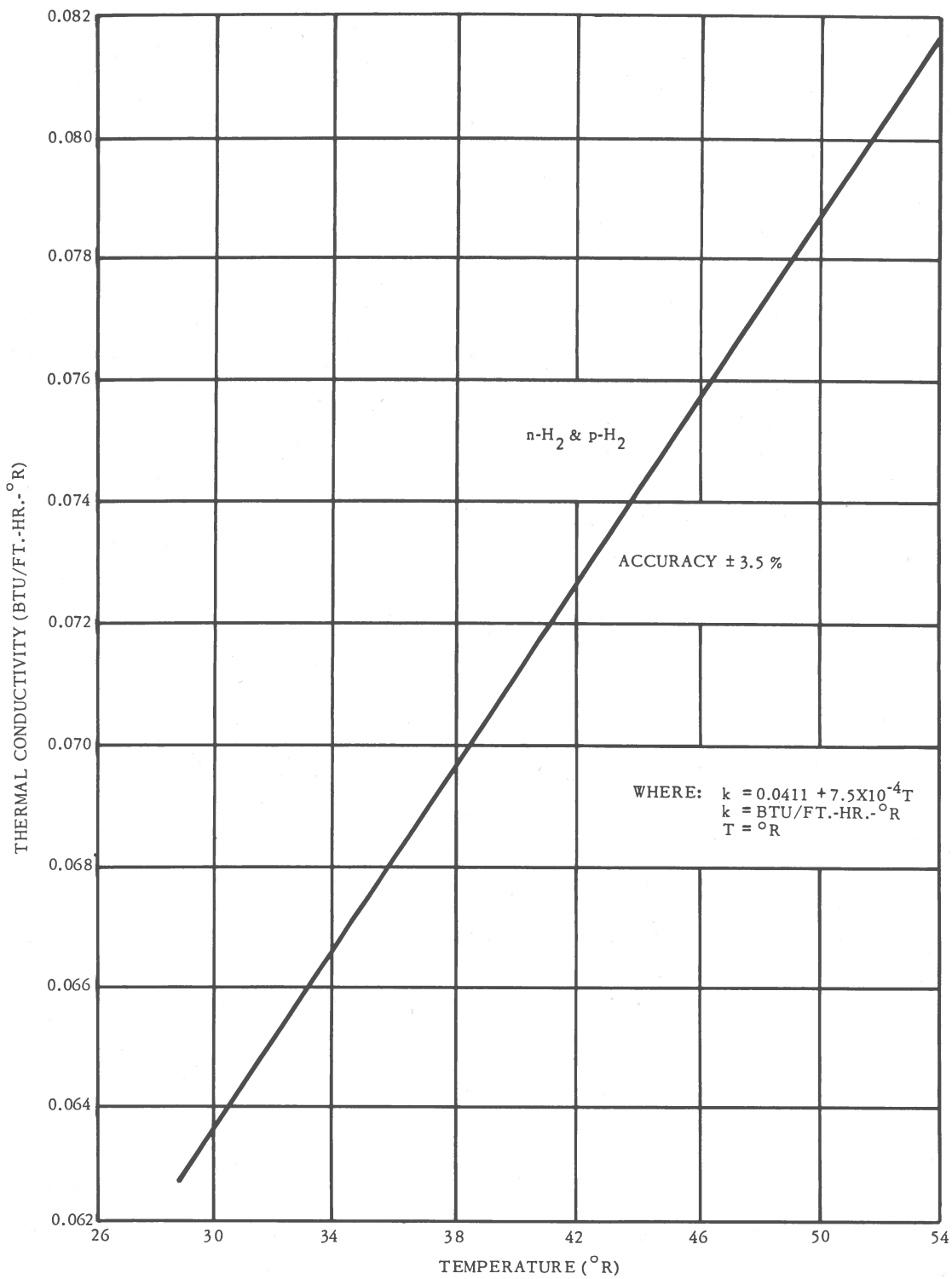


Figure 123. Thermal conductivity of liquid hydrogen as a function of temperature.



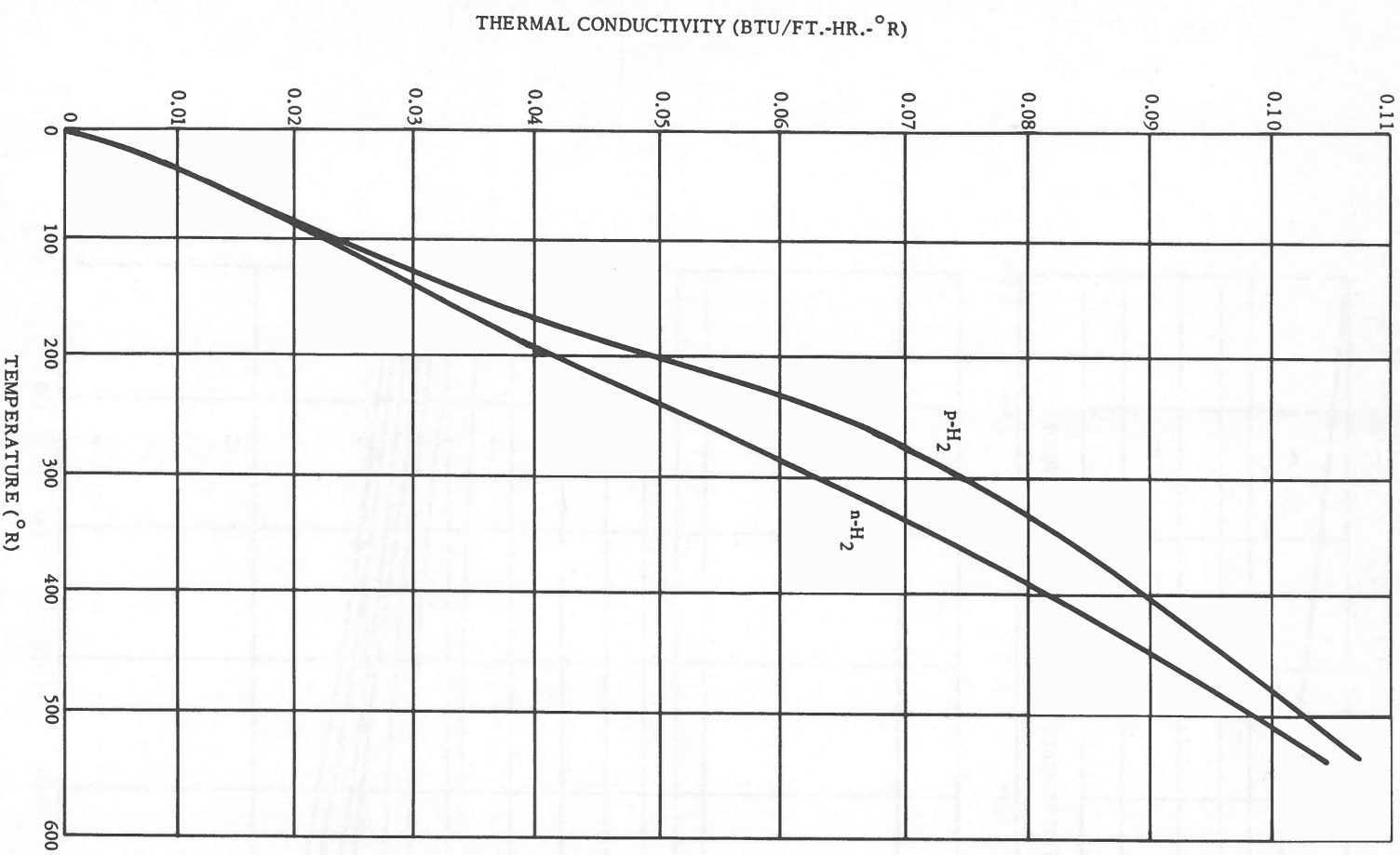


Figure 124. Thermal conductivity of gaseous hydrogen at 14.7 psia as a function of temperature.

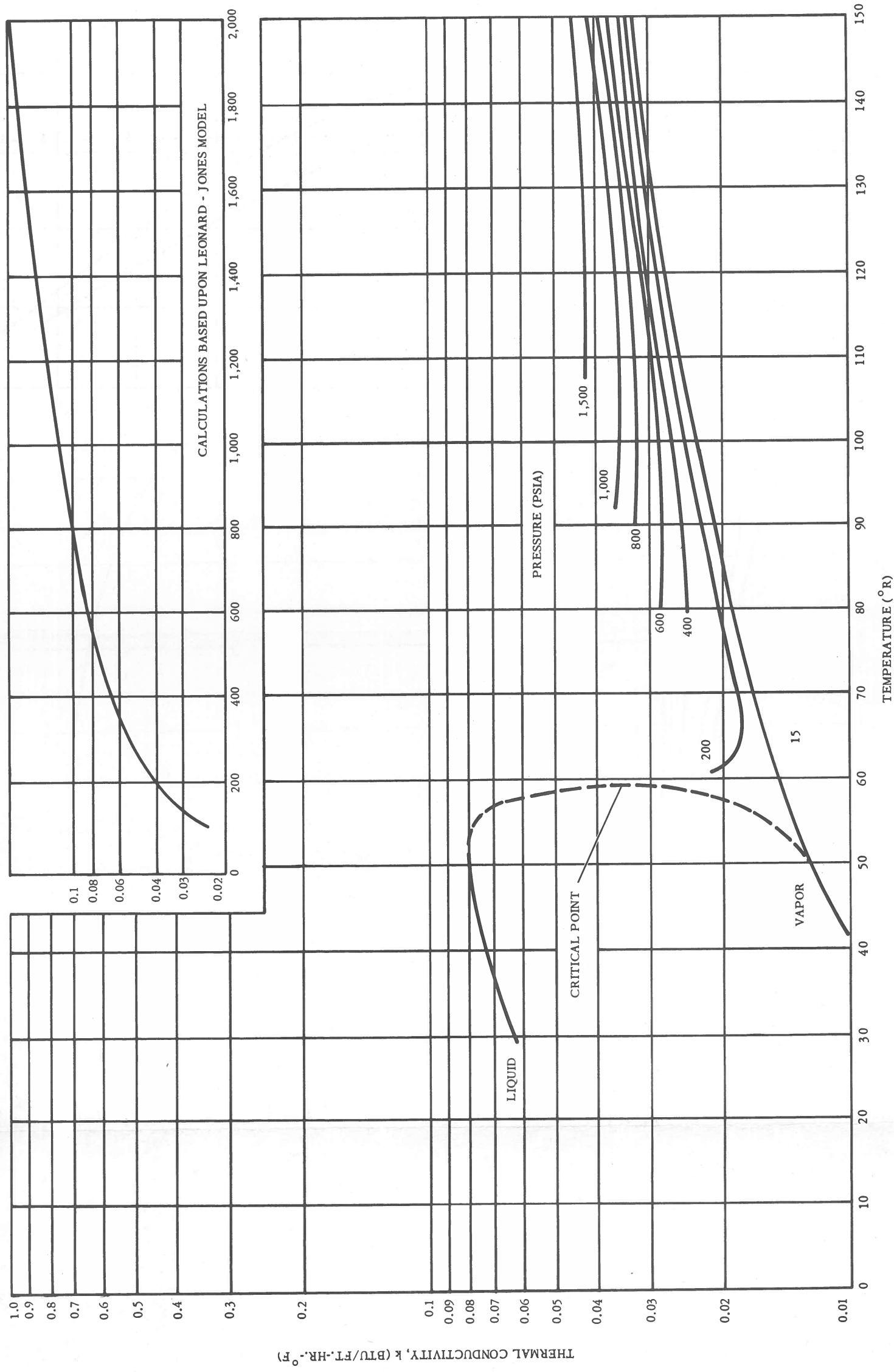


Figure 125. Thermal conductivity of hydrogen.



# GENERAL DYNAMICS | ASTRONAUTICS

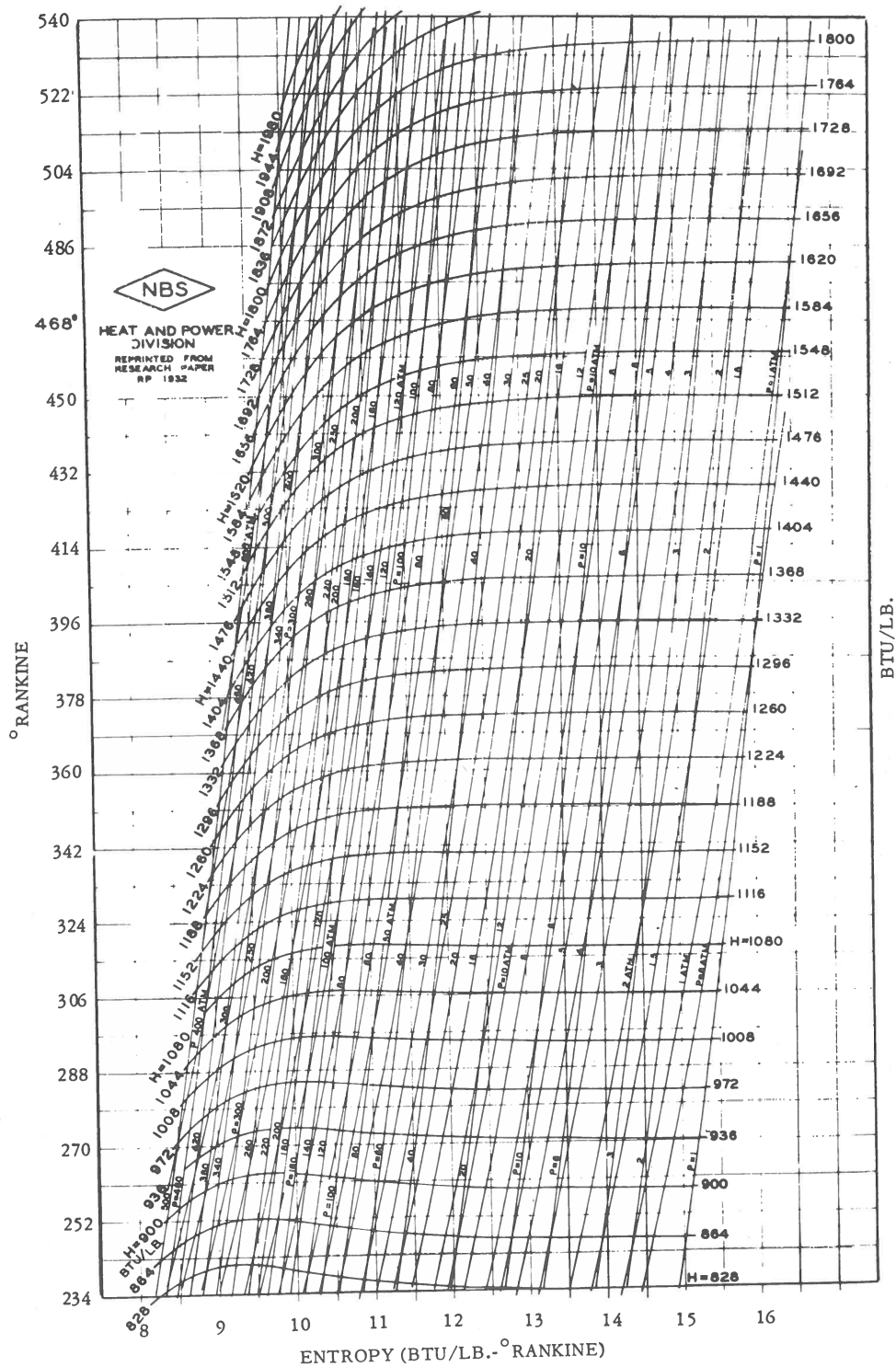


Figure 127. Temperature-entropy diagram for normal hydrogen (234° to 540°R).



GENERAL DYNAMICS | ASTRONAUTICS

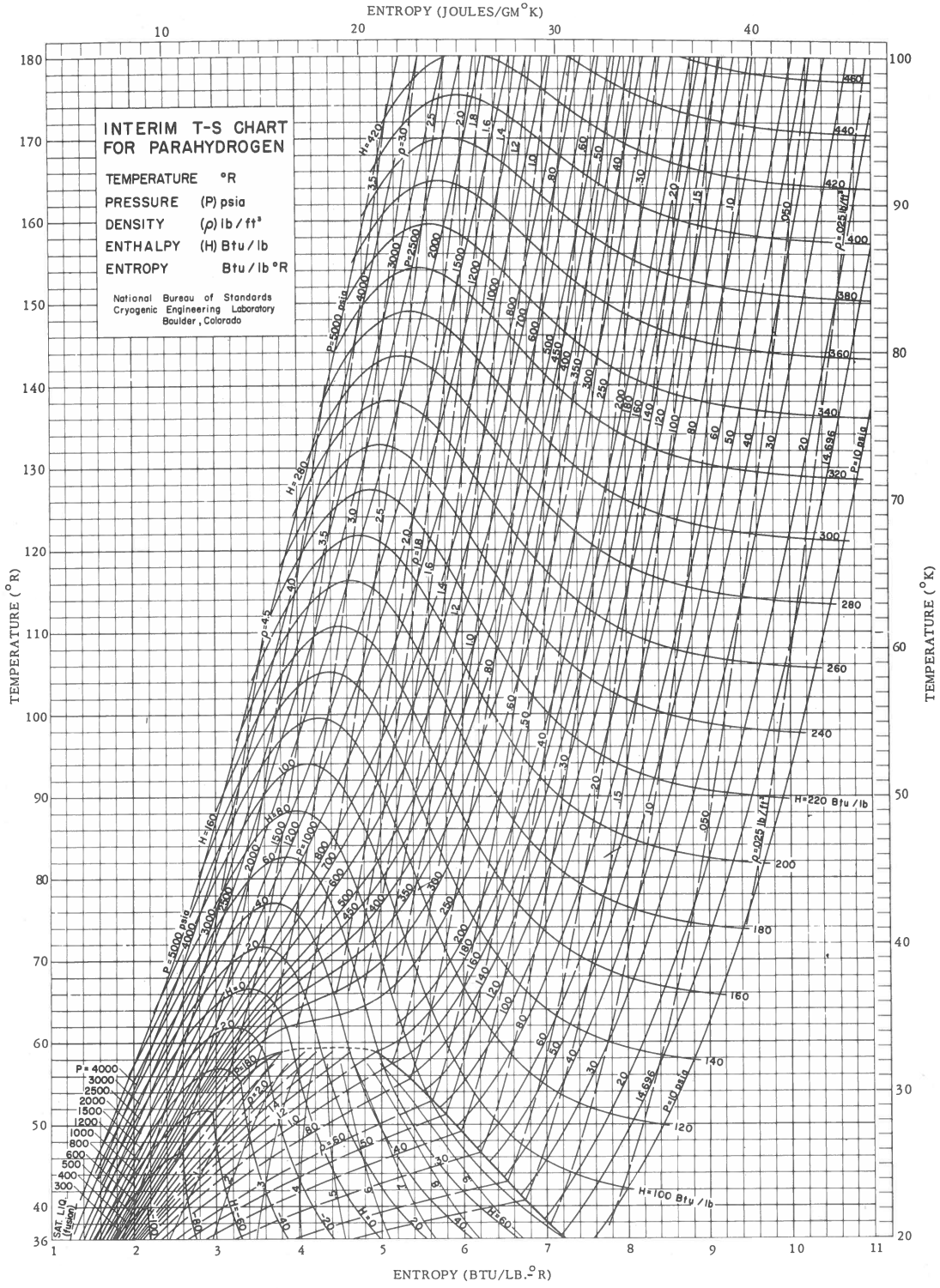


Figure 129. Temperature-entropy diagram for parahydrogen (36° to 180°R).





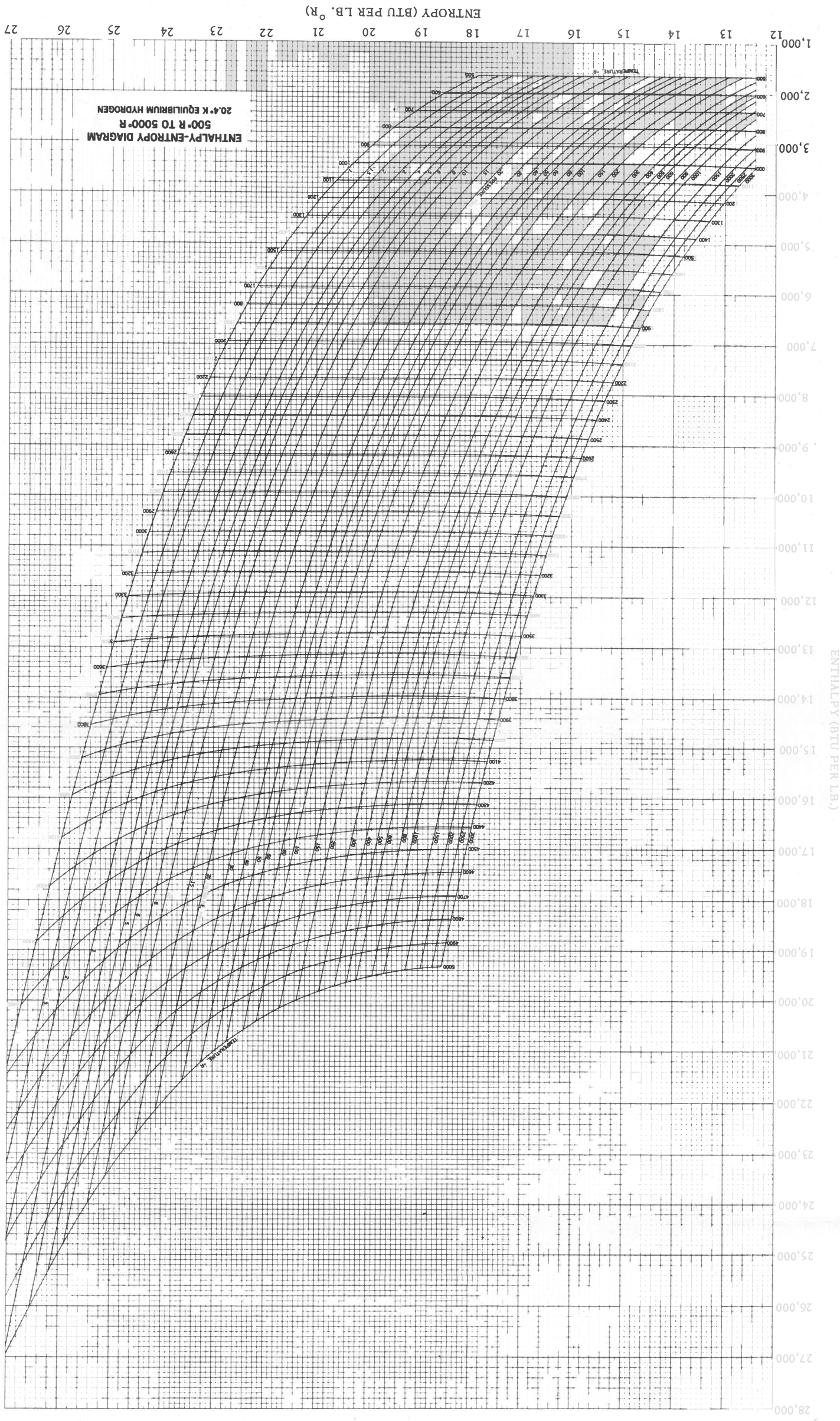


Figure 131. Enthalpy-entropy diagram for parahydrogen (500° to 5,000°R).



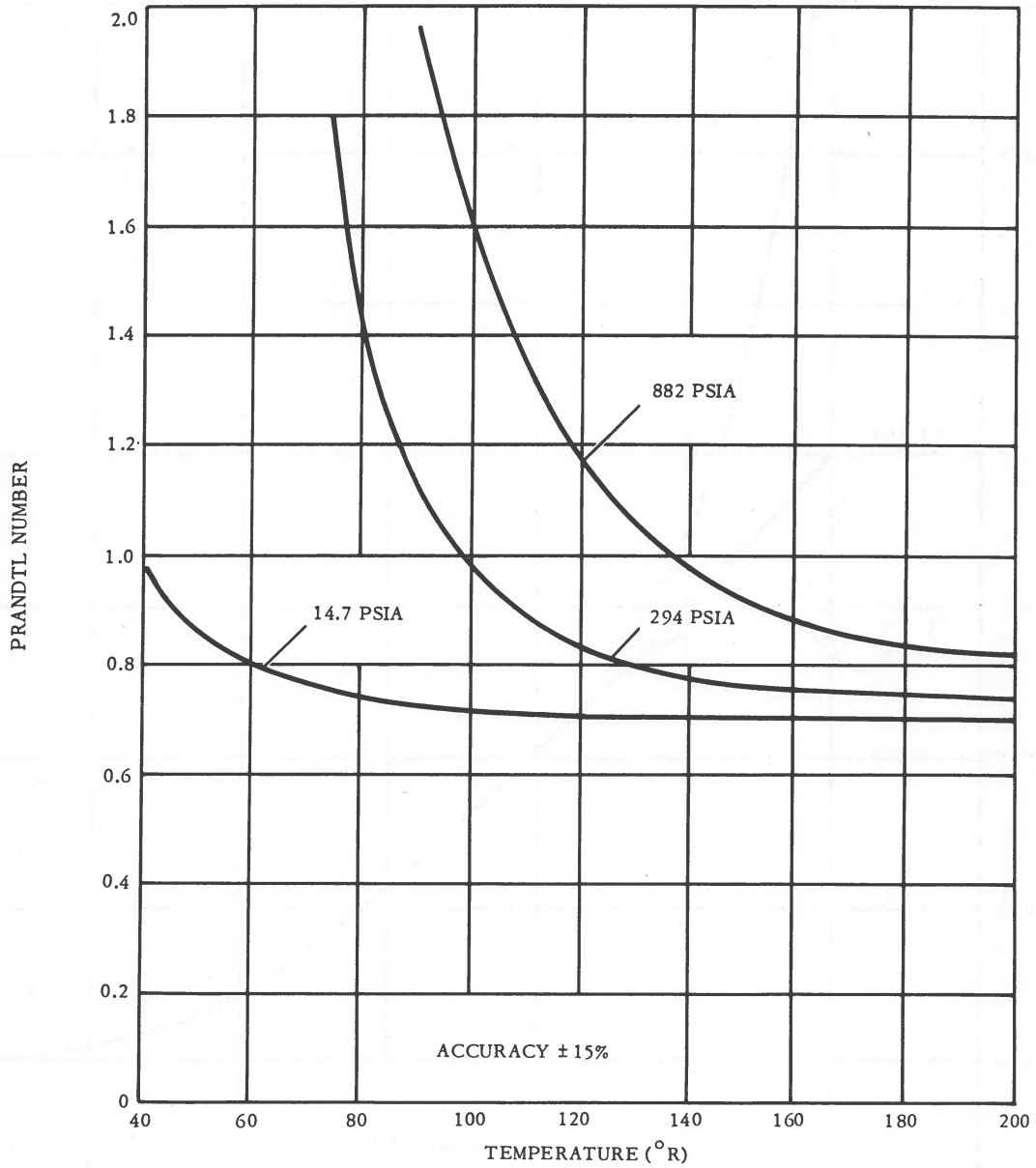


Figure 132. Prandtl number of hydrogen as a function of temperature and pressure.

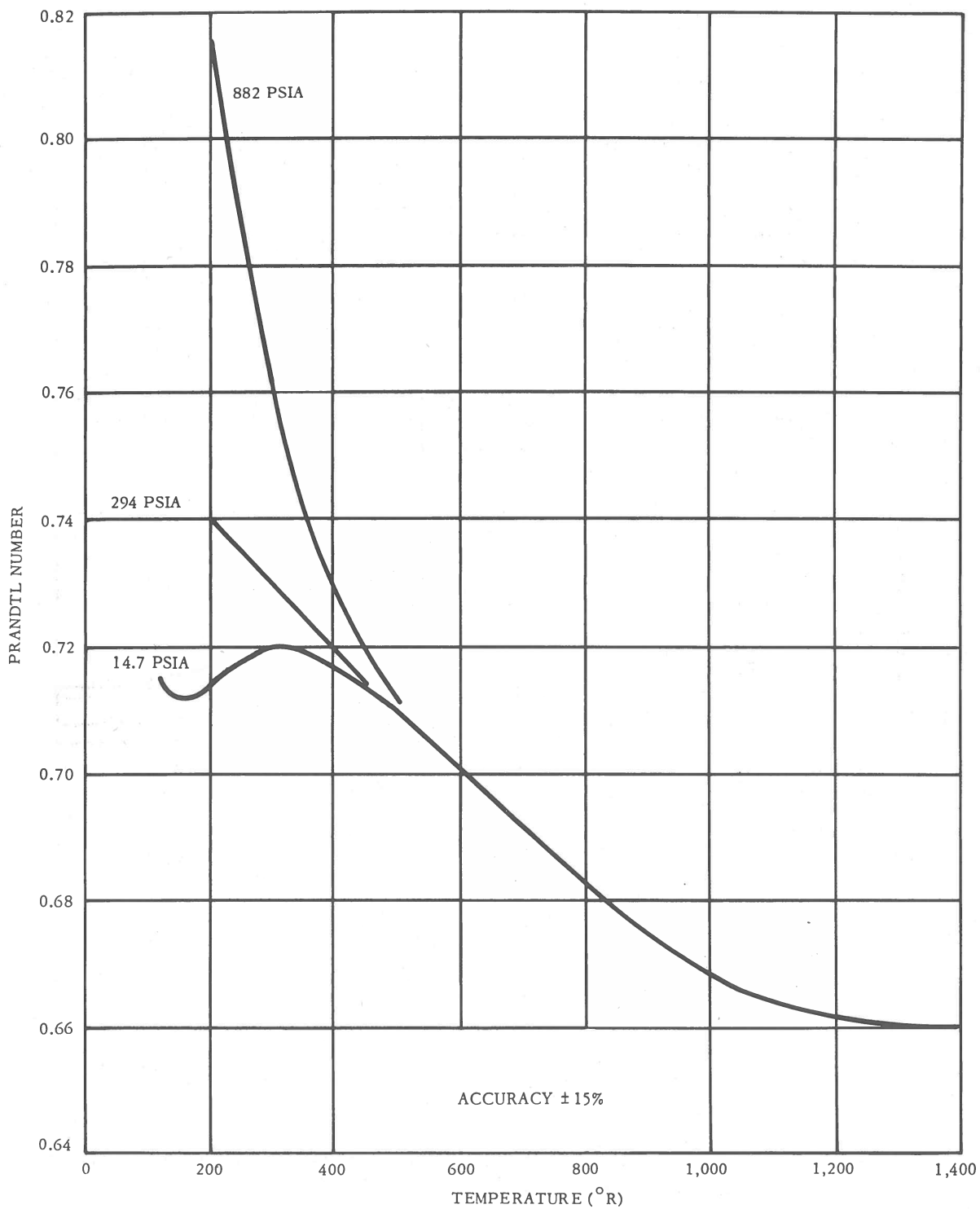


Figure 133. Prandtl number of hydrogen as a function of temperature and pressure.

14.5 NUCLEAR PROPERTIES

Nuclear properties of hydrogen are presented in Table XXIV (Ref. 39) and Figures 134 through 143.

Table XXIV. Isotopic mass.

NUCLIDE	% NATURAL ABUNDANCE	ISOTOPIC MASS
${}^1_1\text{H}^1$	99.9849 to 99.9861	1.008142
${}^1_1\text{H}^2$	0.0139 to 0.0151	2.014735

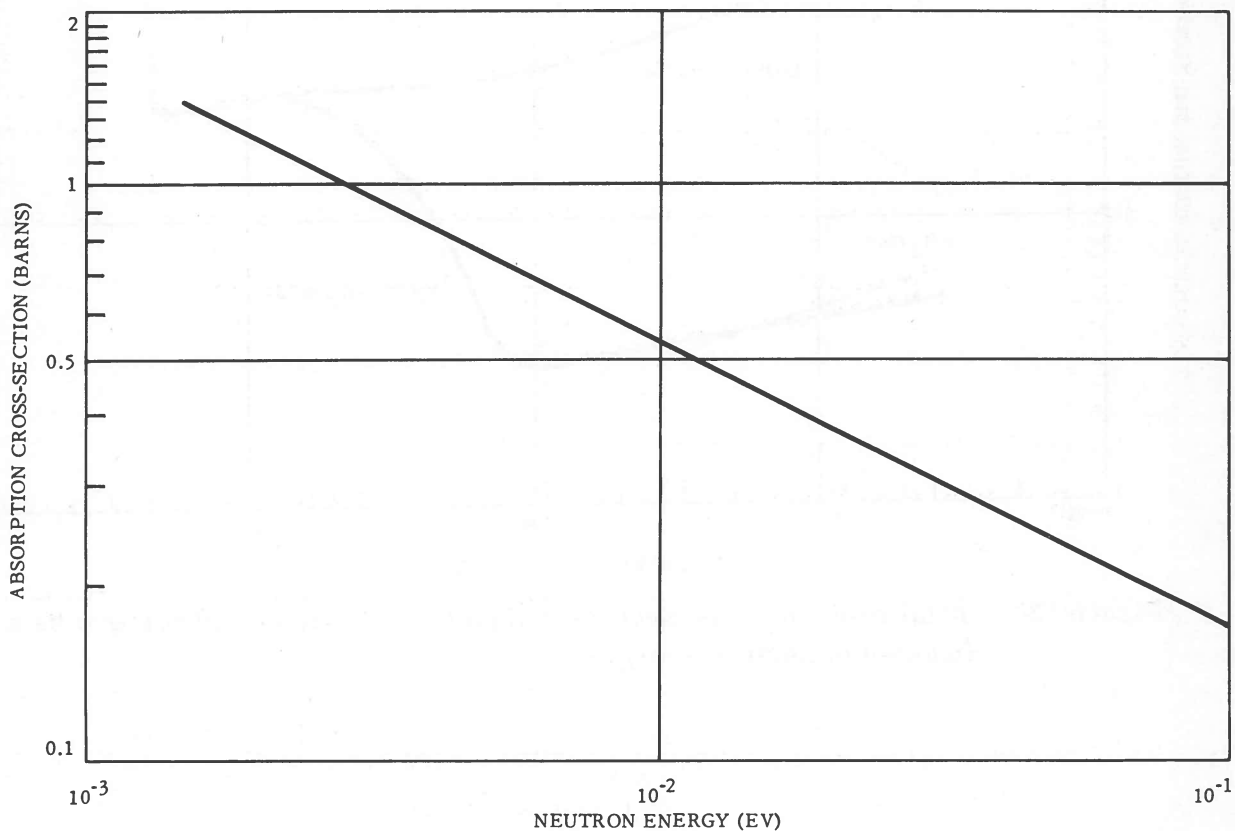


Figure 134. Absorption cross-sections for hydrogen as a function of neutron energy.

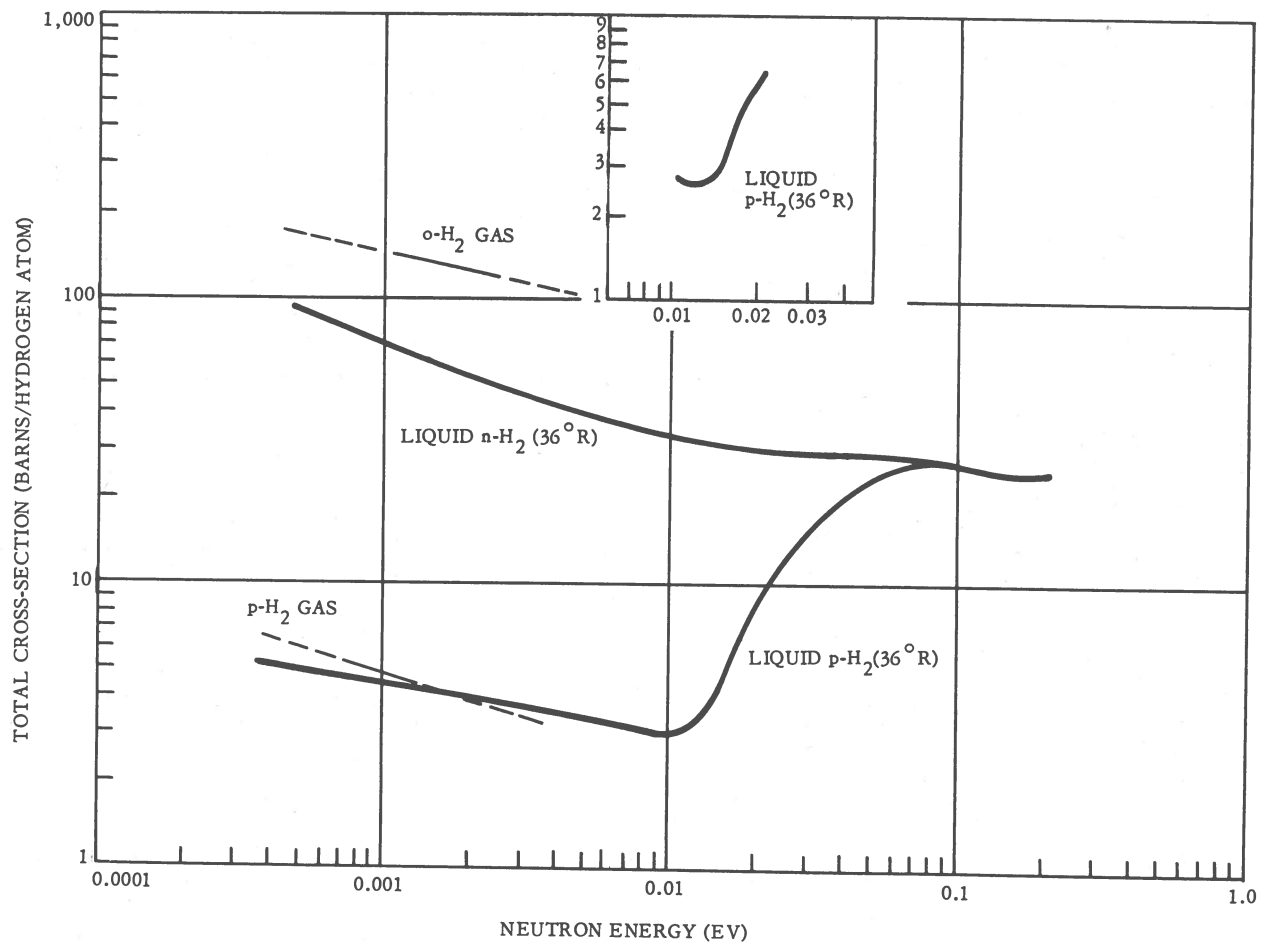


Figure 135. Total neutron cross-section of liquid normal and parahydrogen as a function of neutron energy.

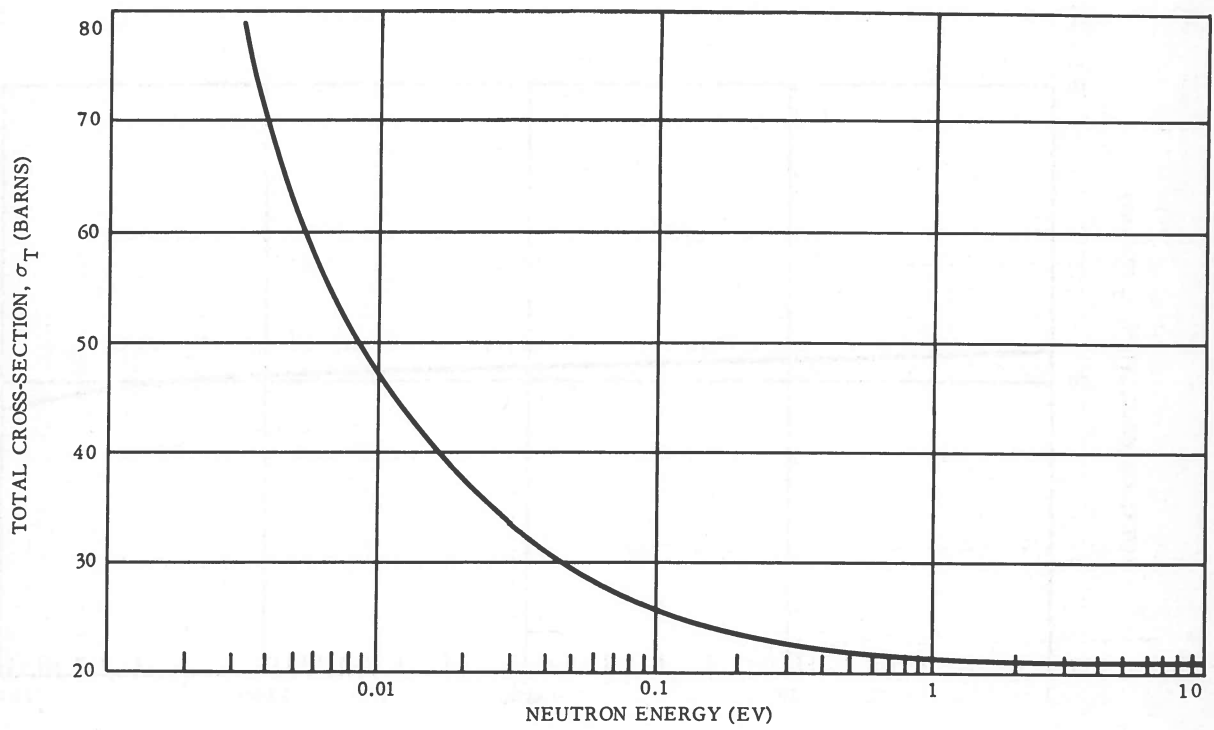


Figure 136. Total neutron cross-sections for hydrogen as a function of neutron energy.

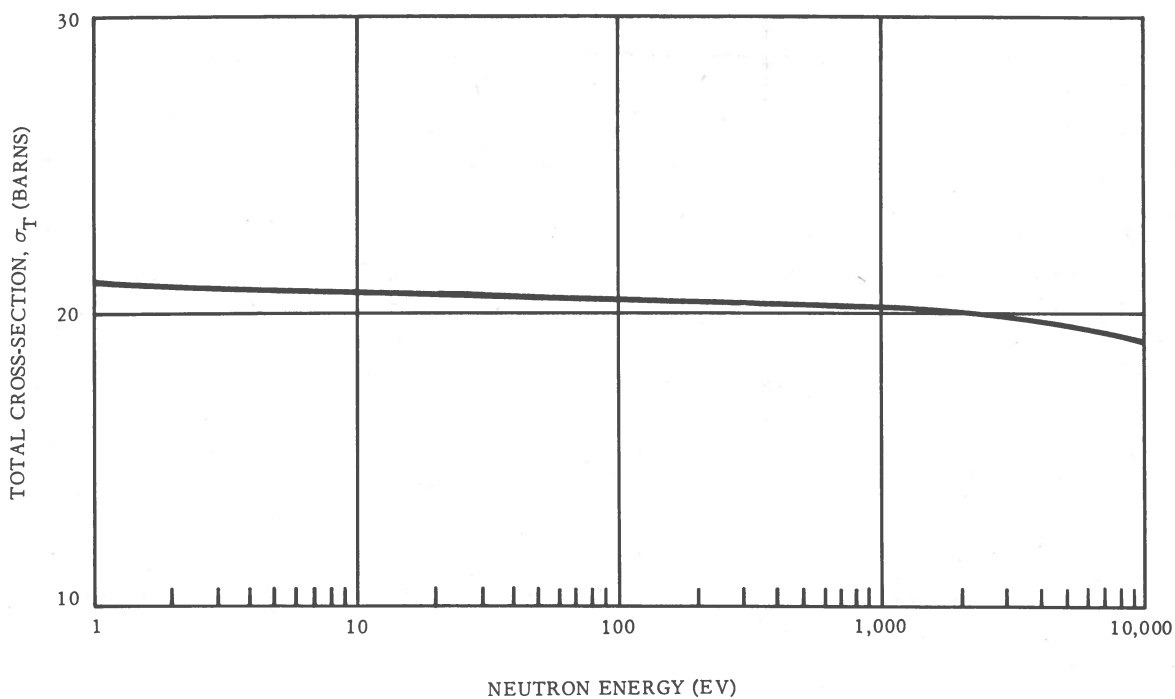


Figure 137. Total neutron cross-sections for hydrogen as a function of neutron energy.

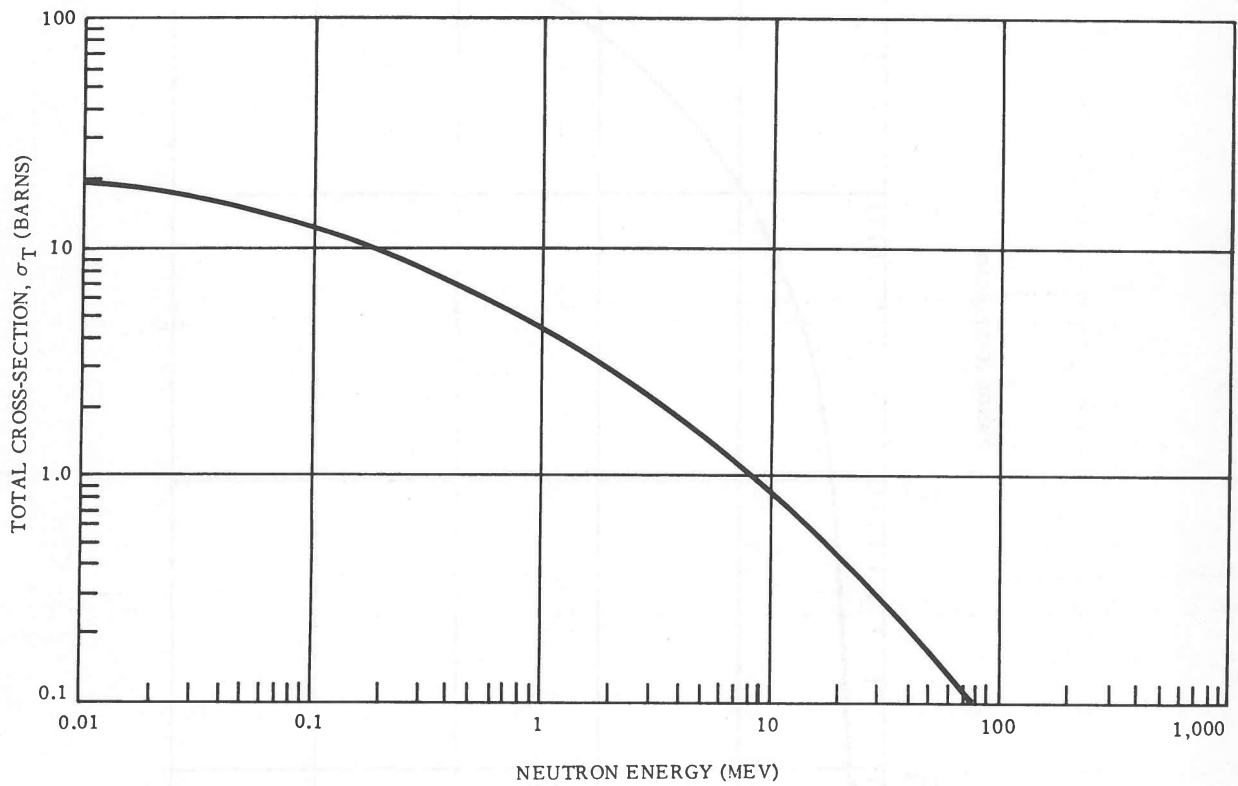


Figure 138. Total neutron cross-section for hydrogen as a function of neutron energy.

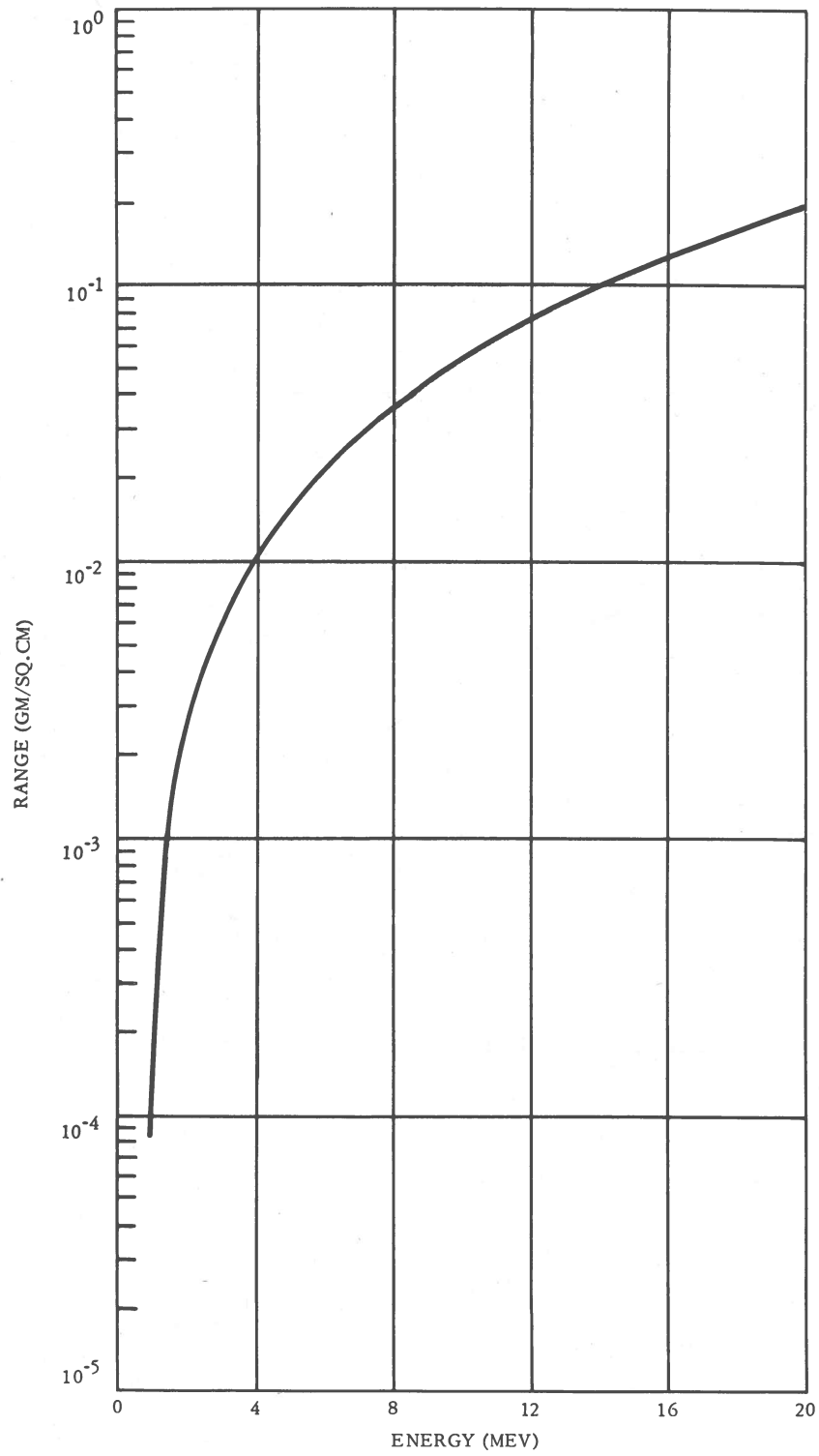


Figure 139. Range of protons in hydrogen as a function of proton energy.



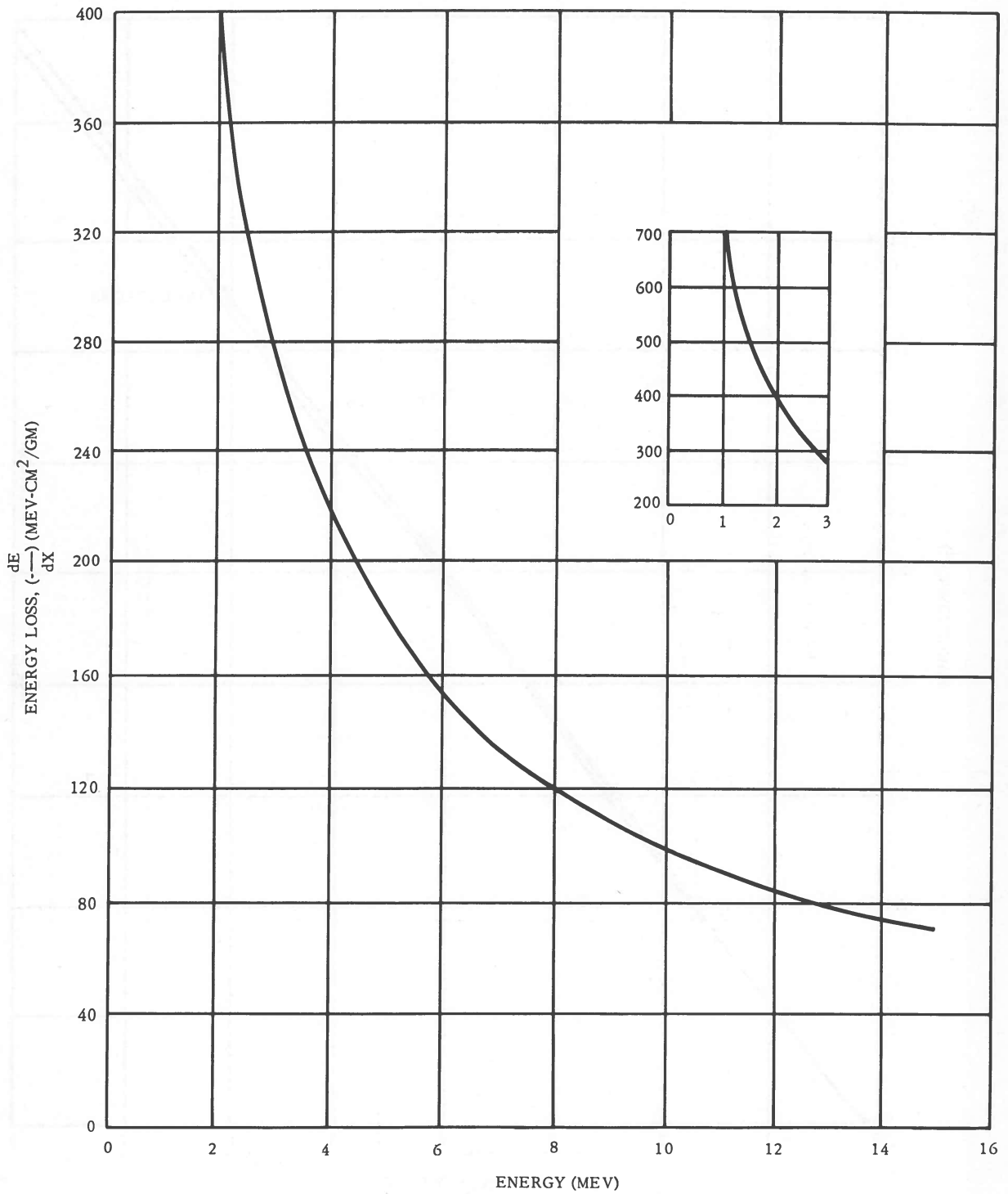


Figure 140. Energy loss of protons in hydrogen as a function of proton energy.

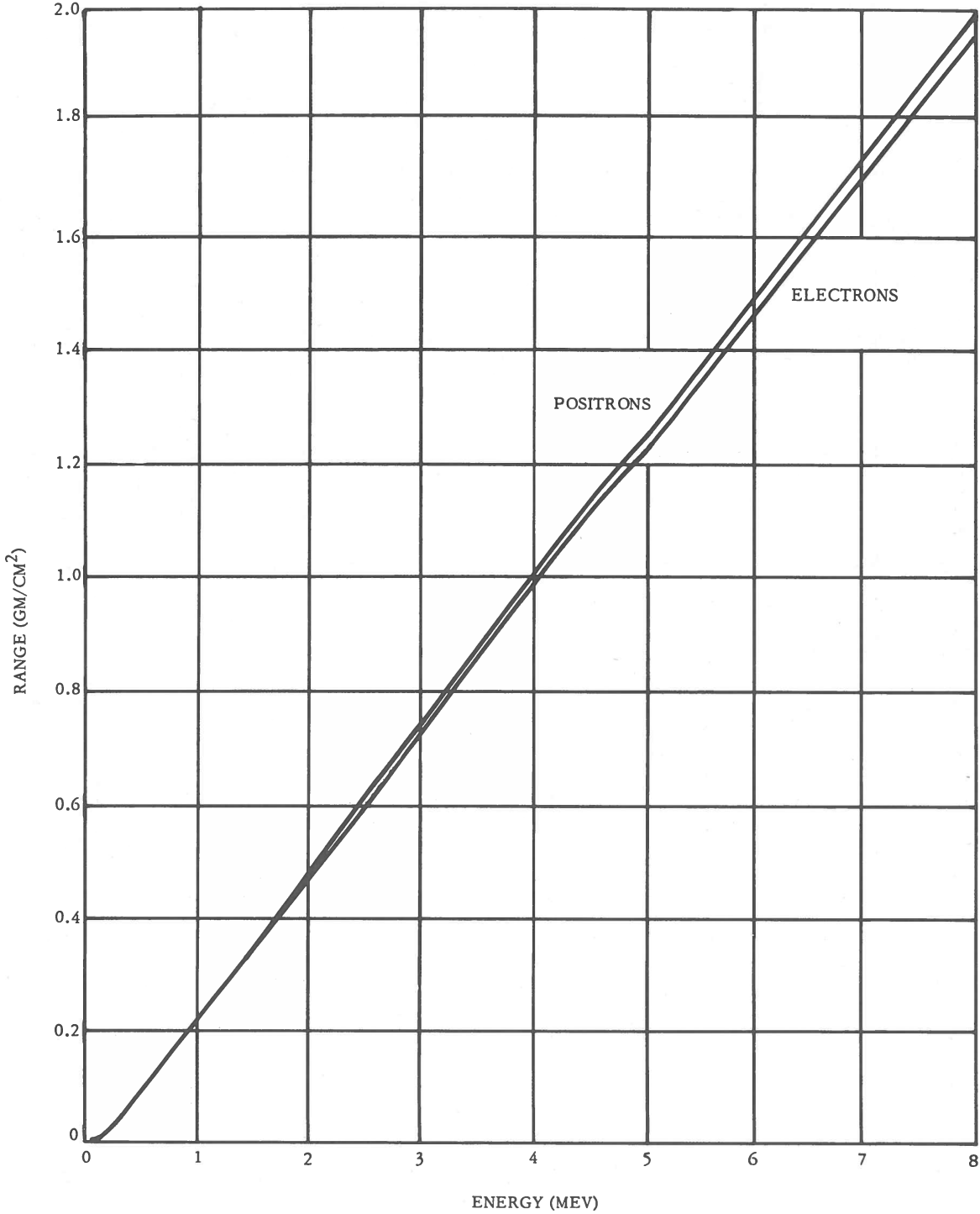


Figure 141. Range of electrons and positrons in hydrogen as a function of energy.

GENERAL DYNAMICS | ASTRONAUTICS

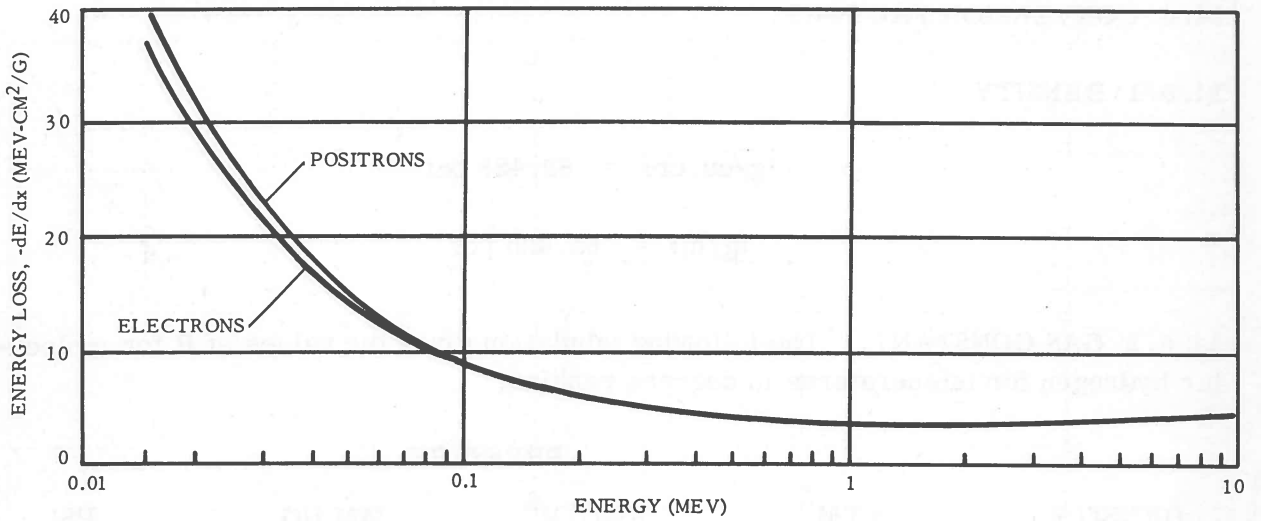


Figure 142. Energy loss of electrons and positrons in hydrogen, including density correction, as a function of energy.

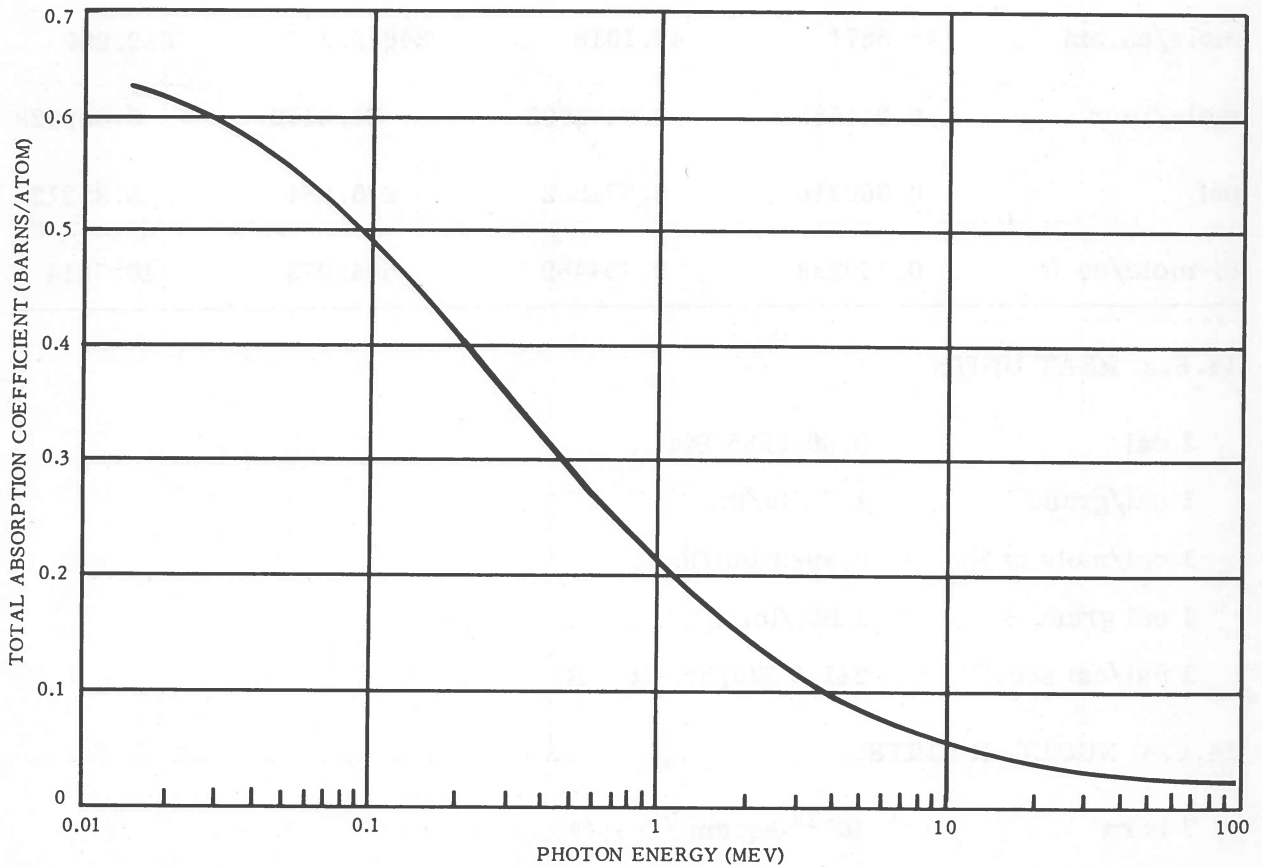


Figure 143. Total absorption coefficients of x-rays and gamma rays for hydrogen.

# GENERAL DYNAMICS | ASTRONAUTICS

## 14.6 CONVERSION FACTORS

### 14.6.1 DENSITY

$$1\text{g/cu. cm} = 62.428 \text{ pcf}$$

$$1\text{g/ml} = 62.426 \text{ pcf}$$

14.6.2 GAS CONSTANT. The following tabulation gives the values of R for molecular hydrogen for temperatures in degrees rankine:

DENSITY	PRESSURE			
	ATM.	KG/CM <sup>2</sup>	MM HG	PSI
g/cu. cm	22.6126	23.3639	17185.6	332.316
mole/cu. cm	45.5871	47.1018	34646.2	669.950
mole/liter	0.0455858	0.0471005	34.6452	0.669928
pcf	0.362216	0.374252	275.284	5.32313
lb-mole/cu. ft.	0.730228	0.754489	554.973	10.7314

### 14.6.3 HEAT UNITS

$$1 \text{ cal} = 0.0039685 \text{ Btu}$$

$$1 \text{ cal/gram} = 1.8 \text{ Btu/lb.}$$

$$1 \text{ cal/mole of H}_2 = 0.8929 \text{ Btu/lb.}$$

$$1 \text{ cal gram } ^\circ\text{K} = 1 \text{ Btu/lb. } ^\circ\text{R}$$

$$1 \text{ cal/cm sec. } ^\circ\text{K} = 241.9 \text{ Btu/hr. -ft. -} ^\circ\text{R}$$

### 14.6.4 NUCLEAR UNITS

$$1 \text{ barn} = 10^{-24} \text{ sq. cm}$$

$$\text{cm}^2/\text{g} = 0.5975 \text{ barns/atom (for hydrogen)}$$

## GENERAL DYNAMICS | ASTRONAUTICS

### 14.6.5 PRESSURE

$$1 \text{ mm of Hg} = 0.019337 \text{ psia}$$

$$1 \text{ atm.} = 14.696 \text{ psia}$$

$$1 \text{ kg/cm}^2 = 14.223 \text{ psia}$$

$$1 \text{ atm.} = 760 \text{ mm}$$

### 14.6.6 TEMPERATURE

$$1^\circ\text{K} = 1.8^\circ\text{R}$$

### 14.6.7 VELOCITY

$$1 \text{ m/sec.} = 3.281 \text{ fps}$$

### 14.6.8 VISCOSITY

$$1 \text{ poise} = 6.7197 \times 10^{-2} \text{ lb./ft.-sec.}$$

### 14.6.9 VOLUME

$$1 \text{ cu. cm} = 3.53144 \times 10^{-5} \text{ cu. ft.}$$

$$1 \text{ ml} = 3.53154 \times 10^{-5} \text{ cu. ft.}$$

$$\frac{\text{cu. cm}}{\text{mole}} = 7.9456 \times 10^{-3} \text{ cu. ft./lb. (for hydrogen)}$$

### 14.6.10 WEIGHT

$$1 \text{ gram} = 2.20462 \times 10^{-3} \text{ lb.}$$

## REFERENCES

1. Handbook of Chemistry and Physics. 40th Ed., Chemical Rubber Co., 1958-1959, p. 3,377.
2. J. Research NBS. H. W. Woolley, R. B. Scott, and F. G. Brickwedde, RP 1932, 41, 1948, pp. 379-475.

## GENERAL DYNAMICS | ASTRONAUTICS

3. NBS Report 7246, 31 March 1962, p. 23.
4. Phil. Mag. H. D. Megaw, 1939, p. 129.
5. Cryogenic Engineering. R. B. Scott, Van Nostrand, 1959, p. 300.
6. A.I. Ch. E. Journal. Schaefer and Thodos, July 1959.
7. Provisional Thermodynamic Functions for Parahydrogen. H. M. Roder and R. D. Goodwin, NBS Tech. Note 130, December 1961, pp. 7-9.
8. Thermodynamic Properties of 20.4°K Equilibrium Hydrogen. A. Shaffer and J. Rousseau, ASD Tech. Report 61-360, October 1961, pp. 20-21.
9. Progress in Low Temperature Physics. A. Van Itterbeck (C. J. Gorter, ed.), International Publishers, Inc., N. Y., North Holland Publishing Co., Amsterdam, 1, 1955, p. 366.
10. Tables of Thermal Properties of Gases. NBS Circular 564, November 1955, p. 283.
11. Expansion Engines for Hydrogen Liquefiers. E. H. Brown, J. Research NBS, Vol. 64C, 1960, p. 25.
12. Hydrogen Handbook. AFFTC TR-60-19, April 1960, p. 103.
13. Dielectric Constant of Liquid Parahydrogen. R. J. Corruccini, NBS Tech. Note 144, April 1962.
14. Thermodynamic Properties of 20.4°K Equilibrium Hydrogen. A. Shaffer and J. Rousseau, ASD Tech. Report 61-360, October 1961, p. 14.
15. Properties and Performance of Hydrogen as a Rocket Fuel. Aerojet-General Corp. Report CR 127-360, 14 March 1960, Figures II-5, II-6.
16. Ibid, Figure II-9.
17. Tables of Thermal Properties of Gases. NBS Circular 564, 1 November 1955, p. 287.
18. A Compendium of the Properties of Materials at Low Temperature. V. Johnson, WADD Technical Report 60-56, Part I., 6:002.

## GENERAL DYNAMICS | ASTRONAUTICS

19. Journal of the American Chemical Society. H. L. Johnson et al. , 72, September-December 1950, pp. 3,935, 3,937.
20. Hydrogen Transport Property Correlations I & II. J. D. Rogers et al. , Los Alamos Scientific Laboratory, LA-2527, May 1961.
21. A Compendium of the Properties of Materials at Low Temperature (Phase I). WADD Tech. Report 60-56, 10.002, October 1960.
22. Properties and Performance of Hydrogen as a Rocket Fuel. Aerojet-General Corp. Report CR 127-360, 14 March 1960, Figure II-29.
23. National Bureau of Standards. R. P. 3282, p. 13.
24. Reacting Propellant Rocket Concept. Convair Report GDC 61-30, November 1961, p. 19.
25. Thermodynamic Properties of 20.4°K Equilibrium Hydrogen. A. Shaffer and J. Rosseau, ASD Tech. Report 61-360, October 1961, p. 16.
26. A Compendium of the Properties of Materials at Low Temperature (Part I). WADD Tech. Report 60-56, 5.002, July 1960.
27. Phil. Mag. R. H. Hill and B. W. A. Ricketson, 45, 1954, p. 227.
28. Tables of Thermal Properties of Gases. NBS Circular 564, 1 November 1955, p. 286.
29. Z. Physik Chem [A], 184, 45, 1939.
30. Tables of Thermal Properties of Gases. NBS Circular 564, 1 November 1955, pp. 277, 282, 291, 292.
31. Properties and Performance of Hydrogen as a Rocket Fuel. Aerojet-General Corp. Report CR 127-360, 14 March 1960, Figures II-16, II-18.
32. Ohio State University Technical Reports. Mattox, Powers, and Johnston, TR 264-10 and TR436-1, 1951.
33. A Compendium of the Properties of Materials at Low Temperature, Phase 1, Properties of Fluids. V. J. Johnson, WADD 60-56, July 1960.

## GENERAL DYNAMICS | ASTRONAUTICS

34. NBS Report 3163, 1954.
35. Cryogenic Data Book. D. B. Chelton and D. B. Mann, WADC Tech. Report 59-8, March 1959, pp. 76-78.
36. Provisional Thermodynamic Functions for Parahydrogen. H. M. Roder and R. D. Goodwin, NBS Tech. Note 130, December 1961.
37. Thermodynamic Properties of 20.4°K - Equilibrium Hydrogen. A. Shaffer and J. Rousseau, ASD Tech. Report 61-360, October 1961, Graph III-C.
38. Properties and Performance of Hydrogen as a Rocket Fuel. Aerojet-General Corp. Report CR 127-360, 14 March 1960, Figure II-24 and II-25.
39. Experimental Nuclear Physics. K. T. Bainbridge, Vol. I, (E. Segre, ed.), John Wiley & Sons, N. Y., 1953.
40. Properties and Performance of Hydrogen as a Rocket Fuel. Aerojet-General Corp. Report CR 127-360, 14 March 1960, Figure II-1.
41. Differential Neutron Thermalization. McReynolds and Whittemore, General Atomic Progress Report GACD-2215, March 1961.
42. Neutron Cross Sections. D. J. Hughes and R. B. Schwartz, 2nd ed., BNL 325, July 1958, pp. 72-74.
43. Range Energy Curves. W. A. Aron et al., AECU-663, 2nd Revision, 28 May 1951, p. 9.
44. Energy Loss and Range of Electrons and Positrons. A. T. Nelms, NBS Circular 577, 30 July 1958, p. 5.
45. X-Ray Attenuation Coefficients from 10 Kev to 100 Mev. G. W. Grodstein, NBS Circular 583, 30 April 1957, p. 23.



# GENERAL DYNAMICS | ASTRONAUTICS

## BIBLIOGRAPHY

### MANUFACTURE

How the Air Force Liquefies Hydrogen. Chemical Engineering, Vol. 67, 25 January 1960, pp. 86-89.

New Details Round Out Liquid H<sub>2</sub> Story. Chemical Engineering, Vol. 67, 22 February 1960, pp. 61-62.

The Master Fuel of a New Age. Lawrence Lessing, Fortune, May 1961, pp. 152-156, 238-244.

Cryogenic H<sub>2</sub>. Pratt & Whitney Aircraft, February 1960.

Large-Scale Production, Handling and Storage of Liquid Hydrogen. P. C. Vander Arend, Advances in Cryogenic Engineering, Plenum Press, Inc., New York, Vol. 5, 1960, pp. 49-54.

Which Process Best for Producing Hydrogen? G. R. James, Chemical Engineering, Vol. 67, 12 December 1960, pp. 161-166.

Cryogenic Engineering. R. B. Scott, D. Van Nostrand Co., Inc., August 1960.

### TRANSPORTATION

New Combinations of Liquid H<sub>2</sub>, Liquid O<sub>2</sub>, Fluorine, Ozone Ready for Rockets. R. F. Fremed, Chemical Engineering, 2 November 1959.

Practical Storage and Distribution of Liquid Hydrogen and Helium. W. E. Perkins et al., Advances in Cryogenic Engineering, Plenum Press, 1959, pp. 69-76.

### HYDROGEN SAFETY

Storage, Transfer and Servicing Equipment for Liquid Hydrogen. B. M. Bailey et al., Arthur D. Little, Inc., WADC Tech. Report 59-386, July 1959.

## GENERAL DYNAMICS | ASTRONAUTICS

Liquid Hydrogen Safety Manual. J. F. Watson, Astronautics Report MRG-66, May 1959.

Properties and Performance of Hydrogen as a Rocket Fuel. Aerojet-General Corp. Report No. CR 127-360, 14 March 1960.

Advances in Cryogenic Engineering. K. D. Timmerhaus, Plenum Press, Inc., N. Y., Vol. 4 and 5, 1960.

Hydrogen Handbook. Arthur D. Little, Inc., AFFTC TR-60-19, April 1960.

Handbook for Hydrogen Handling Equipment. B. M. Bailey et al., Arthur D. Little, Inc., WADC Tech. Report 59-751, February 1960.

Research on the Hazards Associated with the Production and Handling of Liquid Hydrogen. M. G. Zabetakis et al., Bureau of Mines, WADD TR-60-141, June 1960.

Electrostatic Hazards Associated with the Transfer and Storage of Liquid Hydrogen. A. D. Little Report C-61092, 15 May 1961.

The Handling and Storage of Liquid Propellants. Office of the Director of Defense Research and Engineering, Washington 25, D. C., March 1961.

Convair-Astronautics Safety Rules and Regulations. A. W. Wright, Astronautics report.

The Science of High Explosives. M. A. Cook, Reinhold Publishing Co., N. Y.

### MATERIALS

Advances in Cryogenic Engineering. Vol. 1-7, Plenum Press.

Cryogenic Materials Data Handbook. T. F. Durham et al., NBS Cryogenic Engineering Laboratory, 15 February 1962.

Hydrogen Handbook. A. D. Little Report AFFTC TR-60-19, April 1960.

A Compendium of the Properties of Materials at Low Temperature (Phases I and II). R. B. Stewart and V. J. Johnson, NBS Cryogenic Engineering Laboratory, WADD Tech. Report 60-56, July 1960 and December 1961.

## GENERAL DYNAMICS | ASTRONAUTICS

Cryogenic Data Book. D. B. Chelton and D. B. Mann, NBS Cryogenic Engineering Laboratory, WADC Tech. Report 59-8, March 1959.

A Compilation of Mechanical Properties of Materials at Cryogenic Temperatures. R. M. McClintock and H. P. Gibbons, NBS Report 6064, 1 July 1959.

Properties of Materials at Liquid Oxygen and Liquid Hydrogen Temperatures. A. Hurlich, Astronautics Report AA-M-23, March 1957.

Bibliography on Low Temperature Characteristics of Steels. K. Janis, International Nickel Co., 1954.

Metals Handbook. ASM, Cleveland, Ohio.

Low Temperature Bibliography for the Field of Cryogenics (with eight supplements). Engineering Division, A. D. Little, Inc., 1958.

Report on Research and Development of Metals and Alloys for Low Temperature Applications. Report No. MAB-65-M, Materials Advisory Board, National Academy of Sciences National Research Council, Washington, D.C., 23 April 1954.

Low Temperature Properties of Metals. A. E. White and C. A. Siebert, Ann Arbor, Mich., 1947.

A Bibliography on the Effect of Low Temperature on the Mechanical Properties of Materials. R. H. Kropschot and D. McCohm, National Bureau of Standards Report 5058, 1957.

Mechanical Properties of Metals at Low Temperatures: A Survey. L. Seigle and R. M. Brick, Trans. ASM, 40, 1948.

The Properties of Metallic Materials at Low Temperatures. P. L. Teed, John Wiley Co., New York, N. Y., 1950.

Mechanical Properties of Metals at Low Temperatures. National Bureau of Standards Circular 520, 7 May 1952.

Metallurgy at Low Temperatures. C. S. Barrett, Trans. ASM, 50, 1957.

Hydrogen in Metals. D. P. Smith, The University of Chicago Press, 1948.

## GENERAL DYNAMICS | ASTRONAUTICS

Effect of the Temperature of Liquid Hydrogen ( $-252.8^{\circ}\text{C}$ ) on the Tensile Properties of Forty-One Specimens of Metals Comprising (a) Pure Iron 99.85% (b) Four Carbon Steels (c) Thirty Alloy Steels (d) Copper and Nickel (e) Four Non-Ferrous Alloys. W. J. DeHaas and R. A. Hadfield, Philosophical Trans., 232, 1933.

Properties of Engineering Materials at Extreme Subzero Temperatures with Supplementary Information of Liquid Hydrogen. J. F. Watson, Astronautics Report MRG-44, 8 December 1958.

Behavior of Metals at Low Temperatures. R. M. Brick, J. R. Low and C. H. Lorig, American Society for Metals, Cleveland, Ohio, 1953.

A Study of the Effects of Nuclear Radiation on High-Strength Aerospace Vehicle Materials at the Boiling Point of Hydrogen ( $-423^{\circ}\text{F}$ ). J. F. Watson et al., Astronautics Report ERR-AN-085, 27 September 1961.

Hydrogen Embrittlement of Steel Review of the Literature. R. W. Buzzard and H. E. Cleaves, NBS Circular 511, 1951.

Lubrication for Space Vehicles. G. W. Oliver, Astronautics Report ERR-AN-104.

### CRYOGENIC INSULATION

Interim Status Report on the Development of Wet-Wall Insulation for Saturn S-IV. Douglas Report 38797, August 1961.

Properties of Foams, Adhesives, and Plastic Films at Cryogenic Temperatures. R. N. Miller et al., Lockheed-Georgia Co., paper presented to American Chemical Society, Div. of Organic Coatings and Plastics Chemistry, Vol. 22, No. 1, March 1962.

Design Selection of Insulation for Airborne Liquid Hydrogen Tanks. B. C. Blankenship and M. B. Hammond, North American Aviation, Inc., Report SID 61-423, November 1961.

Bonded and Sealed External Insulations for Liquid-Hydrogen-Fueled Rocket Tanks During Atmospheric Flight. V. H. Gray et al., Lewis Research Center, NASA TN D-476, October 1960.

## GENERAL DYNAMICS | ASTRONAUTICS

Evaluation of Rift Insulation Test Program. J. Hertz, Astronautics Report AR-592-1-334, August 1962.

Evaluation of Composite Insulations for Centaur F-2 Liquid Hydrogen Tank. H. R. Pearson, Astronautics Report AR-592-1-333, August 1962.

Thermal Expansion Characteristics of Fiberglass Honeycombs at Low Temperatures. M. Campbell, Astronautics Report MRG-327, July 1962.

Thermal Conductivity and Coefficient of Expansion of Fiberglass Honeycomb Panels at Low Temperature. J. Haskins, Astronautics Report MRG-323, June, 1962.

Thermal Conductivity of Plastic Foams from  $-423^{\circ}\text{F}$  to  $75^{\circ}\text{F}$ . J. Haskins and J. Hertz, Astronautics Report MRG-242, July 1961.

Cryogenic Engineering. R. B. Scott, D. Van Nostrand Co., Inc., August 1960.

Storage, Transfer and Servicing Equipment for Liquid Hydrogen. B. M. Bailey et al., WADC Tech. Report 59-386, July 1959.

Cryogenic Adhesive Evaluation Study. J. Hertz, Astronautics Report ERR-AN-032, 25 January 1961.

### TRANSFER

Storage, Transfer and Servicing Equipment for Liquid Hydrogen. B. M. Bailey et al., WADC Tech. Report 59-386, July 1959.

Advances in Cryogenic Engineering. Vol. 1-7, Plenum Press.

Cryogenic Engineering. R. B. Scott, D. Van Nostrand Co., Inc., August 1960.

Geysering Study of the SF-1 Transfer Line. D. Fulmer, Astronautics Report 55B-2349, 3 November 1960.

Research on Zero Gravity Expulsion Techniques. A. Krivetsky, Bell Aerosystems Report 7129-933003, March 1962.

## GENERAL DYNAMICS | ASTRONAUTICS

### CRYOGENIC MEASUREMENTS

Instrumentation Transducer Identification. H. Norton, Astronautics Report ZN-7-182-TN, 1 April 1961.

Calibration of Platinum Resistance Thermometers. R. J. Corruccini, NBS Project 8131, File No. 57-25.

Cryogenic Engineering. R. B. Scott, D. Van Nostrand Co., Inc., August 1960.

Instrumentation Calibration Procedures for Centaur Vacuum Stub Tank Heat Transfer Test. R. N. Franklin, Astronautics Report STL-P17, 2 July 1962.

NBS Circular 561.

Low Temperature Thermocouples - Gold Cobalt or Constantan vs. Copper or Normal Silver. R. L. Powell et al., Cyrogenics, Vol. I, No. 3, March 1961.

Storage, Transfer and Servicing Equipment for Liquid Hydrogen. B. M. Bailey et al., WADC Tech. Report 59-386, July 1959.

Transducers for Electronic Measuring Systems. H. Norton, Prentiss-Hall Publishing Co., to be published in December 1963.

### PROPULSION METHODS

Reacting Propellant Rocket Concept. Convair Report GDC-61-30, November 1961.

Rocket Propulsion. M. Barrère et al., Elsevier Publishing Co., 1960.

Nuclear Rocket Propulsion. R. W. Bussard and R. D. De Lauer, McGraw-Hill Book Co., Inc., 1958.

Space Flight. G. Merrill, Editor, D. Van Nostrand Co., Inc., 1960.

Comparison of Advanced Propulsion Systems: Solar-Heating, Arc Thermodynamics and Arc Magneto Hydrodynamics. K. A. Ehricke, Astronautics report.

The Solar-Powered Space Ship. K. A. Ehricke, presented at ARS Meeting, Cleveland, Ohio, 18-20 June 1956.

## GENERAL DYNAMICS | ASTRONAUTICS

On the Application of Solar Power in Space Flight. K. A. Ehricke, Astronautics report.

Status of Electric Propulsion Systems for Space Missions. W. E. Moechel, Advances in Cryogenic Engineering, Vol. 6, 1960, pp. 1-19.

Chemical Rocket Propulsion Systems. F. J. Hendel, Chem. Eng., 6 March 1961, pp. 99-114.

Advanced Rocket Propulsion. F. J. Hendel, Chem. Eng., 3 April 1961, pp. 131-148.

Exotic Rocket-Propulsion Systems. F. J. Hendel, Chem. Eng., 24 July 1961, pp. 135-142.

### SLOSHING

Propellant Sloshing Control Problems in Large Ballistic Boosters. A. F. Schmitt, Astronautics paper.

Orientation Control of Satellites and Space Vehicles. A. F. Schmitt, paper presented to School of Aeronautical Engineering, Purdue University, September 1960.

Measured Two-Dimensional Damping Effectiveness of Fuel-Sloshing Baffles Applied to Ring Baffles in Cylindrical Tanks. H. A. Cole et al., NASA Tech. Note D-694, February 1961.

Propellant Sloshing Test for "C" Missile During 2nd Stage. G. L. Kugler, Astronautics Report 7A1380, 13 November 1958.

### VORTEXING

Vortex Motion in Draining Liquids - The Discharge Rate. M. S. Plesset, 28 May 1956.

Vortex Motion in Draining Liquids - II Viscous Decay of Rotational Motion. M. S. Plesset, 9 July 1956.

Vortex Motion in Draining Liquids - III Decay of the Circulating Motion in a Tank of Infinite Radius. M. S. Plesset, 14 December 1956.

## GENERAL DYNAMICS | ASTRONAUTICS

Vortex Motion in Draining Liquids - IV Remarks on Similitude Scaling of Vortex Motion in Draining Liquids. M. S. Plesset, 10 April 1957.

The Behavior of Vortex Motion in an Emptying Container. P. Dergarabedian, Proceedings of the 1960 Heat Transfer and Fluid Mechanics Institute, Stanford University Press, 1960, P. 47.

Fuel Tank Vortexing Test B and C Series. R. T. Tuttobene, Astronautics 7B1591-1, 12 January 1959.

Fuel Tank Vortexing Test D Series. R. T. Tuttobene, Astronautics Report 7B2319-1, 5 August 1959.

### PROPELLANT HEATING

A Stable Numerical Solution of Transient Heat Conduction Problems. A. Cohen, Astronautics Report AE 60-0744, 8 September 1960.

The Variable-Boundary Transient Heat Conduction Program. R. F. O'Neill and C. D. Rozendaal, Astronautics Report AE 62-0401, 1 May 1962.

Analytical Methods and Equations for Use in an IBM 704 Program, to Determine the Effects of Aerodynamic Heating by the Reference Enthalpy Method. D. J. Smith and L. Fisher, Convair Report T-C-15, 28 October 1958.

Space Vehicle Radiant Energy Program (Saint Nero). H. E. Hogfors and R. S. Dummer, Astronautics Report ERR-AN-146.

Cryogenic Tank Thermal Design for Planet Missions. C. C. Love Jr., Astronautics Report ASD 44-62, 10 August 1962.

Liquid Hydrogen in a Nuclear Environment, D. G. Abshier (Project Leader), Astronautics Report ERR-AN-150.

Convection in a Liquid Contained in an Axisymmetric Tank with Prescribed Heat Input and Gravity. Ta Li, Astronautics Report ERR-AN-149, 8 March 1962.

Thermodynamic Analysis of Centaur Cryogenic Propellant Tanks. J. J. Fitts and E. Sotak, Astronautics Report AE 62-0408, 16 April 1962.



## GENERAL DYNAMICS | ASTRONAUTICS

### ZERO GRAVITY BEHAVIOR

Liquid Behavior in a Zero-G Field. Ta Li, Astronautics Report AE60-0682, September 1960.

Preliminary Studies of Liquid Behavior in a Low-G Field. Ta Li, Astronautics Report ERR-AN-036, March 1961.

Hydrostatics in Various Gravitational Fields. Ta Li, Astronautics report.

The Effect of the Liquid Volume on Its Behavior Under Zero-G Conditions. John Vasiliu, Astronautics Report ERR-AN-043, 27 March 1961.

A Description of the Laboratory and Aircraft Zero-G Test Program. Astronautics Report AE60-0942, 15 November 1960.

August - October Progress Report for the Combined Laboratory and KC-135 Aircraft Zero-G Test Program. Astronautics Report AE60-0886, 8 November 1960.

The Center-Vent Shape. C. K. Perkins, Astronautics Report 55D859, 25 July 1961.

Liquid Oscillations and Damping. G. B. Wood, Astronautics Memo 562-1-550, 25 April 1961.

Laboratory Simulation of Centaur Fuel-Tank Ullage Configuration in Zero-Gravity. G. B. Wood, Astronautics Memo 562-1-577, 27 September 1961.

The Effect of Zero Gravity on Fluid Behavior and System Design. J. J. Neimer, WADC Tech. Note 59-149, April 1959.

Zero-Gravity Flight Tests with Cryogenic Liquids at WADC, Dayton, Ohio. H. E. Hogfors, Astronautics Report AZJ-55-006 TN, 7 August 1959.

A Proposal for a Combined Laboratory and Airplane Zero-G Test Program. Astronautics Report AE-60-0564, 27 June 1960.

### SPACE STORAGE

Cryogenic Tank Thermal Design for Planet Missions. C. C. Love Jr., Astronautics Report ASD 44-62, 10 August 1962.

Researches on Meteorites. C. B. Moore, John Wiley and Sons, Inc., N. Y., 1962.

## GENERAL DYNAMICS | ASTRONAUTICS

A Study of Early Manned Interplanetary Missions. K. A. Ehricke, Astronautics Report ASO 1-4, 30 July 1962.

Study of Principles of Meteoroid Protection. R. F. Rolsten et al., Astronautics Report AE 62-6413, April 1962.

Investigation of Recovered Fragments from Atlas 109-D Booster. J. J. Sheppard Jr., Astronautics Report AE 62-0558, 1 July 1962.

Preliminary Investigation of Impact on Multiple-Sheet Structures and an Evaluation of the Meteoroid Hazard to Space Vehicles. R. C. Nysmith and J. L. Summers, NASA TN D-1039, September 1961.

A Technique of Evaluating Fuel Losses Due to Meteoroid Puncture and Some Timely Examples. A. H. Jazwinski, Astronautics paper.

Satellite Pressure Losses Caused by Meteoroid Impacts. M. Kornhauser, ARS Journal, 30(5), May 1960.

Meteoroids Versus Space Vehicles. R. L. Bjork, ARS Journal, 31, June 1961.

Fuel Losses on a Typical 6.2 Hour Centaur Mission Due to Meteoroid Puncture. A. H. Jazwinski, Astronautics Report AE61-1042, August 1961.

The Production of Meteoroid Hole Area in a Space Vehicle Near the Earth. R. M. Edmiston, IAS Paper No. 62-29, January 1962.

Cosmic Dust Showers by Direct Measurements. M. Dubin, W. M. Alexander, and O. E. Berg, Symposium on the Astronomy and Physics of Meteors, 1961.

Between the Planets. F. G. Watson, Harvard University Press, 1956, Ch. 7.

The Meteoritic Risk to Space Vehicles. F. L. Whipple, Vistas in Astronautics, 1958.

The Density of Mass Distribution of Meteoritic Bodies in the Neighborhood of the Earth's Orbit. Harrison Brown, J. Geophys. Research, 65, 1679, June 1960.

The Distribution of Small Interplanetary Dust Particles in the Vicinity of Earth. C. W. McCracken and W. M. Alexander, Symposium on the Astronomy and Physics of Meteors, 1961.

## GENERAL DYNAMICS | ASTRONAUTICS

Interplanetary Dust Distribution. D. B. Beard, *Astrophys. J.*, 192, 1959, pp. 496-506.

Interplanetary Dust Near the Earth. S. F. Singer, *Nature*, 28 October 1961.

Particulate Contents of Space. F. L. Whipple, Chapter in *Medical and Biological Aspects of the Energies of Space*, Columbia University Press, New York, 1961.

Survey of Hypervelocity Impact Information. W. Herrmann and A. H. Jones, MIT ASRL Report 99-1, September 1961.

Effects of Meteoroid Impact on Space Vehicles. R. L. Eichelberger and J. W. Gehring, BRL Report 1155, December 1961.

Advances in Cryogenic Engineering. Papers D-1 through D-5 on Laminar Insulation, Plenum Press, 1959.

### PROPERTIES

Compilation of Thermal Properties of Hydrogen in Its Various Isotopic and Ortho-Para Modifications. H. W. Woolley, NBS Research Paper 1932, Vol. 41, November 1948.

A Tabulation of the Thermodynamic Properties of Normal Hydrogen from Low Temperatures to 300° K and from 1 to 100 Atmospheres. J. W. Dean, NBS Tech. Note 120, November 1961.

Provisional Thermodynamic Functions for Parahydrogen. H. M. Roder and R. D. Goodwin, NBS Tech. Note 130, December 1961.

The Thermodynamic Properties of Parahydrogen from 1° to 22° K. J. C. Mullins et al., NBS Report MR-6, 1 November 1961.

Cryogenic Data Book. D. B. Chelton and D. B. Mann, WADC Tech. Report 59-8, March 1959.

A Compendium of the Properties of Materials at Low Temperature (Phase I and II). R. B. Stewart and V. J. Johnson, WADD Tech. Report 60-56, December 1961.

Hydrogen Handbook. Air Force Flight Test Center Report TR-60-19, April 1960.

## GENERAL DYNAMICS | ASTRONAUTICS

Properties and Performance of Hydrogen as a Rocket Fuel. Aerojet-General Corp. Report CR 127-360, 14 March 1960.

Thermodynamic Properties of 20.4 °K - Equilibrium Hydrogen. A. Schaffer and J. Rousseau, Aeronautical Systems Division Report 61-360.

Hydrogen Transport Properties. J. D. Rogers et al., Los Alamos Scientific Laboratory Report LA-2527, May 1961.

Tables of Thermal Properties of Gases. J. Hilsenrath et al., NBS Circular 564, 1 November 1955.